

# **GEOCHEMISTRY AND PETROGRAPHY OF SPELEOTHEMS FROM TURKEY AND IRAN: PALAEOCLIMATE AND DIAGENESIS**

**LERETTA BROOK WICKENS**

A thesis submitted to for the degree of  
Doctor of Philosophy

University of East Anglia

School of Environmental Sciences

June 2013

This copy of the thesis has been supplied on condition that anyone who consults it is understood to recognise that its copyright rests with the author and that use of any information derived there from must be in accordance with current UK Copyright Law. In addition, any quotation or extract must include full attribution

## Abstract

Speleothems contain key archives of palaeoclimatic information, which can be interpreted through multiple geochemical and petrographic proxies, and precisely dated by Uranium Series dating. As U/Th dating is only viable for samples up to approximately 700 kyr of age, U/Pb dating must be used to date older samples. In this study, U/Pb methods were used to date an aragonite layer in a speleothem from Iran, following the use of autoradiography to select samples with appropriately high uranium.

Aragonite is metastable at earth surface conditions, and is therefore prone to recrystallisation as calcite if it comes into contact with a fluid that is undersaturated with respect to aragonite. This process affected two speleothems from Dim Cave, SW Turkey, and one speleothem from Torang Cave, Iran. The older Dim Cave stalagmite, which precipitated during MIS 5e, was not identified as a recrystallised stalagmite at first, as the mineralogy of the growth axis appeared to show a change in primary mineral rather than recrystallisation. Despite the fact that recrystallisation had occurred, it was possible to create an age model, as the system had not opened to a great degree. The persistence of an aragonite layer in this speleothem, as well as several other geochemical proxies, indicates that an arid phase occurred during early MIS 5e in SW Turkey. The second recrystallised speleothem from Dim Cave provides useful insights into the geochemical and petrographic character of recrystallised speleothems. The recrystallised speleothem from Torang Cave produced a record of climatic instability in southern Iran during MIS period 9-7, although the age model was not precise enough to draw precise conclusions.

A small aragonitic Holocene growth from Dim Cave grew during a time which corresponds to an early Holocene pluvial period that affected the entire eastern Mediterranean Basin, coinciding with the deposition of Sapropel 1.

## Contents

Abstract.....	2
Contents.....	3
List of Figures .....	11
List of Tables .....	16
Acknowledgements.....	17
<i>1 Chapter 1</i> Introduction.....	18
1.1 Why Use Speleothems as Palaeoclimatic Proxies? .....	19
1.1.1 Comparison with Other Records.....	20
1.1.2 Problems with Speleothems as Palaeoclimatic Proxies.....	21
1.2 The Need for Palaeoclimate Records from the Eastern Mediterranean – Middle East (EM-ME) Region .....	22
1.3. Project Aims and Objectives .....	22
1.4 Geography and Present Day Climate of the EM-ME Region.....	24
1.4.1 The Mediterranean Sea.....	24
1.4.2 Climate of the Eastern Mediterranean Region.....	24
1.4.2.1 Atmospheric Circulation in the EM-ME Region .....	25
1.4.2.1.1 Anticyclone Ridge.....	25
1.4.2.1.2 Cyprus Lows .....	25
1.4.2.1.3 The Persian Trough and Etesian Winds .....	26
1.4.3 Controls on EM Climate.....	26
1.4.3.1 The North-Atlantic Oscillation .....	26
1.4.3.2 The North Sea-Caspian Pattern and Eastern Atlantic-Western Russia Pattern	28
1.4.3.3 The Eastern Mediterranean Pattern .....	30
1.4.4 Mediterranean Low Pressure Systems.....	31
1.4.5 Isotope Composition of Air Moisture.....	32
1.4.6 Present Day Climate of Turkey.....	34
1.4.6.1 The Climate Zones of Turkey.....	35
1.4.7 Present Day Climate of Iran.....	37
1.4.7.1 Topography of Iran and its Relation to Precipitation.....	37
1.4.7.2 Precipitation Amount and Distribution.....	38
1.4.7.3 Seasonal Variability .....	40

2	<i>Chapter 2</i> Speleothems as Archives of Palaeoclimatic Information .....	41
2.1	The Components of the Karst System.....	42
2.2	Cave Formation .....	42
2.3	Speleothem Formation .....	43
2.3.1	The Soil Zone.....	43
2.3.2	The Karst Zone.....	45
2.3.3	The Cave Environment.....	46
2.3.3.1	Degassing of Drips.....	46
2.3.3.2	Speleothem Precipitation .....	47
2.4	Types of Speleothem .....	48
2.4.1	Flowstones.....	48
2.4.2	Stalactites.....	49
2.4.3	Stalagmites.....	49
2.5	Speleothem Growth Rates .....	50
2.5.1	Factors affecting growth rate.....	50
2.5.1.1	Supersaturation .....	50
2.5.1.2	Cave Air Ventilation and Cave Air pCO <sub>2</sub> .....	51
2.5.1.3	Variations in Drip Rate .....	52
2.5.1.4	Other factors .....	53
2.6	Physical Properties of Speleothems.....	54
2.6.1	Stalagmite Width and Shape.....	54
2.6.2	Annual Layers.....	54
2.6.3	Hiatuses.....	55
2.7	Speleothem Mineralogy and Petrography.....	55
2.7.1	Cave Carbonate Minerals.....	55
2.7.2	Mineralogy of Speleothems used for Palaeoclimatic Studies.....	56
2.7.2.1	Benefits of Performing Petrographic Observations of Speleothems.....	57
2.7.3	Calcite.....	58
2.7.4	Aragonite.....	59
2.7.4.1	Characteristics of Aragonite.....	59
2.7.5	Isotopic Characteristics of Speleothem Fabrics.....	60
2.7.6	Diagenesis and Recrystallisation.....	60
2.7.6.1	Replacement of Aragonite by Calcite.....	60
2.7.6.1.1	Appearance of Recrystallised Speleothems.....	61

2.7.6.1.2	Geochemical Indicators of Recrystallisation .....	62
2.7.6.2	The Effects of Recrystallisation on U-Series Dating .....	63
3	<i>Chapter 3 Palaeoclimatic and Palaeoenvironmental Proxies Recorded within Speleothems</i> .....	64
3.1	Stable Isotopes in Speleothems .....	65
3.1.1	Notation of Stable Isotope Values .....	65
3.1.1.1	The Delta Value .....	65
3.1.1.2	Symbols for Components of the Speleothem-Forming System .....	66
3.1.2	Equilibrium .....	66
3.1.2.1	The Hendy Test .....	67
3.1.2.2	Palaeotemperature Equations .....	69
3.1.2.3	Aragonite and Equilibrium .....	70
3.1.3	Oxygen Isotopes .....	71
3.1.3.1	Notation .....	71
3.1.3.2	Interpretation in Terms of Temperature .....	71
3.1.3.3	Relationship between Components of the $\delta^{18}\text{O}$ System .....	72
3.1.3.4	Changes in the Isotopic Composition of Air Masses .....	72
3.1.3.4.1	The Temperature Effect .....	73
3.1.3.4.2	The Altitude Effect .....	73
3.1.3.4.3	The Continental Effect .....	74
3.1.3.4.4	The Amount Effect .....	74
3.1.3.4.5	The Source Effect .....	74
3.1.3.4.6	The Ice Volume Effect .....	75
3.1.3.5	$\delta^{18}\text{O}$ of Karst Waters .....	75
3.1.3.6	$\delta^{18}\text{O}_d$ and $\delta^{18}\text{O}_c$ .....	76
3.1.4	Carbon Isotopes .....	78
3.1.4.1	Origin of Speleothem $\text{CaCO}_3$ Carbon .....	78
3.1.4.1.1	Atmospheric carbon dioxide .....	78
3.1.4.1.2	Soil Biogenic Carbon Dioxide .....	79
3.1.4.1.3	Dissolution of Karst Bedrock and Calcareous Soils .....	79
3.1.4.2	Open-System vs. Closed-System .....	80
3.1.4.2.1	Open-System .....	80
3.1.4.2.2	Closed-System .....	80
3.1.4.3	Causes of variations in $\delta^{13}\text{C}$ .....	81

3.1.4.3.1	The Palaeovegetation Signal.....	81
3.1.4.3.2	Climatic Causes .....	83
3.1.4.3.3	Growth Rate.....	83
3.1.4.3.4	Prior Calcite Precipitation .....	83
3.1.4.3.5	Degassing .....	84
3.1.4.3.6	Ventilation.....	84
3.2	Minor and Trace Elements.....	85
3.2.1	Origins of Trace Elements.....	85
3.2.1.1	Initial Carbonate Dissolution.....	85
3.2.1.2	Mobilisation of Trace Elements in Soils and Epikarst .....	85
3.2.2	Incorporation of Trace Elements into Speleothems.....	86
3.2.3	Methods of Trace Element Analysis.....	86
3.2.4	Interpreting Trace Element Variations.....	87
3.2.4.1	Distribution Coefficients .....	87
3.2.4.2	Mg and Sr Variations.....	88
3.2.4.3	Precipitation Variations.....	89
3.2.4.4	Prior Calcite Precipitation .....	90
3.2.4.5	In Combination with Other Proxies.....	92
3.3	Strontium isotopes.....	93
3.3.1	The Isotopes of Strontium.....	93
3.3.2	<sup>87</sup> Sr/ <sup>86</sup> Sr in Cave Waters and Speleothems.....	93
3.4	Uranium Isotopes as a Palaeoclimatic Proxy .....	94
3.5	Fluorescence .....	96
3.5.1	Fluorescence in Speleothems.....	96
3.6	U-Series Dating.....	97
3.6.1	U/Th Dating.....	97
3.6.2	U-Pb Dating.....	97
3.6.2.1	Sample Selection.....	98
3.6.2.2	Mass Spectrometric Analysis and Isochron Construction.....	99
3.6.2.3	Disequilibrium Corrections .....	101
4	<i>Chapter 4 Calcite - Aragonite Relationships and Climate of early MIS 5e and the early Holocene Recorded in Speleothems from SW Turkey</i> .....	102
4.1	Introduction .....	103
4.1.1	Dim Cave.....	103

4.1.2	Monitoring of Dim Cave.....	104
4.1.2.1	Temperature and Humidity.....	104
4.1.2.2	Water Samples.....	104
4.2	Isotopic Composition of Precipitation and Groundwater near Dim Cave, Dim Cave Drip Waters and Modern Speleothem Growth .....	107
4.2.1	IAEA Weather Station Data.....	107
4.2.1	Dim Dripwaters and Meteoric Water Lines.....	111
4.2.1.1	Water-Calcite Equilibrium.....	113
4.3	Stalagmites DIM-1, DIM-2 and DIM-3.....	114
4.3.1	Physical Characteristics of DIM-1, DIM-2 and DIM-3.....	114
4.3.1.1	Hiatus in DIM-1 .....	114
4.3.1.2	Stalagmite Shape.....	116
4.3.1.3	Interfingering “wings” .....	116
4.3.1.4	3D Evolution of DIM-1 Structure and Laser-Photostimulated Luminescence .....	116
4.3.1.5	Crystallography .....	117
4.3.1.5.1	DIM-1 .....	117
4.3.1.5.2	DIM-3 .....	117
4.3.1.5.3	DIM-2 .....	122
4.3.2	Uranium Series Dating.....	125
4.3.2.1	Sampling Strategy .....	125
4.3.2.1.1	DIM-1 .....	125
4.3.2.1.2	DIM-3 .....	125
4.3.2.1.3	DIM-2 .....	125
4.3.2.2	Results.....	125
4.3.2.2.1	DIM-1 .....	131
4.3.2.2.1.1	Problems with the DIM-1 Age Model .....	131
4.3.2.2.1.2	Age Model and Growth Rates.....	135
4.3.2.2.1.3	Initial ( $^{234}\text{U}/^{238}\text{U}$ ) <sub>0</sub> .....	137
4.3.2.2.2	DIM-3 .....	137
4.3.2.2.3	DIM-2 .....	139
4.3.3	Stable Isotope Measurements.....	140
4.3.3.1	Hendy Tests.....	140
4.3.3.2	Axial Profile Stable Isotope Results.....	146

4.3.3.2.1	Sampling Strategy .....	146
4.3.3.2.2	DIM-1 .....	146
4.3.3.2.2.1	Oxygen Isotopes.....	146
4.3.3.2.2.2	Carbon Isotopes .....	147
4.3.3.2.2.3	Oxygen and Carbon Isotope Variations .....	148
4.3.3.2.3	DIM-3 .....	150
4.3.3.2.4	DIM-2 .....	150
4.3.4	Strontium Isotope Measurements.....	153
4.3.4.1	Sampling Strategy .....	153
4.3.4.2	Results.....	153
4.3.4.2.1	DIM-1 .....	160
4.3.4.2.2	DIM-3 .....	160
4.3.4.2.3	DIM-2 .....	162
4.3.5	Trace Element Measurements.....	164
4.3.5.1	DIM-1 .....	164
4.3.5.1.1	Sampling Strategy .....	164
4.3.5.1.2	Trace Element Results.....	164
4.3.5.2	DIM-2 .....	169
4.3.6	Palaeoclimatic and Palaeoenvironment Interpretations.....	171
4.3.6.1	DIM-1 .....	171
4.3.6.1.1	The Growth of DIM-1 and Subsequent Diagenesis.....	171
4.3.6.1.1.1	Aragonite as the Primary Mineral of DIM-1 .....	171
4.3.6.1.1.2	Replacement of DIM-1 Aragonite by Calcite .....	172
4.3.6.1.2	The Eemian Record in DIM-1 .....	178
4.3.6.1.3	The Aragonite Region and Hiatus .....	180
4.3.6.2	DIM-3 .....	187
4.3.6.2.1	Absence of the 8.2 kyr Event .....	187
4.3.6.2.2	The Growth of DIM-3 .....	188
4.3.6.2.2.1	The Early Holocene Wet Period .....	188
4.3.6.2.2.1.1	Causes of the Pluvial Period.....	191
4.3.6.2.3	Cessation of Growth .....	192
4.3.6.2.4	Archaeological Evidence and the Mesolithic to Neolithic Transition	194
4.3.6.3	DIM-2 .....	195
5	<i>Chapter 5 A Record of arid events during MIS 9-7 from Torang Cave, Southern Iran</i>	197

5.1	Torang Cave .....	198
5.2	Isotopic Composition of Precipitation and Groundwater near Torang Cave.....	199
5.2.1	IAEA Weather Station Data.....	199
5.3	Stalagmite TG-6.....	202
5.3.1	Uranium Series Dating.....	203
5.3.1.1	Sampling Strategy .....	203
5.3.1.2	Results.....	204
5.3.1.3	Age Model and Growth Rates .....	204
5.1.1	Physical Characteristics.....	205
5.1.1.1	Stalagmite Shape.....	205
5.1.1.2	Crystallography .....	206
5.1.2	Stable Isotope Measurements.....	207
5.1.2.1	Sampling Strategy .....	207
5.1.2.2	Hendy Tests.....	208
5.1.2.3	Axial Isotope Measurements .....	208
5.1.2.4	Oxygen Isotopes.....	212
5.1.2.5	Carbon Isotopes .....	212
5.1.3	Trace Element Measurements.....	214
5.1.3.1	Sampling Strategy .....	214
5.1.3.2	Results.....	214
5.1.4	Fluorescence Imaging.....	216
5.3.6	Palaeoclimatic Interpretation of TG-6.....	217
6	Chapter 6 U/Pb dating of a Speleothem from Sehlak Cave, Iran.....	223
6.1	Sehlak Cave .....	224
6.2	Stalagmite SK-1 .....	225
6.2.1	Previous Attempts to Date SK-1.....	226
6.2.2	Preliminary Screening of Samples.....	226
6.2.3	High Resolution Sampling by LA-ICP-MS.....	228
6.2.4	Digital Autoradiography and Fluorescence.....	229
6.2.5	ID-TIMS Results.....	232
7	Chapter 7 Conclusions and Further Work.....	234
7.1	Introduction .....	235
7.2	Dim Cave, SW Turkey .....	235
7.2.1	Stalagmite DIM-1.....	235

7.2.2	Stalagmite DIM-3.....	237
7.2.3	Stalagmite DIM-2.....	237
7.3	Iranian Speleothems .....	238
7.3.1	Stalagmite TG-6.....	238
7.3.2	Stalagmite SK-1.....	238
7.4	Future Work.....	239
	References .....	240
	Methods Appendix.....	276

## List of Figures

Figure 1.1	Location of study sites from this research	p23
Figure 1.2	The connection between the NAO and EM rainfall	p28
Figure 1.3	NCP-related circulation anomalies affecting the Mediterranean	p30
Figure 1.4	The paths of atmospheric cyclones which affect Turkey	p31
Figure 1.5	The geographical regions of Turkey	p34
Figure 1.6	Air masses influencing the eastern Mediterranean region	p35
Figure 1.7	The Climate Zones of Turkey	p36
Figure 1.8	Simplification of precipitation regimes of Turkey into coastal, transitional and inland regions	p36
Figure 1.9	Simplified map of major elements of Iranian topography	p38
Figure 1.10	A) Mean annual rainfall of Iran, B) Precipitation regions of Iran	p40
Figure 3.1	Example of a Tera-Wasserburg isochron	p99
Figure 4.1	Dim Cave location within Turkey	p103
Figure 4.2	Dim Cave plan	p103
Figure 4.3	Trace element data for water samples from Dim Cave	p106
Figure 4.4	Map of locations used in calculation of Meteoric Water Lines (MWLs) in relation to Dim Cave	p107
Figure 4.5	Average monthly precipitation and temperature data for Antalya	p109
Figure 4.6	Percentage contributions of time periods to total annual precipitation at Antalya IAEA Station	p110
Figure 4.7	Comparison of local and global meteoric water lines with Dim Cave dripwaters	p112
Figure 4.8	Stalagmites DIM-1, DIM-3 and DIM-2	p115
Figure 4.9	Schematic indicating how progressive slabs through DIM-1 were used for analyses	p118
Figure 4.10	Diagnostic imaging of DIM-1 (upper portion)	p119
Figure 4.11	Location of a microhiatus in DIM-1	p120

Figure 4.12	Thin section microphotographs of DIM-1	p120
Figure 4.13	Additional XRD and SLPL analyses of DIM-1	p121
Figure 4.14	Crystallography of DIM-2 established via A) XRD and B) SLPL	p123
Figure 4.15	Thin section microphotographs of DIM-2	p124
Figure 4.16	Location of U/Th dating samples in DIM-1, DIM-2 and DIM-3	p127
Figure 4.17	Last set of U/Th dates, selected from areas identified as primary aragonite	p131
Figure 4.18	$^{230}\text{Th}/^{238}\text{U}$ versus $^{234}\text{U}/^{238}\text{U}$ for DIM-1	p133
Figure 4.19	DIM-1 dating locations before selection of samples in Figure 4.19	p134
Figure 4.20	DIM-1 age model	p136
Figure 4.21	Initial $[^{234}\text{U}/^{238}\text{U}]$ vs. $^{230}\text{Th}/^{238}\text{U}$ variations in DIM-1	p138
Figure 4.22	Initial $[^{234}\text{U}/^{238}\text{U}]$ activity ratio variations in DIM-1 plotted against distance from base	p138
Figure 4.23	Location and ages of U/Th samples from DIM-2	p139
Figure 4.24	Location of Hendy Tests in the Dim Stalagmites	p141
Figure 4.25	Hendy tests for stalagmite DIM-1 (A-C) and DIM-3 (D), $\delta^{18}\text{O}$ and $\delta^{13}\text{C}$ variations along a single lamina	p142
Figure 4.26	Hendy tests for stalagmite DIM-1(A-C) and DIM-3 (D), covariation between $\delta^{18}\text{O}$ and $\delta^{13}\text{C}$	p143
Figure 4.27	Hendy tests for stalagmite DIM-2, $\delta^{18}\text{O}$ and $\delta^{13}\text{C}$ variations along a single lamina	p144
Figure 4.28	Hendy tests for stalagmite DIM-2, covariation between $\delta^{18}\text{O}$ and $\delta^{13}\text{C}$	p145
Figure 4.29	$\delta^{18}\text{O}$ variations in DIM-1 through time	p146
Figure 4.30	$\delta^{13}\text{C}$ variations in DIM-1 through time	p147
Figure 4.31	$\delta^{18}\text{O}$ and $\delta^{13}\text{C}$ cross plot for isotopic axial profile of DIM-1	p149
Figure 4.32	$\delta^{18}\text{O}$ (red) and $\delta^{13}\text{C}$ (navy) variations in DIM-1 through time	p149
Figure 4.33	$\delta^{18}\text{O}$ and $\delta^{13}\text{C}$ variations for DIM-3 through time	p150
Figure 4.34	$\delta^{18}\text{O}$ and $\delta^{13}\text{C}$ variations for DIM-2 against depth	p152

Figure 4.35	$^{87}\text{Sr}/^{86}\text{Sr}$ of DIM-1, DIM-2 and DIM-3, modern Dim Cave aragonite, Dim Cave bedrock and soil, and modern seawater	p155
Figure 4.36	$^{87}\text{Sr}/^{86}\text{Sr}$ vs. $1/[\text{Sr}]$ for DIM-1 and DIM-3	p157
Figure 4.37	Exogenic source of Sr to Dim Cave	p157
Figure 4.38	$\delta^{18}\text{O}$ vs. $^{87}\text{Sr}/^{86}\text{Sr}$ for the Dim Stalagmites p159	
Figure 4.39	$\delta^{13}\text{C}$ vs. $^{87}\text{Sr}/^{86}\text{Sr}$ for the Dim Stalagmites	p159
Figure 4.40	$^{87}\text{Sr}/^{86}\text{Sr}$ profile for DIM-1 in comparison to $\delta^{18}\text{O}$	p161
Figure 4.41	$^{87}\text{Sr}/^{86}\text{Sr}$ profile for DIM-3 in comparison to $\delta^{18}\text{O}$ and $\delta^{13}\text{C}$	p162
Figure 4.42	$^{87}\text{Sr}/^{86}\text{Sr}$ profile for DIM-2 in comparison to $\delta^{18}\text{O}$ and $\delta^{13}\text{C}$	p163
Figure 4.43	$^{87}\text{Sr}/^{86}\text{Sr}$ profile for DIM-2 in comparison to mineralogy	p163
Figure 4.44	Mg/Ca * 1000 and Sr/Ca * 1000 variations for sections of DIM-1	p165
Figure 4.45	Crossplot of Mg/Ca * 1000 vs. Sr/Ca * 1000 for sections of DIM-1	p166
Figure 4.46	Crossplot of Sr/Ca * 1000 vs. Ba/Ca * 1000 for sections of DIM-1	p166
Figure 4.47	Mg/Ca * 1000, Sr/Ca * 1000 and Ba/Ca * 1000 variations for the $\delta^{18}\text{O}$ region of DIM-1	p167
Figure 4.48	Mg/Ca * 1000, Sr/Ca * 1000 and Ba/Ca * 1000 variations for the $^{87}\text{Sr}/^{86}\text{Sr}$ collapse region of DIM-1	p168
Figure 4.49	Mg/Ca * 1000, Sr/Ca * 1000 and Ba/Ca * 1000 variations for the Above Shift region of DIM-1	p168
Figure 4.50	Mg/Ca * 1000 data for DIM-2	p170
Figure 4.51	Sr/Ca * 1000 data for DIM-2	p170
Figure 4.52	The growth and recrystallisation of DIM-1	p176-177
Figure 4.53	$\delta^{18}\text{O}$ and $\delta^{13}\text{C}$ data for DIM-1 with 10-point running mean	p178
Figure 4.54	Comparison of $\delta^{18}\text{O}$ record of DIM-1 with records from Soreq Cave, Israel, Corchia Cave, Italy and Bourgeois-Delaunay Cave, France	p179
Figure 4.55	The expression of the arid phase in DIM-1 in multiple proxies	p182

Figure 5.1	Location of Torang Cave	p198
Figure 5.2	Map of Iran showing location of Torang Cave and Tehran IAEA station	p199
Figure 5.3	Average monthly precipitation and air temperature data at Tehran IAEA station	p201
Figure 5.4	Stalagmite TG-6	p202
Figure 5.5	Location of U/Th dates previously performed on TG-6	p203
Figure 5.6	Age model for TG-6	p205
Figure 5.7	Microscope images of TG-6	p206
Figure 5.8	$\delta^{18}\text{O}$ and $\delta^{13}\text{C}$ data for TG-6. A) Original data compiled by Sa'ad Al-Omari, B) Additional data from this research	p207
Figure 5.9	Hendy tests for stalagmite TG-6, $\delta^{18}\text{O}$ and $\delta^{13}\text{C}$ variations along a single layer	p209
Figure 5.10	Hendy tests for stalagmite TG-6, covariation between $\delta^{18}\text{O}$ and $\delta^{13}\text{C}$	p210
Figure 5.11	Crossplot of $\delta^{18}\text{O}$ and $\delta^{13}\text{C}$ data for TG-6, split into regions of differing coherence between $\delta^{18}\text{O}$ and $\delta^{13}\text{C}$	p211
Figure 5.12	$\delta^{18}\text{O}$ data for TG-6	p212
Figure 5.13	$\delta^{13}\text{C}$ data for TG-6	p213
Figure 5.14	Mg/Ca * 1000 for the lower hiatus region, in comparison to $\delta^{18}\text{O}$	p214
Figure 5.15	Sr/Ca * 1000 for the lower hiatus region, in comparison to $\delta^{18}\text{O}$	p215
Figure 5.16	Ba/Ca * 1000 for the lower hiatus region, in comparison to $\delta^{18}\text{O}$	p215
Figure 5.17	Fluorescence imaging of TG-6	p216
Figure 5.18	Point to point age model for TG-6. Dashed blue vertical lines represent the approximate position of the two hiatuses	p217
Figure 5.19	Point to point age model for TG-6, with hypothetical lengths of growth hiatuses included. The four ages are included as black circles	p220
Figure 5.20	$\delta^{18}\text{O}$ and $\delta^{13}\text{C}$ data for TG-6, plotted against the amended age model described above, and in comparison to benthic $\delta^{18}\text{O}$ data	p221

Figure 6.1	Location of Sehlak Cave within Iran	p224
Figure 6.2	Stalagmite SK-1	p200
Figure 6.3	Tera-Wasserburg diagrams for the top of SK-1	p202
Figure 6.4	Mineralogy of the top of SK-1	p203
Figure 6.5	Tera-Wasserburg diagram of composite of several sets of LA-ICP-MS analyses of the aragonite layer in SK-1.	p203
Figure 6.6	Autoradiography image of SK-1	p204
Figure 6.7	Fluorescence intensity of SK-1	p205
Figure 6.8	Tera-Wasserburg Diagram for SK-1 ID-TIMS data	p206

## List of Tables

Table 4.1	Dim Cave drip water cation data	p105
Table 4.2	Geographic data for Dim Cave and Antalya IAEA station	p107
Table 4.3	Number of water samples analysed for isotopic data per month at Antalya IAEA Station	p110
Table 4.4	Percentage contribution of time periods to total annual precipitation at Antalya IAEA Station	p110
Table 4.5	Summary of measured $\delta^{18}\text{O}$ values of Dim Cave drip waters ( $\delta^{18}\text{O}_w$ ) and soda straw calcite ( $\delta^{18}\text{O}_c$ )	p113
Table 4.6	U/Th age data for DIM-1 arranged by sample depth	p128
Table 4.7	U/Th age data for DIM-2 and DIM-3 arranged by sample depth	p129
Table 4.8	U/Th Age Data for DIM-1 arranged chronologically	p130
Table 4.9	Representative $\delta^{18}\text{O}$ and $\delta^{13}\text{C}$ of primary aragonite and secondary calcite in DIM-2	p151
Table 4.10	Strontium isotope data for the Dim Cave stalagmites and environmental components	p154
Table 4.11	Representative Mg/Ca * 1000 and Sr/Ca * 1000 of primary aragonite and secondary calcite in DIM-2	p169
Table 5.1	Geographic data for Torang Cave and Tehran IAEA Station	p200
Table 5.2	U/Th age data for stalagmite TG-6	p204
Table 6.1	ID-TIMS U/Pb data for SK-1	p232
Table 6.2	Corrected U/Pb data for SK-1 via ID-TIMS analysis	p233

## **Acknowledgements**

I would like to express my very great appreciation to my supervisors, Julian Andrews and Peter Rowe, for the opportunity to work on this research, and for all the encouragement, guidance and advice they have given me along the way.

I am particularly grateful for the excellent analytical assistance I received from Alina Marca-Bell, Graham Chilvers, Bertrand Lezé and Robert Posey at UEA. I am also very thankful to all the staff at NIGL for allowing me to use their facilities, and for the great results and advice I received, especially Steve Noble, Randy Parrish, Dan Condon, Tony Milodowski and Ian Millar.

I would like to thank Sa'ad Al-Omari for collection of the Iranian stalagmites, and Mehmet Özkul and Oruç Baykara for helping us gain access to Dim Cave, and for collection of drip water samples.

My special thanks to my office mates and friends through the years for the endless moral support over cups of tea, particularly Sarah, Amy, and Eddie, whose support got me through the hard times. And special thanks too to my family, whose pride in me was the greatest motivation I could ask for.

# *Chapter 1*

## Introduction

## 1.1 Why Use Speleothems as Palaeoclimatic Proxies?

Speleothems may contain many physical and chemical proxies, which can be interpreted to yield high-resolution modified climate signals (McDermott, 2004, McDermott et al., 2006, Fairchild et al., 2006). Recently, authors have indicated the benefits of analysing several proxies from one sample to aid interpretation of proxies which may be driven by several factors, and to account for the fact that some proxies may not record certain events (Hellstrom and McCulloch, 2000, Asrat et al., 2007). Comparative spectral analysis of proxies known to be reflecting factors external to the cave, such as growth rate, and oxygen and carbon isotopes, which could either be reflecting variations in cave-external parameters or conditions within the cave, can aid interpretations of the latter by distinguishing between cave-internal and –external driving mechanisms (Asrat et al., 2007)

The mechanisms of speleothem growth are sensitive to external parameters, and often climatically driven (Lauritzen and Lundberg, 1999, Fairchild et al., 2006). One such external property is mean annual temperature (MAT) above the cave, which has been shown to be represented by cave air temperatures at most sites, which remain relatively constant and within approximately  $\pm 1^\circ\text{C}$  of MAT (McDermott, 2004). Speleothem growth will cease if the cave is overlain by ice due to stripping of the soil, lack of groundwater recharge, minimal vegetation, and/or cave flooding due to drainage becoming blocked (Winograd, 2002), allowing speleothem growth periods to be used as a proxy for the retreat of glaciers or ice sheets. If speleothems contain magnetic minerals, they may provide a record of palaeomagnetic variations through geological time (Latham et al., 1982, Perkins, 1996).

The Devil's Hole calcite vein record demonstrated the potential of speleothems and other terrestrial carbonates for palaeoclimatic research (Winograd et al., 1992, 1997), with the countless studies published since realising the benefits of using cave carbonates (e.g. Dorale et al., 1998), discovering new proxies which can be obtained from speleothems, and refining those proxies already used. Proxies which can be retrieved from speleothems include mineralogy, growth rate and speleothem diameter, oxygen and carbon isotopes, strontium isotopes, trace elements, organic compounds, and pollen. For interpretation of oxygen and carbon isotopes, the fact that speleothems are often deposited close to isotopic equilibrium aids retrieval of climatic information from the other factors affecting the signal (McDermott et al., 2006), and where speleothems grow in cool, temperate regions, high humidity (typically 95-99%) minimises evaporation, which may otherwise have caused kinetic isotope fractionation (McDermott, 2004).

Speleothems benefit from the protection of the cave environment, which reduces external erosion and allows speleothems to survive for very long periods of time, up to  $10^4$ - $10^6$  years (Lauritzen and Lundberg, 1999, McDermott, 2004). This allows speleothems to grow for very long periods of time, if the prerequisites for growth are met, which makes them extremely valuable compared to records which are not as long (Frisia and Borsato, 2010). Their closed crystalline nature also means that speleothems are not usually susceptible to contamination or degradation (Lauritzen and Lundberg, 1999), or other forms of secondary alteration (Fairchild et al., 2006), and so are often preserved as relatively pure calcium carbonate (McDermott, 2004).

### **1.1.1 Comparison with Other Records**

Speleothems are able to provide proxy information which may complement other records, for example their terrestrial nature makes them valuable for comparison against deep-sea and ice-core records (Lauritzen and Lundberg, 1999).

In some cases, the benefits of speleothem records may allow them to improve upon the available information from other records. For example, ice cores provide very useful records of global palaeoclimate, but dating uncertainties lead to difficulty resolving trends at high resolution, for example on the scale of Dansgaard-Oeschger events, while speleothem dating by U-Series methods can be accurate enough to identify the imprint of these millennial-scale events on the records recovered (Wang et al., 2001, Genty et al., 2003), and so speleothem records can be used to refine Greenland ice-core records (McDermott, 2004). Marine cores may also have problems with their dating chronology due to  $^{14}\text{C}$  issues (Beck et al., 2001, Genty et al., 2003). In comparison, U-series dating of speleothems can obtain precise, robust, accurate and absolute chronologies (Lauritzen and Lundberg, 1999, Richards and Dorale, 2003, Fairchild et al., 2006), which is vital for palaeoclimatic interpretation. Such chronologies can be presented in calendar years, with a precision approaching 0.3 – 0.6 % ( $2\sigma$ ) for dates less than 100,000 years due to the advent of thermal ionization mass spectrometric methods of U-Series dating, which among other benefits allow much smaller sample sizes than previous methods (Edwards et al., 1987, Lauritzen and Lundberg, 1999, McDermott, 2004, McDermott et al., 2006).

While both ice cores and marine cores can provide very long, continuous records of climate (as can speleothems), lake cores may not provide long-term records due to the fact that lakes can be transient features, and so records may be short or fragmented, and in arid regions lakes may dry up completely (Gat and Magaritz, 1980). On the contrary,

speleothems may exhibit continuous growth for up to  $10^3$ - $10^5$  years (Fairchild et al., 2006), and as they exhibit a relatively rapid growth rate compared to other archives (McDermott et al., 2006), they can be studied on a wide variety of timescales, from intra-annual to orbital timescales (Fairchild et al., 2006).

Speleothem records are very appropriate to use to test and validate general circulation models (GCMs), for example Yuan et al. (2004) suggested that changes in humidity and moisture availability between glacial and interglacial periods could cause additional important amplifications to climatic change due to the greenhouse gas properties of water vapour. Due to the high resolution of speleothem records, they can be used to investigate and assess inter-hemispheric and latitudinal leads and lags in the climate system (McDermott, 2004), and identify teleconnections (McDermott et al., 2006), for example Wang et al. (2001) identified a link between the East Asian Monsoon and Greenland temperatures during the precipitation of a speleothem from Hulu Cave, China.

### **1.1.2 Problems with Speleothems as Palaeoclimatic Proxies**

One of, if not the most commonly used proxies in speleothem analysis is  $\delta^{18}\text{O}$ . Use of  $\delta^{18}\text{O}$  is complicated by several control factors (e.g. Hendy, 1971, Lachniet, 2009, Dayem et al., 2010), and previous studies have over-simplified the controls on isotopes of precipitation, such as temperature (Fairchild et al., 2006). Despite this,  $\delta^{18}\text{O}$  is still considered to be usable as a measure for precipitation in certain climatic settings (e.g. Wang et al., 2001, 2008, Yuan et al., 2004, Cheng et al., 2009, Li et al., 2011).

Although the cave environment is valuable in providing a protected environment for the speleothem, allowing it to persist for very long periods of time, it is not without problems. Evaporation may occur close to the cave entrance, creating an unsuitable soft, porous deposit (Lauritzen and Lundberg, 1999). Also, there has been insufficient research into the complicating processes in the karst and cave system (Fairchild et al., 2006). While post-depositional recrystallization is rare, it can occur and can be detected as randomly orientated, equidimensional crystals in an irregular mosaic (Lauritzen and Lundberg, 1999).

Although speleothems are very common in humid areas, and are also able to deposit in semi-arid areas (e.g. Bar-Matthews et al., 1996, Auler and Smart, 2004), they will not be able to precipitate where water availability is too scarce, limiting their geographical extent. However, this can be used as a proxy for precipitation amount if speleothems have been able to form at times when the climate was more humid (e.g. Burns et al., 2001, Vaks et al.,

2003), and a high frequency of speleothems can also be used to infer high water availability, warm temperatures, good soil and vegetation cover (Gascoyne, 1992, Lauritzen, 1995), although this proxy may not be viable for the Eastern Mediterranean region (Ayalon et al., 1999). Non-hydrological effects may also be responsible for initiation of growth however; examples are karst evolution or fissures which had been blocked, becoming unblocked (Asrat et al., 2007).

## **1.2 The Need for Palaeoclimate Records from the Eastern Mediterranean – Middle East (EM-ME) Region**

The eastern Mediterranean – Middle East region is a transition zone between the Eurasian, Asian and African climatic belts, making it highly sensitive to changes in the relative influence of the climatic systems association with these zones (Roberts et al., 1999b). In addition, Turkey is subject to severe water shortages at present, with climate projections indicating that increased aridity is likely in the next 100 years (Christensen et al., 2007). Despite this, palaeoclimatic data from this region is often sparse; for example in reconstructions of northern Hemisphere palaeoprecipitation, Turkey is often under-represented (e.g. Luterbacher and Xoplaki, 2003, Pauling et al., 2006). The coverage of speleothem records from the region is improving, with a record spanning a large range of time from Soreq Cave, Israel (Bar-Matthews et al., 1991, 1996, 1997, 1999, 2000, 2003, 2011) forming the most complete record, but many gaps still exist, both spatially and temporally. Therefore, there is scope for additional speleothem data from the region.

## **1.3. Project Aims and Objectives**

The overall purpose of the thesis is to use speleothems from the Eastern Mediterranean-Middle East region to reconstruct palaeoclimate during the Pleistocene-Holocene period. More specific objectives include:

- To obtain multi-proxy records from speleothems from the Holocene and MIS 5e from a cave in SW Turkey (red circle in Figure 1.1). These proxies include stable isotopes, high resolution LA-ICP-MS analysis of trace elements, strontium isotopes, and fluorescence.

- To obtain stable isotope and trace element data from a speleothem from a cave in S Iran (blue square in Figure 1.1) that grew during MIS 9-7, to give palaeoclimatic insight to these periods in the area. In particular, MIS 8 is not well represented in the literature.
- To identify teleconnections with palaeoclimatic records from other regions.
- To investigate the causes of recrystallisation of aragonite speleothems to calcite, and the effects this process has on the geochemistry of the speleothems.
- To attempt to date materials from a cave in S Iran (yellow diamond on Figure 1.1) that are outside the range of U/Th dating by U/Pb methods.



**Figure 1.1**  
**Location of study sites from this research: Dim Cave in SW Turkey (red circle), Sehlak Cave (yellow diamond) and Torang Cave (blue square) in S Iran.**

## **1.4 Geography and Present Day Climate of the EM-ME Region**

### **1.4.1 The Mediterranean Sea**

The Gibraltar Strait is the sole connection between the Mediterranean Sea and the Atlantic Ocean, making the basin almost isolated from the moderating influence of the Atlantic Ocean (Zhou et al., 2008c, Almogi-Labin et al., 2009). The land-locking effect in the present day leads to increases towards the east in both salinity and sea surface temperature (SST), which in turn causes productivity to decrease in the same direction (Antoine et al., 1995, Malanotte-Rizzoli et al., 1999, Pinardi and Masetti, 2000). The main freshwater flux to the Mediterranean Sea is through the Black Sea system (Gat and Magaritz, 1980).

The Mediterranean Sea acts as a modulating influence on vapour sources of precipitation (Gat and Carmi, 1987, Ayalon et al., 1998), and causes the area around it to experience a milder and less arid climate (Gat and Magaritz, 1980). In the summer, extremes of heat are moderated by the influence of the Mediterranean Sea, while during the autumn and winter, cyclogenesis occurs over the sea due to the juxtaposition of cold, dry continental air and a relatively warm sea (Gat and Magaritz, 1980, Alpert et al., 1990, Tatli et al., 2004). The responsible convergence zone occurs due to the fact that the Azores high shifts to the south at this time (Tatli et al., 2004).

### **1.4.2 Climate of the Eastern Mediterranean Region**

The Eastern Mediterranean (EM) is located between the arid Sahara-Arabian deserts, and the humid temperate European climatic zone (Bar-Matthews et al., 1999, Frumkin and Stein, 2004). The climate of the Eastern Mediterranean-Middle East (EM-ME) region is sensitive to environmental change, especially with regards to N-S shifts in the climate belts (Frumkin and Stein, 2004), such as advance and regression of the arid-zone boundary (Gat and Magaritz, 1980). There is a clear increased continental effect from the western to eastern Mediterranean (Almogi-Labin et al., 2009). This effect, combined with a decreasing moderating influence of the Atlantic Ocean to the east, leads to a W-E moisture gradient (Pierre, 1999).

The climate of the eastern Mediterranean region is affected by the inter-relationship between the climate patterns of North Africa, Asia, and Europe (Bar-Matthews et al., 2000), with the monsoon systems, Atlantic disturbances and Mediterranean cyclogenesis all potentially affecting the region (Gat and Magaritz, 1980). The combination and/or interplay of these climatic inputs means that local climate within the EM region may not be

in phase with the glacial cycles or the local climates of other areas within the region (Gat and Magaritz, 1980). Currently, the southern part of the EM basin is affected by the low latitude monsoons (Rossignol-Strick, 1985), and this influence dissipates rapidly to the north, so that the northern extreme of the eastern Mediterranean Sea is mostly influenced by the North Atlantic/Mediterranean climate system (Almogi-Labin et al., 2009). Mediterranean cyclogenesis, brings precipitation that is winter-dominated, and has a large  $d$  excess (Gat and Magaritz, 1980). These two variables contrast with precipitation delivered by the monsoon system, as monsoonal rains are mostly summer- rather than winter-dominated, and have a very low  $d$  excess as well as being enriched in heavy isotopes (Gat and Magaritz, 1980). Atlantic depressions are year-round events, and in contrast to monsoon precipitation, precipitation from Atlantic storms has depleted isotopic values (Gat and Magaritz, 1980). A change in the area of influence of these three precipitation source types (Mediterranean cyclogenesis, Atlantic depressions, and monsoonal systems) can have severe effects on local climate.

The Mediterranean climate of dry summers and wet winters is representative of the Cs climate type, in which at least eight months must have average temperatures of  $\geq 10$  °C, and the average annual precipitation must be  $< 900$  mm (Trewartha, 1980). Synoptic classification of the seasons in the EM shows that both the winter and summer seasons are in fact longer than either the astronomical or meteorological durations given for the seasons, and are 3 months and 23 days each (Alpert et al., 2004).

Weather systems reaching Turkey at present generally follow a pattern of being north-westerly in spring, westerly to north-westerly in winter, south-westerly in autumn and easterly to south-easterly in summer (Kutiel and Maheras, 1998, Kutiel et al., 1998).

#### **1.4.2.1 Atmospheric Circulation in the EM-ME Region**

##### *1.4.2.1.1 Anticyclone Ridge*

An anticyclone ridge extends over the Near East region, with the northern part being an extension of the Siberian anticyclone, and the southern part related to the subtropical high pressure belt (Zhou et al., 2008a). The ridge leads to predominance of north-east surface winds over the Caspian and Black seas (Zhou et al., 2008a). In mountainous areas however, surface winds may not conform to the surface pressure pattern (Zhou et al., 2008a).

##### *1.4.2.1.2 Cyprus Lows*

Cyprus Lows are mid-latitude disturbances which develop when upper troughs or cut-off lows penetrate into the Eastern Mediterranean (Zangvil et al., 2003), bringing cool air

originating from Eastern Europe over the warmer Mediterranean Sea where it becomes unstable (Shay-El and Alpert, 1991). The passage of a warm sector during a Cyprus Low pressure system can lead to dust storms originating in the Sahara affecting the eastern Mediterranean (Ganor and Mamane, 1982).

#### *1.4.2.1.3 The Persian Trough and Etesian Winds*

The Persian Trough is a low-pressure extension of the Asian monsoon (Bitan and Saaroni, 1992), which in summer extends to the northwest through the Persian Gulf extends across the EM to the Aegean Sea via southern Turkey (Ziv et al., 2004), at which point it meets the Azores High/Ridge (Bitan and Saaroni, 1992). The interaction of the Persian Trough and the Azores High leads to the Etesian Winds, which are generally north-south direction winds that blow over the EM during summer and early autumn (Tritakis, 1982), yielding cool advection from eastern Europe into the EM (Ziv et al., 2004). Near the south-western Turkish coast, the Etesian winds are north-westerly (Kotroni et al., 2001).

In the eastern Mediterranean, summer aridity and a stable temperature regime are caused by a linkage between the climate systems of the EM and the Asian Monsoon, which leads to mid-level subsidence caused by Rossby wave-induced adiabatic descent (Rodwell and Hoskins, 1996) and enhancement of the Etesian winds when the Asian monsoon is more intense, due to the increased pressure gradient between the two (Ziv et al., 2004). This connection is in the higher troposphere, and involves a 1-day lag between the Asian Monsoon and subsidence in the Levant, while in the mid-troposphere the EM is connected to eastern North Africa, where the Hadley cell is located, and in the lower troposphere it is connected to Europe (Ziv et al., 2004). In summer, sea level pressure over the EM anticorrelates with the Indian monsoon and is correlated with the Etesian winds (Raicich et al., 2003). The eastern Mediterranean can also be affected by an extension of the Indian summer monsoon depression in summer (Karaca et al., 2000).

### **1.4.3 Controls on EM Climate**

#### *1.4.3.1 The North-Atlantic Oscillation*

The North Atlantic Oscillation (NAO) is a large-scale phenomenon affecting the northern hemisphere (Wallace and Gutzler, 1981). The basic structure of the oscillation is a modulation of the relative intensity of the Icelandic Low and the Azores High (Hurrell, 1995), which affects downstream climates far from the Atlantic such as the Middle East (Visbeck et al., 2001) via variation in the intensity and spatial distribution of the westerlies

(Eshel and Farrell, 2000). A positive NAO refers to an enhanced pressure difference between the two centres, while a negative NAO occurs when the pressure difference between the two is reduced (Hurrell, 1995)

The NAO affects precipitation, stream flow and maximum and minimum temperatures in Turkey, making it a very important climate input to the region, although the extent to which the NAO controls temperature and precipitation in Turkey is still under debate. The NAO may contribute up to 27% of Turkish winter precipitation variability (Cullen and deMenocal, 2000). Whether there is a strong link between the NAO and EM temperature is less clear; evidence has been presented which suggests that temperature is less sensitive to the NAO (Karabork et al., 2005), while other data suggest that a strong relationship exists between the NAO and temperature in the EM (Luterbacher and Xoplaki, 2003).

During an NAO negative phase, anomalously high pressure over Greenland coincides with anomalously low pressure over the Mediterranean region, leading to warming southerlies in the EM which causes weakened subsidence due to dynamic adjustment, resulting in increased EM precipitation (Eshel and Farrell, 2000) and warmer, wetter conditions in Turkey (Luterbacher and Xoplaki, 2003, Karabork et al., 2005). When the NAO is in the positive phase, which happens most often and with highest intensity in boreal winter (Walker and Bliss, 1932), low pressure anomalies exist over Iceland and the Arctic, while high pressure persists over the subtropical Atlantic, the Mediterranean and southern Europe, leading to stronger-than-average midlatitude westerlies and cooling northerlies in the EM, which results in colder and drier winters in the Mediterranean (Cullen and deMenocal, 2000, Visbeck et al., 2001, Krichak and Alpert, 2005), including Turkey (Luterbacher and Xoplaki, 2003, Karabork et al., 2005). The effects of positive and negative NAO conditions on EM climate are shown in Figure 1.2.

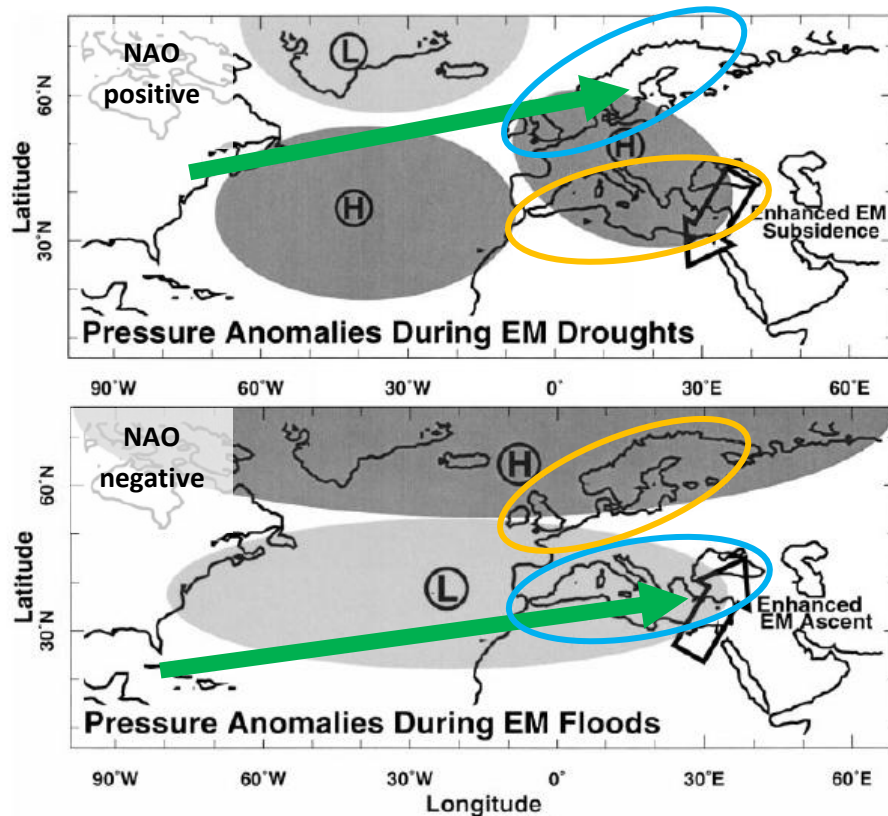


Figure 1.2  
The connection between the NAO and EM rainfall, showing pressure anomalies during both EM droughts and floods. Green arrows indicate dominant depression tracks. L = low pressure, H = High pressure. Orange oval indicates arid conditions, blue oval indicates wet conditions Modified from Eshel and Farrell (2000)

A positive NAO leads to winters with a rainfall deficit, and hot, dry conditions in the summer following in the Eastern Mediterranean (Wang et al., 2011). The NAO has been in the positive phase increasingly in the last 40 years (Visbeck et al., 2001), possibly due to anthropogenic climate change (Shindell et al., 1999), which may have been a cause of the increased frequency of heat waves and drought in the Mediterranean region in recent years (Wang et al., 2011).

#### 1.4.3.2 *The North Sea-Caspian Pattern and Eastern Atlantic-Western Russia Pattern*

The North Sea-Caspian Pattern (NCP) and Eastern Atlantic-Western-Russia Pattern (EA-WR) are two atmospheric teleconnections linked to pressure differences between the North Sea and Caspian Sea at different geopotential heights; the NCP is active at 500 hPa while the EA-WR occurs at 700 and 850 hPa (Hatzaki et al., 2007). The locations of the two “poles” of the NCP as defined by Kutiel and Benaroch (2002) are shown in Figure 1.3. The NCP can have a severe effect on air temperatures and precipitation amounts in Turkey, especially

during the months October-April (Kutiel and Benaroch, 2002), causing variations in seasonal mean temperature of 1-3°C and seasonal precipitation totals of hundreds of mm (Kutiel et al., 2002). The EA-WR pattern is active during the months December-February and shows a significant relationship with precipitation (Krichak and Alpert, 2005).

Specifically, when the NCP is in negative phase, higher pressure over the northern Caspian Sea and lower pressure over the North Sea leads to increased anticlockwise circulation around the western pole of the NCP and increased clockwise circulation around the eastern pole of the NCP, leading to southerly/south westerly circulation, which results in increased precipitation and higher temperatures in western Turkey (Kutiel et al., 2002, Kutiel and Benaroch, 2002). When the NCP is in positive phase, the above conditions are reversed, and it is eastern Turkey and the Black Sea coast which receive higher rainfall, along with decreased temperatures over the whole of Turkey, due to the increased northerly circulation that arises (Kutiel and Benaroch, 2002, Kutiel et al., 2002).

The EA-WR may be responsible for some of the precipitation trends over Europe during the last ~60 years that have been attributed to the NAO (Krichak and Alpert, 2005). The physical mechanisms causing the EA-WR pattern are not well understood, but it is known that when EA-WR is low, circulation from the Atlantic characterises precipitation in the eastern Mediterranean region, while in high EA-WR years eastern Mediterranean circulation is linked to central Europe; and that the pattern may be linked to the NAO, ENSO and/or movements of the Siberian anticyclone (Krichak and Alpert, 2005).

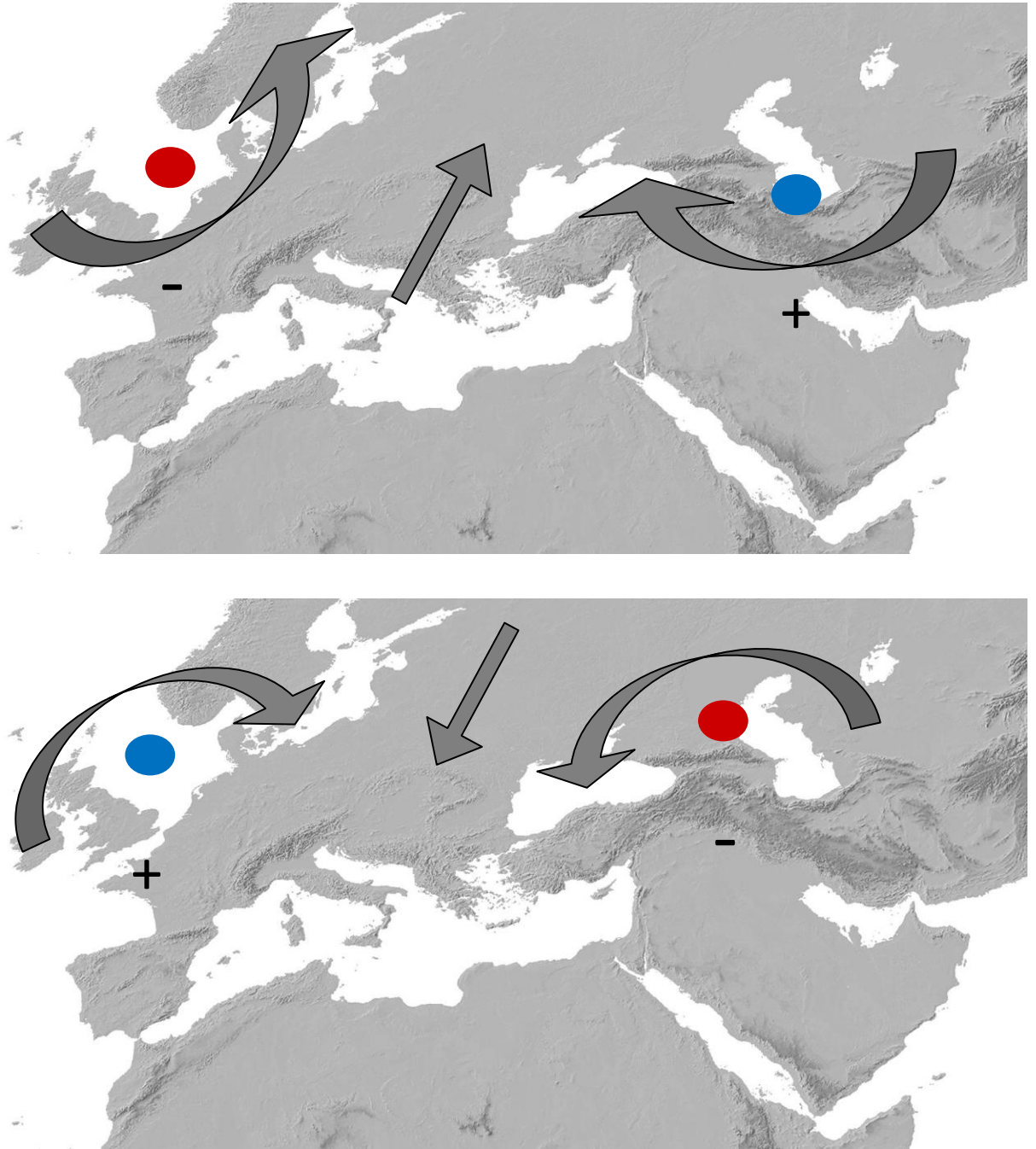


**Figure 1.3**  
 The circulation anomalies affecting the Mediterranean and surrounding regions during an NCP negative (a) and NCP positive (b) phase. After Kutiel and Benaroch (2002)

### ***1.4.3.3 The Eastern Mediterranean Pattern***

The Eastern Mediterranean Pattern (EMP) is a dipole pattern between the EM and north-eastern Atlantic at 500 and 300 hPa geopotential height (also at 700 hPa but weakened), which is linked to the NCP and EA-WR pattern but independent from the NAO (Hatzaki et al., 2007). The pattern is strong during winter, especially in December when it forms an independent mode of upper circulation, in place but weakened and associated with the

NCP and EA-WR during spring and autumn, and does not exist in summer (Hatzaki et al., 2007). When the EMP is in negative phase, zonal flow over Europe is increased, while the positive phase results in an intensification of the Atlantic anticyclone, leading to increased northerly meridional flow (Hatzaki et al., 2007).

#### 1.4.4 Mediterranean Low Pressure Systems

Cyclogenesis over the Mediterranean is favoured due to the land-sea temperature contrast and excursions of the polar front jet and the European trough (Wigley and Farmer, 1982).

The paths of cyclones which affect Turkey are shown in Figure 1.4.



Figure 1.4 The paths of atmospheric cyclones which affect Turkey, after Karaca et al. (2000)

The rainy season in the Mediterranean begins in October, and continues through winter. Winter is characterised by low pressure in the Mediterranean and regular cyclonic disturbances (Karaca et al., 2000). During winter, low pressure systems enter the Mediterranean region and move from west to east, along preferred tracks (Holmgren et al., 1995). Some depressions migrate from the Atlantic to the western Mediterranean, while others develop over the Mediterranean Sea, especially in the Adriatic and Cyprus regions and in the Gulf of Genoa (Zhou et al., 2008a). The strength of the Siberian high and zonality of upper flow control the movement of depressions in the eastern Mediterranean basin (Wigley and Farmer, 1982).

It has been suggested that seasonal resolution is not high enough to capture all the climate features that interact in the Mediterranean region due to the complex terrain (Alpert et al.,

1990). For instance, while during winter most storm tracks enter the Mediterranean along the northern section of the Mediterranean, the way they exit differs, as in December most cyclones leave through the EM, while in January more leave through the Aegean Sea to the Black Sea (Alpert et al., 1990). When the subtropical and polar jet streams interact, winter depressions in the eastern Mediterranean are deepened (Zhou et al., 2008a).

In Spring, cyclones transition from tracking across the northern Mediterranean to moving along the north African coast, this change most pronounced between March and April, and the exit point for cyclones progresses from the EM in March to the WM in May (Alpert et al., 1990).

In summer, the polar front and strong jet stream move to about 60°N, and therefore have a diminished effect on the Mediterranean region (Karaca et al., 2000). The subtropical high has a strong influence over the central and eastern Mediterranean and north African region in July and August, most cyclones are non-migratory, and intermonthly variations are the smallest compared to the other seasons (Alpert et al., 1990). Summer heat waves through Turkey, Greece and Italy are sometimes linked to an elongation of the Indian monsoon trough over the Arabian Gulf (Zhou et al., 2008a).

A study into the isotope composition of atmospheric moisture over the Mediterranean Sea stressed the importance of the convective motions in the north-eastern margin of the Mediterranean in controlling attributes of the “Mediterranean climate” (Zhou et al., 2008c).

At the present day, continental air masses (mainly from the north) impinge on seawater under conditions of large differences in temperature and isotopic disequilibrium between atmospheric moisture and the sea surface, and large humidity deficits, especially in winter (Zhou et al., 2008c). This leads to high instability in the air and water column, which affects precipitation distribution and intensity in the Mediterranean (Zhou et al., 2008c).

#### **1.4.5 Isotope Composition of Air Moisture**

Mediterranean Sea Water is the major source of vapour in the Eastern Mediterranean region (Gat and Carmi, 1987, Ayalon et al., 1998), and so changes in SSTs and sea-surface salinity will affect the isotopic composition of rainfall, and it follows, speleothems (Bar-Matthews et al., 2000). Strong evaporation of incoming Atlantic Surface water flowing eastward leads to a sharp W-E gradient in  $\delta^{18}\text{O}$  values, with the Levantine basin

experiencing an increase of up to 1‰ relative to the Western Mediterranean (Pierre, 1999, Almogi-Labin et al., 2009).

In the Mediterranean Sea, the equation relating evaporation, precipitation and runoff is as follows:

$$\frac{E}{(P + R)} \sim 2.61$$

*Equation 1.1: Relationship between evaporation, precipitation and runoff in the Mediterranean Sea (Bethoux, 1979)*

Where E = evaporation, p = precipitation and r = runoff. This leads to high salinity (up to 39‰) and heavy isotope signatures (up to  $\delta^{18}\text{O} = +1.8\text{‰}$ ) (Gat and Magaritz, 1980).

When both cold air originating over the European continent and warm, dry air originating from North Africa converge over the Mediterranean Sea, intensive air-sea interaction (evaporation) in coincidence with a large humidity deficit creates atmospheric moisture with a large deuterium-excess near the coast (Zhou et al., 2008c). Deuterium-excess ( $d$ ), which is defined as  $d = \delta\text{D} - 8(\delta^{18}\text{O})$ , is very high in the Eastern Mediterranean, especially in winter, with values of  $d > 20\text{‰}$  (Gat and Carmi, 1970, Zhou et al., 2008b). Deuterium-excess is affected by several factors, for example decreased sea surface temperatures lead to a reduction in deuterium excess for a given value of relative humidity, while high humidity during formation of moist air masses leads to lower deuterium excess, and vice versa (Clark and Fritz, 1997).

Air moisture in the Bay of Antalya was found to have one of the highest deuterium values in the eastern Mediterranean basin, at a time when the air masses involved originated over the European continent; therefore cold, dry European air was impinging on the warmer Mediterranean waters (Zhou et al., 2008c). In a study of precipitation from 1963-2001, precipitation at Antalya was found to have  $\delta^{18}\text{O}$  of  $-5.4\text{‰}$ ,  $\delta^2\text{H}$  of  $-27.2\text{‰}$  and deuterium excess of 16.2 (Dirican et al., 2005).

Ayalon et al. (2003) found that for individual rainfall events at Soreq Cave, Israel, there was high correlation between increasing rainfall amount and negative  $\delta^{18}\text{O}$  anomaly. Therefore it is beneficially to analyse individual rainfall events. Unfortunately, the IAEA data that will be used to characterise the precipitation regimes of the regions discussed in later chapters is accumulated into months, so this level of detail is not possible in this study.

Daily rain events at Soreq cave, Israel with >20mm rain and temperatures below 10°C were found to fall on the MMWL, while rain events of <20mm and temperatures ranging from 10-25°C deviate from the MMWL, falling on evaporative lines (Raich et al., 2003). In that study, all cave dripwaters fell on the MMWL, indicating that the rainfall from the light rain showers (<20mm) was practically all lost by evaporation and therefore had very little effect on the cave waters (Raich et al., 2003).

#### 1.4.6 Present Day Climate of Turkey

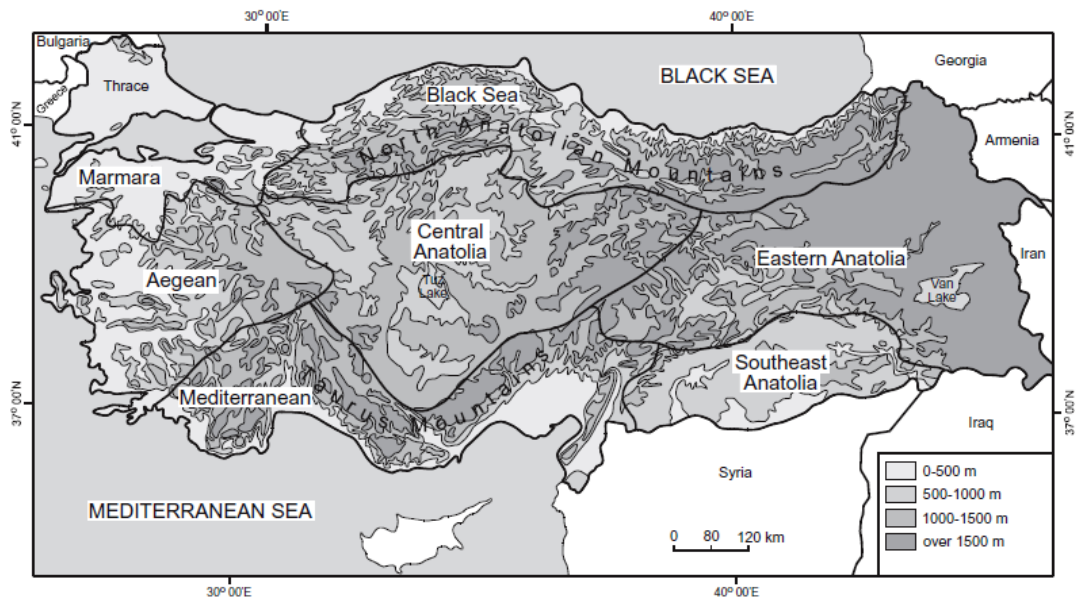


**Figure 1.5 The Geographical Regions of Turkey (Saris et al., 2010)**

The major geographical regions of Turkey are shown in Figure 1.5. The geography and topography of Turkey influences its climate greatly. The Black Sea, Mediterranean and Southeast Anatolian regions are all mountainous, Central Anatolia and Eastern Anatolia are of plateau and high plateau topography respectively, and Marmara and the Aegean region are low altitude plains (Saris et al., 2010).

Turkey has a climate which can be broadly described as Mediterranean, i.e. winter rainfall is at least three times that of summer rainfall (Tatli et al., 2004). Air masses originating in both polar and tropical regions affect the country in winter and summer respectively (Tatli et al., 2004). As can be inferred from earlier descriptions of atmospheric circulation in the Eastern Mediterranean, Turkey's climate is affected by inputs from several atmospheric circulation systems, including those over Asia, eastern Europe and North Africa (Turkes et al., 2002).

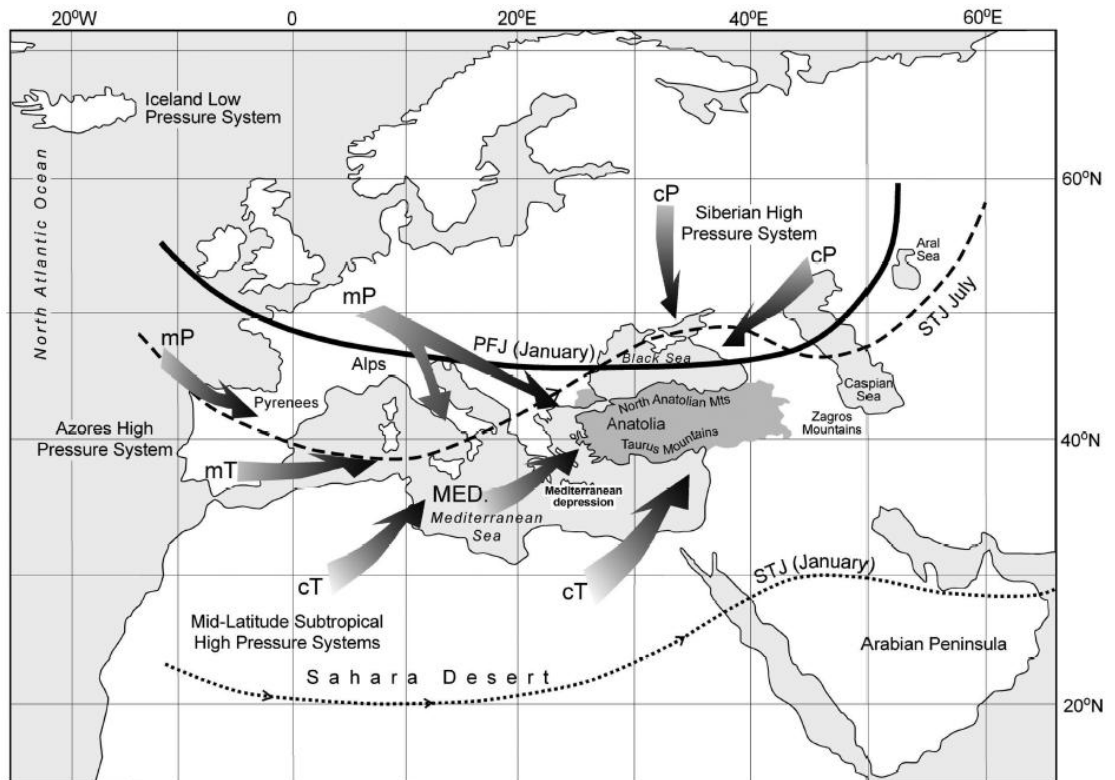


**Figure 1.6** Air masses influencing the eastern Mediterranean region, after Saris et al. (2010). Air masses are identified as follows: MED = Mediterranean, mP = marine polar, cP= continental polar, mT = marine tropical, cT = continental tropical, PFJ = polar front jet, STJ = sub-tropical jet.

In comparison to its neighbours to the south and east, Turkey is a relatively humid country (Jex et al., 2010). However, in recent decades the country has experienced reduced rainfall and increased temperatures (Sönmez et al., 2005, Camci Çetin et al., 2007). Projections for the coming century predict increased aridity (Christensen et al., 2007).

#### **1.4.6.1 The Climate Zones of Turkey**

Several studies have sought to separate Turkey into regions of similar rainfall regime. Türkeş (1996) used seasonality to divide Turkey into 7 precipitation regions: Black Sea, Marmara Transition, Mediterranean, Continental Mediterranean, Mediterranean to Central Anatolia Transition, Continental Central Anatolia, Continental Eastern Anatolia. Unal et al. (2003) used cluster analysis to redefine the climate zones of Turkey as shown in Figure 1.7. These regions were the Marmara region, the Aegean – western Mediterranean region, the Black Sea region, the central Anatolian region, the eastern Anatolian region, the south-eastern Anatolian region, the eastern Mediterranean region.

Saris et al. (2010) also redefined the precipitation regions of Turkey as shown in Figure 1.8. Specifically, they found that the most important division was into coastal, transitional and

inland regimes. The coastal group comprises all coastal areas of Turkey, is characterised by a December or October peak and intermediate to very high magnitude of rainfall, and is under the control of cyclogenesis and orographic rains. The transitional group are controlled by a combination of frontal and convective rainfall, which shows a December peak with the rainy period extending into spring with intermediate to moderately high magnitude. The inland group experiences a May peak in precipitation with low to intermediate magnitude of rainfall, and is characterised by convective rains.

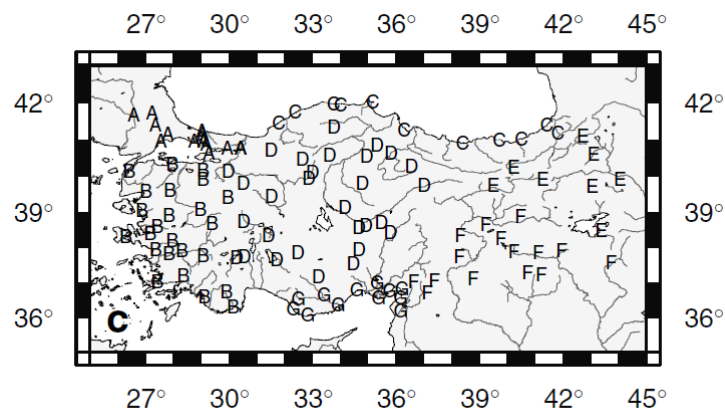


**Figure 1.7 The Climate Zones of Turkey**

A = the Marmara region, B = the Aegean – western Mediterranean region, C = The Black Sea region, D = the central Anatolian region, E = the eastern Anatolian region, F = the south-eastern Anatolian region, G = the eastern Mediterranean region. From Unal et al. (2003)

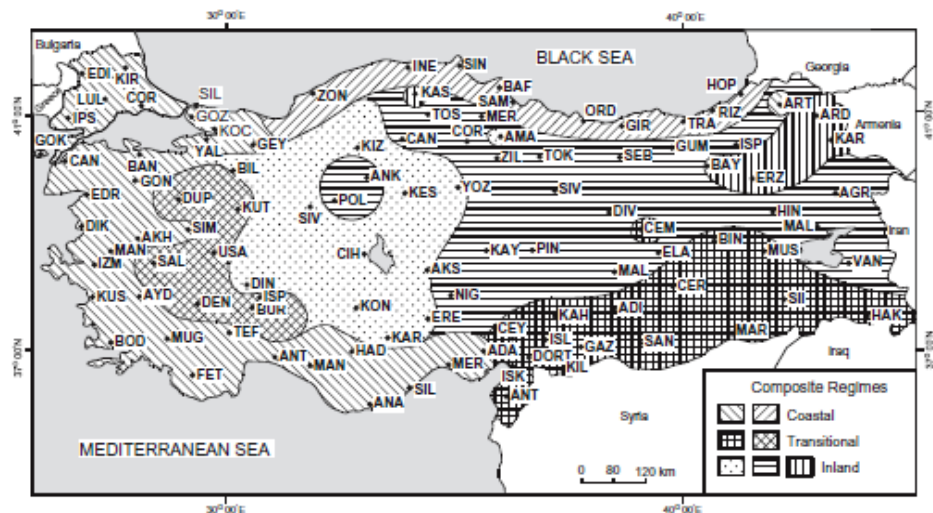


**Figure 1.8**

Simplification of precipitation regimes of Turkey into coastal, transitional and inland regions, from Saris et al. (2010)

The Mediterranean coastal region of Turkey experiences mild, wet winters and hot, dry summers, with snow rare but present on mountain tops (Holmgren et al., 1995, Unal et al., 2003). The rainy season is winter and spring, with the highest number of cyclones occurring in winter (Karaca et al., 2000). However rainfall is unreliable, with long droughts and heavy rainfall events common (Holmgren et al., 1995). July and August are usually rain-free months (Holmgren et al., 1995). The coastal regions of Turkey, including the Mediterranean coastal region, are under the influence of large-scale pressure systems and upper-air circulations, while in central parts and the black Sea region, local processes have much more of an influence, and the south-eastern area of Turkey is affected by monsoonal systems in addition to Mediterranean systems (Tatli et al., 2004). The interior of the country, by contrast, is characterised by arid and continental climates, while the northern fringe (i.e. the Black Sea coast) experiences a more temperate climate (Unal et al., 2003).

There is a decreasing trend in the winter precipitation of Turkey, especially over the Mediterranean region, while at the same time the precipitation totals of spring, summer and autumn are increasing (Türkeş et al., 2009).

#### **1.4.7 Present Day Climate of Iran**

The climate of Iran is governed by interaction of the Siberian High, the SW Asian Monsoon and the Atlantic westerly cyclones (Kehl, 2009). Extreme continental conditions prevail, with some mediation due to topography and the proximity of the Caspian Sea and the Persian Gulf (Stevens et al., 2001).

Precipitation is highly seasonal, and its distribution is strongly influenced by topographic factors. In summer, a thermal low over southern Iran combined with relative high pressure over Eurasia causes a dry, broadly northerly airstream across the country (Kehl, 2009). In winter, North Atlantic/Mediterranean cyclones enter Iran from the west, their intensities and trajectories depending on the strength of the Siberian high pressure system. An exception to this pattern is the coastal zone of the Caspian Sea, where rainfall is much more evenly distributed throughout the year (Kehl, 2009).

##### ***1.4.7.1 Topography of Iran and its Relation to Precipitation***

There are two major mountain ranges in Iran; the Zagros in the west and the Alborz in the north of the country, bordering the Caspian Sea. These two mountain ranges act as a barrier to rainfall reaching the arid and semi-arid central plateau regions of Iran (Modarres and Sarhadi, 2011). The Zagros mountains form the north-eastern boundary of the Fertile

Crescent, and separate the Mesopotamian lowlands from the Iranian plateau (Stevens et al., 2001). The major precipitation sources to the Zagros Mountains are depressions from the North Atlantic, the Mediterranean and the Black Sea, which in winter are steered by the prevailing westerlies (Alijani and Harman, 1985, Stevens et al., 2001). The Alborz Mountains form the major northern highlands of Iran, bordering the Iranian Plateau on its northern edge (Kendrew, 1961). These two mountain ranges receive much higher amounts of precipitation than the Plateau, mostly in the form of snow (Kendrew, 1961). There exists a sharp contrast between the vegetated, wet windward sides of the mountains, and the arid, bare inward-facing slopes (Kendrew, 1961). The central part of Iran, between the Zagros and Alborz ranges, is mostly comprised of two salt deserts; Dasht-e Lut and Dasht-e Kavir, which combined occupy approximately one sixth of Iran's land area (Fisher, 1968). The major topographic features of Iran are shown in Figure 1.9.

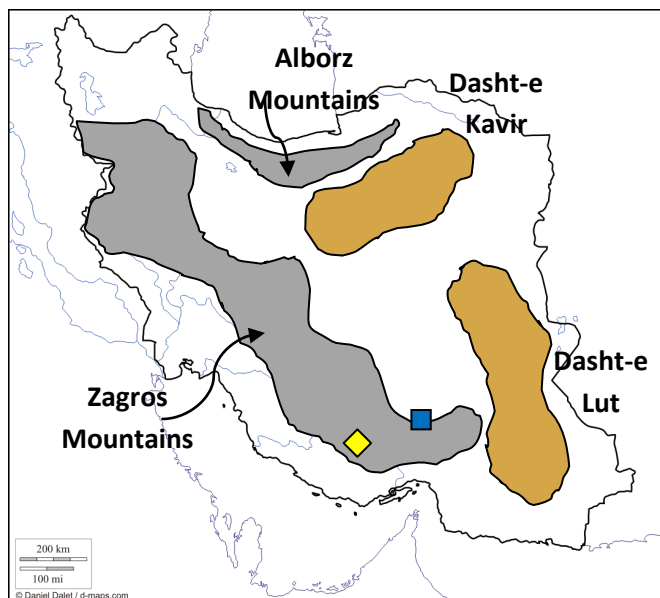


**Figure 1.9**  
Simplified map of major elements of Iranian topography. Modified after Nasab et al. (2012). Approximate locations of Sehlak (yellow diamond) and Torang (blue square) cave are shown.

#### **1.4.7.2 Precipitation Amount and Distribution**

Mean annual precipitation over the whole of Iran is approximately 250 mm (Nazemosadat and Cordery, 2000, Dinpashoh et al., 2004), but with strong regional disparities. More than 50% of Iran receives less than 200 mm of rain annually (Dinpashoh et al., 2004), such as the region between the Zagros mountains and the Persian Gulf (Djamali et al., 2010). In excess of 75% of the country receives less than 300 mm/year, while only 8% receives more than

500 mm of rain/year (Dinpashoh et al., 2004), concentrated along the Caspian Sea coast and the high Zagros. The spatial distribution of average annual precipitation is shown in Figure 1.10A.

The climate regions of Iran are influenced by elevation, proximity to seas, and large atmospheric systems (Modarres and Sarhadi, 2011). The wettest region of Iran is the southern coastal area of the Caspian Sea (Dinpashoh et al., 2004) (areas G8 and G6 in Figure 1.10B), which has a rainfall regime in which rainfall is more evenly distributed throughout the year compared to other regions of Iran (Kehl, 2009). In general, the precipitation which reaches this area originates from the Caspian Sea (Alijani, 1997). The driest region of Iran is the south-eastern region (Dinpashoh et al., 2004). The central region of Iran is also very dry. These two regions form the arid and semi-arid regions of Iran, and cover nearly two-thirds of the country (G1 in Figure 1.10B).

Western Iran experiences almost no summer precipitation (Dinpashoh et al., 2004), due to the subtropical Azore's High extending its influence into the Middle East, while in winter the westerly Mediterranean wind brings moisture from the Mediterranean Sea (Alijani, 1997). The north and north-west region of Iran receives a high proportion of rainfall in October (Dinpashoh et al., 2004). The coastal lowlands to the south and southwest receive most of their rain during winter (Kendrew, 1961). Thunderstorms are also common during spring due to destabilization of the atmosphere caused by rapid heating of the land surface (Stevens et al., 2001), with moisture supplied (at least to the southern part of the country), by advection from the Persian Gulf (Taha et al., 1981).

The mountainous areas of Iran have a distinct climatology, due to their elevation. Areas G2, G5 and G7 in Figure 1.10B cover high mountainous areas of the Zagros mountains, and receive precipitation from Mediterranean rainfall systems (Modarres and Sarhadi, 2011).

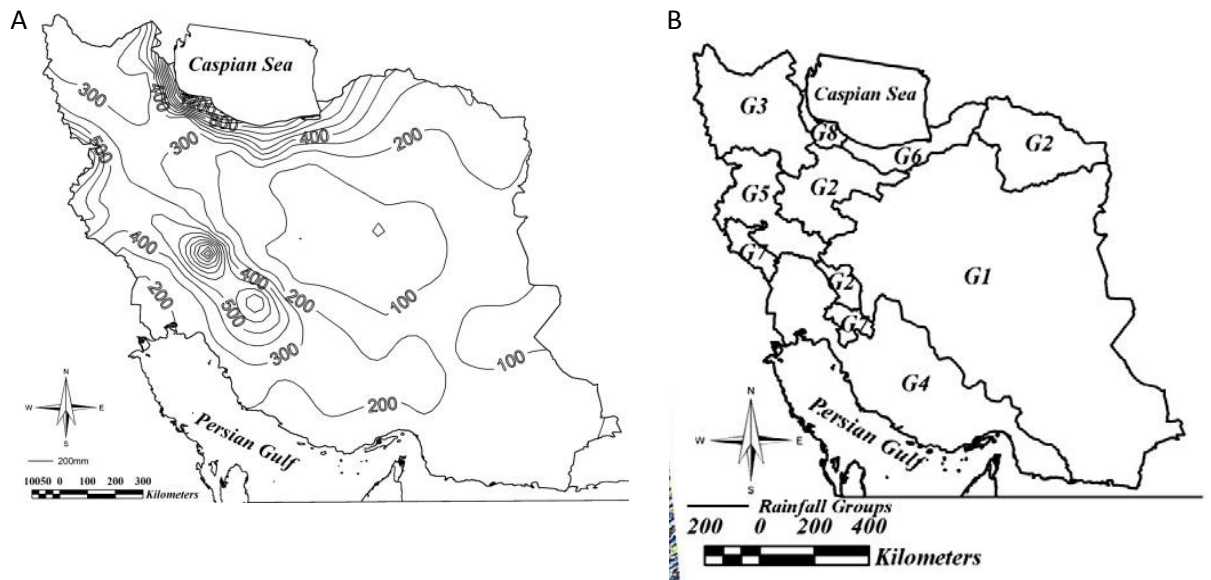


**Figure 1.10**  
**A) Mean annual rainfall of Iran (mm). From Modarres & Sarhadi (2011).**  
**B) Precipitation Regions of Iran. From Modarres and Sarhadi (2011). Labelled regions are discussed in the text**

### **1.4.7.3 Seasonal Variability**

Over half (53%) of precipitation over Iran falls in the months January-March, with 20% in April-June, 4% in July-September, and 23% in October-December (Dinpashoh et al., 2004). As these numbers show, in general, summers are hot and dry in Iran, although the relative amount of spring and summer precipitation increases to the north and east (Stevens et al., 2001, Raziei et al., 2008).

During the period October to April, the air pressure gradients between the equatorial low pressure system and the Siberian high steer depressions formed in the Atlantic or Mediterranean towards Iran (Kehl, 2009). These are able to penetrate the Siberian High Pressure which dominates the atmosphere over Iran during the winter (Kehl, 2009), aided by active cyclogenesis over southern Iraq and the Persian Gulf (Barth and Steinkohl, 2004).

# *Chapter 2*

## Speleothems as Archives of Palaeoclimatic Information

## **2.1 The Components of the Karst System**

Karst comprises “terrain with distinctive hydrology and landforms that arise from a combination of high rock solubility and well developed secondary (fracture) porosity” (Ford and Williams, 2007). The soil, epikarst and transmission zone constitute the vadose zone, where most of the mobilization, transportation and reprecipitation of ions occurs (Frisia and Borsato, 2010). The epikarst, or subcutaneous zone is a near surface zone with a high capacity for water storage which may extend from 3 m to 30 m (Gunn, 1983, Williams, 1983, 2008, Frisia and Borsato, 2010). High porosity (10 – 30% secondary porosity) and high permeability cause it to be a source of stored H<sub>2</sub>O, functioning as a perched aquifer, feeding major conduits and lower transmissivity fissures, which in turn feed cave dripwater zones (Fairchild et al., 2006, 2007, Williams, 2008, Frisia and Borsato, 2010). The epikarst functions as a dual-porosity system, with inputs from both matrix pore-held seepage water and more rapid fissure flow, with some conduits only activated under very high flows (Fairchild et al., 2000). The transmission zone underlies the epikarst, and is characterised by minimal water storage (Williams, 2008).

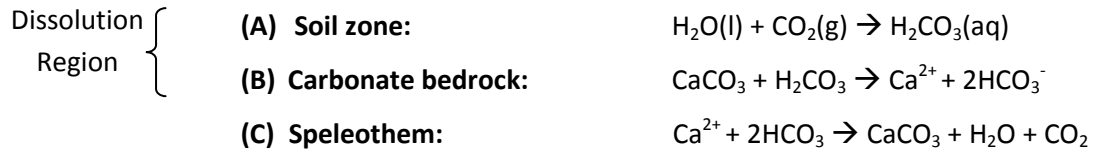
## **2.2 Cave Formation**

Approximately 80% of dissolutional caves are formed as a result of downward percolation of meteoric waters with elevated CO<sub>2(aq)</sub> levels dissolving relatively soluble host rocks, which are typically karstified carbonate aquifers with little or no water drainage (Ford, 1988, Gunn, 2004, Fairchild et al., 2006).

Karstic cave characteristics such as size, morphology, and hydrology are controlled by many properties of the host rock, such as its solubility, permeability, hydrogeology, structure and composition; as well as by climatic conditions (Alonso-Zarza et al., 2011). Most caves are less than 1000 m in length or 100 m in depth, and in fact the majority of open spaces in karst are too small for a human to enter, but some have been discovered which are over 100 km in length or 1000 m deep (Ford, 1988).

## 2.3 Speleothem Formation

The reaction scheme leading to speleothem deposition can be simplified as follows (Fairchild et al., 2007):



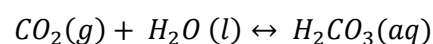
***Equations 2.1A, B, C: The reactions leading to speleothem formation, in the soil zone (A), bedrock (B), and at the speleothem site (C).***

The “Dissolution Region” is located in the soil and upper epikarst, and is dominated by carbonate dissolution (Fairchild et al., 2006). The simplified process is that rainwater seeps through the soil zone, which has a high  $pCO_2$ , dissolving calcite particles, and will dissolve calcite in the karst rock as it reaches it if still not at equilibrium, until equilibrium is reached with respect to calcite (Dreybrodt and Scholz, 2011), which may take up to three weeks (Ford, 1988). Approximately 70% of carbonate dissolution occurs within the top 10 m of the dissolution zone, and dissolution then decreases with depth (Williams, 2008).

Drake (1983) provided the distinction between the “Coincident System”, in which  $CaCO_3$  is dissolved to saturation at the  $pCO_2$  of the soil environment, and the “Sequential System”, in which carbonate-poor soils lead to solutions undersaturated with-respect-to  $CaCO_3$ , and saturation is reached under conditions closed to  $CO_2$  re-supply.

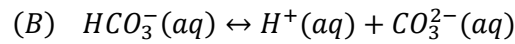
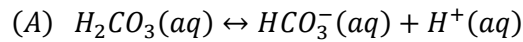
### 2.3.1 The Soil Zone

In the soil, plant respiration and organic matter decay produce  $CO_2$  (Fairchild et al., 2006). Green plants respire about 40% of the  $CO_2$  they intake from the atmosphere into the soil (Frisia and Borsato, 2010). Percolating  $H_2O$  equilibrates with this soil-zone  $CO_2$ , dissolving the  $CO_2$  to form carbonic acid (Lauritzen and Lundberg, 1999). This process is known as carbonation (Bar-Matthews et al., 1991), and can take from a few minutes to a few hours (Frisia and Borsato, 2010). Carbonation can be expressed as:



***Equation 2.2: Carbonation in the soil zone***

Carbonic acid dissociates in two steps, with each step releasing one hydrogen ion:



***Equations 2.3 A, B: The two step dissociation of carbonic acid***

Soil zone  $pCO_2$  is not constant, as differing factors can increase or decrease  $CO_2$  production in the soil. For example, increased temperatures lead to increased biomass, so the  $pCO_2$  of the soil will be raised (Harmon et al., 1975), and plant root activity also increases with temperature, with the same effect (Frisia and Borsato, 2010). As a result, when percolating water equilibrates with the soil- $CO_2$ , it will have a higher  $pCO_2$  and so dissolve more carbonate from the host rock (Lauritzen and Lundberg, 1999, Fairchild et al., 2007). In tropical climates, this process has been shown to lead to increased speleothem formation (Bögli, 1960). Well-drained, tropical karst soils in warm and wet climates that show little seasonal variation in temperature will produce very high and constant levels of  $CO_2$ , while in the mid-latitudes, soil  $CO_2$  will be very low in the cold season and very high in the warm season (Baldini et al., 2008a, Frisia and Borsato, 2010). However,  $CO_2$  solubility is inversely proportional with temperature, approximately halving between  $0^\circ C$  and  $20^\circ C$  (Ford, 1988). This allows karst dissolution to occur in the absence of soil in cold climates (Frisia and Borsato, 2010)

The dissolution of  $CaCO_3$  in soils and host limestone may vary due to changes in the  $CO_2$  concentration of the soil zone (Banner et al., 1996). Changes in soil zone  $CO_2$  concentration are mainly driven by variations in soil productivity and organic matter degradation (Banner et al., 1996), which may in turn be caused by variations in rainfall and the associated shift in vegetation type and productivity (Dorale et al., 1992), and/or variations in temperature (Baker et al., 1995).

Varying fluid flow-routes through the soil may lead to variations in soil geochemistry (Trudgill et al., 1983). The way in which groundwater moves through the soil, as well as when, where and the length of time it will be stored and the extent to which it will experience evaporation in the soil are controlled by the surface climate and the soil's physical properties (Shurbaji and Phillips, 1995). Soil waters have mobile and static fractions (Fairchild et al., 2006). In the mobile fractions, water may move through soils in several ways, including macropore flow, which allows waters from individual events to

bypass older waters which have become stationary in the soil system, piston flow, and fingered flow (Fairchild et al., 2006).

The extent to which groundwater is evaporated in the soil zone is an important factor because evaporation leads to enrichment of D and  $^{18}\text{O}$  in soil water near the surface (Hsieh et al., 1998), and some of this is likely to be transported to the groundwater, especially during periods when there is sufficient summer heat to cause some surface evaporation, followed by a rapid increase in precipitation (Fairchild et al., 2006).

### **2.3.2 The Karst Zone**

Water flow through the karst is predominantly vertically, as shown by models (Perrin et al., 2003) and tracers (Bottrell and Atkinson, 1992), and moves by a combination of seepage, conduit and fracture flow (Fairchild et al., 2007).

The time taken for waters to travel from the surface to the drip site can vary from hours to years, and differing hydrological behaviours may affect each drip site within a cave (Smart and Friederich, 1987). Bomb  $^{14}\text{C}$  has been used as a marker to estimate a 5-10 year lag between soil carbon production and transport to a speleothem in which it is captured, although mixing of groundwaters of differing ages could have had an influence (Genty et al., 1998). Mixing of waters of different ages may occur within the karst, but this process is minimal if the cave is at shallow depth (Fairchild et al., 2000).

Fractures deliver the largest proportion of faster flow dripwater, while conduits are the most variable flow systems, and tend to flow only after heavy rainfall (Fairchild and McMillan, 2007). Changes in the relative proportion of each kind of water flow can occur due to several factors, including local deforestation, which causes decreased evapotranspiration, increasing the proportion of seepage water reaching caves (Fairchild et al., 2007).

Recharge of the aquifer with  $\text{H}_2\text{O}$  and  $\text{CO}_2$  is influenced by a combination of the degree and style of karstification, the surface topography and the nature of the deposits, and soil characteristics, for example soil animal activity can lead to macropores which focus recharge into the karst (Fairchild et al., 2007).

### 2.3.3 The Cave Environment

Waters entering a cave can either be hypogenic, i.e. sourced from below the cave (Klimchouk, 2009), or hypergenic, i.e. recharged from the surface (Alonso-Zarza et al., 2011).

In the idealised case of speleothem precipitation, a stalactite forms at each drip site which acts as a “catchment area”, over which the water flows in thin films of ~0.01 cm thickness, which contributes to the process of drip formation (Dreybrodt, 2011a). The catchment area of a drip and the flow velocity of the water which travels to it can be identified and calculated by marking the water with uranine and shining UV-light on it (Dreybrodt, 2011a).

Drip waters are usually fed by a combination of a diffuse component, i.e. groundwater, which has a long residence time, and a rapid component, which has a short residence time and often travels via fissures (Asrat et al., 2007). Seepage flow drips are commonly slow drip sites, associated with large storage components, and most appropriate for multi-annual resolution (McDermott et al., 2006). The drip water  $\delta^{18}\text{O}$  reflects annual precipitation  $\delta^{18}\text{O}$  (Yonge et al., 1985). “Flashy” drip sites typically result in fast drips which show a large seasonal variation in  $\delta^{18}\text{O}$ , reflecting minimum storage and homogenisation in the epikarst (McDermott et al., 2006). Speleothems which precipitate from flashy drip sites are less likely to be geometrically simple, which can make interpretation more difficult, however they have considerable value due to their ability to record high-resolution seasonal changes (McDermott et al., 2006). Little short-term variation in drip-rate indicates that storage water dominates the feed to the drip site (Fairchild et al., 2000).

#### 2.3.3.1 Degassing of Drips

Calcite deposition will only be initiated in caves if nucleation occurs, which can either proceed by the raising of supersaturation or through the presence of nucleation sites, such as clastic sediments (Frisia and Borsato, 2010). Degassing raises supersaturation by removing  $\text{CO}_2$  from solution and releasing it to the cave atmosphere, which drives the following reaction to the right, leading to calcite precipitation (Frisia and Borsato, 2010):



**Equation 2.4: Calcite precipitation as a consequence of  $\text{CO}_2$  degassing**

When percolating waters come into contact with the cave atmosphere, the  $p\text{CO}_2$  of the

cave air is lower than that with which the waters first equilibrated (Lauritzen and Lundberg, 1999, Fairchild et al., 2006). The partial pressure of CO<sub>2</sub> may be up to two orders of magnitude higher in the soil than in the free atmosphere (Dulinski and Rozanski, 1990, Kaufmann, 2003). The pCO<sub>2</sub> of the soil is typically in the region of 0.1-3.5%, while the pCO<sub>2</sub> of the cave air is generally closer to 0.06-0.6%, and it is this difference that causes the dripwaters to degas (McDermott, 2004). As the CO<sub>2</sub> in the water is present as molecular carbon dioxide, when the solution meets the lower pCO<sub>2</sub> of the cave atmosphere, degassing occurs by molecular diffusion (Dreybrodt, 2011a). This process of degassing is fast, on time scales of 10s for waters films of <0.02 cm thickness, although for thicker films the time will be longer and in this case the normally-subsequent change to equilibrium will take place simultaneously (Dreybrodt, 2011a). During degassing, pH and Ca-concentration stay constant, but when degassing has equilibrated the pCO<sub>2</sub> of the dripwater with the cave atmosphere, pH, [HCO<sub>3</sub><sup>-</sup>] and [CO<sub>3</sub><sup>2-</sup>] are no longer in equilibrium with the CO<sub>2</sub> of the solution (which is now lower) (Dreybrodt, 2011a). The waters must then undergo a move to chemical and isotopic equilibrium, which leads to an increase in pH (about 1 pH-unit) and supersaturation with respect to calcite. Thus, dripwaters which have degassed completely will have a pH >8.3. This change takes place in timescales of 100s (Dreybrodt, 2011a).

Other causes of speleothem precipitation have been suggested, but Holland et al. (1964) confirmed that the key process of speleothem precipitation was degassing of CO<sub>2</sub> and not evaporation.

### **2.3.3.2 *Speleothem Precipitation***

This supersaturation of CaCO<sub>3</sub> leads to precipitation of speleothems (Fairchild et al., 2006, Lauritzen and Lundberg, 1999). If a drip has not achieved full equilibrium (and so not achieved supersaturation either) when it reaches the cave floor/stalagmite, deposition will not begin at the impact point, but will occur after the drip has travelled for a long enough time for equilibrium to occur (Dreybrodt, 2011a).

The growth of crystals requires nucleation to occur, which always occurs under thermodynamic disequilibrium, as the supersaturation of drip waters with respect to calcium carbonate is a necessary condition for nucleation, and this is a departure from thermodynamic equilibrium as the drip water is no longer of uniform composition (Frisia and Borsato, 2010). Supersaturation must persist, or nuclei will become unstable and

redissolve (Frisia and Borsato, 2010). The number of nuclei, and consequently the number of crystals increases with increasing supersaturation (Frisia and Borsato, 2010).

Speleothems are expected to grow through “synchronous crystallization”, in which each successive growth layer precipitates at almost the same time as the layer before it (Stepanov, 1997). Speleothems precipitate as syntaxial overgrowths, in which the c-axis is generally perpendicular to the growth surface (Ford, 1988). Crystals can range in size from a few micrometers to several centimetres long, and single crystals visible to the naked eye are commonly actually composed of scores of very small crystals, only visible with electron microscopes (Frisia and Borsato, 2010). These “building blocks” are known as crystallites in carbonate petrology (Kendall and Broughton, 1978). Crystal defects may occur due to incorporation of foreign ions or misfits (Wenk et al., 1983). Defects such as steps and kinks increase the number of surfaces exposed (Kendall and Broughton, 1978).

Speleothems vary from compact to porous and may contain levels of impurities such as clay or organic matter anywhere between 0 to several tens of % (Fairchild et al., 2006). Surface growth irregularities are on a scale of less than 1-10  $\mu\text{m}$ , often forming between crystals. This favours the development of fluid inclusions, which are often elongate parallel to growth and constitute 0.05-0.5 wt% of speleothems (Fairchild et al., 2006).

## **2.4 Types of Speleothem**

The types of speleothem most typically used for palaeoclimatic research are stalagmites and flowstones (Lauritzen and Lundberg, 1999). Stalagmites are useful for analysis as they have a relatively simple geometry (McDermott et al., 2006). Stalactites are generally not used for palaeoclimatic analysis, as superposition cannot necessarily be assumed due to the fact that internal discontinuities sometimes occur (Lauritzen and Lundberg, 1999), and there are concerns over stalactite lamina geometry including the fact that there is insufficient control over lateral changes in composition (Hendy, 1971).

### **2.4.1 Flowstones**

Flowstones are laminated deposits which form on cave floors or walls, from thin sheets of flowing water film that is slightly supersaturated with respect to calcium carbonate (Frisia and Borsato, 2010) or from relatively strong conduit/fissure flows (Fairchild et al., 2006). They are commonly formed of stacked layers of crystals elongated normal to the substrate (Frisia and Borsato, 2010). They may be tens to hundreds of meters downstream of the  $\text{H}_2\text{O}$  source (Ford and Williams, 1989). They are laterally extensive, up to tens or hundreds

of metres long (Frisia and Borsato, 2010), allowing repeated coring, but non-uniform calcite growth rates and flow-switching behaviour lead to complex internal stratigraphy (Fairchild et al., 2006). Flowstones can be several metres thick, and grow at a rate of up to  $100 \mu\text{m year}^{-1}$  (Frisia and Borsato, 2010), for up to tens of thousands of years, but high levels of impurities compromise U-series dating (Fairchild et al., 2006, 2007). Flowstones often cease to grow during dry and/or cold intervals (Fairchild et al., 2007), making them very useful for constraining the timing of glacial to interglacial transitions and of warm events during glacial (Spötl et al., 2002a, Drysdale et al., 2007). A “flashy” response to rainfall events at parts of the cave in which dripwater is fed by fractures is likely to result in a flowstone being deposited (McDermott et al., 2006).

#### **2.4.2 Stalactites**

Massive stalactites are conical or cylindrical growths from cave ceilings (Frisia and Borsato, 2010) with internal growth layering parallel to the surface (Fairchild et al., 2006). They are made up of concentric layers of crystals elongated perpendicular to an axis running from the cave ceiling to floor (Frisia and Borsato, 2010)

Soda straw stalactites are hollow and cylindrical, and very delicate (Fairchild et al., 2006). They form at seepage zones on cave ceilings (Fairchild et al., 2006), and accrete downwards rather than outwards (Frisia and Borsato, 2010). They only provide information on the youngest few decades of the cave record (Fairchild et al., 2006), and have regularly spaced banding which has been suggested to be annual (Huang et al., 2001, Fairchild et al., 2007).

Conical stalactites begin their growth as straws, after which the central hole becomes blocked by sparite crystals, which necessitates water to flow along the outer surface of the stalactite instead of through the hollow centre, and a cone forms (Bar-Matthews et al., 1991, Frisia and Borsato, 2010).

#### **2.4.3 Stalagmites**

Stalagmites grow upwards from the cave floor, with a cylindrical to conical growth pattern (Fairchild et al., 2006), commonly under water dripping from a stalactite (Frisia and Borsato, 2010). Crystals grow with their growth axis perpendicular to the substrate (Frisia and Borsato, 2010). Where stalagmites are candle-shaped, with little precipitation centred on the flanks, this indicates high efficiency of  $\text{CaCO}_3$  precipitation (Fairchild et al., 2007). Stalagmites shaped like stacked dishes, or conical stalagmites with a central splash cup, indicate a great drip height (Fairchild et al., 2007).

Stalagmites are considered particularly useful for palaeoclimate interpretation because they originate from a single point source (i.e. one drip), their growth can be understood in terms of mathematical principles (Dreybrodt, 1999, Kaufmann, 2003), and their geometry is generally simple (Fairchild et al., 2006).

## **2.5 Speleothem Growth Rates**

Changes in speleothem growth rate can be used as a palaeoenvironmental indicator (Baker and Smart, 1995, Baker et al., 1998b, 2007, McDermott et al., 1999, Frisia et al., 2003, Baldini et al., 2005, Banner et al., 2007). Constant speleothem growth rate is generally assumed, but this is likely to be simplistic, with the actual situation including variations on the annual cycle (Finch et al., 2003). Monitoring of cave sites is therefore profitable as seasonal biases can be detected (Spötl et al., 2005, Banner et al., 2007, Baldini et al., 2008a, Matthey et al., 2008), and the controls on intra-annual variations in growth rate better understood (McDermott et al., 2006). Additionally, changes in growth rate can alter the stable isotope and trace element signal contained within a speleothem, cause complications for palaeoclimatic interpretation (Sherwin and Baldini, 2011), and affect the fabric of the crystals which precipitate (Frisia and Borsato, 2010).

Stalagmite growth rates vary greatly, depending on such factors as temperature and the concentration of calcium ions in the precipitating drip-waters, and typically fall within the range of 0.01-1.0 mm/year (Baker et al., 1998a, Genty et al., 2001b, McDermott, 2004). Maximal growth rates are predicted at 70-100  $\mu\text{m}/\text{yr}$  at 6°C to 800  $\mu\text{m}/\text{yr}$  at 13°C, but in reality growth rates are typically slower due to high cave  $p\text{CO}_2$  or low drip rate, such that realistic growth rates are 10-100  $\mu\text{m}/\text{yr}$  in cool temperate conditions to 300-500  $\mu\text{m}/\text{yr}$  in sub-tropical climates (Fairchild et al., 2006). A fast growing stalagmite from Ethiopia exhibited growth of ca. 0.53 mm  $\text{yr}^{-1}$  (Asrat et al., 2007).

Asrat et al. (2007) identified four hydrological switches within less than 500 years of growth in a very fast growing speleothem, and suggested that in slower growing samples, the amount of calcite precipitated in that time would limit the number of geochemical analyses that could be performed, making it harder to identify the complex hydrological changes.

### **2.5.1 Factors affecting growth rate**

#### **2.5.1.1 *Supersaturation***

Growth rate is a function of degree of supersaturation (Chernov, 1984, Morse and Mackenzie, 1990, Fernández-Díaz et al., 1996). Drip water supersaturation is controlled by

drip rate and outgassing, which are in turn controlled by factors such as ventilation, cave temperature and rate of water discharge (Dreybrodt, 1988). Higher supersaturation results in faster precipitation of speleothems (Fairchild et al., 2007), and may potentially favour aragonite precipitation (Folk, 1974, Chafetz et al., 1991).

Where cave air  $p\text{CO}_2$  is at atmospheric levels, the dominant influence on supersaturation of the fluid is the  $\text{Ca}^{2+}$  content of the drip water, and therefore  $\text{Ca}^{2+}$  is the main control of stalagmite growth overall (Baker et al., 1998b, Genty et al., 2001b, Fairchild and McMillan, 2007, Baldini, 2010, Sherwin and Baldini, 2011). Ca concentration is itself a function of the maximum  $p\text{CO}_2$  the drip water encountered in the soil zone or upper epikarst (i.e. where it was in contact with carbonate rock), and the maximum  $p\text{CO}_2$  is moderated strongly by surface temperature (Genty et al., 2001b, Fairchild and McMillan, 2007) and density of vegetation (Dulinski and Rozanski, 1990, Genty et al., 2001b, Baldini et al., 2005). As temperature increases, aragonite precipitation increases at a far greater rate than calcite (Burton and Walter, 1987, Railsback et al., 1994). Water availability is also important, as aridity can lead to reduced soil  $p\text{CO}_2$ , resulting in lower than expected cave water Ca concentration (Genty et al., 2001b). Also, rapid infiltration events lead to high discharge, which results in low supersaturation (Frisia et al., 2000).

Thus, environmental temperature can exert a control over speleothem growth rate (Fairchild and McMillan, 2007). However, it is possible for sites with high mean annual temperature to have low drip rate Ca ion concentration, possibly due to either prior calcite precipitation (PCP) or lack of soil cover (Genty et al., 2001b). Also, as growth rate is sensitive to both temperature and aridity, with either able to enhance or reduce growth, other proxies must be used to disentangle the effects on growth rate (Baker et al., 1993b). Furthermore, as temperature, precipitation, soil  $p\text{CO}_2$  and therefore drip water Ca concentration vary seasonal, speleothem growth rate may as a result experience seasonal variations related to these fluctuations (Genty et al., 2001b).

#### **2.5.1.2 Cave Air Ventilation and Cave Air $p\text{CO}_2$**

Cave air ventilation is not constant throughout the year; radon tracers have shown increased circulation in winter (Hakl et al., 1997). The key control on cave ventilation is the pressure difference between the cave and the exterior. This pressure difference responds to synoptic weather patterns (Fairchild et al., 2007). Where ventilation is controlled by a cave stream, relative humidity will be 100% and so  $p\text{CO}_2$  will be controlled by the stream, which varies seasonally (Troester and White, 1984).

Speleothem growth rate may be affected by seasonal changes in cave ventilation (Pflitsch and Piasecki, 2003, Perrier et al., 2005, Richon et al., 2005, Spötl et al., 2005, Baldini et al., 2006b, Baldini et al., 2008b, Baldini et al., 2008a, Tremaine et al., 2011). Air stagnation in summer can lead to high cave air  $p\text{CO}_2$ , which reduces degassing of drip water  $\text{CO}_2$ , thus lowering growth rate of calcite, but only if all other growth rate parameters remain unchanged (Frisia et al., 2000, Fairchild et al., 2007, Tremaine et al., 2011). This effect would lead to a seasonal aliasing of the climate signal preserved within speleothem calcite towards that of the winter (Tremaine et al., 2011). This process is typical of poorly ventilated caves in temperate-humid settings (Moore, 1962) and would occur, in theory, in all caves that breathe (Tremaine et al., 2011).

Ventilation-driven outgassing of cave-air  $\text{CO}_2$  controls drip water degassing of  $\text{CO}_2$ , therefore controlling speleothem growth rate (McDermott, 2004, Mickler et al., 2004, Spötl et al., 2005, Mickler et al., 2006, Banner et al., 2007, Baldini et al., 2008a, Kowalczyk and Froelich, 2010). Cave air  $p\text{CO}_2$  is a secondary control on speleothem growth, with drip water  $\text{Ca}^{2+}$  concentration remaining the most important factor, but  $p\text{CO}_2$  can become a much more important modulating factor through time if annual variations in drip water  $\text{Ca}^{2+}$  are similar from year to year (Baldini, 2010, Sherwin and Baldini, 2011)

The isotopic composition of the drip-water and subsequently precipitated calcite are also affected by this ventilation-driven outgassing (Mattey et al., 2008, Cosford et al., 2009, Oster et al., 2010, Frisia et al., 2011, Lambert and Aharon, 2011), although it is not yet clear how strongly calcite  $\delta^{18}\text{O}$  and  $\delta^{13}\text{C}$  are affected by ventilation effects on seasonal, diurnal and multi-decadal scales (Tremaine et al., 2011).

### **2.5.1.3 Variations in Drip Rate**

In some situations, variations in drip rate may be the main factor influencing growth rate over time; for example where the ion supply from drip waters is slow (drip interval >100 seconds) (Fairchild and McMillan, 2007). The length of time outgassing occurs is directly related to drip rate (Dreybrodt, 1988). Drip rate does not greatly influence intra-annual growth rate of fast drips, with drip water Ca concentration exerting the most influence, but slow drips will be much more affected by drip rate on the seasonal scale (Genty et al., 2001b). Under normal conditions, there is a positive relationship between infiltrating rainwater and drip discharge (Fairchild and McMillan, 2007). Therefore, in this situation, the simplification would be that growth rate reflects precipitation amount above the cave

(Fairchild and McMillan, 2007), with seasonal rainfall patterns and shifts in hydrology affecting growth rate (Treble et al., 2003, Cruz et al., 2005, Baldini et al., 2006a, Lambert and Aharon, 2010, Pape et al., 2010). Higher volumes of flow can also lead to increased entrainment of organic material from the soil and detrital particles (Ayalon et al., 1999), which can help to identify the cause of increased growth rate.

However, this simplification involves a few problems: Firstly, speleothems are still able to form in semi-arid areas in cases of infiltration from heavy rains and adequate aquifer storage (Fairchild et al., 2007). Secondly, where speleothems are forming of aragonite, high flow can in fact lead to dissolution of previously deposited material (Railsback et al., 1994). High water flow can lead to dissolution of the tops of aragonite layers, if flow is so fast that the waters cannot reach equilibrium with the bedrock, resulting in un-buffered soil-zone carbonic acid reaching the speleothem, and flowing over the speleothem too quickly to degas completely, so causing dissolution of aragonite until flow rates decreased enough for calcite to precipitate (Railsback et al., 1994). Thirdly, it is possible for both prior calcite precipitation (PCP) and dilution of the drip water (a response to high rainfall) to occur in drips which have very low variability and are assumed to be fed by well-mixed seepage flow (Baldini et al., 2006a, Sherwin and Baldini, 2011). Lastly, flowstones and stalagmites which are not fed by soda straw stalactites may show non-linear response to surface rainfall events (Baker et al., 1999, Baker and Brunson, 2003, Asrat et al., 2007).

#### **2.5.1.4 Other factors**

The presence of impurities such as phosphorus can reduce speleothem growth (Frisia and Borsato, 2010).

In cases where stalagmites are fed by drips falling from stalactites, as the stalactites grows in size it may cause a decrease in the growth rate of the corresponding stalagmite, eventually resulting in a cessation of the stalagmite's growth. This occurs due to the fact that drips will spend an increasing amount of time degassing on the stalactite as it grows in size, which reduces  $\text{Ca}^{2+}$  concentration in the drip water, leading to reduction of growth in the stalagmite as  $\text{Ca}^{2+}$  is the dominant factor governing stalagmite growth rate (Sherwin and Baldini, 2011). This process would result in increased  $\delta^{13}\text{C}$  and trace element concentrations due to the fact that increased degassing and PCP have taken place (Johnson et al., 2006a, Frisia et al., 2011).

## **2.6 Physical Properties of Speleothems**

### **2.6.1 Stalagmite Width and Shape**

It is expected that a positive correlation exists between drip rate and the width of the stalagmite precipitating from the drip (Dreybrodt, 1999, Kaufmann, 2003, Fairchild et al., 2006, Asrat et al., 2007). Very fast drips result in precipitation of calcium carbonate along the flanks of the stalagmite, increasing the width, while slow drips result in tall, thin stalagmites (Hill and Forti, 1997), and if there is little deposition on the stalagmite flanks, this suggests low drip rate (Asrat et al., 2007). Stalagmite width is also affected by drip height; the higher the drip fall height, the larger the splash effects will be at the speleothem deposition site, and so the wider the stalagmite itself will be (Gams, 1981).

Slowly dripping sites which are fed by vadose seepage flow water are likely to result in columnar, constant diameter stalagmites (McDermott et al., 2006), and uniformity in diameter can be interpreted as indicating that the flow regime was fairly regular and drip rate was constant over time (Hill and Forti, 1997). Stalagmite shape is also affected by changes in the overlying regolith or the feeding system of drips (Fairchild et al., 2006), evaporation and amount of bicarbonate in solution (Hill and Forti, 1997).

### **2.6.2 Annual Layers**

Some speleothems exhibit annual layers (e.g. Genty and Massault, 1997, Roberts et al., 1998, Frisia et al., 2003, Tan et al., 2006, Asrat et al., 2007, Borsato et al., 2007, Boch et al., 2011). Annual laminae can be characterised by colour, luminescence and petrographic changes (Baker et al., 1993a, Genty and Quinif, 1996, Frisia et al., 2000) and often consist of a couplet of dark and light calcite (van Beynen et al., 2001). It is now possible to study these annual layers with sufficient precision due to improvements in techniques such as secondary ionization mass spectrometry (SIMS), synchrotron microprobes and eximer laser ablation inductively-coupled plasma mass spectrometry (ELA-ICPMS) (Kuczumow et al., 2003).

Thus, analysing the geochemical proxies contained in these annual laminations can provide very high resolution information about seasonal precipitation (Finch et al., 2003, Treble et al., 2003, 2005b), bio-productivity above the cave (Huang et al., 2001, Baldini et al., 2002, Treble et al., 2003) and soil/rock weathering variations (Roberts et al., 1998, Fairchild et al., 2001).

### **2.6.3 Hiatuses**

A temporary cessation in growth may be expected to result from a period of below-average rainfall, which may be identifiable in a stalagmite as reduced stalagmite width, culminating in a hiatus (Holmgren et al., 1995), at which either insoluble matter accumulates or an irregular corrosion surface develops (Dreybrodt, 1999). This cause is for a hiatus is typical for arid areas, while in northern latitude caves, hiatuses often occur as a result of glaciation (e.g. Schwarcz et al., 1976, Schwarcz, 1986, Gascoyne, 1992, Lauritzen, 1995). Hiatuses can provide valuable information for palaeoclimatic interpretation, particularly when immediately preceded by geochemical change (e.g. McMillan et al., 2005). It is important to fully constrain the length of growth hiatuses, to ensure accurate interpretation of palaeoclimatic events (McDermott et al., 2006).

Growth was found to be completely suppressed some years in a speleothem from SW Australia, leading to pinching-out of annual layers, which can cause complex growth patterns, uneven thickness of annual growth layers and annual hiatuses (Treble et al., 2005a). This growth suppression was related to periods of reduced rainfall, most likely in the summer and indicated that the surface of the previous year's growth will impact the following year's growth nucleation, via a combination of crystal defect density and/or crystallite morphology (Treble et al., 2005a). Dislocations in crystal structure may cause mismatch of coalescing crystals, or incorporation of foreign ions such as clay or organic ions which can provide additional nucleation sites for crystal growth (Wenk et al., 1983, Treble et al., 2005a). A change in crystallite morphology due to drip water chemistry could also influence crystal nucleation (Frisia et al., 2000).

## **2.7 Speleothem Mineralogy and Petrography**

### **2.7.1 Cave Carbonate Minerals**

More than 100 minerals can occur as secondary precipitates in caves, with calcite the most common by volume (Ford, 1988). 95% of the cave minerals of the world are aragonite or calcite, which are both polymorphs of calcium carbonate (Onac, 2005). Speleothems may be formed of several carbonate forms, including not only calcium carbonate minerals. Such carbonates include low-magnesium calcite, high-magnesium calcite (metastable), aragonite, dolomite, calcian dolomite, huntite, vaterite, hydromagnesite and nesquehonite (White, 1976, Hill and Forti, 1997). Magnesium carbonate hydrates such as hydromagnesite and nesquehonite are highly unstable and therefore likely to undergo early replacement (Bar-Matthews et al., 1991). Hydromagnesite is a stable mineral phase

at typical cave temperatures (10-15°C) (Hill and Forti, 1997) where extremely high Mg/Ca ratios exist (Fischbeck and Müller, 1971). It is likely the third most common cave mineral after calcite and aragonite (Hill and Forti, 1997).

Huntite,  $\text{CaMg}_3(\text{CO}_3)_4$ , may coat aragonite needles (e.g. Frisia et al., 2002), and is believed to form through evaporation of the water film the aragonite precipitated from (Harmon et al., 1983), during periods of extreme evaporation and elevated Mg concentrations and Mg/Ca (González and Lohmann, 1988), indicating diminishing water flow (Frisia et al., 2002). Vaterite is the highest temperature polymorph of  $\text{CaCO}_3$ , and is highly metastable, so it is possible that where it does form in caves, it is quickly replaced by calcite or aragonite (Hill and Forti, 1997). At extremely high Sr concentration, strontianite ( $\text{SrCO}_3$ ) forms, rather than aragonite (Astilleros et al., 2003). Strontianite is isostructural with aragonite, along with witherite ( $\text{BaCO}_3$ ) (de Villiers, 1971).

### **2.7.2 Mineralogy of Speleothems used for Palaeoclimatic Studies**

In general, speleothems which are used for palaeoclimatic studies are formed of calcium carbonate,  $\text{CaCO}_3$  (Hill and Forti, 1997), which precipitates from calcite/aragonite super-saturated cave waters (Lauritzen and Lundberg, 1999). Typically speleothems consist of macro-crystalline calcite (McDermott, 2004). It is also possible for speleothems to be formed of aragonite, although this occurs less frequently, particularly in situations where host-rocks contain high-Mg calcite or dolomite, and/or dolomite dissolution of partially dolomitised host rocks is increased due to longer contact times between water and rock during drier periods (McDermott, 2004). Moore (1956) suggested that aragonite speleothems could be used as indicators of temperature.

Aragonite and calcite can coexist harmoniously in caves (Murray, 1954, Alonso-Zarza et al., 2011); for example aragonite stalagmites may be fed by counterpart calcite stalactites (Hill and Forti, 1997). It is also possible for a speleothem layer to contain lateral variations between calcite and aragonite, interpreted to be caused by variations in degree of evaporation across the speleothem surface (Railsback et al., 1994), or aragonitic botryoids within primary calcite, indicating that both forms were capable of forming almost simultaneously (Spötl et al., 2002b). Very strong seasonal dryness leading to a reduction in drip rate combined with increased prior calcite precipitation may result in seasonal mineralogical changes from calcite to aragonite (Railsback et al., 1994). Another possibility is that high flow rates would reduce the residence times on the speleothem surface to such an extent that there was insufficient time for  $\text{CO}_2$  to degas and initiate calcite precipitation,

resulting in aragonite dissolution by waters in equilibrium with calcite or dolomite until calcite precipitation became possible (Dreybrodt, 1980, Railsback et al., 1994). Both processes could possibly occur together (Railsback et al., 1994).

Caves which contain actively growing calcite and aragonite speleothems often show zonation of mineralogy; with areas with more continuous water supply containing calcite speleothems, and less continuous drips such as those fed by seepage water more likely to precipitate aragonite (Frisia et al., 2002, Alonso-Zarza et al., 2011). Massive speleothems tend to be formed of calcite, as they require a more continuous water supply to form (Frisia et al., 2002).

Use of aragonitic speleothems is considered to be problematic (Fairchild et al., 2006), due to the instability of aragonite at certain temperature and pressure conditions, leading to phase-change and recrystallization (Frisia et al., 2002, Fairchild et al., 2006). However, some studies have successfully made use of wholly or partly aragonitic speleothems for palaeoclimatic reconstruction (e.g. Bar-Matthews et al., 1991, Railsback et al., 1994, 2011, Denniston et al., 2000, Finch et al., 2001, 2003, McMillan et al., 2005, Cosford et al., 2008, Li et al., 2010, 2011), while accounts of the effects of recrystallization and phase-change are also useful (e.g. Frisia et al., 2002, Martín-García et al., 2009, Alonso-Zarza et al., 2011). Aragonitic speleothems from tropical and sub-tropical, semi-arid environments have been found useful in palaeoclimatic reconstruction (e.g. Brook et al., 1999, 2006). Aragonite stalagmites are particularly sensitive to climate, making them useful indicators of drought (Finch et al., 2003).

Measurements of oxygen and carbon isotope fractionation between drip waters and aragonite speleothems have been carried out in some caves (e.g. McDermott et al., 1999, Frisia et al., 2000, McMillan et al., 2005), although as these caves are all European, the relationships discovered may not be applicable to other geographical regions (Li et al., 2011). Li et al. (2011) found that in Furong Cave, China, active (primary) aragonite deposition was in oxygen isotope equilibrium with drip water, and showed coherence with the  $\delta^{18}\text{O}$  signatures of Hulu (Wang et al., 2001) and Dongge Caves (Yuan et al., 2004, Dykoski et al., 2005), while complicated carbon isotope fractionation necessitates further study before palaeoclimate conclusions can be drawn.

### **2.7.2.1 Benefits of Performing Petrographic Observations of Speleothems**

Petrographic analysis of speleothems can help to identify diagenetic processes (Frisia and Wenk, 1993), which can be a particular problem with aragonite speleothems.

Microorganisms could cause important small-scale diagenetic processes (Jones and Kahle, 1995). Phase transformations from aragonite to calcite or vice versa may alter the original oxygen and carbon isotopic signature, so it is important to identify recrystallisation before inferring palaeoclimatic information from speleothem isotopic records (Fairchild et al., 2006).

Another reason to perform petrographic analysis of speleothems is to assist in the palaeoclimatic interpretation; textural variations may be related to drip-water availability (Frisia et al., 2000), the nature of flow or transport of water (González et al., 1992, Gratz et al., 1993, Jones and Kahle, 1993) and/or evaporation (Frisia, 1996). However, it is important to show that changes in crystallography or petrography are synchronous throughout a particular region before using them to aid interpretation of stable isotope data, as they may have been influenced by drip- or cave-specific hydrological routing effects (McDermott, 2004).

### **2.7.3 Calcite**

“Calcite” refers to calcite containing less than 0.5 mole %  $\text{MgCO}_3$  (Howson et al., 1987, Bar-Matthews et al., 1991). Low-magnesium calcite (LMC) refers to calcite which contains less than 5 mole %  $\text{MgCO}_3$ , and high magnesium calcite (HMC) contains more than 5 mole %  $\text{MgCO}_3$  (Scoffin, 1987).

Calcite, a trigonal mineral, is the most common and stable polymorph of  $\text{CaCO}_3$  under earth surface conditions (Lippmann, 1973, Hill and Forti, 1997). The most stable form of calcite at earth surface temperature and pressure is calcite or LMC which contains <4 mole %  $\text{MgCO}_3$  (Berner, 1966, Winland, 1969, Lippmann, 1973, de Boer, 1977). Calcite is believed to be the most abundant carbonate mineral as a result of limestone’s dominance of carbonate rocks, and the fact that limestone is essentially composed of calcite (Lippmann, 1973).

Calcite is rhombohedral, with each Ca atom surrounded by six  $\text{CO}_3$  groups, and the oxygen atoms being the closest neighbours of the calcium atoms (Lippmann, 1973, Speer, 1983). Calcites which develop as rhombohedral crystals, with overlapping, radial-layered patterns are indicators of enhanced supersaturation and growth rate (White, 1976). The density of calcite is 2.71 (Lippmann, 1973).

Calcite in its pure form is colourless (White, 1981), but in natural systems it is often a colourful mineral, depending on trace impurities or other factors (Hill and Forti, 1997), for

example it may be brownish (Alonso-Zarza et al., 2011), dark grey to light yellow-beige (Verheyden et al., 2008), light-brown to light-green (Spötl et al., 2002b) or even blood-red (White, 1981). Colour may be given to speleothem fabric by detrital material and oxides; for example speleothems from Soreq Cave, Israel which had more detrital material and oxides of up to 0.5% were much darker in colour (Ayalon et al., 1999). Fluorescence Index analysis of a stalagmite from Ethiopia indicates that brown colouring in calcite may not arise from higher concentrations of organic matter, but rather from a greater concentration of organic molecules which have a higher molecular weight (Asrat et al., 2007).

Calcite may be less shiny or bright than aragonite, and show more visible banding than aragonite areas of a stalagmite (Martín-García et al., 2009, Alonso-Zarza et al., 2011), although Ortega et al. (2005) found that the calcitic parts of a French speleothem contained no visible or luminescent banding .

## **2.7.4 Aragonite**

### **2.7.4.1 Characteristics of Aragonite**

Aragonite is the high pressure polymorph of  $\text{CaCO}_3$  (Helgeson et al., 1978). Aragonite is orthorhombic, and each  $\text{Ca}^{2+}$  is bonded to nine oxygen atoms, which are derived from 6  $\text{CO}_3$  groups, with 3  $\text{CO}_3$  groups bonding to the  $\text{Ca}^{2+}$  with two oxygens, and the remaining 3 bonding to the  $\text{Ca}^{2+}$  with one oxygen atom, giving the structural formula  $\text{A}^{\text{IX}}\text{C}^{\text{III}}\text{O}^{\text{IV}}_3$  (Lippmann, 1973, Speer, 1983). The density of aragonite is 2.93 (Lippmann, 1973). Aragonite crystals in speleothems are fibrous and orientated parallel to growth (Fairchild et al., 2006). Aragonite often appears as fans growing out from a common point (Alonso-Zarza et al., 2011). Aragonite appeared as acicular crystals with a length to width ratio  $\geq 6:1$  in Castañar Cave, Spain (Alonso-Zarza et al., 2011). Layers of aragonite were found to thin towards the centre in alternating aragonite-calcite couplets in a Botswanan speleothem (Railsback et al., 1994).

Aragonite is usually pure white, (e.g. Spötl et al., 2002b), but can also precipitate as a colourless, grey or yellow mineral (Morse and Mackenzie, 1990, Hill and Forti, 1997). It is often shiny and transparent (Alonso-Zarza et al., 2011). Needle aragonite forms from drips which experience slow, continuous, prolonged degassing and evaporation, and are the most isotopically enriched aragonite fabrics (Frisia et al., 2002). Prismatic aragonite forms where drip discharge rate is very slow ( $<0.00035$  ml/min) and dripwater Mg/Ca is  $>1.1$  (Frisia et al., 2002).

The conditions of aragonite formation are complex. They will be discussed in Chapter 4 in relation to speleothems from Dim Cave, SW Turkey.

### **2.7.5 Isotopic Characteristics of Speleothem Fabrics**

Caves which precipitate both calcite and aragonite have consistently been found to have lighter isotopic values in the calcite compared to the aragonite (McDermott et al., 1999, Frisia et al., 2002, Woo and Choi, 2006, Alonso-Zarza et al., 2011). Constant, slow, prolonged degassing encourages incorporation of  $^{13}\text{C}$  in aragonite (Frisia et al., 2002). Where aragonite enrichments are larger than expected compared to calcite, this may indicate that the aragonite formed under more prolonged degassing conditions than the calcite (Frisia et al., 2002).

The  $\delta^{18}\text{O}$  equilibrium separation factor between aragonite and calcite is 0.6‰ at 25°C (Tarutani et al., 1969), and 0.7‰ at 3-19°C (Grossman and Ku, 1981). The  $\delta^{13}\text{C}$  equilibrium separation factor between aragonite and calcite is  $1.7 \pm 0.4\text{‰}$ , and is independent of temperature between 10 and 40°C (Romanek et al., 1992).

The various phenomena controlling  $\delta^{13}\text{C}$  in aragonite are extremely complex; therefore it is impossible to use such a record as an indicator of past vegetation changes (Bar-Matthews et al., 1991, Frisia et al., 2002, Hopley et al., 2009). Secondary calcite is problematic for carbon isotope reconstruction also, as  $^{13}\text{C}$  enrichment was found to be inherited from the precursor phase (Frisia et al., 2002).

### **2.7.6 Diagenesis and Recrystallisation**

#### **2.7.6.1 *Replacement of Aragonite by Calcite***

Aragonite is metastable at surface pressures and temperatures (Frisia et al., 2002), making it susceptible to changes in hydrothermal conditions (Ortega et al., 2005), and therefore aragonite speleothems may undergo secondary replacement to calcite, the more stable polymorph (Folk and Assereto, 1976, Bar-Matthews et al., 1991, Frisia, 1996, Hill and Forti, 1997, Ortega et al., 2005, Woo and Choi, 2006). Calcitisation of components of marine limestones has been well-documented (Wardlaw et al., 1978, Buchardt and Weiner, 1981, Sandberg and Hudson, 1983, Martin et al., 1986, Brand, 1989, Maliva and Dickson, 1992), as has replacement of aragonite by calcite in speleothems (Folk and Assereto, 1976, Cabrol and Coudray, 1978, 1982, Frisia, 1996, Frisia et al., 2002, Spötl et al., 2002b, Hopley et al., 2009).

Aragonite sediments of Tertiary age or older are rare, with the assumption being that this is because all older aragonites have converted to calcite (Lippmann, 1973), as the complete conversion of aragonite into calcite may occur in 5-16 kyr in the phreatic, meteoric diagenetic environment (Budd, 1988), and has also been known to occur in less than 1kyr (Frisia et al., 2002). However, metastable aragonite can exist in caves for thousands to millions of years (Fairchild et al., 2006).

#### 2.7.6.1.1 *Appearance of Recrystallised Speleothems*

It may be difficult to identify calcitized aragonite speleothems in caves, as the entire outer surface may be comprised of aragonite, while the inner regions may have been calcitized (Lachniet et al., 2012).

To the naked eye, sampled speleothems which have been recrystallised appear more massive, matt, brownish, and grainy (due to calcite mosaics, which also cause them to lose their acicular texture if they had it) when cut open (Martín-García et al., 2009, Alonso-Zarza et al., 2011). Secondary calcite was found to show virtually no fluorescence or cathodoluminescence, while both primary calcite and primary aragonite show both at least moderately (Spötl et al., 2002b). "Islands" of aragonite embedded in secondary calcite may occur as a result of extensive but not complete replacement, and these may be visible either to naked eye or under the microscope (Spötl et al., 2002b).

Under the microscope, aragonite which has been recrystallised as calcite will exhibit a mosaic of equigranular calcite crystals (Bischoff and Fyfe, 1968, Hopley et al., 2009), preserving either relic fibres of original aragonite, or aragonite ghosts, as well as some twinned or deformed calcite crystals (Frisia et al., 2002, Martín-García et al., 2009, Hopley et al., 2009). Relics are common features of neomorphism (Folk, 1965, Mazzullo, 1980). Incomplete recrystallisation will result in solid inclusion aragonite relics within the calcite crystals, while complete recrystallisation will preserve only the textural imprint of the aragonite, resulting in ghosts (Martín-García et al., 2009). For example, where the commencement of calcite precipitation following aragonite dissolution raises the local supersaturation of the solution so that it is supersaturated with respect to aragonite, this may facilitate the preservation of undissolved aragonite relics (Frisia et al., 2002). Frisia et al. (2002) found that in a speleothem from Clamouse Cave, France, replacement phenomena were sometimes fabric-destructive, indicating some scale of chemical openness (Maliva et al., 2000). A very fine-grained "chalky" fabric with no aragonite relics is also possible for secondary calcite (Hopley et al., 2009).

#### 2.7.6.1.2 *Geochemical Indicators of Recrystallisation*

Recrystallisation modifies the geochemical signals of the primary aragonite, which is problematic if the speleothem records are intended for palaeoclimatic interpretation (Railsback et al., 2002, Fairchild et al., 2006, Alonso-Zarza et al., 2011).

Hopley et al. (2009) found that primary fabrics of South African speleothems had on average lower  $\delta^{13}\text{C}$  than secondary fabrics, and while  $\delta^{13}\text{C}$  values were variable,  $\delta^{18}\text{O}$  was invariant. Martín-García et al. (2009) found that transformation of aragonite to calcite will result in calcite which has higher isotopic values than original calcite, but lower than original aragonite, regardless of the composition of the cave waters. However, the isotopic signature of the cave water may be important if, for example, it contains very heavy values due to an extremely arid interval (Martín-García et al., 2009).

The equilibration of oxygen isotopes with aqueous carbonate ions occurs as the replacement reaction is progressing, and after aragonite has dissolved, calcite is precipitated by incorporating ions from the solution (Perdikouri et al., 2011). Calcite derived from recrystallisation of aragonite can achieve oxygen-isotope equilibrium with the solution in a short amount of time, regardless of what the original aragonite's isotopic composition may have been (Perdikouri et al., 2011).

The chemical composition of neomorphic calcite is partly controlled by the chemical composition of the precursor aragonite (Woo and Choi, 2006). However, the extent to which the primary aragonite influences the trace element and stable isotope compositions of the secondary calcite depends on ionic exchange rates between the alteration site and diagenetic waters, and the size of the alteration front (Woo and Choi, 2006). Therefore, the isotopic and elemental composition of secondary calcite will depend on the method of reprecipitation from the original aragonite. Secondary calcites containing aragonite relics were reprecipitated via a thin film (a few microns thick) under closed system conditions (Brand and Veizer, 1980, Pingitore, 1982, Hopley et al., 2009) and will have stable isotope and trace elemental compositions close to the dissolved aragonite and aragonite micrite (Hopley et al., 2009, Martín-García et al., 2009). Secondary calcites which do not contain aragonite relics were most likely reprecipitated via the chalkification process across a broad zone (Pingitore, 1976), in which the cave waters are more closely associated with the diagenetic fabric and as such exert the dominant control over the secondary calcite's chemical properties, with the primary aragonite having little influence (Martín-García et al., 2009, Hopley et al., 2009). In this situation the chemical distinction between the original

and reprecipitating waters may become blurred (Hopley et al., 2009), but values close to primary calcite (Spötl et al., 2002b), or close to primary calcite with a slight shift towards aragonitic values has also been observed (Martín-García et al., 2009). Thus, it has been suggested that carbon and oxygen isotopes may help to distinguish between primary and secondary calcites, but as there is some overlap, this is not an exact science (Hopley et al., 2009, Alonso-Zarza et al., 2011).

During recrystallization, the degree of exchange of trace elements depends on the volume and composition of the diagenetic waters (Brand and Veizer, 1980). However, where aragonite recrystallizes into calcite, abnormally high Sr contents (for calcite) may be found, as a portion of the aragonite's Sr remains in the neogenic calcite (Frisia, 1996, Ortega et al., 2005).

#### **2.7.6.2 *The Effects of Recrystallisation on U-Series Dating***

A large (>1.0 ppm) range of U concentrations within a speleothem is an indicator of possible recrystallization and U loss (Railsback et al., 2002) as is abnormally high U in calcite (Ortega et al., 2005). Uranium loss during recrystallisation can occur because the  $\text{UO}_2^{2+}$  cation is relatively soluble (Langmuir, 1978), while  $\text{Th}^{4+}$  has been found to be practically insoluble in aqueous environments (Kaufman, 1969). As a result, during recrystallisation uranium may be mobilised and leached, while thorium remains in the recrystallised speleothem, leading to anomalously old ages (Frisia et al., 2002, Railsback et al., 2002, Ortega et al., 2005). However, recrystallization can occur with no subsequent loss of dating integrity, if the system is not open and therefore U loss does not occur, for example in the case of a recrystallized Alpine speleothem (Spötl et al., 2002b).

# *Chapter 3*

## *Palaeoclimatic and Palaeoenvironmental Proxies Recorded within Speleothems*

### 3.1 Stable Isotopes in Speleothems

The historic method for oxygen and carbon isotopic analysis is spot-sampling of sample powders, followed by dissolution in orthophosphoric acid (Sharp, 2007). Alternatively, laser-ablation or ion microprobe may be used (Fairchild et al., 2006).

Oxygen isotope data can now be analysed on the seasonal scale, (e.g. Treble et al., 2005a), allowing summer and winter precipitation to be distinguished from each other, provided the drip contains a fracture-fed component (Fairchild et al., 2006), as otherwise the drip may have a homogenised composition (Williams et al., 2004).

#### 3.1.1 Notation of Stable Isotope Values

##### 3.1.1.1 The Delta Value

The delta value was introduced by McKinney et al. (1950) to report stable isotope data, and is the current method used to report stable isotope data for speleothems. The symbol for delta is  $\delta$ . The value represents:

$$\delta = \left( \frac{R_x - R_{std}}{R_{std}} \right) \times 1000$$

*Equation 3.1: The delta value*

where R is the ratio of heavy to light isotope,  $x$  is the sample, and std denotes a universal standard. For example, in the case of  $\delta^{18}\text{O}$  (Sharp, 2007):

$$\delta^{18}\text{O} = \left( \frac{{}^{18}\text{O}/{}^{16}\text{O}_x - {}^{18}\text{O}/{}^{16}\text{O}_{std}}{{}^{18}\text{O}/{}^{16}\text{O}_{std}} \right) \times 1000$$

*Equation 3.2: The derivation of  $\delta^{18}\text{O}$*

The units of delta values are per mil, given as ‰. When comparing  $\delta$  values, a more positive value indicates that the ratio of heavier to light isotopes is higher (Sharp, 2007).

### 3.1.1.2 Symbols for Components of the Speleothem-Forming System

For simplicity, the following symbols will be used from now on to distinguish between the  $\delta^{18}\text{O}$  of different components of the speleothem-forming system:

$\delta^{18}\text{O}_p$	The $\delta^{18}\text{O}$ of meteoric precipitation
$\delta^{18}\text{O}_d$	The $\delta^{18}\text{O}$ of the cave dripwater
$\delta^{18}\text{O}_c$	The $\delta^{18}\text{O}$ of speleothem calcite
$\delta^{18}\text{O}_s$	The $\delta^{18}\text{O}$ of seawater
$\delta^{18}\text{O}_v$	The $\delta^{18}\text{O}$ of water vapour of air masses
$\delta^{18}\text{O}_k$	The $\delta^{18}\text{O}$ of waters moving through the karst

### 3.1.2 Equilibrium

Demonstrating that modern calcite is precipitating in isotopic equilibrium at the cave site is important, but it is even more important to demonstrate that isotopic equilibrium was maintained during the speleothem growth history (McDermott et al., 2006), usually through the application of Hendy tests (Hendy, 1971).

Drips which fall about half a metre to the drip site are most likely to be in chemical and isotopic equilibrium and therefore record climate conditions above the cave (Dreybrodt, 2011a). Speleothems often precipitate in quasi-equilibrium with their drip waters (McDermott et al., 2006), with low supersaturation, constant drip rate and relative humidity of approximately 100% (Fairchild et al., 2007). In cool temperate locations, relative humidity is likely to be high (95-100%), which results in decreased evaporation (McDermott et al., 2006), which is beneficial for interpretation of oxygen isotopic data. Although speleothems often precipitate in “quasi-equilibrium”, most cave carbonates are not strictly in isotopic equilibrium, and on the basis that positive correlation between  $\delta^{13}\text{C}$  and  $\delta^{18}\text{O}$  is caused by kinetics effects, Mickler et al. (2006) suggested that most studied speleothems were deposited in isotopic disequilibrium. When applying equilibrium calibrations the choice of fractionation factor applied will change the output critically (McDermott et al., 2006). This also has implications for the use of transfer functions to

extract temperature or precipitation data from stable isotope records (Frisia and Borsato, 2010).

Many speleothems, despite precipitating in quasi-equilibrium with their dripwaters, have heavier oxygen isotope signals than predicted by equilibrium fractionation factors (Desmarchelier et al., 2000, Plagnes et al., 2002, Genty et al., 2003, Mickler et al., 2004, Mangini et al., 2005, Coplen, 2007, Sinha et al., 2007, Genty, 2008, Boch et al., 2009), with enrichments of 0.5-1‰ relative to predicted values (Kim and O'Neil, 1997). Kinetic enrichment accompanying relatively rapid degassing of drip waters could be the reason for this, as when this occurs the  $\delta^{18}\text{O}$  of the calcite approaches the  $\delta^{18}\text{O}$  of the dissolved bicarbonate reservoir (Mickler et al., 2004). High supersaturation can lead to this rapid degassing, initiating disequilibrium (Asrat et al., 2007). Evaporation on the stalagmite cap during degassing would also could disequilibrium (Mickler et al., 2004).

In a situation where degassing rates are slow and there is no evaporation, calcite will be deposited in thermodynamic equilibrium with the dripwater, making the isotopic signature easier to interpret. The distribution of light/heavy isotopes will only be a function of temperature (Lauritzen and Lundberg, 1999). Where there is fast crystallisation and/or evaporation, isotopic fractionation will be controlled by kinetic effects, and so there may not be equilibrium between the calcite and the dripwater (Lauritzen and Lundberg, 1999).

### **3.1.2.1 The Hendy Test**

The Hendy Criteria or similar can be used to assess if calcite was precipitated under equilibrium conditions (Hendy, 1971, Schwarcz, 1986). In the Hendy Method, a series of coeval samples are taken along the same growth horizon. Loss of isotopically light carbon in  $\text{CO}_2$  would lead to  $\delta^{13}\text{C}$  change progressively outwards from the apex and down the sides of the growth layer, while  $\delta^{18}\text{O}$  would be invariant. If evaporation was occurring,  $\text{H}_2^{16}\text{O}$  would be lost progressively down the growth layer so both isotopes would be enriched (Hendy, 1971). Therefore, if equilibrium deposition has occurred,  $\delta^{18}\text{O}$  should remain constant along the growth layer while  $\delta^{13}\text{C}$  varies irregularly, with no correlation between  $\delta^{18}\text{O}$  and  $\delta^{13}\text{C}$  along the growth layer (McDermott, 2004). Positive correlation between  $\delta^{13}\text{C}$  and  $\delta^{18}\text{O}$  suggests kinetic isotope fractionation during calcite/aragonite precipitation (Hendy, 1971).

Performing Hendy tests can be difficult due to the physical difficulty of sampling along the same, coeval horizon (Lauritzen and Lundberg, 1999), and the fact that lamina may be thinner on the stalagmite flanks than at the central growth axis (McDermott, 2004). Furthermore, in some cases it has been shown that while the calcite deposited along the central growth axis may have been deposited in isotopic equilibrium, the calcite deposited along the flanks was not (Talma and Vogel, 1992). Modelling of stable isotope fractionation has shown that a positive Hendy test (i.e. isotopic enrichment of  $\delta^{13}\text{C}$  and  $\delta^{18}\text{O}$  along a growth layer) can only be achieved if isotope fractionation occurred under disequilibrium conditions, while a negative Hendy test can happen under the same situation (Mühlinghaus et al., 2009).

Several authors have suggested improvements to the Hendy test, for example to combat the above problem, Mühlinghaus et al. (2009) suggest that the enrichment of  $\delta^{13}\text{C}$  alone along an individual growth layer is a more reliable indicator of disequilibrium fractionation. Frisia et al. (2000) suggest that Hendy's (1971) criteria for assessing isotopic equilibrium be expanded to include consideration of the calcite crystal fabric, specifically identification of columnar, fibrous or microcrystalline fabrics and flat-faced rhombohedral crystallites, and the need for a low degree of supersaturation of the parent waters. Mickler et al. (2006) suggested that  $\delta^{18}\text{O}$  and  $\delta^{13}\text{C}$  covariation through time (i.e. along the vertical axis rather than horizontally) may be due to kinetic effects that the Hendy Test cannot test for, although this may also be caused by PCP, a change in drip rate or evapotranspiration, which are climatically controlled and therefore a useful proxy (Frisia and Borsato, 2010, Frisia et al., 2006). Oster et al. (2010) suggested that an improvement on the Hendy Test would be to analyze off-axis  $\delta^{18}\text{O}$  and  $\delta^{13}\text{C}$  profiles. Tremaine et al. (2011) suggest that a whole-cave Hendy test could be a very useful ventilation proxy.

Many records have been published which include speleothems that have been affected by non-equilibrium processes (e.g. Frumkin et al., 1999, Plagnes et al., 2002, Spötl and Mangini, 2002, Drysdale et al., 2004, Wurth et al., 2004, Asrat et al., 2007), and it has been shown that most speleothem isotope records may be affected by kinetic effects (Mickler et al., 2006). The experiments of Wiedner et al. (2008) suggested that a certain degree of kinetic fractionation is always possible, and that specifically speleothem growth may be enriched in  $^{13}\text{C}$  and  $^{18}\text{O}$  in the down-flow direction due to progressive degassing and slower flow.

### 3.1.2.2 *Palaeotemperature Equations*

It has been difficult to produce reproducible extraction and analysis of fluid inclusions, which prevented a simple solution to the palaeotemperature equation (Fairchild et al., 2006), leading to attempts to calibrate  $\delta^{18}\text{O}$  of atmospheric moisture with long-term temperature (Lauritzen and Lundberg, 1999).

Kim and O'Neil (1997) proposed the following equation for the oxygen isotope fractionation between calcite and water at low temperatures:

$$1000 \cdot \ln\alpha = \frac{18030}{T} - 32.42$$

*Equation 3.3: The Kim and O'Neil (1997) calcite-water oxygen isotope fractionation equation*

Where  $\alpha$  is the fractionation factor and  $T$  is temperature in Kelvin.

Demeny et al. (2010) analysed data from two Hungarian caves to test the suitability of using existing fractionation-temperature relationships when dealing with natural environments. They created the following equation for use with cave deposits which precipitated in the range 10 to 25°C:

$$1000 \cdot \ln\alpha = \frac{17500}{T} - 29.89$$

*Equation 3.4: The Demeny et al. (2010) ambient temperature calcite-water oxygen isotope fractionation equation*

Due to the fact that modern *in situ* calibration of calcite  $\delta^{18}\text{O}$ -temperature fractionation factors has shown that inorganic calcite precipitated from very slow drips that are slightly supersaturated is on average  $+0.82 \pm 0.24$  ‰ more enriched in  $^{18}\text{O}$  than expected, Tremaine et al. (2011) proposed the following equation for isotope-temperature fractionation of cave calcites:

$$1000 \cdot \ln\alpha = \frac{16100}{T} - 24.6$$

*Equation 3.5: The Tremaine et al. (2011) cave calcite oxygen isotope fractionation equation*

Mickler et al. (2004) use the equations of O'Neil et al. (1969) as modified in Friedman and O'Neil (1977) to calculate the relationship between the oxygen isotopic composition of calcite and its corresponding drip water and the temperature of formation. They also use the equations of Deines et al. (1974) to define the relationship between the C isotopic content of  $\text{HCO}_3^-$ , the dominant species in the DIC, calcite and the formation temperature.

Several equations have been presented to empirically derive the relationship between temperature of deposition and  $\delta^{18}\text{O}_c$  such as the Craig (1965) equation and the equation of Anderson & Arthur (1983). Such equations often yield temperatures closer to expected cave air temperature (McDermott et al., 2006), probably partly because they used mixed calcite and aragonite fractionation factors (Leng and Marshall, 2004), and equilibrium fractionation factors for aragonite predict higher temperatures than calcite equilibrium fractionation factors at the same temperature (Grossman and Ku, 1986). Therefore it would seem that mixed mineralogy empirical calibrations are not appropriate for wholly calcite speleothems (McDermott et al., 2006). Field experiments have shown that calcite may be more likely to be precipitated close to oxygen isotopic equilibrium with its corresponding dripwater if the drip is very slow, and calcite is deposited at a slow rate (Mickler et al., 2004).

### **3.1.2.3 Aragonite and Equilibrium**

Evaluating if aragonite precipitated in equilibrium is more complicated than for calcite, as there are many and conflicting  $\delta^{18}\text{O}_{\text{water}} - \delta^{18}\text{O}_{\text{temperature}}$  equations (McCrea, 1950, Grossman and Ku, 1986, Thorrold et al., 1997, Zheng, 1999, Bohm et al., 2000, Zhou and Zheng, 2003, Kim et al., 2007), which use many different experimental conditions (Kim et al., 2007). The equation recommended by Lachniet (2009), who reviewed the available literature, for determination of aragonite equilibrium fractionation, is that of Kim et al. (2007):

$$1000 \ln \alpha = 17.88 (\pm 0.13) \times \frac{1000}{T} - 31.14 (\pm 0.46)$$

*Equation 3.6: The Kim et al. (2007) Equation for aragonite equilibrium fractionation*

where  $\alpha =$  the  $^{18}\text{O} / ^{16}\text{O}$  fractionation between aragonite and water and T = temperature at deposition (K).

### 3.1.3 Oxygen Isotopes

#### 3.1.3.1 Notation

$\delta^{18}\text{O}$  is reported relative to two standards; Pee Dee Belemnite (PDB) (Craig, 1957), and Standard Mean Ocean Water (SMOW). SMOW is now often referred to with the prefix “Vienna”, abbreviating the whole to VSMOW (Gonfiantini, 1978). In terms of speleothem isotopic studies, PDB is used to relate values for the carbonate, while SMOW is used for drip- and rain-waters (Sharp, 2007). The  $\delta^{18}\text{O}$  value of both PDB and SMOW is defined as 0.0‰ (Coplen, 1996). The two scales can be related to each other via the relationships (Coplen et al., 1983):

$$\delta^{18}\text{O}_{\text{SMOW}} = 1.03091(\delta^{18}\text{O}_{\text{PDB}}) + 30.91$$

*Equation 3.7: Relation between SMOW and PDB*

$$\delta^{18}\text{O}_{\text{PDB}} = 0.97002(\delta^{18}\text{O}_{\text{VSMOW}}) - 29.98$$

*Equation 3.8: Relation between PDB and SMOW*

#### 3.1.3.2 Interpretation in Terms of Temperature

Early researchers such as Gascoyne et al. (1980) sought to reconstruct absolute changes in mean annual air temperature from speleothem oxygen isotope data, as it is understood that if the  $\delta^{18}\text{O}$  of the water from which authigenic carbonates such as speleothems precipitated is known or can be independently calculated, then it may be possible to reconstruct a record of relative or possibly absolute temperature changes (e.g. Goede et al., 1986, Schwarcz, 1986, Winograd et al., 1988, Gascoyne, 1992, Talma and Vogel, 1992, Lauritzen, 1995, Dorale et al., 1998, Ku and Li, 1998). However, as air temperature is not the only factor to affect speleothem calcite  $\delta^{18}\text{O}$  (McDermott, 2004), other factors influencing  $\delta^{18}\text{O}$  of precipitation such as changing moisture sources, air mass history, moisture recycling, and rainfall seasonality and rainfall amount (Hendy, 1971, Grootes, 1993) must be taken into account. However, speleothems were found to be reliable recorders of a combination of air temperature and precipitation oxygen isotope signals in a study of spatial variability of  $\delta_{18}\text{O}$  in European Holocene speleothems (McDermott et al., 2011).

Additional factors affect speleothems, especially in arid and semi-arid regions, as  $\delta^{18}\text{O}_p$  may be modified by evaporation processes at or near the surface (Bar-Matthews et al., 1996).

For eastern Mediterranean sites, the majority of precipitation falls in winter, coinciding with lower temperatures and lower  $\delta^{18}\text{O}_p$ , such that the effects of each on  $\delta^{18}\text{O}_c$  cannot be differentiated without independent data (Bar-Matthews et al., 1997).

### **3.1.3.3 Relationship between Components of the $\delta^{18}\text{O}$ System**

$\delta^{18}\text{O}_p$  exerts a first order control on  $\delta^{18}\text{O}_c$  (McDermott et al., 2006), as  $\delta^{18}\text{O}_c$  is dependent on  $\delta^{18}\text{O}_d$ , and it is known that ideally,  $\delta^{18}\text{O}_d$  reflects the weighted mean of regional  $\delta^{18}\text{O}_p$  (McDermott, 2004). If the speleothem calcite can be demonstrated to have been precipitated under isotopic equilibrium, then  $\delta^{18}\text{O}_c$  reflects a combination of  $\delta^{18}\text{O}_d$ , which in turn is related to  $\delta^{18}\text{O}_p$ , and the temperature driven isotopic fractionation between the depositing drip waters and the deposited calcite (Dansgaard, 1964, McDermott, 2004, McDermott et al., 2006). The fractionation is the smaller input, and thus changes in water isotopic composition are the main control for changes in  $\delta^{18}\text{O}_c$  (Fairchild et al., 2007).

In caves with near 100% humidity and no significant cave temperature variations, speleothem  $\delta^{18}\text{O}_c$  is most often interpreted in terms of variations in  $\delta^{18}\text{O}_p$ . There have been many studies of seasonal and spatial variations in the  $\delta^{18}\text{O}$  of modern precipitation e.g. (Rozanski et al., 1982, Rozanski et al., 1993, Gat, 1996). The oxygen isotope composition of precipitation is a consequence of the effects of several factors, which include latitude, altitude, distance from the sea, amount of precipitation, amount of previous rainout, surface air temperature and the global ice volume effect on glacial timescales (McDermott, 2004). Other possible factors include changes in the proportion of precipitation which was derived from sources other than the ocean, e.g. recycling from continental surficial waters, which should increase as temperature increases (McDermott et al., 1999, Koster et al., 1993).

### **3.1.3.4 Changes in the Isotopic Composition of Air Masses**

There are several factors which may change the oxygen isotopic signature of an air mass. These various isotope effects are primarily related to latitude, altitude, and the location of the moisture source (Dansgaard, 1964, Rozanski et al., 1993, Lachniet, 2009).

During cooling, Rayleigh fractionation leads to condensation which results in a more negative  $\delta^{18}\text{O}_p$  (Fairchild et al., 2007). The principles of Rayleigh fractionation can be used to model the fraction of water vapour removed from an air mass between the source region and cave site (Yuan et al., 2004). Where water vapour is advected from inland,  $\delta^{18}\text{O}_v$

often reflects upstream precipitation changes, and so  $\delta^{18}\text{O}_p$  and  $\delta^{18}\text{O}_c$  do not reflect local precipitation amount changes, but changes in upstream precipitation (Drysdale et al., 2004). After vapour is evaporated from the ocean, it is isotopically depleted by condensation and subsequent interaction with falling raindrops (Lee et al., 2008).

#### *3.1.3.4.1 The Temperature Effect*

The temperature effect describes the positive correlation between a site's mean annual temperature (MAT) and the mean  $\delta^{18}\text{O}$  of precipitation at the site, and can be expressed as  $d\delta^{18}\text{O}_p / dT$  (Dansgaard, 1964, Fricke and O'Neil, 1999).  $d\delta^{18}\text{O}_p / dT$  is variable and site dependent (Dansgaard, 1964, Rozanski et al., 1982, 1993), and may have been different in the past (McDermott, 2004). Changes in the seasonality of precipitation, or changes in moisture source, could also lead to variations in  $d\delta^{18}\text{O}_p / dT$  over time (Charles et al., 1994, Denton et al., 2005).

The average temperature dependence of  $\delta^{18}\text{O}$  of modern precipitation in the mid-to-high latitudes is approximately 0.6‰/°C, with a range of 0.58 to 0.9‰/°C in the region 40°N-60°N (Winograd et al., 1988, Gascoyne, 1992, Rozanski et al., 1993, Lauritzen, 1995, Dorale et al., 1998, Ku and Li, 1998). In the western Mediterranean region, the value was found to be +0.2 - 0.34‰/°C (Bard et al., 2002, Domínguez-Villar et al., 2008). This temperature dependence does not apply in low latitudes or monsoon-affected areas (Dansgaard, 1964, Rozanski et al., 1993). Thus, latitude has a large effect on the isotopic composition of air masses.

The temperature effect also has an effect on seasonal scales, as  $\delta^{18}\text{O}_p$  is generally lower in winter, when temperatures are colder, and higher in summer when they are warmer. The temperature effect is the primary cause of these variations, but seasonal variations in moisture source may also have an effect (Lachniet, 2009).

#### *3.1.3.4.2 The Altitude Effect*

The altitude effect describes the decrease in  $\delta^{18}\text{O}$  values as altitude increases (Clark and Fritz, 1997), which has an approximate range of -2 to -3‰  $\delta^{18}\text{O}$  km<sup>-1</sup> (Gonfiantini et al., 2001, Poage and Chamberlain, 2001, Fleitmann et al., 2004, Lachniet and Patterson, 2006). This is caused by the decreasing temperature of condensation with altitude, and to increased Rayleigh distillation due to orographic uplift (Lachniet, 2009). As a result of this effect, a pronounced "isotopic rain shadow" may be visible in the lee-side of high mountain ranges (Blisniuk and Stern, 2005).

#### 3.1.3.4.3 *The Continental Effect*

The continental effect describes the progressive rainout and cooling of an air mass as it moves over a continent, away from the ocean, leading to a decrease in water  $\delta^{18}\text{O}$  (Dansgaard, 1964, Rozanski et al., 1993, Clark and Fritz, 1997). However, the continental effect may be counteracted by moisture recycling in some areas, where high  $\delta^{18}\text{O}$  continental moisture is returned to the atmosphere by evaporation of water bodies such as lakes, rivers, and even soil water (Koster et al., 1993), leading to a reduction in the degree to which  $\delta^{18}\text{O}$  decreases with distance from the ocean (Lachniet, 2009).

#### 3.1.3.4.4 *The Amount Effect*

$\delta^{18}\text{O}_p$  is inversely correlated with precipitation amount in low latitude and coastal regions, i.e.  $\delta^{18}\text{O}_p$  gets lower as rainfall amount increases (Dansgaard, 1964, Rozanski et al., 1993). This is known as the amount effect. The amount effect is most pronounced in the tropics, especially tropical ocean island locations close to the ITCZ with mean annual temperature exceeding  $15^\circ\text{C}$  (Dansgaard, 1964, Rozanski et al., 1993, Wang et al., 2001, Yuan et al., 2004). The amount effect is the dominant effect on  $\delta^{18}\text{O}_c$  in the tropics, monsoonal areas (e.g. Johnson et al., 2006b, Wang et al., 2008), and some semi-arid areas as partial re-evaporation of weak rains in the atmosphere may occur (Fairchild and McMillan, 2007).

Sites some distance inland may not be suitable for interpreting in terms of local precipitation amount, with  $\delta^{18}\text{O}_p$  instead being modified by changes in upstream  $\delta^{18}\text{O}_v$  (Drysdale et al., 2004).

#### 3.1.3.4.5 *The Source Effect*

The source of an air mass has a prominent effect on its isotopic composition, due to various factors such as air mass history, temperature of a moisture source and regional  $\delta^{18}\text{O}$  variation of the ocean (LeGrande and Schmidt, 2006, Lachniet, 2009) and air masses originating from different source regions will have distinct  $\delta^{18}\text{O}$  signatures (Rozanski et al., 1993, Clark and Fritz, 1997, Cole et al., 1999, Friedman et al., 2002).

This effect also interplays with changes in seasonality to bring about large changes in mean annual  $\delta^{18}\text{O}$  on palaeoclimatic timescales, as a change in the relative proportion of summer vs. winter precipitation may lead to more precipitation deriving from one moisture source over another (Lachniet, 2009). Advection of air masses along trajectories which are warmer or cooler will also lead to variations in the degree of rainout, which also affects  $\delta^{18}\text{O}$  of precipitation (McDermott et al., 1999).

Changes in meteoric moisture sources have been inferred as the main driver for  $\delta^{18}\text{O}$  variations in a number of speleothem studies (Bar-Matthews et al., 2003, Fleitmann et al., 2003b, Cobb et al., 2007).

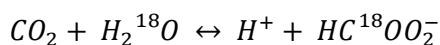
#### 3.1.3.4.6 *The Ice Volume Effect*

Changes in continental ice volume at glacial/interglacial transitions result in a change in the  $\delta^{18}\text{O}$  of the ocean (Lauritzen and Lundberg, 1999, McDermott, 2004).  $\delta^{18}\text{O}$  of the ocean will increase as continental ice volume increases, due to the fact that evaporation of ocean water preferentially removes light isotopes from the ocean (Lachniet, 2009). The maximum  $\delta^{18}\text{O}$  change attributed to this effect during the Quaternary is approximately 1.0-1.2 ‰ (Schrag et al., 1996, 2002, Lea et al., 2002), and the collapse of ice caps in the early Holocene led to a  $\delta^{18}\text{O}$  decrease of 0.3‰ (Stuiver et al., 1995). However, a cooler glacial sea surface temperature would affect the temperature-dependent equilibrium fractionation between liquid and water vapour at the ocean surface, such that rainfall  $\delta^{18}\text{O}$  would decrease, which would partially or even wholly offset the increase in  $\delta^{18}\text{O}$  caused by increased ice volume (Lauritzen and Lundberg, 1999, Lachniet, 2009).

#### 3.1.3.5 $\delta^{18}\text{O}$ of Karst Waters

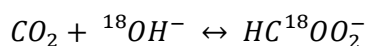
The oxygen isotopic signal of speleothem calcite reflects a component of the isotopic signature of cave seepage waters, which are affected not only by the factors which affect the  $\delta^{18}\text{O}$  of precipitation listed above, but also processes in the surface-karst-cave system, such as evaporative enrichment at the surface or in the epikarst zone, changing water transit times in the karst system, complex mixing histories or seasonal changes in the rate of calcite deposition (McDermott et al., 2006).

Oxygen atoms in the seepage waters can be exchanged with oxygen atoms in the carbonate bedrock by the reactions (Dreybrodt, 2011a):



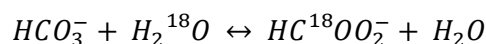
*Equation 3.9: Oxygen atom exchange between bedrock and seepage waters (A)*

And



*Equation 3.10: Oxygen atom exchange between bedrock and seepage waters (B)*

Which can be summarised as



*Equation 3.11: Oxygen atom exchange between bedrock and seepage waters (Summary)*

After a sufficiently long time (8 hours at 25°C, 29 hours at 10°C, 54 hours at 5°C) (Beck et al., 2005), the oxygen atoms in the carbonate will be in equilibrium with the oxygen atoms in the seepage water, and will contain a climatic signal, but waters which reach the cave in less time than is required for this equilibrium to take place will not represent a climatic signal (Dreybrodt, 2011b).

The high frequency signal may be dampened by mixing of older stored waters and younger waters relating to specific infiltration events in the epikarst, and rate of infiltration (Fairchild et al., 2006). Different parts of the aquifer may store water from different seasons, which will have different isotopic composition (Fairchild et al., 2007).

**3.1.3.6  $\delta^{18}O_d$  and  $\delta^{18}O_c$**

The drip water composition is dependent on several factors, including the composition of  $\delta^{18}O_p$ , and interactions in the unsaturated zone between water, soil and rock (Hendy and Wilson, 1968, Hendy, 1971, Bar-Matthews et al., 1996, Ayalon et al., 1998). The cave temperature effect causes thermodynamic fractionation between dripwater and calcite in precipitation, although this effect is small (Lauritzen and Lundberg, 1999).

The isotopic composition of dripwater most likely constitutes a mixture of longer residence time stored water, with event water of short term residence time (Jex et al., 2010).

“Flashy” drip sites typically result in fast drips which show a large seasonal variation in  $\delta^{18}O$ , reflecting minimum storage and homogenisation in the epikarst (McDermott et al., 2006).

Seepage flow drips are slow drips associated with large storage components (McDermott et al., 2006), in which  $\delta^{18}O$  typically reflects annual precipitation  $\delta^{18}O$  (Yonge et al., 1985).

Increased residence times (for example in drier periods) lead to the attenuation of seasonal  $\delta^{18}O$  variations which result in the  $\delta^{18}O$  of dripwater being closer to the  $\delta^{18}O$  of precipitation in the region above the cave (McDermott et al., 2006). In shallow temperate-zone caves in which drip-sites are fed by seepage flow,  $\delta^{18}O_d$  is likely to represent mean regional precipitation (McDermott et al., 1999, Frumkin et al., 2000).

In arid or semi-arid areas, a negative balance between precipitation and evaporation during the summer months may lead to near-surface evaporative effects, which may shift  $\delta^{18}O$  to higher values (Bar-Matthews et al., 1996, Bar-Matthews et al., 1997). At such sites, while in theory warm-dry conditions could cause higher  $\delta^{18}O$  and cold-wet conditions could cause lower  $\delta^{18}O$ , the isotopic signal could in fact be cancelled out if other combinations of

temperature and precipitation amount existed (McDermott et al., 1999). Using meteorological data, it is possible to assess whether a negative balance between precipitation and evapotranspiration occurs during the summer months in the present day, but to assess whether this also occurred in the past, high  $\delta^{18}\text{O}$  values in speleothem calcite should be compared with the growth rate, to see whether precipitation amount or temperature was causing the  $\delta^{18}\text{O}$  variation (McDermott et al., 1999).

It was suggested by Hendy (1971) that in cases of drip waters from which  $\text{CO}_2$  was rapidly degassed,  $\delta^{13}\text{C}$  would move to higher values while  $\delta^{18}\text{O}$  would remain unchanged by this effect provided that continuous  $^{18}\text{O}$  equilibrium exchange with oxygen isotopes in the water reservoir was possible. Both  $\delta^{13}\text{C}$  and  $\delta^{18}\text{O}$  would be driven to higher values in situations where rapid precipitation also occurred (Hendy, 1971).

If drip times are fast, i.e.  $T_d \leq 0.1(\tau_p)$ , where  $T_d$  is the drip interval, and  $\tau_p$  is the time constant for the precipitation of calcite, the oxygen and carbon isotopic composition of the dripwater carbonate increases due to Rayleigh distillation by less than 0.3‰ (Dreybrodt and Scholz, 2011). Fractionation of carbon and oxygen increases to a few ‰ heavier for drip times  $T_d > 3(\tau_p)$  (Dreybrodt, 2008, Scholz et al., 2009, Dreybrodt and Scholz, 2011).

Kinetic effects such as high supersaturation (Kim and O'Neil, 1997) or  $\text{CO}_2$  outgassing and evaporation (González and Lohmann, 1988) during calcite precipitation may lead to high frequency noise in the isotopic signal which may be identifiable by Hendy tests (Hendy, 1971). Covariation of  $\delta^{18}\text{O}$  and  $\delta^{13}\text{C}$  through time suggests the possibility of kinetic fractionation (Hendy, 1971). Kinetic fractionation may occur due to evaporation of dripwater in low humidity cave environments, or due to rapid degassing of super-saturated drip waters (Mickler et al., 2004). It may be possible to identify if rapid degassing has occurred if drip rates are fast or if the drip waters have a high saturation index (Jex et al., 2010). Seasonal variation in drip water  $p\text{CO}_2$  may be identifiable by sub-annual covariation between  $\delta^{18}\text{O}$  and  $\delta^{13}\text{C}$  in speleothem calcite (Jex et al., 2010).

At mid to high latitudes there is a positive correlation between temperature and  $\delta^{18}\text{O}_c$  (i.e. in the opposite direction to  $d\delta^{18}\text{O}_p / dT$ ), but this should be tested at each site (Fairchild et al., 2007). At 25°C,  $d\delta^{18}\text{O}_c / dT$  is approximately -0.23‰/1°C, a value which is an average of numerous experiments where calcite has been precipitated in the laboratory, (O'Neil et al., 1969, Tarutani et al., 1969, Kim and O'Neil, 1997, Jiménez-López et al., 2001).

However, in experiments carried out at such low temperatures as these (i.e. <40°C), it is

difficult or impossible to prove that calcite precipitation is occurring in oxygen isotopic equilibrium with the water (Coplen, 2007). As calcite precipitated in caves as speleothems is precipitated more slowly than in laboratory experiments, it is more likely to be closer to equilibrium (Tremaine et al., 2011).

Theoretically, an increase in air temperature could lead to an increase, decrease or maintenance of  $\delta^{18}\text{O}_c$ , as the degree to which  $\delta^{18}\text{O}$  of precipitation changes with temperature may be greater, smaller or equal to the temperature-dependent fractionation which accompanies calcite deposition within the cave ( $d\delta^{18}\text{O}_c / dT$ ) (McDermott, 2004, McDermott et al., 2006). As the temperature dependence of  $\delta^{18}\text{O}_p$  is on average more positive than the calcite-water fractionation, it is expected that in the absence of other processes, a rise in temperature would result in a net shift to heavier O isotopes, but only where near surface evaporative effects are minimal (McDermott et al., 1999). However, as the temperature-dependent fractionation between drip-waters and calcite can potentially be either positive or negative,  $\delta^{18}\text{O}_c$  cannot be simply interpreted relative to temperature change, and therefore it is important to utilise additional proxies from the speleothem, such as fluid inclusion data, changes in growth rate and annual layer thickness variations in order to reach a more meaningful interpretation (McDermott et al., 1999, McDermott, 2004, McDermott et al., 2006).

### **3.1.4 Carbon Isotopes**

There are two stable isotopes of carbon,  $^{12}\text{C}=98.89\%$  and  $^{13}\text{C}=1.11\%$  (Nier, 1950). Values of  $\delta^{13}\text{C}$  are generally reported in comparison to the Pee Dee Belemnite (PDB) standard (Morse and Mackenzie, 1990), and the  $\delta^{13}\text{C}$  of PDB is zero (Sharp, 2007).

#### ***3.1.4.1 Origin of Speleothem $\text{CaCO}_3$ Carbon***

Sources of carbon in drip water are atmospheric carbon dioxide, soil biogenic carbon dioxide and dissolution of karst bedrock (Fairchild et al., 2007). The bulk of dripwater carbon comes from organic sources, with dripwater and modern speleothems typically containing 80-95% modern carbon (Genty et al., 2001a).

##### ***3.1.4.1.1 Atmospheric carbon dioxide***

Rainwater droplets may absorb carbon dioxide as they fall through the atmosphere, but the amount is thought to be small and not contribute a large proportion to the bicarbonate in soil water (Vaks et al., 2010). Atmospheric carbon dioxide has a lower  $\delta^{13}\text{C}$  value over the

continents than over oceanic areas due to influence from respiration, decay of plant matter, and in modern times, fossil fuel combustion (Develle et al., 2011).

#### 3.1.4.1.2 *Soil Biogenic Carbon Dioxide*

Soil atmosphere carbon dioxide may be up to several orders of magnitude higher in concentration than atmospheric carbon dioxide (Salomons and Mook, 1986). It has been shown that soil CO<sub>2</sub> may contribute up to 80-95% of speleothem carbon (Genty et al., 2001a, Genty and Massault, 1999, Genty et al., 1999), although some speleothems form in the absence of soils (Fairchild and Baker, 2012). Overproduction of carbon dioxide promotes equilibration and leads to complete equilibration. This is known as the “oversupplied open system” (Fairchild and Baker, 2012).

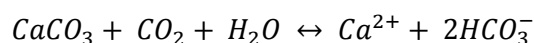
In temperate climates, soil CO<sub>2</sub> derives mostly from decomposition of organic matter and plant root respiration (Lasaga, 1981). In the Mediterranean, soil CO<sub>2</sub> production is low in the dry summer, increases in the autumn due to increased precipitation, followed by a decrease in winter due to low temperatures (Billès et al., 1971).

Soil-CO<sub>2</sub> varies on a seasonal cycle; values are close to atmospheric levels in the winter, and exhibit a rapid decrease in the growing season (Rightmire, 1978). This is believed to be caused by invasion of atmospheric CO<sub>2</sub>, which can cause the δ<sup>13</sup>C value of soil CO<sub>2</sub> to be several ‰ higher than the value which would be derived from plant respiration alone (Dreybrodt and Scholz, 2010).

Soil atmosphere carbon dioxide was found to have δ<sup>13</sup>C values ranging from -10‰ to -28‰, with two maxima at -23‰ and -16‰ (Deines, 1980, Salomons and Mook, 1986). This signal is believed to be related to photosynthetic pathway, which will be discussed below.

#### 3.1.4.1.3 *Dissolution of Karst Bedrock and Calcareous Soils*

The simple model for dissolution of calcium carbonate in calcareous soils is (Münnich, 1957)



*Equation 3.12: Calcium carbonate dissolution in calcareous soils*

The equation is reversible, as the backwards reaction accounts for precipitation of calcite, with associated CO<sub>2</sub> degassing. As degassing occurs, <sup>12</sup>C is lost from the HCO<sub>3</sub><sup>-</sup><sub>(aq)</sub> reservoir,

which cannot be offset by the loss of  $^{13}\text{C}$  through precipitation of calcite, leading to Rayleigh-type enrichment (Mickler et al., 2004).

This equation assumes that the carbon in soil solution derives half from biogenic  $\text{CO}_2$  and half from carbonate rock, which although a simple approximation, does not account for other factors such as the differing isotopic composition of biogenic carbon dioxide produced by C3 and C4 plants, evaporation, exchange with atmospheric carbon dioxide (Salomons and Mook, 1986), and oversupply of  $\text{CO}_2$ .

### ***3.1.4.2 Open-System vs. Closed-System***

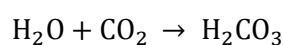
The processes which control the mechanisms by which percolating waters become saturated with calcium carbonate in the soil and bedrock above the cave have been simplified and grouped into two end-member models (Zhou et al., 2008a, Salomons and Mook, 1986).

#### *3.1.4.2.1 Open-System*

In an open system, the groundwater reacts with calcium carbonate while in contact with a gas phase of fixed  $p\text{CO}_2$  (Salomons and Mook, 1986, Hendy, 1971). The open-system model assumes an infinite supply of  $\text{CO}_2$  and continuous equilibrium between the seepage water and  $\text{CO}_2$ , leading to a steady increase in bicarbonate content as dissolution in the unsaturated zone increases (Salomons and Mook, 1986). The  $\delta^{13}\text{C}$  of the dissolved species in an open system is understood to represent the isotopic composition of soil  $\text{CO}_2$ , and not to contain any discernible effects of bedrock carbonate (Salomons and Mook, 1986). During open-system evaporation, the isotopic composition of both carbon and oxygen will change, according to simple Rayleigh processes (Salomons and Mook, 1986).

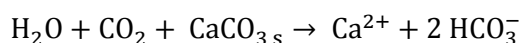
#### *3.1.4.2.2 Closed-System*

In the closed system, the groundwater equilibrates with a carbon dioxide reservoir before coming into contact with the calcium carbonate, and subsequently becomes isolated from the reservoir before calcium carbonate dissolution (Salomons and Mook, 1986, Hendy, 1971). As the  $\text{CO}_2$  is finite, limestone dissolution is limited by the consumption of  $\text{CO}_2$  through carbonation:



*Equation 3.13: Formation of carbonic acid*

The dissolved carbon dioxide then reacts with the CaCO<sub>3</sub> via the reaction (Salomons and Mook, 1986):



*Equation 3.14: Limestone dissolution*

In contrast to the open system in which it is the soil CO<sub>2</sub> which contributes the signal prevailing in δ<sup>13</sup>C of DIC, in the closed system it is the host bedrock which influences the isotopic composition of the DIC (McDermott, 2004). Modelled results show that in a fully closed system, up to 50% of dissolved carbon may be derived from the host rock (Hendy, 1971).

### ***3.1.4.3 Causes of variations in δ<sup>13</sup>C***

Identifying the causes of speleothem δ<sup>13</sup>C variations can be difficult due to the fact that so many processes can have an effect. Such factors include:

- The ratio of C<sub>3</sub> to C<sub>4</sub> plants in the vegetation above the cave (Dorale et al., 1998, Dorale et al., 1992)
- The rate of soil respiration (Genty et al., 2001a, Genty et al., 2003).
- The relative contributions of soil-respired CO<sub>2</sub> and atmospheric CO<sub>2</sub> to dissolved inorganic carbon (Genty et al., 2001a, Genty et al., 2003, Dulinski and Rozanski, 1990).
- Variations in fluid-rock interaction (Hendy, 1971, Genty et al., 2001a).
- CO<sub>2</sub> degassing and prior calcite precipitation (PCP), which is common in semi-arid, highly seasonal epikarst regions, causing more <sup>13</sup>C-enriched dripwater, and subsequently speleothem calcite (Baker et al., 1997, Mickler et al., 2004).
- Isotopic disequilibrium occurring during calcite precipitation (Hendy, 1971, Mickler et al., 2004).
- Progressive enrichment in <sup>13</sup>C with distance along a speleothem that water flows before calcite is precipitated (Baker et al., 1997).

#### ***3.1.4.3.1 The Palaeovegetation Signal***

Where appropriate, large shifts in δ<sup>13</sup>C can be attributed to the difference between δ<sup>13</sup>C of CO<sub>2</sub> respired by a C<sub>3</sub> versus a C<sub>4</sub> assemblage (McDermott, 2004, Dorale et al., 1992, Dorale et al., 1998).

At its simplest,  $\delta^{13}\text{C}$  should be lighter when  $\text{C}_3$  plants dominate and there is unlimited water, and heavier when  $\text{C}_4$  plants dominate or conditions are arid (Dorale et al., 1992, Dorale et al., 1998, Fairchild et al., 2007). In cold, wet conditions,  $\text{C}_3$  photosynthetic pathway plants dominate, resulting in a more negative  $\delta^{13}\text{C}$  value of soil biogenic  $\text{CO}_2$ , compared to the soils in which  $\text{C}_4$  grasses grow, when drier conditions prevail (Fairchild et al., 2007). For changes in the ratio of  $\text{C}_3$  to  $\text{C}_4$  plants to be considered as a mechanism for changes in speleothem  $\delta^{13}\text{C}$ , it is important to consider whether both types of plants are known to have grown at a location during the time period (Genty et al., 2003).

The difference in  $\delta^{13}\text{C}$  signal which arises from vegetation changes is linked to the photosynthetic pathway utilised by vegetation in the area. The Calvin-Benson (or non-Kranz) photosynthetic pathway is known more simply as " $\text{C}_3$ ", which includes almost all trees and many grasses, and allows plants to be better suited to cooler, moister growing seasons (Holland et al., 1964). It produces plant material with  $\delta^{13}\text{C}$  ranging from -22 to -34 ‰, with a peak at  $-27 \pm 2$  ‰ (Salomons and Mook, 1986). The Hatch-Slack (or Kranz) pathway is known as " $\text{C}_4$ ", and allows other grasses to thrive in hot, dry climates (Holland et al., 1964). It produces plant material with  $\delta^{13}\text{C}$  between -9 to -19 ‰, with a peak at  $-12 \pm 2$  ‰ (Salomons and Mook, 1986). The Crassulacean Acid Metabolism (CAM) cycle produces a carbon isotopic composition that is intermediate between  $\text{C}_3$  and  $\text{C}_4$ , with an average value of ca. -17‰ (Salomons and Mook, 1986).

Soil  $\text{CO}_2$  is always slightly less negative than the  $\delta^{13}\text{C}$  of the plant material, due to preferential uptake of  $^{12}\text{C}$  during plant material formation, preferential release of  $^{13}\text{C}$  in  $\text{CO}_2$  during respiration (Frumkin et al., 2000) and diffusive loss of  $^{12}\text{C}$  from the soil (Cerling, 1984). Soil respired  $\text{CO}_2$  in equilibrium with  $\text{C}_3$  vegetation will have a  $\delta^{13}\text{C}$  of approximately -26‰ to -20‰, with an average of -26‰, while soil respired  $\text{CO}_2$  in equilibrium with a dominantly  $\text{C}_4$  assemblage generally has a  $\delta^{13}\text{C}$  signature in the range of -16‰ to 10‰, with an average of -13‰ (Bar-Matthews et al., 1991, McDermott, 2004, McDermott et al., 2006). The  $\text{C}_4$  signature is noticeably heavier, and even after the fractionations associated with various processes leading to carbonate precipitation, the difference is preserved in the  $\delta^{13}\text{C}$  of the secondary carbonates, as carbonates deposited in equilibrium with  $\text{CO}_2$  respired from  $\text{C}_3$  vegetation will typically fall in the range -14‰ - -6‰, while a  $\text{C}_4$  system yields carbonates with a  $\delta^{13}\text{C}$  range of -6‰ - +2‰ (McDermott, 2004). In dry conditions, the  $\delta^{13}\text{C}$  of respired soil  $\text{CO}_2$  of  $\text{C}_3$  plants is isotopically heavier due to restricted stomatal conductance (Paulsen et al., 2003).

Minimal soil and vegetation cover above the cave can result in increased  $\delta^{13}\text{C}$  (Bar-Matthews et al., 2003, Cerling, 1984), while an increase in vegetation density can also lead to  $\delta^{13}\text{C}$  decrease due to increased input of isotopically light biogenic carbon to the total dissolved organic carbon (DIC) (Baldini et al., 2005).

#### *3.1.4.3.2 Climatic Causes*

Periods of climatic amelioration and/ or increased precipitation may lead to increased levels of soil biogenic  $\text{CO}_2$  (Raich and Schlesinger, 1992), which has a lighter  $\delta^{13}\text{C}$  signal than atmospheric  $\text{CO}_2$ , thus resulting in a lighter  $\delta^{13}\text{C}$  signal in the speleothem signal (Genty et al., 2003).

During wet periods, deluge events may strip soil cover, or lead to such short residence times that it is not possible for significant amounts of soil  $\text{CO}_2$  to be dissolved (Paulsen et al., 2003, Bar-Matthews et al., 1997). This sequence of events may lead to high  $\delta^{13}\text{C}_c$ , low  $\delta^{18}\text{O}_c$ , low deposition rate and increased detritus in the calcite matrix (Bar-Matthews et al., 1997). Prior calcite precipitation may be reduced during periods of increased rainfall (Fairchild et al., 2000), thus removing this mechanism for  $\delta^{13}\text{C}$  enrichment (Zanchetta et al., 2007).

#### *3.1.4.3.3 Growth Rate*

At slow growth rates, thermodynamic isotopic fractionation causes large fractionation as precipitation of the heavier isotope-bearing ions is favoured, while at fast growth rates, the competing effects of thermodynamic fractionation and kinetic fractionation (which favours light isotope-bearing ions) leads to a smaller fractionation (Turner, 1982, Fairchild et al., 2007).

#### *3.1.4.3.4 Prior Calcite Precipitation*

Prior calcite precipitation (PCP) in the vadose zone can cause increased  $\delta^{13}\text{C}$  (Baker et al., 1997). More positive speleothem  $\delta^{13}\text{C}$  was found to correlate with times of lower fractions of  $\text{HCO}_3^-$  (aq) remaining in solution (modelled), which is an indication of increased prior calcite precipitation, and believed to be due to decreased rainfall leading to increased seepage water residence time (Oster et al., 2009, Oster et al., 2010).

Slow seepage rates lead to calcite with isotopically heavier  $\delta^{13}\text{C}$  being precipitated, as more calcite will have been precipitated from the solution at any given point compared with a faster flowing water (Baker et al., 1997).

PCP will be discussed further in Section 3.2.4.4 in relation to trace element variations.

#### 3.1.4.3.5 *Degassing*

There is still some uncertainty concerning the propriety of  $\delta^{13}\text{C}$  for use as a climate proxy, as kinetic fractionation may occur during  $\text{CO}_2$  degassing (Genty et al., 2003), although this process has generally been assumed to have only a small effect on  $\delta^{13}\text{C}$  of speleothem calcite, and equilibrium isotopic fractionation was therefore expected to be sufficient in explaining the process of degassing (Hendy, 1971, Salomons and Mook, 1986). However, the initial, rapid degassing which occurs without calcite precipitation and without a back-reaction, and would result in an increase of  $\delta^{13}\text{C}_{\text{DIC}}$  value (Dulinski and Rozanski, 1990). Recently, Tremaine et al. (2011) have shown a direct connection between calcite growth rates, seasonal calcite  $\delta^{13}\text{C}$  and ventilation-driven  $p\text{CO}_2$ -gradients, with  $\delta^{13}\text{C}$  decreasing along the ventilation pathway. Therefore, they suggest that calcite  $\delta^{13}\text{C}$  may be useful as a proxy for cave air ventilation, in addition to the traditionally used interpretations such as overlying vegetation.

#### 3.1.4.3.6 *Ventilation*

Forced degassing related to oscillating cave ventilation can produce higher  $\delta^{13}\text{C}$  (Frisia et al., 2000, Spötl et al., 2005).

## **3.2 Minor and Trace Elements**

### **3.2.1 Origins of Trace Elements in Speleothems**

There can be significant variations in trace element composition within the cave same cave chamber, as well as temporal variations throughout the year, necessitating awareness of the processes which control trace element concentrations at a site (Fairchild and Treble, 2009).

#### ***3.2.1.1 Initial Carbonate Dissolution***

The bulk of cations incorporated into speleothem carbonate originate from carbonate dissolution in the soil and bedrock and overlying regolith (Fairchild et al., 2007, Fairchild and Treble, 2009). There is also a contribution from marine aerosols and pollutants (Fairchild et al., 2007).

Transport of a trace element into the bedrock originally is dependent on two factors; mobilization of the element in the soil and underlying epikarst, and hydrological processes which influence infiltration into the epikarst (Fairchild and Treble, 2009). Dissolution of carbonate to saturation, either in the soil or epikarst, occurs under high  $p\text{CO}_2$ , under which conditions dissolved chemical species loads will therefore be higher (Fairchild et al., 2000, Fairchild and Treble, 2009, Atkinson, 1977, Drake, 1983).

The relative proportions of calcite and dolomite encountered by water flowing through the karst will affect its trace element chemistry, as will transit time from surface to drip site (Fairchild et al., 2000, Roberts et al., 1998).

#### ***3.2.1.2 Mobilisation of Trace Elements in Soils and Epikarst***

Other ways in which trace elements can be incorporated into groundwaters and subsequently speleothems require mobilisation of such elements in the soils and epikarst, and require varying amounts of time:

Pre-existing solutes, mobilised particles and colloids may become incorporated into the percolating groundwater, weakly adsorbed/absorbed species may be leached from substrates, or dissolution of salts may add trace elements to the groundwater; all these processes are rapid (Fairchild and Treble, 2009). Calcite dissolution can add elements at an intermediate speed, while chemical weathering of various minerals such as dolomite, silicates, phosphates, oxides, and sulphides is a slow process (Fairchild and Treble, 2009).

Slower dissolution processes are of greater influence in seepage flow dominated systems, such as those studied in glacial settings (Fairchild et al., 1994, Fairchild et al., 1999).

Trace element activities in soil waters may be strongly affected by changes in soil acidity, soil CO<sub>2</sub> concentration and organic chemistry; thus the same controls will exert a control on cave seepage waters (Hellstrom and McCulloch, 2000).

### **3.2.2 Incorporation of Trace Elements into Speleothems**

There are several ways in which trace elements can become incorporated into speleothems:

1. Substitution of divalent ions for Ca<sup>2+</sup> or CO<sub>3</sub><sup>2-</sup> in the lattice (Fairchild et al., 2006, Fairchild et al., 2007), defined by the partition coefficient (K) (Fairchild et al., 2007).
2. Interstitial incorporation of ions or molecules, where growth defects exist and so ion size is less important (Fairchild and Treble, 2009, Fairchild et al., 2007, Fairchild et al., 2006). Incorporation of trace elements at defect sites is increased where crystal growth surfaces are rough; which in turn is more likely in speleothems which undergo faster growth and precipitate from solutions with higher levels of supersaturation (Frisia et al., 2000)
3. As part of fluid inclusions, or solid inclusions (i.e. not as part of the CaCO<sub>3</sub> phase) (Fairchild et al., 2007).

Different types of crystal face will have different trace element chemistry, resulting in sector zoning (Reeder and Grams, 1987). Aragonite, as an orthorhombic mineral which develops a number of forms, displays this behaviour to a greater extent than calcite, and as such can exhibit complex lateral changes (Finch et al., 2003). Calcite is generally simpler, growing in most cases as the unit rhombohedron, with micron-scale crystallites conglomerating to form larger crystals (Frisia et al., 2000).

Trace element levels in speleothems are controlled by several factors, such as drip water trace element concentrations, physical conditions such as temperature (Finch et al., 2001), and characteristics of the crystallographic site the trace element will occupy, such as fusing of crystallites or presence of foreign ions (Treble et al., 2005a). Kinetic factors such as drip rate may be important under disequilibrium conditions (Finch et al., 2001).

### **3.2.3 Methods of Trace Element Analysis**

Until the turn of the new millennium, trace element analysis was primarily performed by atomic absorption spectrometry or ICP-AES, involving several milligrams of sample powder

being first dissolved in dilute acid. At the present, analysis is moving towards in situ micro-analysis by laser-ablation (Fairchild et al., 2006).

Laser-ablation-inductively coupled plasma-mass spectrometry (LA-ICP-MS) analysis is advantageous as analysis is very rapid, and sensitive enough to provide annual resolution on moderate to fast-growing samples (Fairchild et al., 2006). Sub-annual resolution should even be possible on all but the slowest growing stalagmites (Treble et al., 2003, Treble et al., 2005a, Desmarchelier et al., 2006). Standards must be matrix-matched to samples (Fairchild and Treble, 2009). Robustness can be increased by stacking parallel traverses (Treble et al., 2003). Where material is not damaged by ablation, a line scan can be used (Fairchild et al., 2006).

### **3.2.4 Interpreting Trace Element Variations**

The causes of trace element variations can be complex, with factors such as the presence of micro domains, replacement phenomena and non-equilibrium incorporation to be considered (Treble et al., 2003, Treble et al., 2005a), and inadequate information about cave water chemistry can make interpretation less reliable (McMillan et al., 2005).

Contemporaneous speleothems from within a single cave can may show trace element variations which are so variable from each other as to shed doubt on the usefulness of trace elements in speleothems for palaeoclimatic interpretation (Roberts et al., 1999a). Trace element variations laterally along growth layers also is a potential problem, to which Treble et al. (2005a) suggested the solution would be to conduct several closely spaced parallel tracks.

Five influences on geochemistry have been identified, which all apply to trace elements: atmospheric input, soil and vegetation, interaction with the karstic aquifer, primary crystal growth at a speleothem, and secondary alteration (Fairchild et al., 2006).

When comparing speleothems from several caves in Korea, some of which were primary calcite/aragonite and some of which were neomorphic calcite, (Woo and Choi, 2006) found that the composition of local cave water had more of an influence on speleothem trace element chemistry than processes such as evaporation and degassing.

#### **3.2.4.1 Distribution Coefficients**

The equation defining the distribution coefficient of a particular trace element is as follows:

$$\left(\frac{Tr}{Ca}\right)_{CaCO_3} = K_{Tr} \left(\frac{Tr}{Ca}\right)_{solution}$$

### Equation 3.15: Defining distribution coefficients of elements

where  $Tr$  is the trace element ion in question and  $K_{Tr}$  is the distribution coefficient (Morse and Bender, 1990). The partition coefficients for Mg and Sr into calcite are  $\ll 1$  (Morse and Bender, 1990), causing Mg/Ca and Sr/Ca to rise as calcite precipitation occurs (Fairchild et al., 2000).

$K_{Tr}$  values for a particular element will be different for aragonite and calcite, so it is important to distinguish between the two phases (McMillan et al., 2005, Ortega et al., 2005, Fairchild and Treble, 2009). For Mg,  $K$  is believed to vary only with temperature for Mg (Huang and Fairchild, 2001, McMillan et al., 2005). Influences on other elements' partition coefficients include growth rate, growth mechanism, and structural characteristics of growth surfaces (Lorenz, 1981, Morse and Bender, 1990, Paquette and Reeder, 1995).

Ratios allow bedrocks to be compared with the solutions expected to arise from congruent dissolution of different mixes of bedrocks (Fairchild and Treble, 2009). Where waters lie above the mixing line, it is likely there are additional processes occurring, which may include the selective release of Mg and Sr from freshly broken calcite surfaces (McGillen and Fairchild, 2005), or redissolution of Mg and Sr-bearing salts precipitated in drying soils in the summer (Fairchild and Treble, 2009).

It is understood that the distribution coefficient approach is inadequate to fully understand trace element variation due to the differences between sites at which trace elements can be incorporated, however as most variations are on such a small scale that their effects are averaged out, the distribution coefficient approach can still be useful (Fairchild and Treble, 2009).

#### ***3.2.4.2 Mg and Sr Variations***

Where Mg/Ca and Sr/Ca vary antipathetically, this can be explained by differential dissolution of dolomite and calcite (Fairchild et al., 2000, Roberts et al., 1998). Where they vary sympathetically, this can be caused by enhanced selective leaching with prolonged contact times between water and rock, and/or prior precipitation (Fairchild et al., 2000). Strong covariation between Mg and Sr in speleothems can be inferred to have been caused by prior calcite precipitation (McMillan et al., 2005, Johnson et al., 2006a).

Drip-water Mg/Ca and Sr/Ca often increase during times of aridity (Huang and Fairchild, 2001). Verheyden et al (2000) concluded that Mg/Ca and Sr/Ca changes in a Belgian speleothem were a result of changes in water residence time in the vadose zone, but

caution that such changes may occur following changes in effective precipitation, or alternatively may simply reflect changes in the routing of seepage water (Domenico and Schwartz, 1990, Roberts et al., 1999a). As speleothem  $\delta^{18}\text{O}$  is not affected by seepage water routing (Harmon, 1979, Yonge et al., 1985), covariation between  $\delta^{18}\text{O}$ , Mg/Ca and Sr/Ca can be interpreted as meaning that routing is not the driver of changes in Mg/Ca and Sr/Ca (Verheyden et al., 2000).

#### **3.2.4.3 Precipitation Variations**

Trace element enrichment can occur as a result of high flow as species may be transported with colloids (Huang et al., 2001, Borsato et al., 2007, Zhou et al., 2008b). For example, zones of enrichment of Mn, P and rare earth elements may be linked to colloidal transport during periods of high flow (Zhou et al., 2008b). Dripwater Mg/Ca can exhibit dilution effects under high flow conditions (Fairchild and Treble, 2009), and large rainfall events can cause a switch from seepage flow to the faster shaft flow, which can cause variations in dripwater (and speleothem) Mg/Ca (Fairchild and Treble, 2009).

At low flow, fracture-fed flow through the aquifer is minimal, and low-permeability components of the aquifer with long mean water residence times have higher influence over drip sites (Fairchild and McMillan, 2007). Increased residence times lead to increased dissolution of dolomite, resulting in increased concentrations of Mg in the groundwater, and subsequently the dripwaters and speleothems (Fairchild and McMillan, 2007), but Sr will vary antipathetically as dolomite is depleted in Sr compared to calcite (Fairchild et al., 2000). Where Sr-rich aragonite is preserved in shaley parts of the aquifer, Sr enrichment may also occur via the same process (Baker et al., 2000, Fairchild et al., 2006).

Increased concentrations of trace elements in speleothem calcite can be an indicator of dry conditions due to prior calcite precipitation, or retention of Ca in soils due to enhanced freezing/evaporation during dry periods leading to incongruent dissolution (Fairchild et al., 2000). Dolomite dissolution is also enhanced during dry periods, leading to increased Mg (Roberts et al., 1998). Dry conditions lead to longer reaction times in the soil and aquifer, allowing higher concentrations of trace elements to be removed into solution/transport (Baker et al., 2000).

A long-term rise in Mg and Sr, which culminated in a switch from calcite to aragonite precipitation, was identified in a speleothem from Clamouse, France, and interpreted as indicating a major drought (McMillan et al., 2005)

Following low flow conditions, when flow rates start to increase, high concentrations may persist as a result of a flush of material which had been entrained in the soil, piston-flow through the aquifer, or interaction between fracture-flow waters and the matrix causing entrainment of ions (Fairchild and Treble, 2009).

#### **3.2.4.4 Prior Calcite Precipitation**

“Prior precipitation” is the expression used for when  $\text{CaCO}_3$  has already been precipitated upflow of the speleothem drip site, which may occur due to the dripwater encountering  $p\text{CO}_2$  lower than that which it assimilated in the soil/upper epikarst (Fairchild and McMillan, 2007).

Prior calcite precipitation is enhanced during seasonal low water recharge, which leads to longer water-rock contact times, and also allows increased volumes of air to penetrate into the aquifer (Fairchild et al., 2000, Fairchild and McMillan, 2007). This gives karst waters better opportunity to degas in air pockets in the aquifer (Fairchild et al., 2000). It is likely that this situation would occur in the summer in Mediterranean climates (Fairchild and McMillan, 2007), working either together with or against the  $p\text{CO}_2$  effect, as discussed below.

Prior calcite precipitation extent may be affected by seasonal cave  $p\text{CO}_2$  variations in addition to or rather than dryness (Fairchild and Treble, 2009). Cave air  $p\text{CO}_2$  may be depleted either in the winter (e.g. Fairchild et al., 2000, Bourges et al., 2001) or the summer (e.g. Matthey et al., 2008, Hoyos et al., 1998). Controls on cave air  $p\text{CO}_2$  include increased ventilation in winter (Spötl et al., 2005) which may be related to thermo-convective instability (Bourges et al., 2006), water-filling of  $\text{CO}_2$ -bearing fissures and temperature and rainfall controls on soil  $p\text{CO}_2$  (Fairchild et al., 2006). Hourly resolved cave air  $p\text{CO}_2$  and drip water chemistry from Crag Cave, SW Ireland indicate that PCP can modulate speleothem growth on extremely short timescale (Sherwin and Baldini, 2011).

The effect of prior calcite precipitation on trace element chemistry is to remove cations from the precipitating solution in the proportion they are incorporated into calcite (Holland et al., 1964). As distribution coefficients for trace elements are typically far less than 1, following prior calcite precipitation Ca will be reduced to a much greater degree than the trace elements, resulting in increased ratio of the trace element to Ca in the solution (Fairchild and Treble, 2009) and positive correlation of Mg/Ca and Sr/Ca (Fairchild et al., 2000).

Covariation of Mg/Ca, Sr/Ca and  $\delta^{13}\text{C}$  in speleothems is an important indicator of prior calcite precipitation which has been noted in speleothem analysis (Verheyden et al., 2000, McDermott et al., 2006, Treble et al., 2005b) and in models (Johnson et al., 2006a, Fairchild and McMillan, 2007). Such patterns have been identified on the seasonal scale in the studies above, and it has been suggested that the same principles could be applied to longer-term records (Johnson et al., 2006a, McMillan et al., 2005).

Sr/Ca and Mg/Ca have often been found to be positively correlated in speleothem calcite and cave waters, a relationship which is generally attributed to prior calcite precipitation (PCP) (e.g. Cruz et al., 2007, Karmann et al., 2007). One way to identify the effects of PCP is that PCP will produce a vector with a constant slope in a log-log cross-plot of Sr/Ca vs. Mg/Ca (Fairchild et al., 2000, McMillan et al., 2005). This identifier for PCP was further proven by Sinclair (2011) who created a mathematical model which found the same relationship, and defined the correlation slope as:

$$\frac{(Kd_{Sr} - 1)}{(Kd_{Mg} - 1)}$$

Equation 3.16: Correlation slope between Sr/Ca and Mg/Ca for waters that have undergone PCP

where  $K_{Sr}$  and  $K_{Mg}$  are the distribution coefficients of Sr and Mg respectively.

This tool for diagnosing PCP is especially useful as it is not affected by host rock or dripwater composition (Sinclair, 2011).

However, limestone leaching experiments designed to recreate the physical and chemical degradation of limestone by glaciers (which involved no PCP), also produced data which plot as straight line in  $\ln(\text{Sr}/\text{Ca})$  vs.  $\ln(\text{Mg}/\text{Ca})$  space, very close to the slope expected for PCP (McGillen and Fairchild, 2005). The slope in these experiments was deemed to be caused by incongruent calcite dissolution (ICD) (McGillen and Fairchild, 2005). During ICD, both Mg and Sr have been shown to be released in preference to Ca during calcite dissolution and diagenesis (Land, 1967, Schroede, 1969, Gomberg and Bonatti, 1970, Reeve and Perry, 1994, Fairchild et al., 1999, Fairchild et al., 2000, McGillen and Fairchild, 2005).

Sinclair (2011) found that the Mg/Ca and Sr/Ca of a solution experiencing ICD plotted as expected along a line with slope  $(Kd_{Sr}-1) / (Kd_{Mg}-1)$  in  $\ln(\text{Sr}/\text{Ca})$  vs.  $\ln(\text{Mg}/\text{Ca})$  space, and

calculated that the slope was  $\sim 0.88 \pm 0.13$ , and passed through the Mg/Ca and Sr/Ca values for the host rock composition. It is still not possible to distinguish the effects of PCP from ICD in this method, but it is a useful diagnostic tool for identifying the effects of calcite-water interaction (Sinclair, 2011). Thus, another identifier is required to assure that the slope produced is due to PCP and not other processes such as ICD (Sinclair, 2011).

#### ***3.2.4.5 In Combination with Other Proxies***

High resolution trace element analyses combined with high precision U-series dating methods can provide a well-constrained palaeoclimatic proxy (Baldini et al., 2002). Trace element variations can have meaningful covariation with  $\delta^{13}\text{C}$  (Hellstrom and McCulloch, 2000, Verheyden et al., 2000, van Beynen et al., 2008) and  $\delta^{18}\text{O}$  (Cruz et al., 2007), which have both been interpreted in terms of rainfall. In the case of  $\delta^{18}\text{O}$ , differences in the trend between trace element variations and  $\delta^{18}\text{O}$  variations in a Brazilian speleothem were used to infer that  $\delta^{18}\text{O}$  was not responding simply to rainfall amount, but rather to changes in the relative proportion of rainfall originating from summer monsoonal and winter extra-tropical sources (Cruz et al., 2007).

### 3.3 Strontium isotopes

#### 3.3.1 The Isotopes of Strontium

Strontium (Sr) is an alkaline earth element (Stewart et al., 1998). There are four isotopes of Sr;  $^{84}\text{Sr}$ ,  $^{86}\text{Sr}$ ,  $^{88}\text{Sr}$  (all of which occur in constant relative proportions within earth materials), and  $^{87}\text{Sr}$ , which is not of a constant proportion, as the decay of  $^{87}\text{Rb}$  (half-life 48.8 billion years) increases the proportion of  $^{87}\text{Sr}$  in the environment (Stewart et al., 1998).

#### 3.3.2 $^{87}\text{Sr}/^{86}\text{Sr}$ in Cave Waters and Speleothems

There is negligible isotopic fractionation during evaporation, degassing and temperature fluctuations (Banner and Kaufman, 1994). Thus, the  $^{87}\text{Sr}/^{86}\text{Sr}$  ratio of speleothems directly record the Sr isotopic composition of the cave water from which they precipitated, which in turn varies as a result of changes in the relative contributions of various Sr sources with differing  $^{87}\text{Sr}/^{86}\text{Sr}$  signatures (Faure and Mensing, 2005). In the soil layer, strontium isotopes are not significantly fractionated by plant or animal metabolism (Capo et al., 1998), and corrections during measurement account for any small fractionation (Stewart et al., 1998).

The host rock provides one of the most important sources of speleothem Sr (Banner et al., 1996, Goede et al., 1998, Ayalon et al., 1999, Bar-Matthews et al., 2000, Verheyden et al., 2000, Frumkin and Stein, 2004, Li et al., 2005, Zhou et al., 2009). Limestone dissolution is affected by many factors, the most important being water availability and  $\text{CO}_2$  availability, and so increased precipitation and/or increased vegetation activity lead to increased limestone dissolution (Ford and Williams, 1989).

The  $^{87}\text{Sr}/^{86}\text{Sr}$  ratio of speleothems and the dripwaters from which they precipitate typically fall between seawater and the cave rock or overlying soil, which may contain aeolian dust (Ayalon et al., 1999, Bar-Matthews et al., 1999, Musgrove and Banner, 2004). Other sources of Sr in speleothems include the overlying soil layer, sea spray, and atmospheric dust (Goede et al., 1998, Ayalon et al., 1999, Capo et al., 1998, Bar-Matthews et al., 2000, Frumkin and Stein, 2004, Zhou et al., 2009). Aeolian dust typically has  $^{87}\text{Sr}/^{86}\text{Sr}$  of ca. 0.7200, which is higher than the  $^{87}\text{Sr}/^{86}\text{Sr}$  for Phanerozoic limestone and dolomite, which averages 0.7070 to 0.7090 (Capo et al., 1998). Seawater  $^{87}\text{Sr}/^{86}\text{Sr}$  has remained higher than 0.70915 throughout the Pleistocene (Capo & DePaolo, 1990).

Where groundwaters have elevated  $^{87}\text{Sr}/^{86}\text{Sr}$  ratios relative to the host aquifer rocks, this indicates that an external source is supplying more radiogenic  $^{87}\text{Sr}$  to the waters (Musgrove

and Banner, 2004). The  $^{87}\text{Sr}/^{86}\text{Sr}$  ratio may differ from that of the limestone due to the inclusion of aeolian-derived silicates, allowing it to be used as an indicator of the relative contributions of limestone weathering and aeolian transport, which can in turn be interpreted a proxy for effective rainfall, with lower  $^{87}\text{Sr}/^{86}\text{Sr}$  ratios occurring during periods of increased residence time (i.e. drier periods) (Musgrove and Banner, 2004, Verheyden et al., 2000, Banner et al., 1996) or aeolian activity (Goede et al., 1998, Bar-Matthews et al., 1999, Frumkin and Stein, 2004, Li et al., 2005).

### 3.4 Uranium Isotopes as a Palaeoclimatic Proxy

$^{234}\text{U}/^{238}\text{U}$  in speleothems has been successfully used as a palaeoclimatic proxy (Kaufman et al., 1998, Ayalon et al., 1999, Hellstrom and McCulloch, 2000, Zhao et al., 2001, Plagnes et al., 2002, Frumkin and Stein, 2004, Zhou et al., 2005, Asrat et al., 2007).

$^{234}\text{U}/^{238}\text{U}$  of speleothem calcite reflects the signature of the groundwater feeding the stalagmite (Asrat et al., 2007). Speleothem ( $^{234}\text{U}/^{238}\text{U}$ )<sub>0</sub> values above equilibrium indicate that U in the speleothems did not originate from simple congruent dissolution of limestone, and that a component of U is enriched in  $^{234}\text{U}$  (Kaufman et al., 1998, Ayalon et al., 1999). There are several causes for deviation of  $^{234}\text{U}/^{238}\text{U}$  from equilibrium in speleothems/groundwater:

Alpha recoil in the soil zone can release  $^{234}\text{U}$  directly into solution after the radioactive disintegration of  $^{238}\text{U}$  (Osmond, 1980, Kaufman et al., 1998, Ayalon et al., 1999, Osmond and Ivanovich, 1992). Groundwater residence time will be important in this case, with short residence times leading to lower  $^{234}\text{U}/^{238}\text{U}$  levels in cave waters (Osmond, 1980, Henderson et al., 1999). Very high  $^{234}\text{U}/^{238}\text{U}$  values were found in a speleothem from Clamouse Cave, France, and were interpreted as indicating that some of the  $^{234}\text{U}$  had come from recoil in the soil zone (Plagnes et al., 2002, Ayalon et al., 1999).

Enrichment of  $^{234}\text{U}$  in speleothems is a consequence of accumulation of  $^{234}\text{U}$  in easily leached sites within soils, due to a reduction in soil  $\text{CO}_2$  levels or a reduction in recharge (or both), that is then leached when precipitation and/or soil  $\text{CO}_2$  levels increase and deposited in speleothem growth (Plagnes et al., 2002). It is for this reason that speleothem  $^{234}\text{U}/^{238}\text{U}$  values may be high after a long period in which a speleothem did not grow, such as a glacial period, as the absence of vegetation may have led to low  $p\text{CO}_2$  in soils, and precipitation would also be reduced (Plagnes et al., 2002). Higher  $^{234}\text{U}/^{238}\text{U}$  during glacial periods could

result from contribution of U from exposed continental shelves, or selective removal of  $^{234}\text{U}$  from soils (Frumkin and Stein, 2004).

Weathering may affect the uranium isotopic signature by either mobilising uranium through erosion, or adding or removing it from the system (Osmond and Ivanovich, 1992, Asrat et al., 2007). Preferential leaching of  $^{234}\text{U}$  from lattice sites which have been damaged by  $\alpha$ -decay can lead to disequilibrium  $^{234}\text{U}/^{238}\text{U}$  in speleothems (Rosholt, 1982). Waters which are aggressive, i.e. with high dissolution rates, will lead to reduced dissolved  $\delta^{234}\text{U}$  values (Hellstrom and McCulloch, 2000).

$^{234}\text{U}/^{238}\text{U}$  ratios can be used to disentangle the temperature and precipitation components of the  $\delta^{18}\text{O}$  signal of speleothems, when used in conjunction with other proxies such as  $\delta^{13}\text{C}$ , Ba and Sr which are affected by changes in vegetation and soil biological activity (which will in turn respond to changes in temperature) (Hellstrom and McCulloch, 2000).

Initial  $(^{234}\text{U}/^{238}\text{U})_0$  was found to correlate with  $\delta^{18}\text{O}$  in speleothems from Soreq cave, Israel, leading to the interpretation that  $^{234}\text{U}/^{238}\text{U}$  in speleothems at this location reflects effects of rainfall and soil weathering conditions (Kaufman et al., 1998, Bar-Matthews et al., 1997). This interpretation stems from the fact that  $^{234}\text{U}/^{238}\text{U}$  in groundwater in low rainfall regimes will be significantly affected by changes in the rate of removal of U from soil as opposed to U released from dissolution of limestone (Kaufman et al., 1998).

Fluorescence Index and  $^{234}\text{U}/^{238}\text{U}$  ratios were used in conjunction with each other in a multi-proxy speleothem record from Ethiopia, as variations in connectivity with the soil and groundwater could explain variations in both (Asrat et al., 2007).

## 3.5 Fluorescence

Fluorescence occurs when an atom emits a photon of light as an electron which had been excited by absorbing electromagnetic radiation returns to its original energy level (McGarry and Baker, 2000). The structural feature of a molecule which cause it to fluoresce are known as fluorophores, and the most influential fluorophore is the frequency of conjugated double or triple bonds within a molecule (McGarry and Baker, 2000).

### 3.5.1 Fluorescence in Speleothems

Far fewer studies have looked at fluorescence in speleothems than the more traditional proxies such as stable isotopes, but several studies do exist (e.g. Baker and Bolton, 2000, McGarry and Baker, 2000, van Beynen et al., 2001, Perrette et al., 2005, Asrat et al., 2007). Fluorescence in speleothems mostly derives from organic acids which have been introduced to the cave environment from the overlying soil and decomposition of vegetation by groundwater (Senesi et al., 1991, McGarry and Baker, 2000).

Another source of fluorescence in speleothems is amino-acid groups in proteins, which may derive from decomposed plant matter, soil bacteria, or decomposed faunal organic material (Senesi et al., 1991, Burstein and Emelyanenko, 1996). The most common source of protein fluorescence is tryptophan (Lakowicz et al., 1983). Inorganic ions such as  $\text{UO}_2^{2+}$  and  $\text{Mn}^{2+}$  are known to produce fluorescence also, but represent a smaller proportion of the fluorescence in speleothems than organic sources (Pedone et al., 1990, Shopov et al., 1994).

Fluorescence variations in speleothems may be related to temperature and precipitation amount, as they influence the rate and degree of humification of organic matter (Heal and French, 1974, Meentmeyer, 1978, Swift et al., 1979).

## 3.6 U-Series Dating

### 3.6.1 U/Th Dating

Speleothems are not appropriate for radiocarbon dating as it is difficult to quantify the proportion of carbon within the  $\text{CaCO}_3$  matrix which is “carbon-dead” as it originated from dissolution of the host limestone (McDermott et al., 2006). Conversely, speleothems are very appropriate for U-Series dating using mass spectrometers, particularly the “daughter deficiency”  $^{230}\text{Th}/\text{U}$  method, as they typically behave as closed systems with respect to uranium and its decay products, a prerequisite for U-Series dating (McDermott et al., 2006). This closed system is important, as it can therefore be assumed that the entirety of the thorium contained in a speleothem is a product of radioactive decay from uranium, as uranium is readily soluble and would be transported to the speleothem growth site in groundwater, while thorium is very insoluble (Fairchild and Baker, 2012).

The reliability of U-series dates hinges on the accuracy with which the mixed  $^{229}\text{Th}/^{236}\text{U}$  spikes have been calibrated to known standards (McDermott, 2004). Therefore, it is important for there to be more thorough inter-lab comparisons, in order to detect systematic errors in mixed  $^{229}\text{Th}/^{236}\text{U}$  spike calibrations, and rectify these errors (McDermott et al., 2006) to ensure that published results from different laboratories can be directly compared (McDermott, 2004). Also, in speleothems which are detritally contaminated it is necessary that there is increased care in correcting for initial  $^{230}\text{Th}$  (McDermott et al., 2006). Another requirement is that there must be improvements in the statistical methods employed to construct speleothem age models from U-series data (McDermott et al., 2006). If these conditions are met, greater confidence can be placed on the output of U-series dating.

Some methodological issues of U/Th dating have not been standardised, for example there is no clear standard for interpolation between dates, and long-term speleothem growth rates may be non-linear, making interpolation difficult and the resultant age models potentially incorrect (Fairchild et al., 2006).

### 3.6.2 U-Pb Dating

Although U/Th dating produces accurate and robust chronologies, it is not applicable to older samples, as by ca. 500 kyr key components of the system approach equilibrium (Woodhead and Pickering, 2012). U/Pb dating allows materials which are older than the

limit for which U/Th is applicable to be dated (Richards et al., 1998), and so is an extremely important emerging technique. There is also an overlap in the limits of U/Th and U/Pb, of several hundred thousand years, allowing direct comparison of ages calculated by both methods on the same material, in order to test the accuracy of U/Pb dating. Such comparisons have so far yielded promising results (e.g. Richards et al., 1998, Cliff et al., 2010).

The important parent-daughter radioactive isotope pairs for U/Pb dating are  $^{238}\text{U}$  and  $^{206}\text{Pb}$ , and  $^{235}\text{U}$  and  $^{207}\text{Pb}$ . As there are two decay systems, two separate ages can be calculated. If these ages are in agreement, the system has remained closed and is in isotopic equilibrium, with no gain or loss of U, Th or Pb, while if they disagree, this “discordance” demonstrates a lack of secular equilibrium, or that the system has become opened at some point (Woodhead et al., 2006).

### ***3.6.2.1 Sample Selection***

Successful U/Pb dating attempts will usually involve high U concentrations and very low Pb concentrations (Pickering et al., 2010). Where Pb is very low, it is assumed that most of it is radiogenic, which is the ideal for U/Pb dating (Richards and Dorale, 2003). However, this assumption is only true for a few minerals, such as zircons. In reality, most samples contain a mix of radiogenic Pb and the inherent Pb which was incorporated at the time of formation, known as “common Pb” (Woodhead et al., 2012). It has recently been observed that some samples have single common Pb sources/transport mechanisms, while others have several. These can include colloidal transport and incorporation of detrital Pb in dust at hiatuses (Woodhead et al., 2012).

A large range of U/Pb ratios is also important for U/Pb dating to be successful, as this is necessary for the generation of U/Pb isochrons (Woodhead and Pickering, 2012). As a result, not all speleothems are viable candidates for U/Pb dating. Also, as U is not evenly distributed throughout speleothems (Fairchild and Treble, 2009), care must be taken when selecting sample locations even in suitable speleothems.

Cole et al. (2003) proposed using digital autoradiography to select suitable speleothems, and further more the most appropriate sampling locations within them. In this method, the natural radiation in the speleothem is used to produce an image of U levels in the speleothems. This is achieved by placing a cut speleothem surface on a phosphor imaging plate for some time (up to several weeks). Radiation from the speleothem will cause the

phosphor crystals to excite. This energy is then released when the plate is scanned with red and/or blue laser light in the autoradiograph, and this released energy is measured to produce an image of radioactivity in the speleothem surface (Pickering et al., 2010).

Although the method is not element specific, for speleothems it can generally be assumed that the larger part of the emitted radiation is from U, and ICP-MS can be used to ensure that this is the case (Pickering et al., 2010). Digital autoradiography is advantageous as it is non-destructive and allows whole speleothems to be analysed at once, provided they are smaller than the phosphor plate. For samples with very low U contents, several weeks contact time with the phosphor plate may be required, and a certain degree of trial and error may be necessary to find the optimal contact time for each sample.

Once subsections of speleothems have been identified by digital autoradiography as having high U content, laser ablation ICP-MS could then be used to ensure that Pb levels are low in these areas (Woodhead et al., 2012). While a useful tool, laser ablation ICP-MS can only be performed on small pieces of speleothem (a few cm<sup>2</sup> large at most), and so is more appropriate to screen areas after they have already been identified as containing high levels of U by autoradiography. Also, care must be taken to ensure that sawing or cutting of sample slabs does not introduce contaminant Pb to the samples.

### ***3.6.2.2 Mass Spectrometric Analysis and Isochron Construction***

Care must be taken when preparing samples for analysis by ICPMS or other methods to avoid contamination of the sample by anthropogenic Pb (Woodhead et al., 2012). Analysis by multicollector inductively coupled plasma mass spectrometry (MC-ICPMS) has several advantages over other techniques for U/Pb dating of speleothems: the method is relatively insensitive to impurities such as organics, there is improved control of instrumental mass fractionation, and sample throughput is increased (Woodhead et al., 2006, Woodhead and Pickering, 2012).

The majority of speleothems studies which use U/Pb dating methods make use of Tera-Wasserburg (T-W) isochron construction (Figure 3.1). A T-W diagram is a concordia plot in  $^{207}\text{Pb}/^{206}\text{Pb}$  against  $^{238}\text{U}/^{206}\text{Pb}$  space (Tera and Wasserburg, 1972), also known as the “semi-total Pb-U isochron” (Ludwig, 1998), which does not have to be corrected for common Pb (Woodhead et al., 2012). T-W diagrams avoid the use of both  $^{208}\text{Pb}$  and  $^{204}\text{Pb}$ , and only use  $^{207}\text{Pb}$ ,  $^{206}\text{Pb}$  and  $^{238}\text{U}$ , which can be well measured by MC-ICPMS (Fairchild and Baker, 2012). Excluding  $^{204}\text{Pb}$  is advantageous as Hg contamination of the argon carrier gas in MC-ICPMS

techniques may lead to interference, reducing the accuracy of the measurement of  $^{204}\text{Pb}$  (Woodhead and Pickering, 2012).

In a T-W isochron, the concordia curve represents the line along which concordant ages (i.e. those which derive only from undisturbed radiogenic Pb, with agreement between both decay schemes) should lie (Woodhead et al., 2012), as shown in Figure 3.1 by the solid line marked Concordia curve. The concordant ages themselves are represented by tick marks on this concordia.

To measure the age of a sample, several individual sub-samples, ideally from the same layer, are analysed, with the aim to produce a large spread in U/Pb ratios. These (almost certainly) discordant ages will plot away from the concordia, forming a mixing line between common Pb and radiogenic Pb (Woodhead et al., 2006), assuming that only the amount of common Pb varies, and not its composition (Woodhead et al., 2012). An example of a mixing line produced in a Tera-Wasserburg plot by several subsamples is shown in Figure 3.1 as Line A. The U-Pb age of the sample is determined from the point at which this line crosses the Tera-Wasserburg concordia.

Single aliquot, common Pb-corrected ages may be employed in certain situations where the composition of common Pb is known and does not vary, producing an anchored isochron (Cliff et al., 2010, Woodhead and Pickering, 2012). This approach is represented by Line B in Figure 3.1.

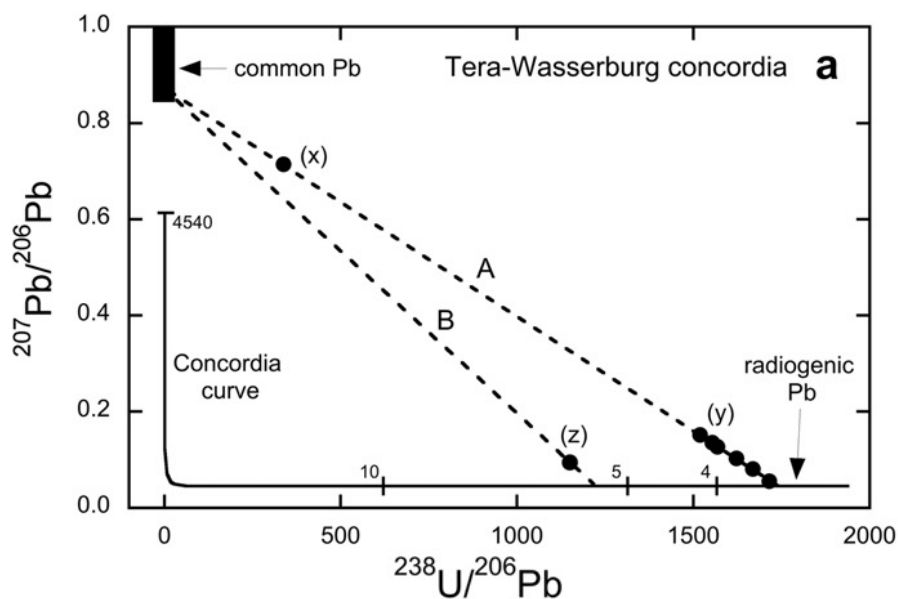


**Figure 3.1**  
**Example of a Tera-Wasserburg isochron, from Woodhead et al. (2012). Line A represents the usually employed method of U/Pb analyses, i.e. analysing several subsamples to produce a mixing line between common Pb and radiogenic Pb. Line B represents a new method in which a single, radiogenic sample is used to produce the isochron, anchored to a known common Pb composition.**

Another type of isochron which may be used is the 3-dimensional Tera Wasserburg, which adds  $^{204}\text{Pb}/^{206}\text{Pb}$  to the T-W concordia, to represent common Pb (Wendt, 1984). This method is advantageous where common Pb contents are high (e.g. Carl et al., 1989), but is limited by the same limitations to  $^{204}\text{Pb}$  measurement as conventional T-W plots.

### **3.6.2.3 Disequilibrium Corrections**

In the application of U/Pb dating methods to samples less than ca. 5 Ma, a correction must be made for initial isotope disequilibrium in the U-series decay chain (Woodhead and Pickering, 2012). Many speleothems precipitate from waters with non-equilibrium  $^{234}\text{U}/^{238}\text{U}$ , as increased availability of  $^{234}\text{U}$  from lattice damaged sites led to  $^{234}\text{U}$  excess (Woodhead and Pickering, 2012). Also, many speleothems are formed with negligible levels of  $^{230}\text{Th}$  (Woodhead and Pickering, 2012). These effects must be corrected for, with these corrections causing shifts of up to several hundreds of thousands of years.

If the present day  $^{234}\text{U}/^{238}\text{U}$  can be measured from young material from the same speleothem or cave, the disequilibrium can be quantified and a correction applied to older samples intended for U/Pb dating (e.g. Pickering et al., 2010). If this is not possible, an estimate of the original state of equilibrium should be made, and used to apply a correction to the U/Pb data, as in Meyer et al. (2009).

# *Chapter 4*

*Calcite - Aragonite  
Relationships and Climate of  
early MIS 5e and the early  
Holocene Recorded in  
Speleothems from SW Turkey*

## 4.1 Introduction

### 4.1.1 Dim Cave

Dim Cave is a show cave located near to the Mediterranean coast of SW Turkey, close to the town of Alanya and 145 km from the large city of Antalya. The location of the cave is shown by the red circle in Figure 4.1. The cave was first explored by speleologists in 1986, and was opened to tourists in 1998 (<http://www.dimcave.com.tr>). The cave is 360 m long and 10-15 m wide and high (<http://www.dimcave.com.tr>), with a lake at one end which has been at a lower level in recent years (Baykara, 2009). The cave plan is shown in Figure 4.2.



Figure 4.1 Dim Cave location within Turkey (red circle)

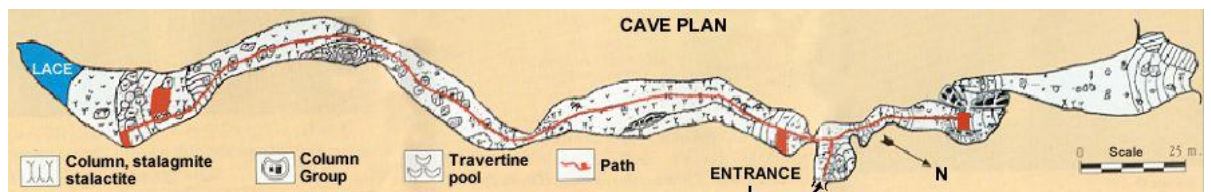


Figure 4.2 Dim Cave plan. Image from <http://www.dimcave.com.tr/magara.htm>

## 4.1.2 Monitoring of Dim Cave

### 4.1.2.1 Temperature and Humidity

The owners of Dim Cave, the MAGTUR Co., report that temperature inside Dim Cave remains relatively constant within the range of 18-19°C, and that humidity is approximately 90% throughout the year (<http://www.dimcave.com.tr>). When visited on the 25<sup>th</sup> and 26<sup>th</sup> of March, 2009, air temperature ranged from 18.1 to 18.6°C, and humidity ranged from 96 to 99%.

### 4.1.2.2 Water Samples

Waters were collected from Dim Cave at the time of stalagmite collection and at several subsequent visits by colleagues Mr Oruç Baykara and Dr Mehmet Özkul. Trace element data for these samples over time are presented in Table 4.1 and Figure 4.3. The water samples were also analysed for hydrogen and oxygen isotopes. These data are compared to meteoric water lines in section 4.2.

The Dim Cave drip waters have Mg/Ca \* 1000 ratios ranging from 625 to 7449, and Sr/Ca \* 1000 ranging from 0.278 to 0.863. Using a  $K_{Mg}$  value of 0.018, as determined by Huang and Fairchild (2001), these drip waters would produce calcite with Mg/Ca \* 1000 ratios in the range of 11.252 to 134.082, while a  $K_{Sr}$  value of 0.15 as suggested by McMillan et al. (2005) indicates that these waters would produce calcite with Sr/Ca \* 1000 ratios ranging from 0.0417 to 0.129. Aragonite precipitated from these waters should have Sr/Ca \* 1000 ratios in the range of 0.314 to 0.534, assuming a  $K_{Sr}$  value of 1.13 (Kinsman and Holland, 1969).

In Figure 4.3, the data are separated by water sample type (drip or stagnant water source) and drip rate. For the pool, lake and spring data, the lake has the lowest Sr/Ca values, and shows similarities in Mg/Ca trend with the pool and spring in winter while spring trends are divergent in both Mg/Ca and Sr/Ca. The spring has the lowest Mg/Ca data in all months except March 2009, perhaps as prior calcite precipitation upstream of the lake and pool may have lead to higher Mg/Ca ratios in these samples.

For the slow dripping samples in B, there are clearly similarities in Sr/Ca between all three drips, although drips “walk” and “high” each have one less data point than drip “short”. Similarly, in the winter months the Mg/Ca data show correlation between drips and with the Sr/Ca data. Thus it is likely that these ratios are being controlled at least in part by a common factor such as precipitation amount. A higher resolution time series of dripwaters

in Dim Cave would be useful to establish if there are true correlations in drip water chemistry between drips of similar drip speed.

One of the fast dripping sites, named “wire” has a very similar trend for both Sr/Ca and Mg/Ca over time, while the other fast drip, “shower” has differing trends for the two elements. These very fast drips are most likely responding to singular rainfall events, with water arriving at the drip by fracture flow. It is also possible that hydrological routing may change following extreme rainfall events. This may suggest that very fast drips in Dim Cave would not be suitable for climatic interpretation due to the bias of single events.

Drip	Drip Rate	Date	Ca (ppm)	Mg (ppm)	Sr (ppm)
“Short”	3 drips s <sup>-1</sup>	Mar 2009	18.0	34.5	0.0311
		May 2009	13.4	60.5	0.0213
		Dec 2009	26.4	35.8	0.0223
		Jan 2010	15.0	32.1	0.0192
		Feb 2010	31.7	39.0	0.0354
“High”	0.33 drips s <sup>-1</sup>	Mar 2009	28.7	45.5	0.0309
		May 2009	11.8	17.2	0.001
		Jan 2010	18.4	41.5	0.0320
		Feb 2010	17.1	43.8	0.0323
“Walk”	1 drip s <sup>-1</sup>	Mar 2009	42.6	29.8	0.0259
		Dec 2009	42.5	33.9	0.0345
		Jan 2010	13.5	12.2	0.0136
		Feb 2010	35.1	30.7	0.0293
“Shower”	Continuous	Mar 2009	15.5	38.7	0.0241
		May 2009	19.3	42.2	0.0167
		Dec 2009	28.4	27.2	0.0274
		Jan 2010	31.6	38.6	0.0289
		Feb 2010	12.1	38.5	0.0098
“Wire”	Continuous	Mar 2009	20.7	35.7	0.0279
		May 2009	19.0	18.5	0.0157
		Dec 2009	22.8	22.4	0.0186
		Jan 2010	20.5	29.9	0.0252
		Feb 2010	44.7	37.3	0.0321
“Pool”	Non-dripping	Mar 2009	32.7	41.8	0.0313
		May 2009	34.8	42.2	0.0349
		Dec 2009	28.0	64.2	0.0230
		Jan 2010	21.0	19.9	0.0225
		Feb 2010	28.3	40.6	0.0301
“Lake”	Non-dripping	Mar 2009	50.5	19.1	0.0375
		May 2009	63.6	51.7	0.0436
		Dec 2009	11.9	17.1	0.0098
		Jan 2010	39.8	22.4	0.0285
		Feb 2010	19.9	17.9	0.0157
“Spring”	Non-dripping	Mar 2009	28.1	16.3	0.0507
		Dec 2009	45.8	11.3	0.0416
		Jan 2010	60.6	11.4	0.0458
		Feb 2010	32.2	11.8	0.0288

**Table 4.1 Dim Cave drip water cation data**

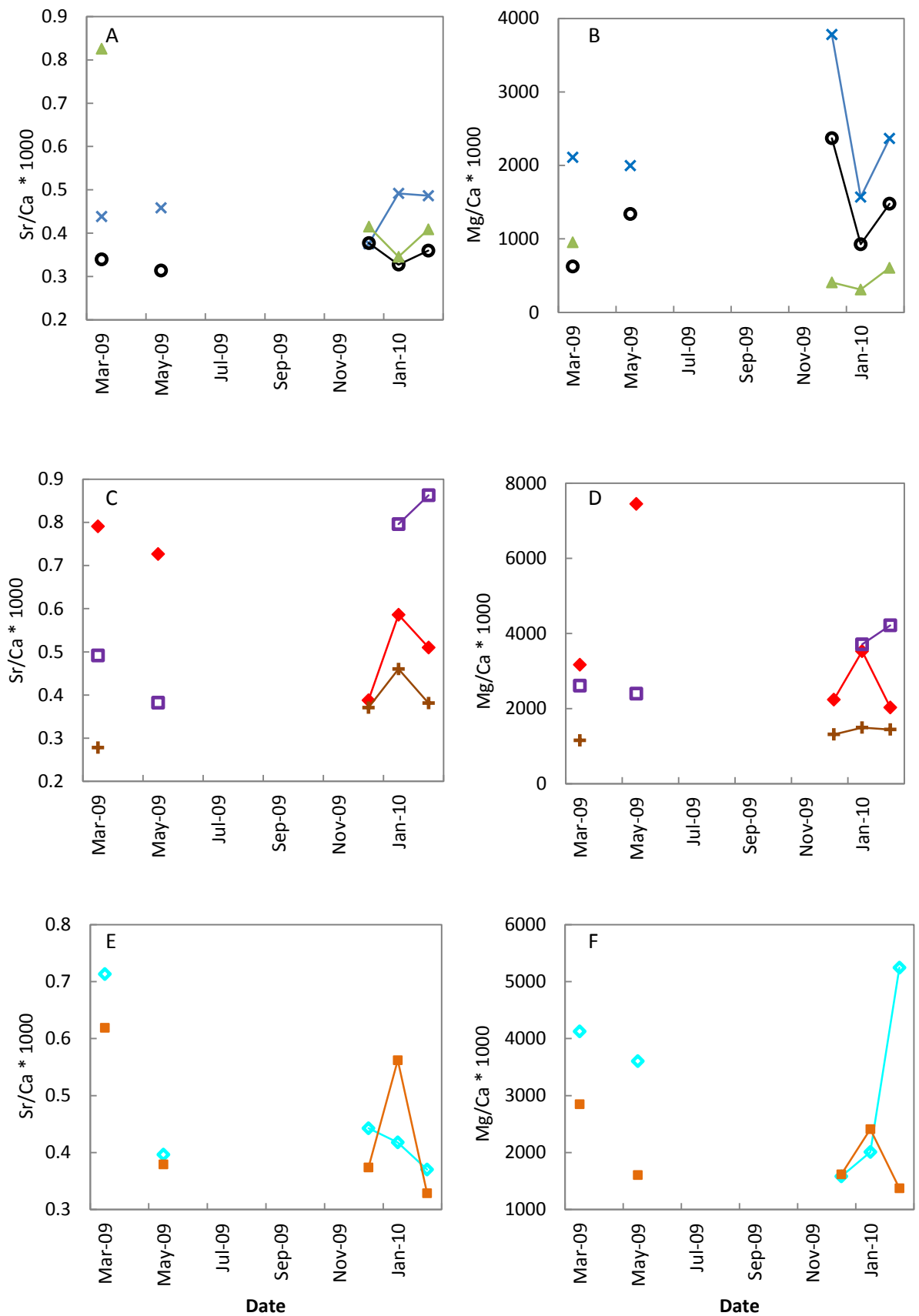


**Figure 4.3**

Trace element data for water samples from Dim Cave. A, C, E = Sr data; B, D, F = Mg data. Data are separated by sample type and drip rate.

A and B = non dripping water samples; a pool (blue crosses) and lake (black open circles) within the cave and a spring (green triangles) in the near vicinity. C and D = Slower dripping drip waters in March 2009 ("short" [red diamonds] = 3 drips per s, "high" [purple open squares] = 0.33 drip per s, "walk" [brown crosses] = 1 drip per s). E and F = Continuous drips in March 2009, "shower" (turquoise open diamonds) and "wire" (orange squares).

## 4.2 Isotopic Composition of Precipitation and Groundwater near Dim Cave, Dim Cave Drip Waters and Modern Speleothem Growth

### 4.2.1 IAEA Weather Station Data

The closest IAEA station to Dim Cave with a large and continuous dataset is at Antalya (Figure 4.4, black triangle). Data from 6 locations in Turkey were used by Dirican et al. (2005) to calculate a Local Meteoric Water Line (LMWL) for Turkey; these locations are shown in Figure 4.4 as open green squares. Geographical data comparing the location of Dim Cave with the Antalya IAEA station is shown in Table 4.2.



**Figure 4.4** Map of locations used in calculation of Meteoric Water Lines (MWLs) in relation to Dim Cave. Red circle = Dim Cave. Green open squares = Locations used by Dirican et al. (2005) to construct the Local Meteoric Water Line (LMWL) for Turkey. Black triangle = Antalya IAEA station.

Location	Latitude / Longitude (degrees)	Elevation (m.a.s.l)
Dim Cave	36.54N 32.1E	232
Antalya IAEA Station	36.88N 30.7E	49

**Table 4.2** Geographic data for Dim Cave and Antalya IAEA station

Saris et al. (2010) used data from 107 Turkish State Meteorological Service stations to classify the precipitation regimes of Turkey. The two closest stations to Dim Cave, Antalya and Manavgat, were both classified as 4A, which is a precipitation regime with a high magnitude December peak with a rapid onset of winter and a gradual cessation towards dry summers.

The monthly averages of several climate variables recorded at Antalya IAEA station are shown in Figure 4.5. Figure 4.5A shows average monthly air temperature and precipitation amount, and indicates that the region experiences hot summers and cool winters (i.e. seasonal contrast) with average temperatures always well above freezing, and that the rainfall regime is winter-heavy, with very low rainfall for the summer months. Figure 4.5B shows mean monthly water excess at Antalya, calculated using the Thornthwaite formula (Thornthwaite, 1948) and mean monthly air temperature and precipitation data (1963-2004) from Antalya IAEA station. The data show that a soil moisture deficit exists at Antalya during the period May-September. Therefore, it is probable that recharge to the aquifer will occur during the winter half-year (Oct-Apr).

The weighted means of  $\delta D$  and  $\delta^{18}O$  of precipitation are shown in Figure 4.5C; both isotopes follow similar patterns throughout the year, with an overall trend towards less negative values from Jan-June, and towards more negative values from Sep-Dec, which is in positive correlation with air temperature and negative correlation with precipitation amount. The months of July and August are contrary to the trend, as they are more negative than the values for September. This is most likely due to the very low sample number for these months, partly due to the fact that some years it did not rain in Antalya during the months of July or August, and exacerbated by the fact that isotopic analyses were not carried out on the samples collected from each year that it did rain. Table 4.3 shows the number of samples per month analysed for isotopes by the IAEA, and illustrates that the summer months are underrepresented in relation to the winter months.

Table 4.4 and Figure 4.6 calculate the percentage contribution of periods of the year to the total annual precipitation at Antalya. The period June-September contributes only 2% of the yearly precipitation; therefore the signal is likely to be heavily skewed towards winter precipitation.

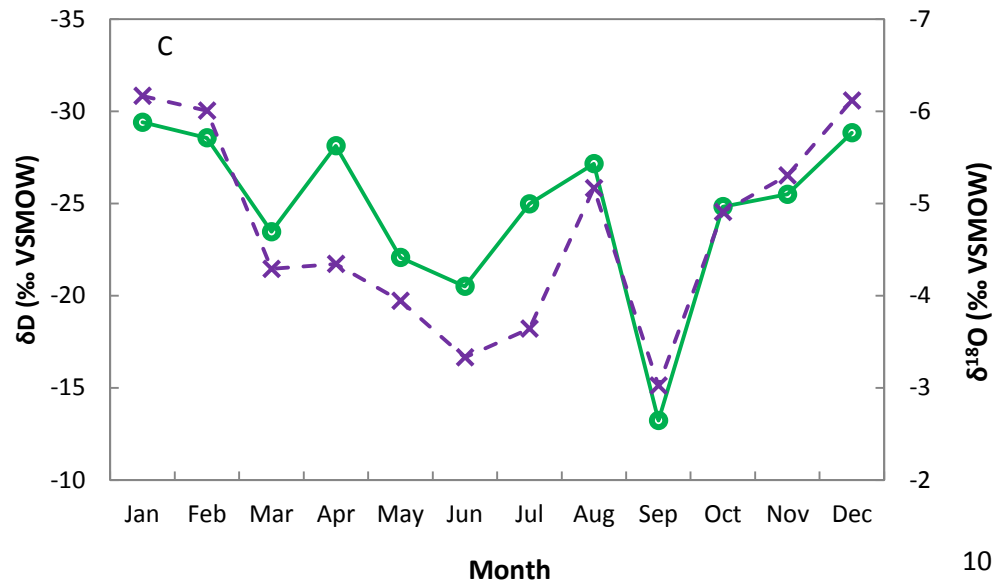
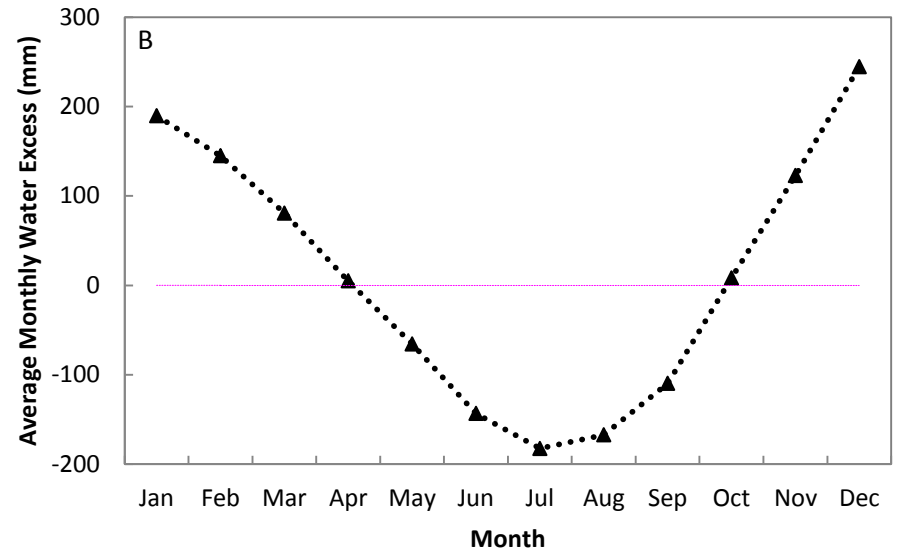
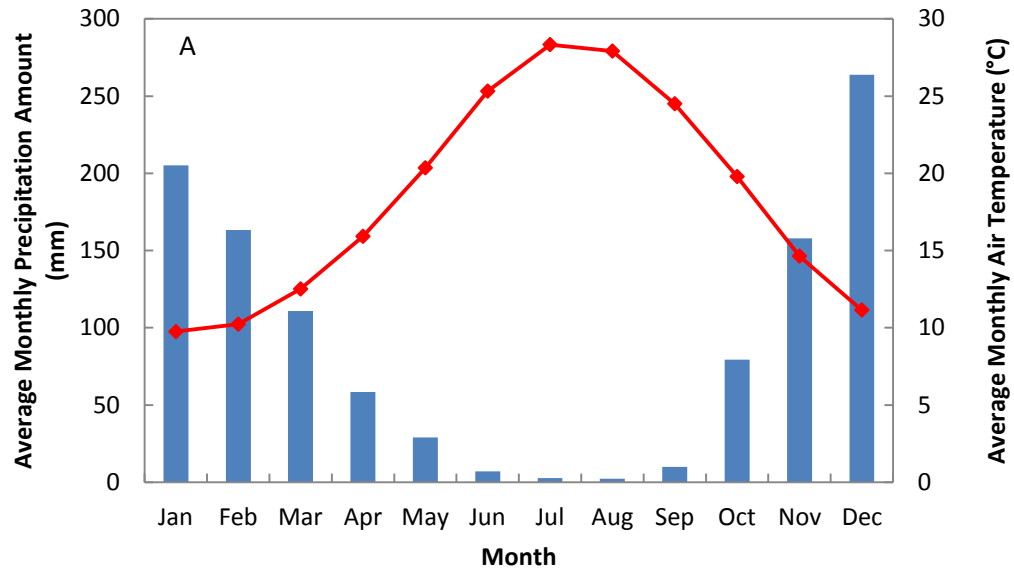


**Figure 4.5** Average Monthly Precipitation and Temperature data for Antalya (IAEA and WMO, 2006), for the period 1963-2004. Months in which less than 20 mm rainfall was recorded were excluded, in an attempt to reduce the effects of evaporation on the averages.

A) Average monthly precipitation amount (blue bars) and average monthly air temperature (red diamonds and solid line).

B) Water Excess (black diamonds and dotted line). Pink dashed line indicates zero water excess.

C) Average monthly weighted  $\delta^{18}\text{O}$  (purple crosses and dashed line) and  $\delta\text{D}$  (green open circles and solid line) of precipitation.

Month	Number of $\delta^{18}\text{O}$ measurements
Jan	30
Feb	28
Mar	32
Apr	27
May	28
Jun	16
Jul	7
Aug	5
Sep	15
Oct	27
Nov	28
Dec	32

**Table 4.3:** Number of water samples analysed for isotopic data per month at Antalya IAEA Station (1963-2004) (IAEA and WMO, 2006).

Period	% of Annual Precipitation
Dec-Feb	58.0
Mar-May	18.2
Jun-Aug	1.1
Sep-Nov	22.7
Oct-Mar	90.0
Apr-Sep	10.0
Oct-May	98.0
Jun-Sep	2.0

**Table 4.4:** Percentage contributions of time periods to total annual precipitation at Antalya IAEA Station (IAEA and WMO, 2006). Periods are as in Figure 4.6.

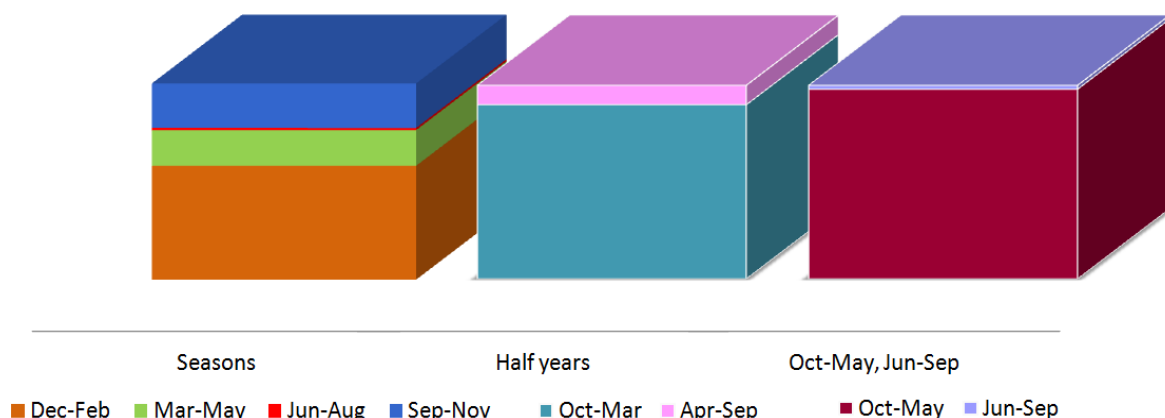


**Figure 4.6:** Percentage contribution of time periods to total annual precipitation at Antalya IAEA Station (IAEA and WMO, 2006). These data are also presented numerically in Table 4.4.

A) Data are separated arbitrarily into the four seasons

B) Data are separated into the winter and summer half years

C) Data are separated into the periods Oct-May, which provides ~98% of the annual rainfall, and Jun-Sep, which provides only ~2% of annual rainfall.

#### 4.2.1 Dim Dripwaters and Meteoric Water Lines

Dripwaters were collected over several months, as described in section 4.1.2.2.

A comparison of Meteoric Water Lines (MWLs) is shown in Figure 4.7. The Antalya IAEA data is represented by the orange, dashed line labelled as Antalya-LMWL, which is described by Equation 4.1. Months in which less than 20 mm of rain fell have been removed from this data set, to exclude evaporative effects.

The Antalya-LMWL is close to the Turkey-LMWL (Equation 4.2) of Dirican et al. (2005), which uses data from several locations along the Mediterranean coast of Turkey, suggesting that rainfall at Antalya is from a Mediterranean source, as expected.

$$\delta^2\text{H} = 6.8 \delta^{18}\text{O} + 9 (\text{‰}_{\text{VSMOW}})$$

*Equation 4.1*

*Antalya IAEA Station Data LMWL Equation*

$$\delta^2\text{H} = 7.74 \delta^{18}\text{O} + 13.1 (\text{‰}_{\text{VSMOW}})$$

*Equation 4.2*

*Turkey-LMWL Equation*

The data for Dim dripwaters (turquoise rings in Figure 4.7) plot closer to the Mediterranean Meteoric Water Line (MMWL, Equation 4.5) than the Turkey LMWL, and far away from the Global Meteoric Water Line (GMWL; Equation 4.4) (Craig, 1961). The equation for the LMWL of the Dim dripwater is shown in Equation 4.3. The MMWL was defined after Gat and colleagues (Gat and Carmi, 1970, 1987, Gat and Dansgaard, 1972, Gat, 1980, 1996, Gat et al., 1996) and documented the high value of the *d* of stable isotopes in winter precipitation in the eastern Mediterranean Sea region.

$$\delta^2\text{H} = 6.5 \delta^{18}\text{O} + 8.4 (\text{‰}_{\text{VSMOW}})$$

*Equation 4.3*

*Dim Dripwaters LMWL*

$$\delta^2\text{H} = 8 \delta^{18}\text{O} + 10 (\text{‰}_{\text{VSMOW}})$$

*Equation 4.4*

*GMWL Equation*

$$\delta^2H = 8 \delta^{18}O + 22 (\text{‰VSMOW})$$

Equation 4.5  
MMWL Equation

$d$  denotes the position of the isotopic composition of a precipitation sample relative to the GMWL

$$\delta D = 8 \delta^{18}O + d_{\text{excess}}$$

Equation 4.6  
Deuterium excess Equation (Dansgaard, 1964)

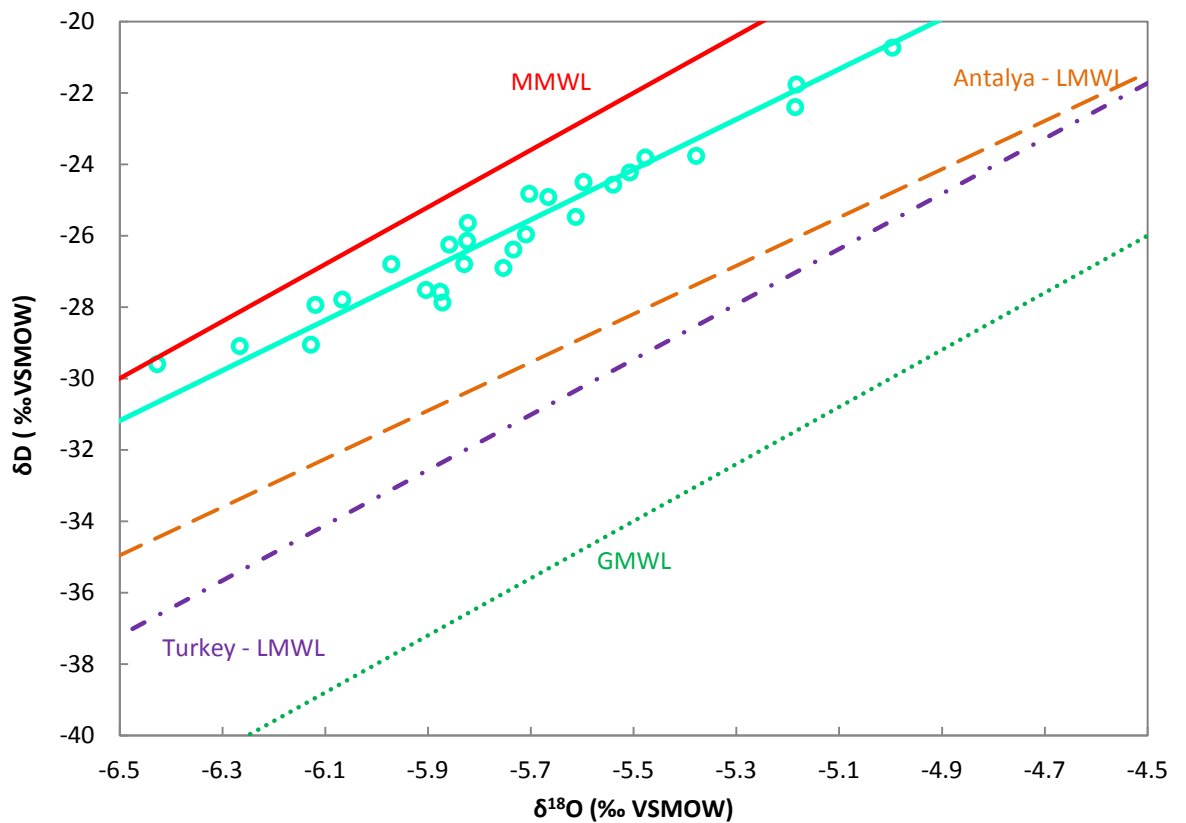


**Figure 4.7** Comparison of local and global meteoric water lines with Dim Cave dripwaters.  
 GMWL = Global Meteoric Water Line (Craig, 1961) [green dotted line]  
 MMWL = Mediterranean Meteoric Water Line (Gat, 1980, Gat and Carmi, 1987, Gat and Carmi, 1970) [red solid line]  
 LMWL = Local Meteoric Water Line;  
     Turkey (Dirican et al., 2005) [purple dotted/dashed line];  
     Antalya (IAEA and WMO, 2006) [orange dashed line]  
 Dim Dripwaters are identified by open turquoise circles; the solid turquoise line running through them represents the overall trend.

#### 4.2.1.1 Water-Calcite Equilibrium

Table 4.5 shows modern calcite  $\delta^{18}\text{O}$  values for 2 soda straws collected from Dim Cave ( $\delta^{18}\text{O}_c$ ), along with high and low values for Dim drip waters ( $\delta^{18}\text{O}_w$ ) and air temperature.

Sample	$\delta^{18}\text{O}_c$ (‰ VPDB)	$\delta^{18}\text{O}_w$ (‰ VSMOW)		Air-Temp. (°C)
DSS 1	-4.049	High	-5.25	18.6
DSS 7	-3.618	Low	-6.13	

**Table 4.5 Summary of measured  $\delta^{18}\text{O}$  values of Dim Cave drip waters ( $\delta^{18}\text{O}_w$ ) and soda straw calcite ( $\delta^{18}\text{O}_c$ )**

Aragonite with  $\delta^{18}\text{O}$  values of -4.049 to -3.618 ‰ precipitated from waters of  $\delta^{18}\text{O}$  value -5.25 to -6.13‰ is expected to have precipitated under air temperatures of approximately 7 -13 °C (Kim et al., 2007). This suggests that modern aragonite is not precipitating in isotopic equilibrium with dripwaters. However, the range of values predicted from several different equilibrium equations is much larger than this range, indicating that these equations may not be of sufficient accuracy to judge equilibrium. Also, it is possible that the equilibrium state may have been different in the past. Therefore, Hendy tests (Hendy, 1971) will also be used to determine whether equilibrium precipitation was occurring.

### **4.3 Stalagmites DIM-1, DIM-2 and DIM-3**

Stalagmites DIM-1 and DIM-2 (Figure 4.8 A and C) are stalagmites collected from Dim Cave in March 2009. Both were toppled when found, and therefore not actively precipitating. The top of DIM-1 was also missing, leaving 568 mm of growth. DIM-2 comprises 230 mm of growth.

At some time after DIM-1 toppled, a new period of growth was deposited on the outer layers of the stalagmite, at a right angle to the original growth direction. Because it is not known if this growth precipitated from the same drip, or if the position of DIM-1 changed significantly after toppling such that the new growth is from a drip in a different part of the cave, we have named the period of new growth DIM-3 (Figure 4.8B), and treat it as though it precipitated from a different drip to DIM-1, but will discuss it in this chapter along with DIM-1.

It is probable that the force required to topple DIM-1 and DIM-2 came from an earthquake, which is possible as the area is close to the Anatolian fault region. Panno et al. (2009) has suggested that growth periods of speleothems may be used to date earthquakes which occurred before instrumental and anecdotal records, provided modern growth can be shown to be interrupted by known earthquake occurrences. Unfortunately, this is not possible for DIM-1 and DIM-2, partly because the top of the stalagmite is missing, and partly because we do not have a modern stalagmite record with which to compare growth periods and earthquake episodes.

#### **4.3.1 Physical Characteristics of DIM-1, DIM-2 and DIM-3**

##### **4.3.1.1 Hiatus in DIM-1**

DIM-1 has one very clear hiatus at ca. 480 mm on the central axis (red line on Figure 4.8 A), followed by a shift in drip axis after growth had resumed. Asrat et al. (2007) highlighted the usefulness of distinct morphological changes in stalagmites from arid or semi-arid regions in aiding palaeoclimatic interpretation if they can be directly related to hydrological change. It is expected that the hiatus in DIM-1 resulted from an increase in aridity, due to the fact that stalagmite diameter reduced immediately before the hiatus.



**Figure 4.8**

**A) Stalagmite DIM-1.** Red line indicates location of hiatus. Blue box indicates one set of the “lateral wings” mentioned in section 4.3.1.3.

**B) DIM-3,** shown as it grew on the outside of DIM-1 at right angles to DIM-1’s growth axis.

**C) Stalagmite DIM-2**

#### **4.3.1.2 Stalagmite Shape**

DIM-1 and DIM-2 are columnar in shape and of near constant diameter throughout growth, with the exception of the area around the hiatus, where width reduces rapidly up to the hiatus, and when growth resumed the previous constant diameter was restored. As mentioned above, this reduction in stalagmite width coupled with a growth hiatus most likely indicates a trend towards increased aridity. Slowly dripping sites which are fed by vadose seepage flow water are likely to result in columnar, constant diameter stalagmites (McDermott et al., 2006), so it could be inferred that DIM-1 was fed by slow dripping, vadose seepage flow-fed drips.

DIM-3 is not columnar in shape, diameter is much wider at the base compared to when growth ceased, however as the stalagmite is not very large (only 34 mm of growth), not much information can be inferred from this. There appears to be a “splash pit” in the growth axis of DIM-3, which may have implications for stable isotope measurements.

#### **4.3.1.3 Interfingering “wings”**

DIM-1 exhibits lateral “wings”, which are less translucent than the area around the central growth axis (see blue box in Figure 4.8A). This is very similar to the structure noted by Verheyden et al. (2008) in stalagmite JeG-stm-1 from Jeita Cave, Lebanon. In JeG-stm-1, the “wings” were found to have much more abundant fluid inclusions compared with the central portion of the stalagmite; it is likely that it is also fluid inclusions which give the “wings” in DIM-1 their more opaque nature.

#### **4.3.1.4 3D Evolution of DIM-1 Structure and Laser-Photostimulated Luminescence**

Sawing of progressive slabs of DIM-1 for various analyses (Figure 4.9) showed that the stalagmite internal structure was not simple at all, and some structures were only visible at certain depths through the stalagmite. This was noticeable to the naked eye in normal light, and was extremely clear when the slabs were imaged using direct scanning laser-photostimulated luminescence imaging (SLPL) (Figure 4.10). From these images, it seems most likely that areas which luminesce (dark areas on the image) are original minerals (aragonite), and non-luminescent areas (white on the image) are recrystallised calcite, which have lost their luminescence. A similar situation was found by Spötl et al. (2002b), although not via SLPL. Sawing of slabs to investigate the 3D evolution of DIM-1’s structure also revealed that some structures which had previously been assumed to be only visible layers were in fact micro-hiatuses (Figure 4.11). This is of particular importance as it may affect U/Th dating.

#### **4.3.1.5 Crystallography**

##### *4.3.1.5.1 DIM-1*

The discovery of the 3D evolution of DIM-1's structure had important implications for understanding the crystallography. Original XRD analysis was performed on Face A, and revealed that the majority of DIM-1 is calcite, with a layer of aragonite immediately preceding the hiatus, which corresponds to the region 467-480 mm on the central growth axis. Thin section microphotographs of this change are shown in Figure 4.12. The calcite crystals lack the equant morphology that often indicates recrystallisation, however this may be because the fabric has been guided by aragonite inclusions. Laser-stimulated photoluminescence imaging on Face A, performed early on in the research, was inconclusive and did not show the very clear structure that was identified in Faces D and E. This clear structure prompted additional XRD analysis on Face E, the results of which are shown in Figure 4.13. The most important discoveries from this analysis are that the area above the hiatus, identified by the green box, is aragonite, and below the aragonite region, the calcite appears to be "eating into" the aragonite from below, identified by the red box. Thus it is likely that at least part of the stalagmite is recrystallised (aragonite to calcite transformation), with recrystallisation still progressing in this portion of the stalagmite. Analysis of the 3D structure was crucial to this interpretation, as the corresponding section of Face A did not show these changes, either in SLPL, thin section microphotography or XRD analysis. As a result of this interpretation of DIM-1s evolution, new U/Th were chosen from aragonitic parts of the stalagmite to attempt to avoid the effects of recrystallisation on U-Series dating.

##### *4.3.1.5.2 DIM-3*

DIM-3 was found by XRD analysis to be comprised entirely of aragonite.

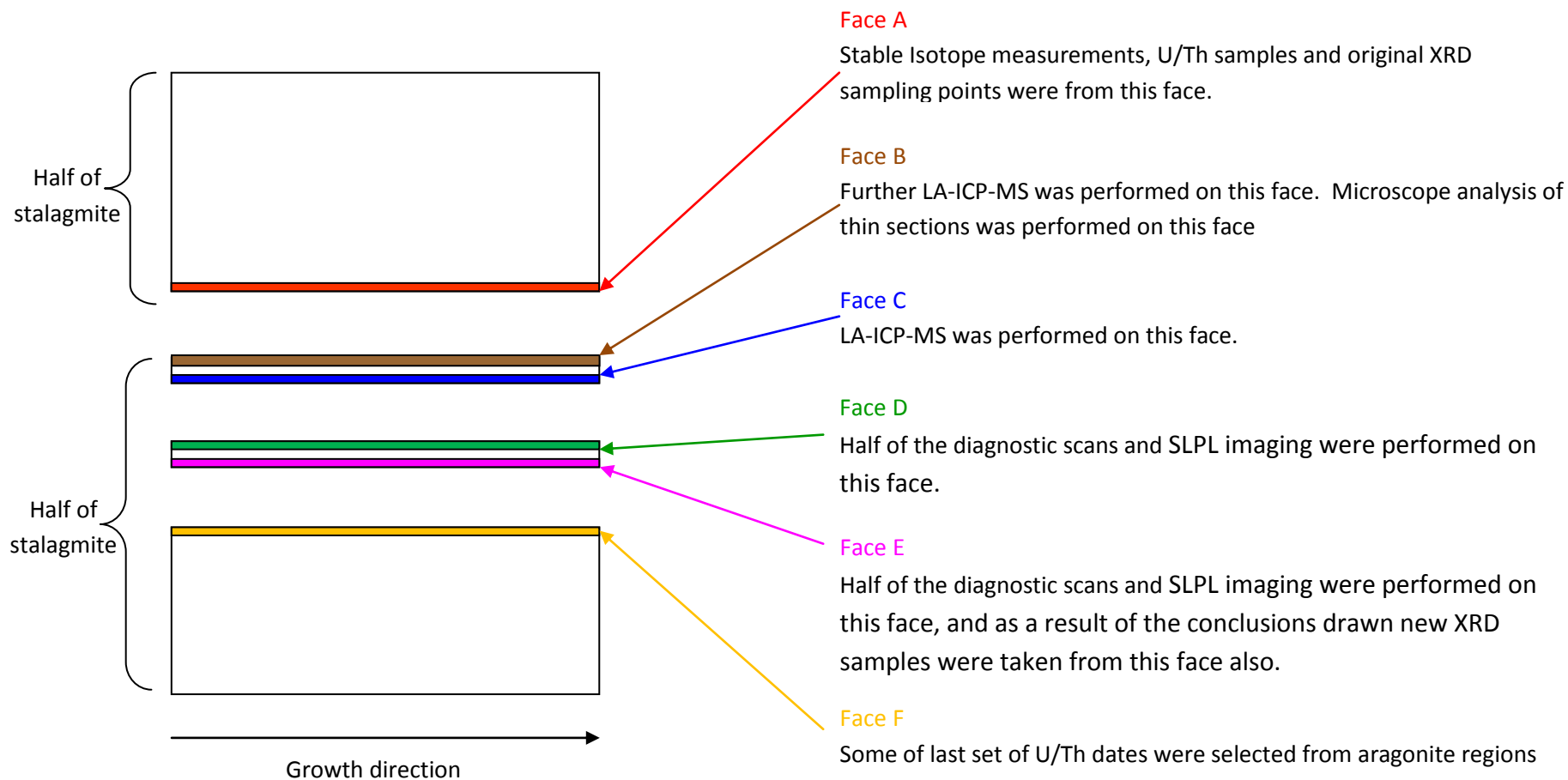


**Figure 4.9** Schematic indicating how progressive slabs through DIM-1 were used for analyses.

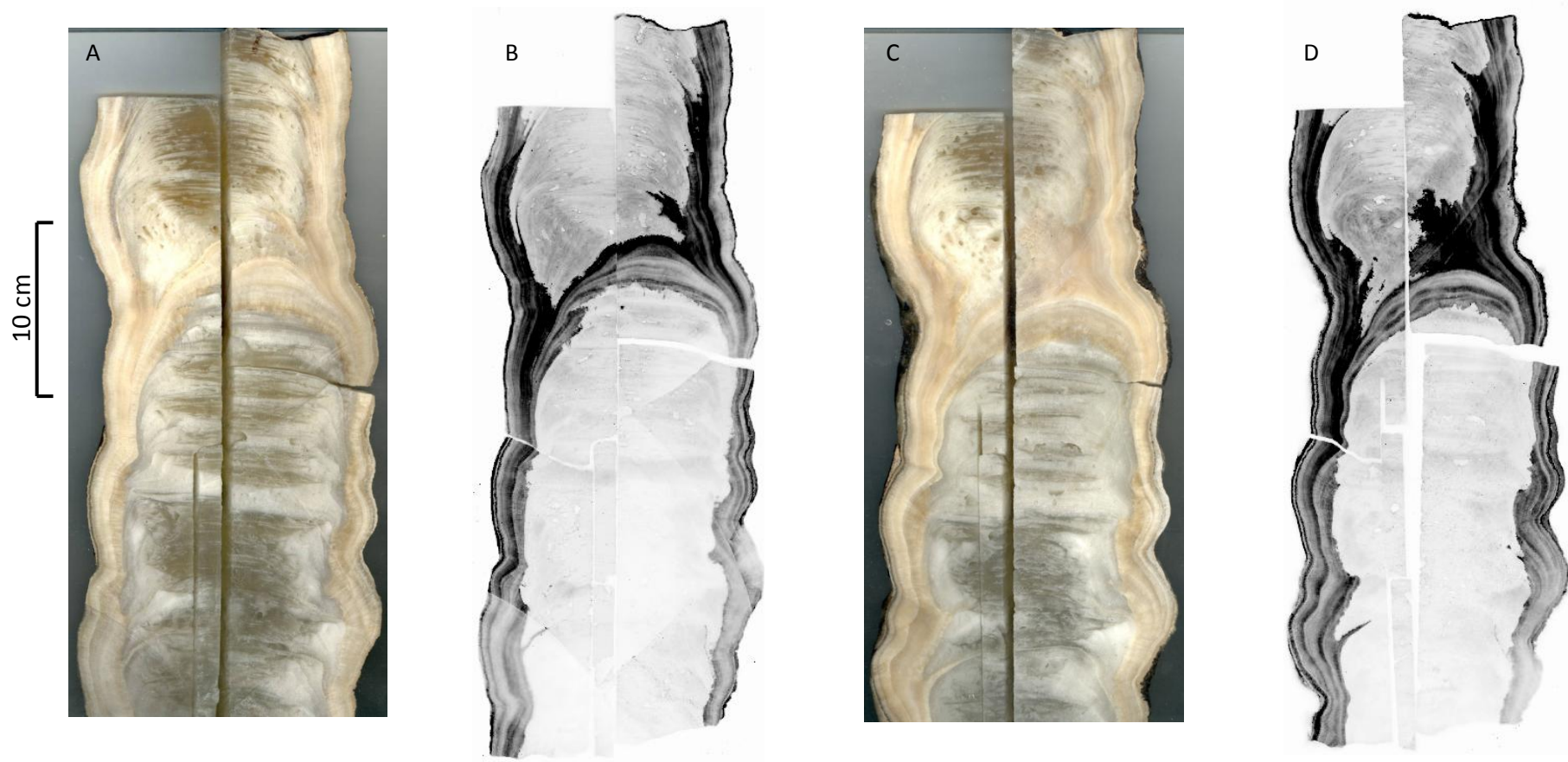


**Figure 4.10 Diagnostic Imaging of DIM-1 (upper portion).**

**A) Face D. Scan in visible light, B) Face D. Direct scanning laser-photostimulated luminescence imaging (SLPL imaging). Dark areas indicate high luminescence. C) Face E. Scan in visible light D) Face E. Direct scanning laser-photostimulated luminescence imaging (SLPL imaging). Dark areas indicate high luminescence.**

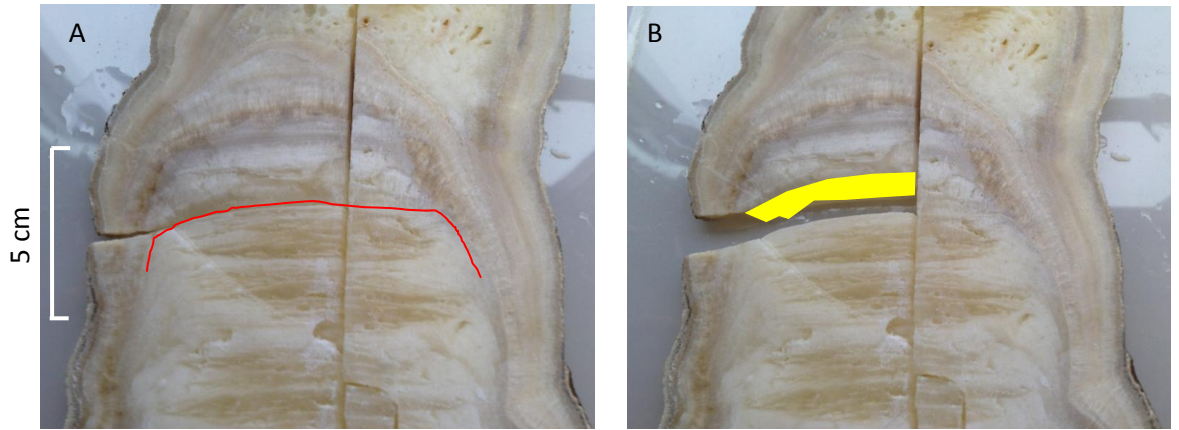


**Figure 4.11** Location of a microhiatus in DIM-1 which was revealed by the stress of sawing causing the slab to split along the microhiatus.  
**A)** Red line indicates position of visible “layer”.  
**B)** Slab cracked along microhiatus. Yellow surface is rough, corroborating the fact that this visible structure is a result of a cessation of growth for a short period.

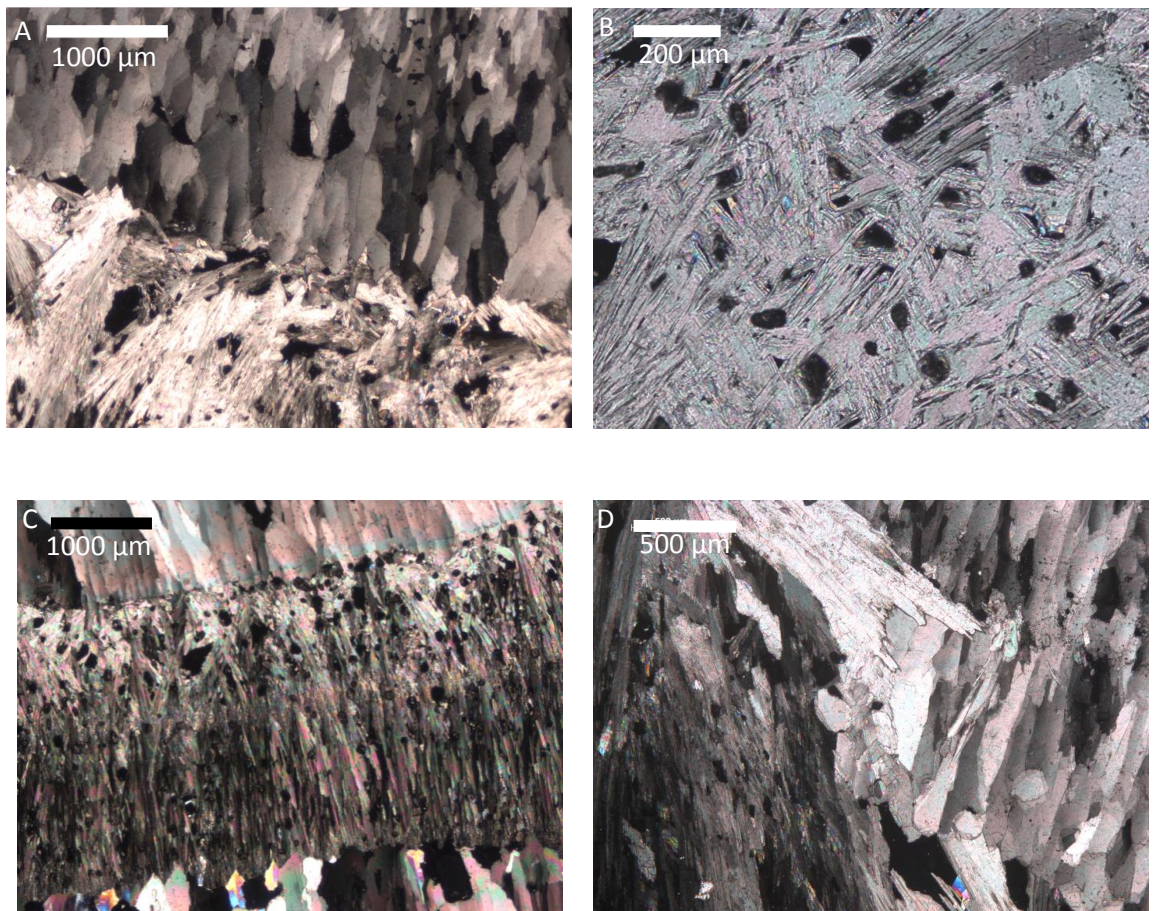


**Figure 4.12** Thin section microphotographs of DIM-1. All images are transmitted, cross-polarized light, and inverted vertically.  
**A)** The intersection between calcite and aragonite growth before the hiatus.  
**B)** Aragonite fabric from the aragonite layer preceding the hiatus.  
**C)** The aragonite layer at a thinner section of its length.  
**D)** The intersection of the aragonite layer with two sections of calcite.

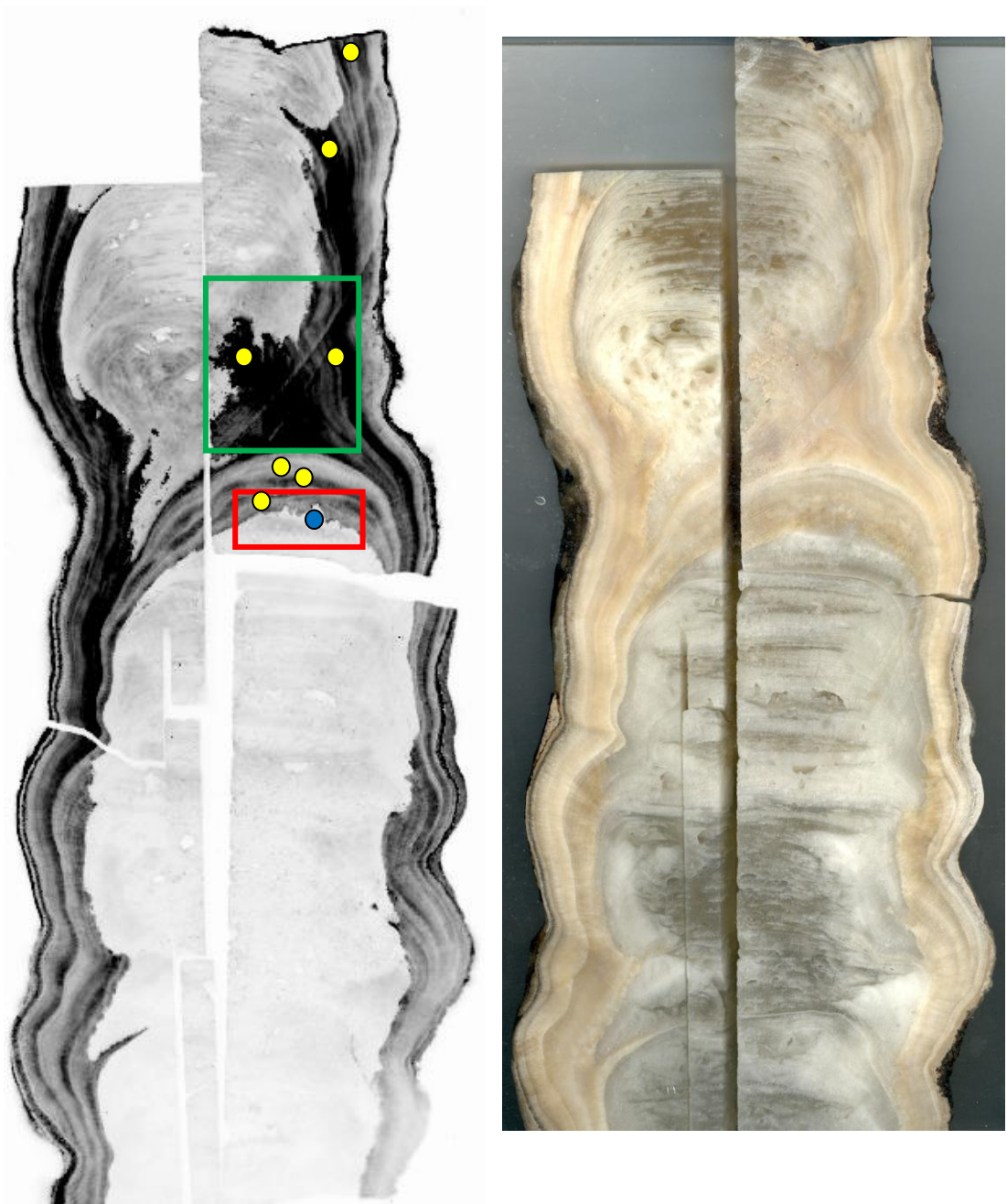


**Figure 4.13** DIM-1 XRD analysis results shown in relation to SLPL image (A) and photograph (B). Dark areas on SLPL image indicate high luminescence. Yellow circles indicate aragonite, blue circle indicates calcite (as identified by XRD analysis). Green rectangle identifies region of interest above hiatus that appears to show recrystallisation in process. Red rectangle indicates area where aragonite is being replaced by calcite, leading to an appearance of the aragonite being “eaten away”.

#### 4.3.1.5.3 DIM-2

Observations of the structure of DIM-2 suggested that some diagenetic alteration, most likely recrystallisation, had occurred. The main reason to suspect this was that some layers clearly crossed areas of differing crystallography (red rectangle in Figure 4.14i). XRD analyses confirmed that the areas of differing appearance in DIM-2 were of different mineralogy. The original fabric of DIM-2 is a bright white, soft, porous aragonite (Figure 4.15A, and regions marked A on Figure 4.14i), which has been replaced in several areas by a dull light brown, hard, dense calcite (regions marked C on Figure 4.14i). One area exhibited both fabrics interspersed (region A+C in Figure 4.14i). Thin section analysis by microscopy supported the conclusion that areas of DIM-2 had been recrystallised from aragonite to calcite (see Figure 4.15). Evidence for recrystallisation in thin section included interlocking of the two fabrics at intersections between the two mineralogies (Figure 4.15C), and “islands” of both fabrics within areas primarily composed of the other polymorph (Figure 4.15B). SLPL imaging also supported the interpretation that DIM-2 was recrystallised in places rather than containing both polymorphs as primary minerals, as while the aragonite regions showed high levels of luminescence (dark colouring in Figure 4.14ii) and layers within this fluorescence, the calcite regions contain little to no luminescence (light colouring in Figure 4.14 ii). The explanation offered here is that the luminescence is caused by organic molecules, which were deposited at high concentrations in the original aragonite due to low discharge rates. Conversely, the subsequent higher discharge rates which led to recrystallisation of the aragonite as calcite resulted in much lower concentrations of organic molecules, and therefore almost no luminescence. A simplified version of the crystallography of DIM-2 is shown in Figure 4.14i.

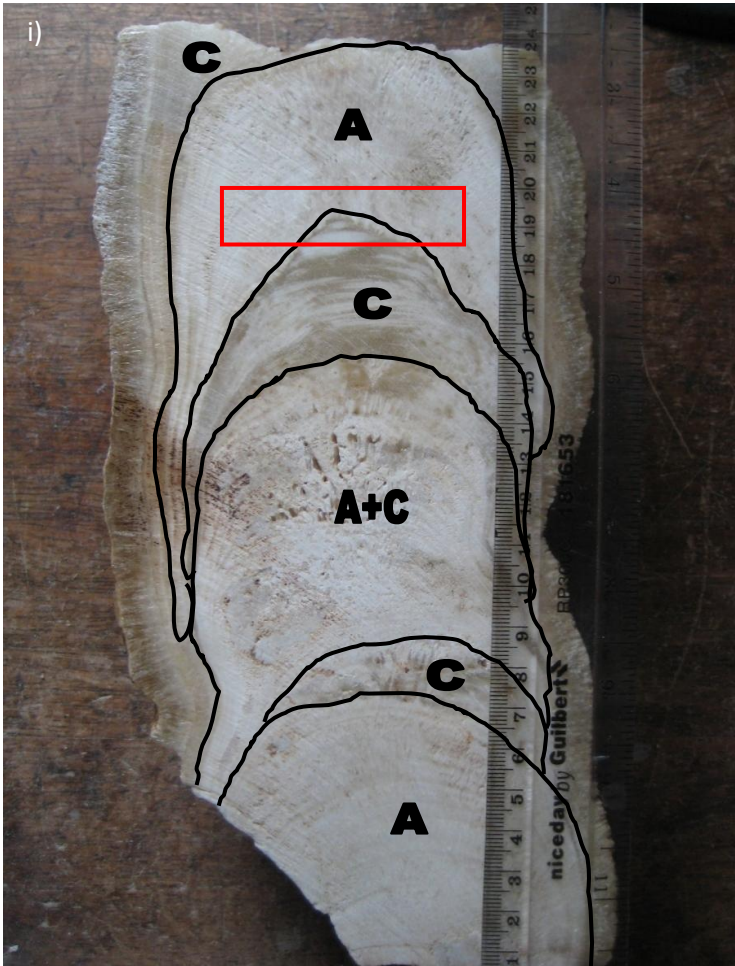


**Figure 4.14** i) Crystallography of DIM-2, according to XRD measurements. A= aragonite, C=calcite. Red box indicates area in which some layers were partially recrystallised, laterally. ii) Direct scanning laser-photostimulated luminescence imaging (SLPL) of DIM-2. Dark areas indicate high luminescence, light areas indicate low luminescence. Note, this image was taken of the opposite half stalagmite slab to i).

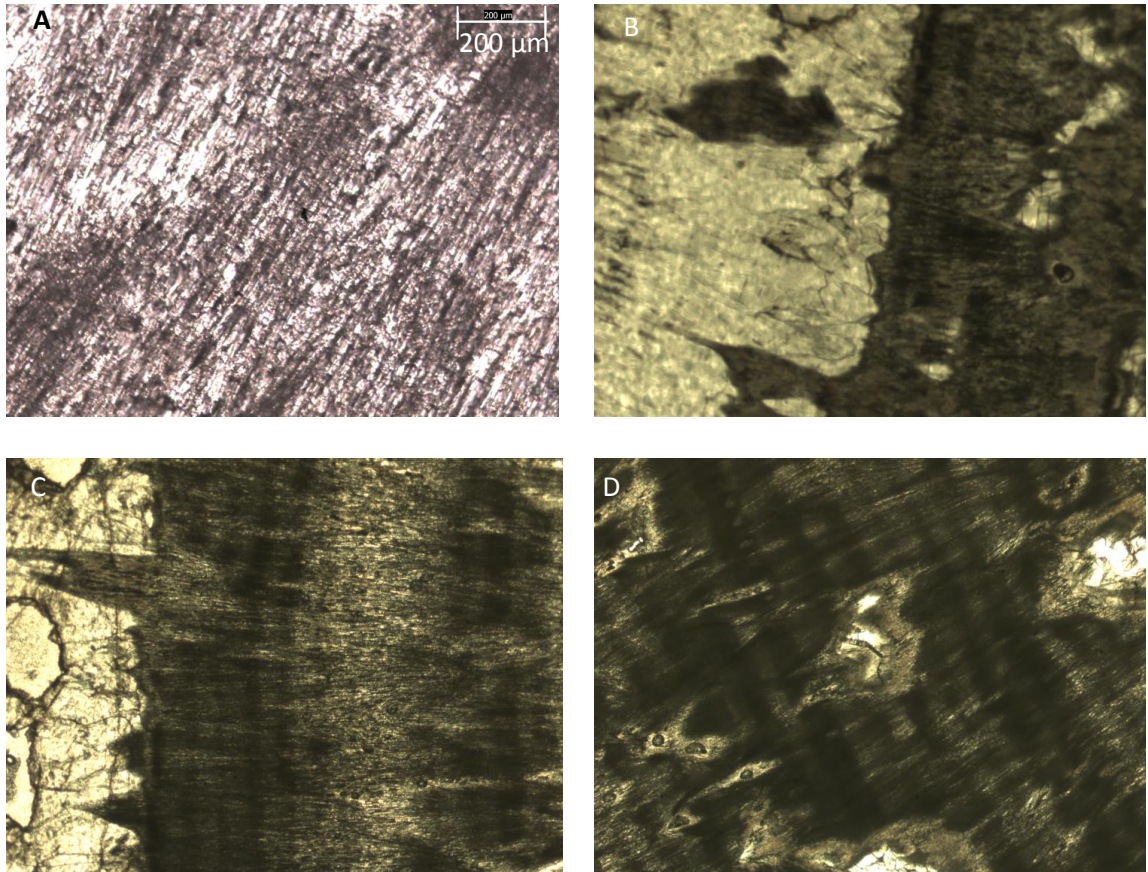


**Figure 4.15** Thin section microphotographs of DIM-2.

**A)** Pristine unaltered aragonite in the lower part of DIM-2, which has not yet undergone recrystallisation at the macro scale.

**B)** Intersection between calcite (lighter) and aragonite areas, with a very clear aragonite relic "island" in the calcite region.

**C)** Intermingling of calcite and aragonite at the boundary, and also what appears to be banding in the aragonite.

**D)** Clearer view of the banding in the aragonite. The voids are due to the thin section making process and are not original features.

## 4.3.2 Uranium Series Dating

### 4.3.2.1 Sampling Strategy

#### 4.3.2.1.1 DIM-1

U/Th samples were selected from DIM-1 with the intention of constructing a chronology for palaeoclimatic reconstruction. Samples were chosen based on stratigraphic features such as shifts in the growth axis, and the hiatus. However, problems with the DIM-1 U/Th chronology (see Section 4.3.2.1.1), most likely due to recrystallisation of aragonite as calcite, necessitated several batches of U/Th dates to attempt to reconcile the problems and retrieve a viable chronology. Figure 4.16A shows the locations of all the sampling locations.

#### 4.3.2.1.2 DIM-3

Due to the small size of DIM-3, only two U/Th locations were chosen, near top and bottom (Figure 4.16B).

#### 4.3.2.1.3 DIM-2

DIM-2 had already been identified before any dating was undertaken as a speleothem which had undergone partial or complete recrystallisation from calcite to aragonite in places. Therefore the aim of U/Th dating this stalagmite was not to build a chronology for palaeoclimatic reconstruction, as it was expected that recrystallisation had lead to U-loss, reducing the accuracy of U/Th dates. However, samples were taken from the two areas of aragonite which appear to not have undergone macro recrystallisation, with the aim of investigating whether speleothems in which the U/Th system has become opened may still be dateable if sample selection is careful (Figure 4.16C). After sampling, it became apparent that like DIM-1, DIM-2 has some evolution of structure in the z-dimension, as pockets of recrystallised calcite could be seen in the aragonite areas at depths further away from the centre of the stalagmite. However, as none of these pockets could be seen on the face sampled, and high U content (up to 5 ppm in the aragonite) allowed small sample sizes, the samples taken were deemed to be unaltered, assuming that recrystallisation was localised to the pockets and had not caused U-migration further afield.

### 4.3.2.2 Results

23 ages were determined throughout DIM-1, 2 ages were determined from DIM-3, and 7 ages were determined throughout DIM-2 (Figure 4.16 and Table 4.6, 4.7 and 4.8). Errors are 2 sigma. A detrital correction ratio ( $^{238}\text{U}/^{232}\text{Th}$ ) of 0.83 was used. This correction

accounts for the fact that most of the Th in the speleothem does not originate from soluble Th in the carbonate-precipitating waters, due to the fact that Th is largely insoluble, but in fact originates from silicate minerals which incorporate into the carbonate. The value of 0.83 is reached by multiplying the average crustal mineral  $^{232}\text{Th}/^{238}\text{U}$  value ( $\sim 3.8$ ) by the decay constants of  $^{232}\text{Th}$  and  $^{238}\text{U}$ , to give a  $[\text{}^{238}\text{U}/\text{}^{232}\text{Th}]$  value of 0.83.

To correct the data, the  $^{232}\text{Th}$  is assumed to be completely from detrital silicate, and from this the amount of  $^{230}\text{Th}$  that needs to be accounted for can be estimated, assuming that the initial Th was at secular equilibrium, i.e.  $[\text{}^{230}\text{Th}/\text{}^{232}\text{Th}] = 1$ . U is also corrected for detrital contamination, using the  $^{238}\text{U}/\text{}^{232}\text{Th}$  detrital correction ratio, and assuming that  $[\text{}^{234}\text{U}/\text{}^{238}\text{U}]$  was at secular equilibrium.



**Figure 4.16** Location of U/Th dating samples from the Dim Cave stalagmites  
**A)** DIM-1, Face A (black filled ovals) and equivalent regions of Face F (open red ovals)  
**B)** DIM-3  
**C)** DIM-2

Mineralogy	Sample ID	Mm from base	U (ppm)	<sup>232</sup> Th (ppb)	[ <sup>234</sup> U/ <sup>238</sup> U]	[ <sup>234</sup> U/ <sup>238</sup> U] <sub>Initial</sub>	[ <sup>230</sup> Th/ <sup>238</sup> U]	[ <sup>230</sup> Th/ <sup>232</sup> Th]	Uncorrected Age (kyr)	Corrected Age (kyr)
Aragonite	52-3	Above top*	1.063	0.925	1.307 ± 0.206	1.439 ± 0.003	0.933	3252	<b>126.59 ± 0.73</b>	<b>126.57 ± 0.73</b>
Calcite	29-10	568	0.430	0.307	1.313 ± 0.057	1.435 ± 0.001	0.893	3795	<b>116.37 ± 0.45</b>	<b>116.36 ± 0.447</b>
Aragonite	52-2	566	3.284	0.681	1.313 ± 0.204	1.449 ± 0.003	0.942	13778	<b>127.51 ± 0.73</b>	<b>127.50 ± 0.73</b>
Calcite	41-8	564	0.422	0.167	1.319 ± 0.060	1.363 ± 0.001	0.462	3543	<b>46.06 ± 0.16</b>	<b>46.05 ± 0.165</b>
Aragonite	52-4	558	4.664	0.279	1.316 ± 0.206	1.453 ± 0.003	0.943	47880	<b>127.23 ± 0.73</b>	<b>127.22 ± 0.73</b>
Aragonite	52-1	506	6.358	3.963	1.313 ± 0.207	1.449 ± 0.003	0.938	4567	<b>126.59 ± 0.78</b>	<b>126.58 ± 0.78</b>
Calcite	37-5	500	0.384	0.749	1.304 ± 0.046	1.437 ± 0.001	0.937	1456	<b>127.97 ± 0.51</b>	<b>127.93 ± 0.515</b>
Calcite	29-9	494	0.772	0.305	1.258 ± 0.054	1.377 ± 0.001	0.922	7085	<b>133.93 ± 0.57</b>	<b>133.92 ± 0.568</b>
Aragonite	41-6	474	2.499	0.193	1.336 ± 0.074	1.343 ± 0.001	0.090	3557	<b>7.60 ± 0.02</b>	<b>7.60 ± 0.023</b>
Aragonite	52-5	472	4.140	0.988	1.318 ± 0.209	1.452 ± 0.003	0.944	12000	<b>126.95 ± 0.73</b>	<b>126.95 ± 0.73</b>
Aragonite	29-7	470	1.863	0.301	1.331 ± 0.045	1.463 ± 0.001	0.917	17226	<b>118.37 ± 0.43</b>	<b>118.36 ± 0.427</b>
Calcite	41-5	460	0.249	0.123	1.318 ± 0.093	1.452 ± 0.002	0.929	5712	<b>123.50 ± 0.65</b>	<b>123.49 ± 0.646</b>
Calcite	41-4	422	0.172	0.082	1.327 ± 0.116	1.328 ± 0.002	0.005	33	<b>0.43 ± 0.01</b>	<b>0.42 ± 0.008</b>
Calcite	37-3	360	0.166	0.989	1.400 ± 0.038	1.578 ± 0.001	1.019	518	<b>129.24 ± 0.69</b>	<b>129.13 ± 0.697</b>
Calcite	33-6	354	0.170	0.268	1.405 ± 0.082	1.576 ± 0.002	1.002	1923	<b>124.52 ± 0.56</b>	<b>124.49 ± 0.559</b>
Calcite	41-2	304	0.147	0.133	1.455 ± 0.090	1.638 ± 0.002	1.016	3428	<b>119.28 ± 0.60</b>	<b>119.26 ± 0.603</b>
Calcite	41-1	166	0.166	0.170	1.648 ± 0.100	1.923 ± 0.002	1.196	3552	<b>124.85 ± 0.65</b>	<b>124.83 ± 0.652</b>
Calcite	33-4	120	0.158	0.452	1.698 ± 0.073	2.004 ± 0.003	1.256	1334	<b>128.4 ± 0.79</b>	<b>128.36 ± 0.790</b>
Calcite	37-1	120	0.185	0.204	1.693 ± 0.032	1.997 ± 0.002	1.251	3447	<b>128.22 ± 0.66</b>	<b>128.20 ± 0.663</b>
Calcite	37-4	110	0.126	0.176	1.755 ± 0.041	2.090 ± 0.002	1.308	2840	<b>129.42 ± 0.53</b>	<b>129.40 ± 0.529</b>
Calcite	33-5	88	0.144	0.443	1.719 ± 0.089	2.008 ± 0.003	1.217	1203	<b>119.07 ± 0.70</b>	<b>119.02 ± 0.698</b>
Calcite	29-6	17	0.104	0.359	1.641 ± 0.103	1.912 ± 0.002	1.188	1043	<b>124.37 ± 0.63</b>	<b>124.32 ± 0.633</b>
Calcite	37-2	0	0.101	0.266	1.664 ± 0.046	1.961 ± 0.002	1.238	1425	<b>130.17 ± 0.70</b>	<b>130.13 ± 0.699</b>

**Table 4.6** *U/Th Age Data for stalagmites for DIM-1, arranged by sample depth. [<sup>234</sup>U/<sup>238</sup>U], [<sup>234</sup>U/<sup>238</sup>U]<sub>Initial</sub>, [<sup>230</sup>Th/<sup>238</sup>U] and [<sup>230</sup>Th/<sup>232</sup>U] are activity ratios. Ages are corrected for detrital interference. Ages in shaded cells are considered unreliable due to problems (see Section 4.3.2.2.1.1).*

*\* This sample was taken from an outer layer which does not have an analogue on the growth axis due to the fact that the stalagmite was broken before sampling.*

Stalagmite	Mm from base	U (ppm)	<sup>232</sup> Th (ppb)	[ <sup>234</sup> U/ <sup>238</sup> U]	[ <sup>234</sup> U/ <sup>238</sup> U] <sub>Initial</sub>	[ <sup>230</sup> Th/ <sup>238</sup> U]	[ <sup>230</sup> Th/ <sup>232</sup> Th]	Uncorrected Age (kyr)	Corrected Age (kyr)
DIM-3	34	5.286	0.277	1.278 ± 0.041	1.284 ± 0.001	0.080	4634	<b>7.01 ± 0.02</b>	<b>7.00 ± 0.018</b>
DIM-3	0	5.658	0.232	1.295 ± 0.108	1.302 ± 0.001	0.093	6859	<b>8.05 ± 0.02</b>	<b>8.05 ± 0.022</b>
DIM-2	226	7.065	0.126	1.181 ± 0.176	1.252 ± 0.003	0.794	135374	<b>116.30 ± 0.63</b>	<b>116.30 ± 0.632</b>
DIM-2	224	6.874	0.178	1.183 ± 0.039	1.253 ± 0.001	0.788	92291	<b>114.49 ± 0.41</b>	<b>114.49 ± 0.413</b>
DIM-2	198	1.043	0.092	1.189 ± 0.046	1.287 ± 0.001	0.908	31105	<b>147.32 ± 0.71</b>	<b>147.32 ± 0.712</b>
DIM-2	64	9.780	0.207	1.189 ± 0.060	1.258 ± 0.001	0.777	111506	<b>110.79 ± 0.53</b>	<b>110.79 ± 0.526</b>
DIM-2	64	10.369	0.198	1.186 ± 0.120	1.253 ± 0.002	0.770	122047	<b>109.60 ± 0.65</b>	<b>109.60 ± 0.655</b>
DIM-2	14	6.699	0.310	1.184 ± 0.052	1.254 ± 0.001	0.779	51119	<b>112.15 ± 0.53</b>	<b>112.14 ± 0.525</b>
DIM-2	5	4.789	0.506	1.181 ± 0.042	1.248 ± 0.001	0.774	22250	<b>111.52 ± 0.40</b>	<b>111.52 ± 0.397</b>

**Table 4.7** U/Th Age Data for stalagmites for DIM-2 and DIM-3, arranged by sample depth. [<sup>234</sup>U/<sup>238</sup>U], [<sup>234</sup>U/<sup>238</sup>U]<sub>Initial</sub>, [<sup>230</sup>Th/<sup>238</sup>U] and [<sup>230</sup>Th/<sup>232</sup>Th] are activity ratios. Ages are corrected for detrital interference. All samples are aragonite. Ages in shaded cells are considered unreliable due to problems

Mineralogy	Sample ID	Mm from base	U (ppm)	<sup>232</sup> Th (ppb)	[ <sup>234</sup> U/ <sup>238</sup> U]	Initial [ <sup>234</sup> U/ <sup>238</sup> U]	[ <sup>230</sup> Th/ <sup>238</sup> U]	[ <sup>230</sup> Th/ <sup>232</sup> Th]	Age (kyr)
Calcite	29-6	17	0.104	0.359	1.641 ± 0.103	1.912 ± 0.002	1.188	1043	<b>124.32 ± 0.633</b>
Aragonite	29-7	470	1.863	0.301	1.331 ± 0.045	1.463 ± 0.001	0.917	17226	<b>118.36 ± 0.427</b>
Calcite	29-9	494	0.772	0.305	1.258 ± 0.054	1.377 ± 0.001	0.922	7085	<b>133.92 ± 0.568</b>
Calcite	29-10	568	0.430	0.307	1.313 ± 0.057	1.435 ± 0.001	0.893	3795	<b>116.36 ± 0.447</b>
Calcite	33-4	120	0.158	0.452	1.698 ± 0.073	2.004 ± 0.003	1.256	1334	<b>128.36 ± 0.790</b>
Calcite	33-5	88	0.144	0.443	1.719 ± 0.089	2.008 ± 0.003	1.217	1203	<b>119.02 ± 0.698</b>
Calcite	33-6	354	0.170	0.268	1.405 ± 0.082	1.576 ± 0.002	1.002	1923	<b>124.49 ± 0.559</b>
Calcite	37-1	120	0.185	0.204	1.693 ± 0.032	1.997 ± 0.002	1.251	3447	<b>128.20 ± 0.663</b>
Calcite	37-2	0	0.101	0.266	1.664 ± 0.046	1.961 ± 0.002	1.238	1425	<b>130.13 ± 0.699</b>
Calcite	37-3	360	0.166	0.989	1.400 ± 0.038	1.578 ± 0.001	1.019	518	<b>129.13 ± 0.697</b>
Calcite	37-4	110	0.126	0.176	1.755 ± 0.041	2.090 ± 0.002	1.308	2840	<b>129.40 ± 0.529</b>
Calcite	37-5	500	0.384	0.749	1.304 ± 0.046	1.437 ± 0.001	0.937	1456	<b>127.93 ± 0.515</b>
Calcite	41-1	166	0.166	0.170	1.648 ± 0.100	1.923 ± 0.002	1.196	3552	<b>124.83 ± 0.652</b>
Calcite	41-2	304	0.147	0.133	1.455 ± 0.090	1.638 ± 0.002	1.016	3428	<b>119.26 ± 0.603</b>
Calcite	41-4	422	0.172	0.082	1.327 ± 0.116	1.328 ± 0.002	0.005	33	<b>0.42 ± 0.008</b>
Calcite	41-5	460	0.249	0.123	1.318 ± 0.093	1.452 ± 0.002	0.929	5712	<b>123.49 ± 0.646</b>
Aragonite	41-6	474	2.499	0.193	1.336 ± 0.074	1.343 ± 0.001	0.090	3557	<b>7.60 ± 0.023</b>
Calcite	41-8	564	0.422	0.167	1.319 ± 0.060	1.363 ± 0.001	0.462	3543	<b>46.05 ± 0.165</b>
Aragonite	52-1	506	6.358	3.963	1.313 ± 0.207	1.449 ± 0.003	0.938	4567	<b>126.58 ± 0.78</b>
Aragonite	52-2	566	3.284	0.681	1.313 ± 0.204	1.449 ± 0.003	0.942	13778	<b>127.50 ± 0.73</b>
Aragonite	52-3	Above top*	1.063	0.925	1.307 ± 0.206	1.439 ± 0.003	0.933	3252	<b>126.57 ± 0.73</b>
Aragonite	52-4	558	4.664	0.279	1.316 ± 0.206	1.453 ± 0.003	0.943	47880	<b>127.22 ± 0.73</b>
Aragonite	52-5	472	4.140	0.988	1.318 ± 0.209	1.452 ± 0.003	0.944	12000	<b>126.95 ± 0.73</b>

**Table 4.8** U/Th Age Data for DIM-1, arranged chronologically, by batch. [<sup>234</sup>U/<sup>238</sup>U], [<sup>234</sup>U/<sup>238</sup>U]<sub>initial</sub>, and [<sup>230</sup>Th/<sup>238</sup>U] are activity ratios. Ages are corrected for detrital interference. Ages in shaded cells are considered unreliable due to problems (see Section 4.3.2.2.1.1).

\* This sample was taken from an outer layer which does not have an analogue on the growth axis due to the fact that the stalagmite was broken before sampling. It was sampled as a test of the other samples; i.e. if all the aragonite samples in batch 52 were in chronological order, this sample (52-3) should be the youngest.

#### 4.3.2.2.1 DIM-1

Aragonite samples from DIM-1 are characterised by high uranium (1.063 - 6.358 ppm), while calcite samples are characterised by lower uranium (0.101 - 0.772 ppm).

##### 4.3.2.2.1.1 Problems with the DIM-1 Age Model

The first 2 batches of dates (analysed together) for DIM-1 (samples beginning 29- and 33- in Table 4.6 and 4.8) did not produce a chronologically ordered profile. However, problems were identified in the analytical procedure, such as an inhomogeneous standard, so these samples were disregarded at first. The following batch of dates (samples beginning 37- ) did produce a chronology that was in stratigraphic order within error, and was therefore used to create an age model.

However, the subsequent batch of U/Th dates, intended to refine the age model (samples 41- ), were far from in stratigraphic order. Analysis of the 3D structure of DIM-1 (see Section 4.3.1.4) revealed evidence of recrystallisation of aragonite to calcite that had not been clear on the central faces. Thus, the final batch of dates (samples 52- ) were all selected from parts of the stalagmite where original aragonite remained, as shown in Figure 4.17 (samples from aragonite in previous batches were found to be too close to the change in mineralogy). These new dates formed a common chronology within error with batch 37. It is worth noting that two samples taken from the same depth on the central growth axis, samples 33-4 and 37-1, which were analysed in separate batches, returned very similar dates ( $128.36 \pm 0.790$  and  $128.20 \pm 0.663$ ).



**Figure 4.17** Last set of U/Th dates, selected from areas identified as primary aragonite.  
**A = Samples selected from Face F**  
**B = Samples selected from Face A**

Thus, a chronology was created for DIM-1 using a combination of primary aragonite and recrystallised calcite samples. Sample 52-3 ( $126.57 \pm 0.73$  kyr BP) was not used as it was not possible to assign a growth axis depth to this sample, as it was taken from an outer layer that did not continue round to the growth axis. Normally, recrystallisation promotes U loss, as uranium is highly soluble as the  $\text{UO}_2^{2+}$  uranyl ion complexes (Langmuir, 1978), with the consequence that the ages calculated are much too old (e.g. Hoffmann et al., 2009, Lachniet et al., 2012). However it does not appear that U loss was a large factor in the anomalous dates from secondary calcite in DIM-1, with the possible exception of sample 29-9 (data point ringed in blue in Figure 4.19), which gave an age older than expected. Instead, many of the ages appear far too young, e.g. sample 41-4 which gave an age of 0.42 kyr BP. As there is no evidence of U uptake during recrystallisation (e.g. in the form of abnormally high U content) it appears that Th may have been lost from some locations. For example, the sample mentioned above for its young age, 41-4, has a  $^{230}\text{Th}/^{238}\text{U}$  activity ratio of only 0.005. Figure 4.18 plots  $^{230}\text{Th}/^{238}\text{U}$  against  $^{234}\text{U}/^{238}\text{U}$ , and clearly shows that samples not selected for the age model have U/Th systems which have been disturbed, by Th loss in all examples except sample 29-9, which appears to have undergone U loss. Thorium is expected to have a low solubility (Langmuir and Herman, 1980, Ryan and Rai, 1987, Vandenborre et al., 2010), so this is unexpected, and it is not clear at this point by what mechanism Th could have been lost from DIM-1.

In addition to Th-loss as an explanation for why some samples from the recrystallised areas were unusable, there is also the fact that there is at least one major hiatus in DIM-1 (as discussed in section 4.3.1.1) and perhaps several micro-hiatuses (as discussed in section 4.3.1.4). Figure 4.19 shows the location of some dates which may have been affected by these hiatuses, as U or Th isotopes may migrate along hiatuses, but there may be many more, as they can be hard to identify.

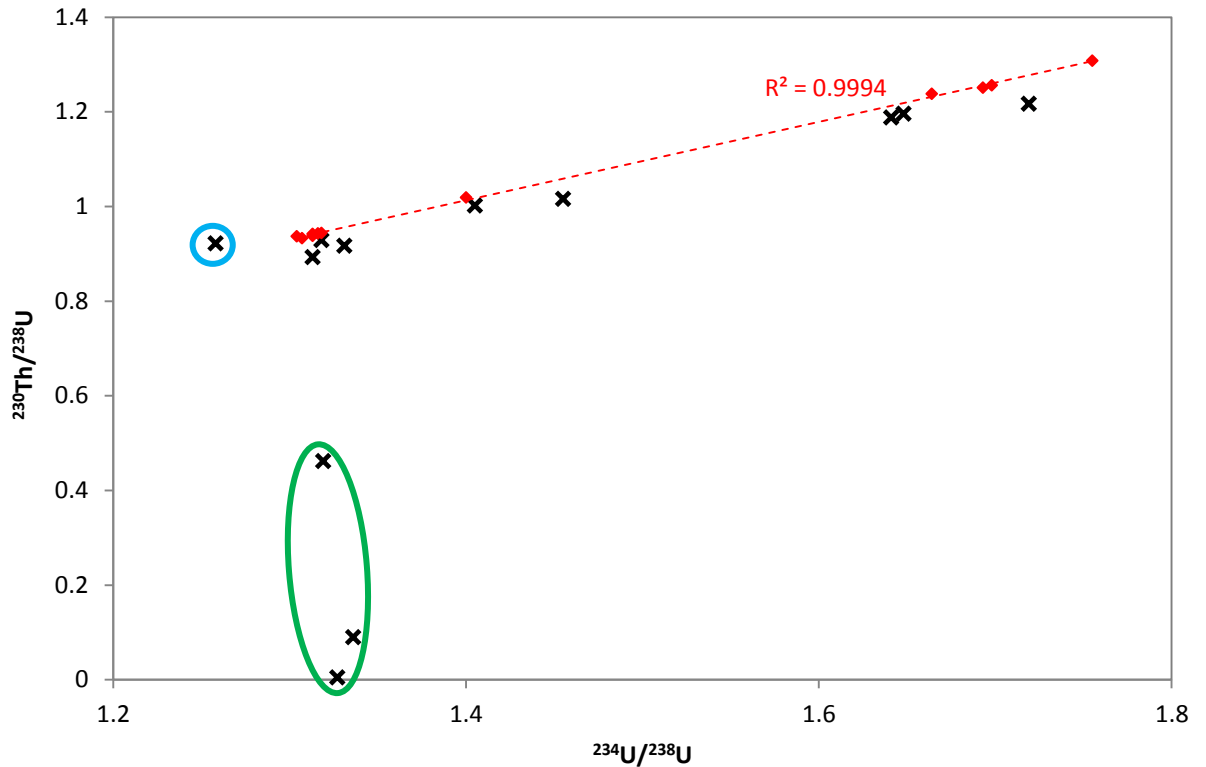


**Figure 4.18**  
 $^{230}\text{Th}/^{238}\text{U}$  versus  $^{234}\text{U}/^{238}\text{U}$  for DIM-1. Red diamonds represent dates selected for the age model. The red dashed line indicates the best-fit line for these data, and the  $R^2$  value for this line is shown (0.9994). Black crosses represent data not selected for the age model. The data point ringed in blue represents sample 29-9 (see discussion of this sample in text). 3 of the points not selected for the age model fall significantly below the rest on the  $^{230}\text{Th}/^{238}\text{U}$  axis, while falling within range of the other points on the  $^{234}\text{U}/^{238}\text{U}$  axis (these data points are identified by the green ring).

It is unusual to use ages from a recrystallised speleothem in an age chronology, even where ages are not generally too old, meaning that U loss was not a large factor. The fact that one of the recrystallised calcite samples was taken from above the hiatus and fits well within the age model of the aragonite samples in this part of the stalagmite suggests that the recrystallised samples can be used to complement the aragonite samples. However, it is clear that there has been some isotopic disturbance, leading to possible Th loss and anomalously young ages. For this reason, the age model must be treated with some caution. Those ages from recrystallised areas which produce acceptable dates and have been used in the chronology appear to have been sampled from areas in which the system opened only minimally.

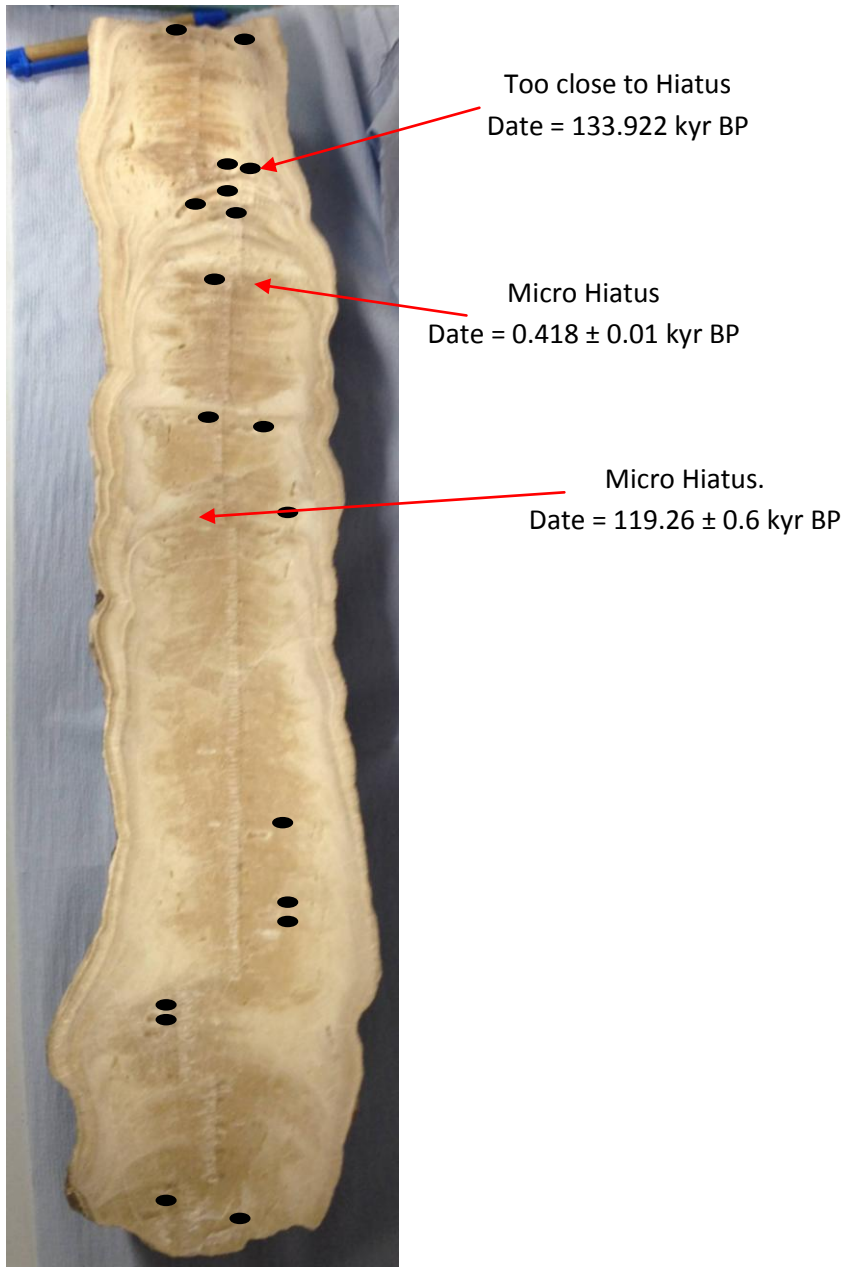


**Figure 4.19**  
*DIM-1 dating locations before selection of samples in Figure 4.19. Arrows identify structures which may have affected the U/Th chemistry of samples selected nearby.*

#### 4.3.2.2.1.2 *Age Model and Growth Rates*

An age model for DIM-1 was constructed from those dates deemed reliable (identified in Table 4.7 by non-shaded cells). The age model was constructed using the StalAge algorithm for the program R (Scholz and Hoffmann, 2011), and is presented in Figure 4.20. StalAge creates an age model by first screening for major outliers. Screening for minor outliers and age inversions follows, after which an iterative procedure is used to increase the uncertainty of outliers. A Monte-Carlo simulation is then applied, fitting ensembles of straight lines to sub-sets of the age data, to produce the age model and 95% confidence limits (Scholz and Hoffmann, 2011).

The growth rates of DIM-1 appear to be very fast in places. Indeed, the age model suggests that the portion of the stalagmite between ca 400 and ca 200 mm from the top of the stalagmite was deposited in a very short period of time, on the order of 100 years, although with the large error envelope, this period could actually be over 1 kyr (Figure 4.20). This section of the stalagmite has very few dates, due to the absence of primary aragonite in this region, and the problems with the majority of calcite dates. Therefore it is unlikely that the age model could be improved upon much in this region of the chronology. It is also possible that one age, sample, 37-3 (129.13 kyr BP  $\pm$  0.697) may be older than the true age due to U loss during recrystallisation. However, the primary aragonite ages above it constrain how much younger the true age could be; therefore if the age is too old it is likely only approximately 1 kyr too old, and in fact most likely is within the date's own analytic error. The other calcite dates also likely have true ages within their analytical errors, as if the true ages are much more than 1 kyr older than the calcite ages, the growth rate of DIM-1 would be unfeasible. Parts of DIM-1 which have a more certain chronology have growth rates of 0.1-1mm yr<sup>-1</sup>. This growth rate is fast, but not at a rate unheard of in the literature, for example a fast growing stalagmite from Ethiopia was found to have a growth rate of  $\sim$ 0.53 mm yr<sup>-1</sup> (Asrat et al., 2007).

As the errors on the age model are large, another approach is to assume relatively constant growth. In this scenario the 568 mm of growth would have been precipitated in approximately 3 kyr. This method assumes that the hiatus was of short duration, and results in average growth rates on the order of 0.2 mm yr<sup>-1</sup>. As DIM-1 appears to have laminations, which may be of an annual nature, future research on DIM-1 could investigate if these layers are indeed annual, and if so, whether they contain annual geochemical signals.

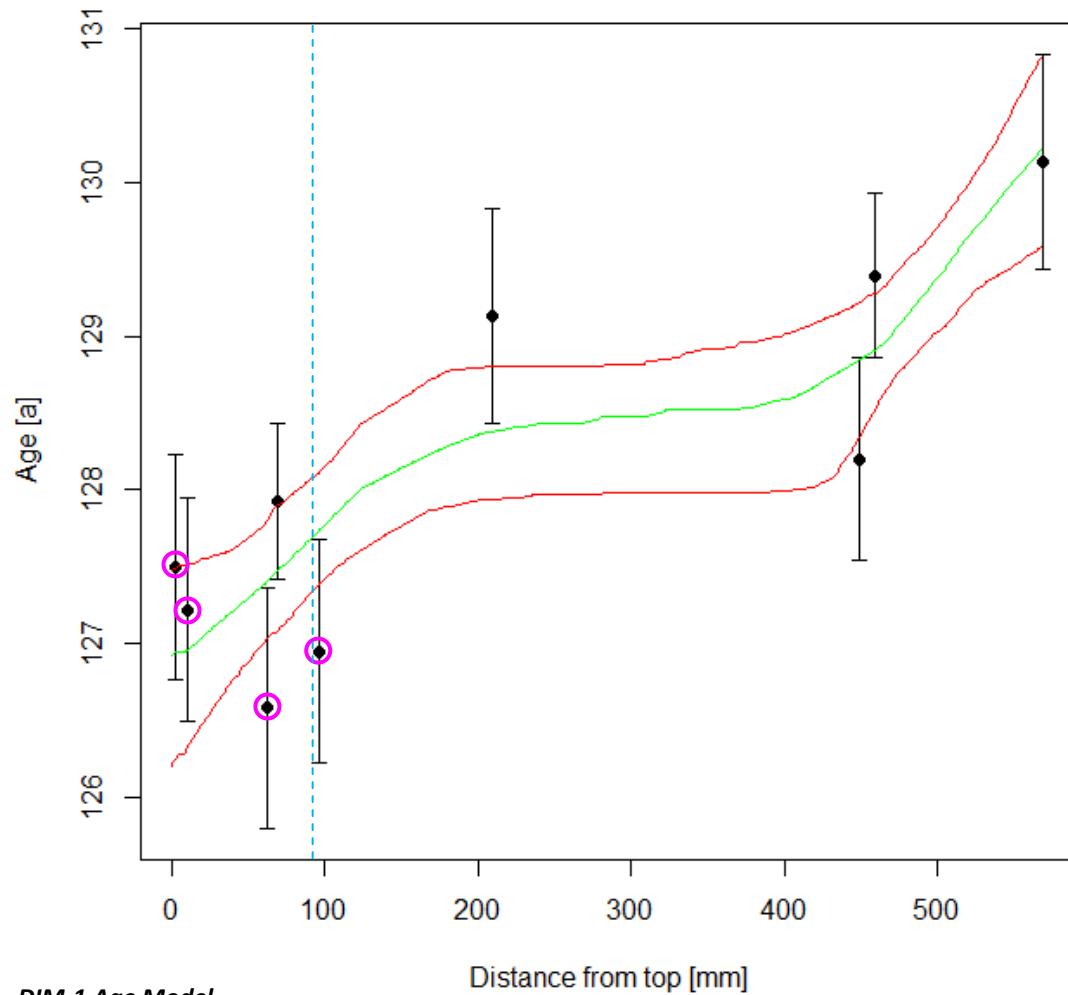


**Figure 4.20 DIM-1 Age Model**  
**A) Final Age Model for DIM-1, constructed using *StalAge* (Scholz and Hoffmann, 2011). Green line indicates age model, red lines indicates error envelope. Dashed blue vertical line indicates approximate location of the hiatus. Data points ringed in pink indicate that the samples were aragonite. B) Location of dates used in age model. Symbols as in Figure 4.16.**

#### 4.3.2.2.1.3 Initial $(^{234}\text{U}/^{238}\text{U})_0$

The initial  $(^{234}\text{U}/^{238}\text{U})_0$  data of DIM-1 are plotted against  $^{230}\text{Th}/^{238}\text{U}$  in Figure 4.21. They appear to show a trend of high values in the base of the stalagmite (green ring), with values reducing in the upper portion of the stalagmite (orange ring). This is most likely a result of alpha recoil effects in the epikarst during the period before DIM-1 grew, i.e. MIS 6. Enrichment of  $^{234}\text{U}$  in speleothems is a consequence of accumulation of  $^{234}\text{U}$  in easily leached sites within soils and overlying rock during periods when leaching activity is much reduced, for example during arid phases.  $^{234}\text{U}$  is then leached when precipitation levels increase and is subsequently deposited in speleothems (Plagnes et al., 2002). The trend of the samples in Figure 4.21 also closely follows an isochron between ca. 130-120 kyr BP, which supports the veracity of the age model adopted for DIM-1.

There are three anomalous points in Figure 4.21, identified by the pink ring. These samples all produced anomalously young ages (0.42, 7.60 and 46.05 kyr BP respectively), and it is for this reason that they do not follow the trend of the other points, as their  $^{230}\text{Th}/^{238}\text{U}$  values are very low.  $(^{234}\text{U}/^{238}\text{U})_0$  values for the 3 points still follow the trend outlined above, as shown in Figure 4.22, which plots the data against the depth in the stalagmite. Figure 4.22 also separates aragonite and calcite samples, and shows that there is no noticeable difference between the two mineralogies in terms of  $(^{234}\text{U}/^{238}\text{U})_0$ , unlike a partially calcitized stalagmite from Mexico in which secondary calcite was characterised by lower  $(^{234}\text{U}/^{238}\text{U})_0$  values than layers of primary aragonite (Lachniet et al., 2012). Thus the fluid which recrystallised the primary aragonite appears to have had a  $(^{234}\text{U}/^{238}\text{U})_0$  composition very close to that of the fluid from which the primary aragonite itself precipitated.

#### 4.3.2.2.2 DIM-3

The two U/Th dates from DIM-3 are in stratigraphic order, and demonstrate that DIM-3 grew during the period ca. 8.05-7.00 kyr BP (see Table 4.8), although a small overgrowth remains undated.

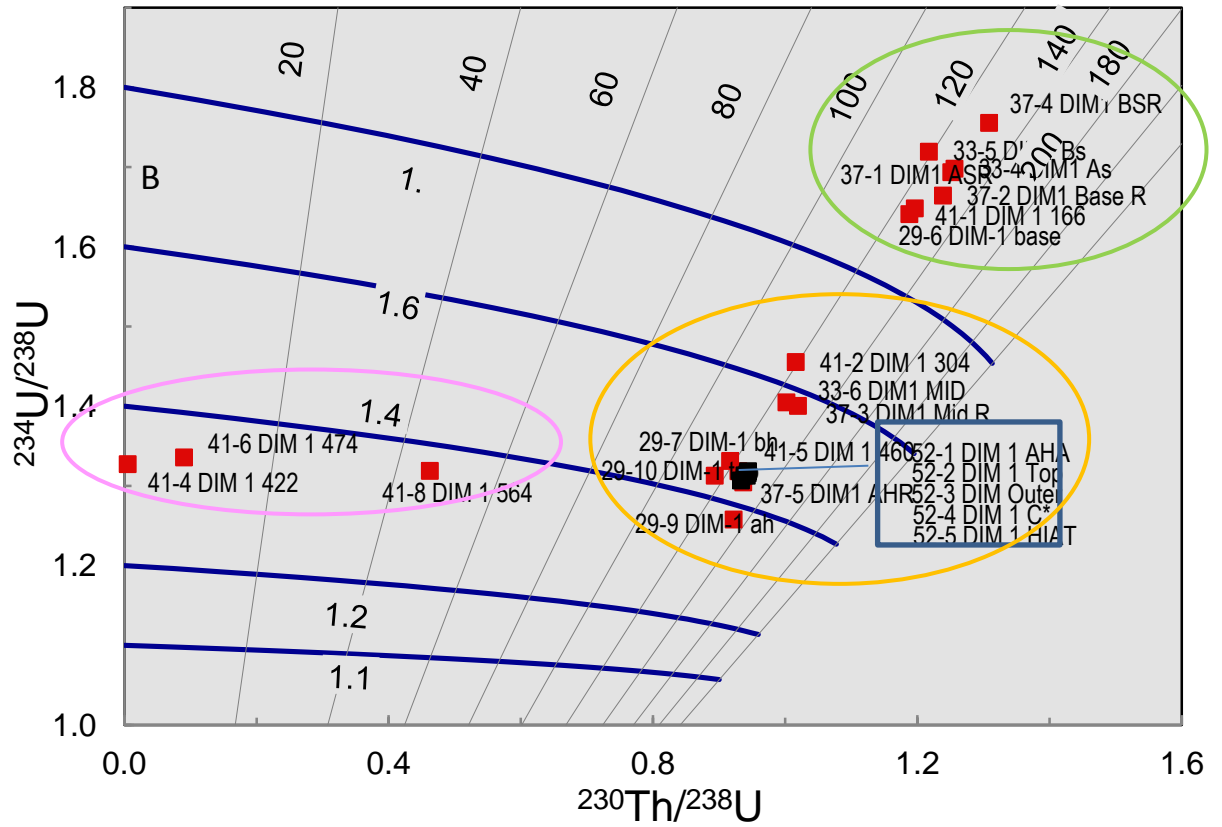


**Figure 4.21** Initial [ $^{234}\text{U}/^{238}\text{U}$ ] vs.  $^{230}\text{Th}/^{238}\text{U}$  variations in DIM-1. Green ring = base of stalagmite, orange ring = upper portion of stalagmite, pink ring = anomalous points.

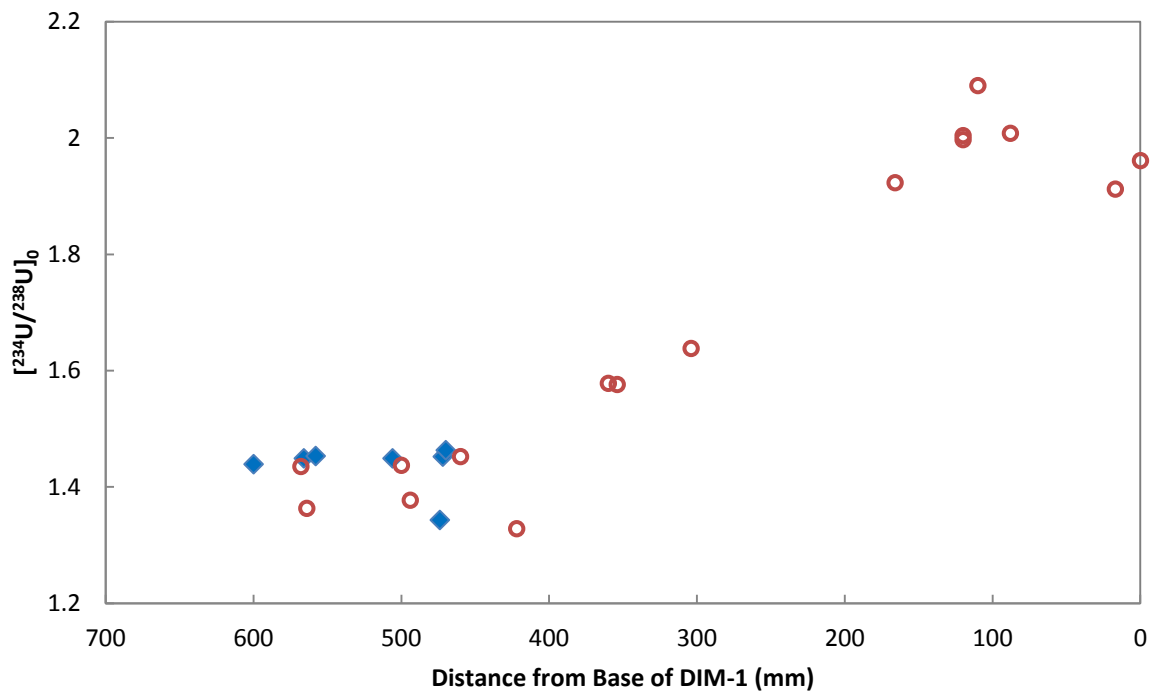


**Figure 4.22** Initial [ $^{234}\text{U}/^{238}\text{U}$ ] activity ratio variations in DIM-1 plotted against distance from base. Aragonite samples are identified by blue diamonds, calcite samples are red rings.

#### 4.3.2.2.3 DIM-2

DIM-2 was sampled for U/Th dating with a hope of ascertaining whether parts of the stalagmite had remained protected from the recrystallisation that had occurred in the areas identified in Figure 4.14i. Dating of DIM-2 was partially successful in this regard. Figure 4.23 shows the location of the U/Th samples from DIM-2 and the dates they produced. In the lower section of primary aragonite, reproduction of dates (note, dates were not true replicates as they were from slightly different depths) at both the lower and upper limits of the region produced ages in stratigraphic order, and reproducible within error. This suggests that dating of the primary aragonite in DIM-2 would produce a usable chronology. However, in the upper section of primary aragonite U/Th dating was not so successful. The lower date produced an anomalously old age, most likely due to U loss, as [U] is 1.043 ppm for that sample, compared with 4.8 - 10.4 ppm for the rest of the aragonite samples. It is likely that this sample was taken too close to the boundary between original and altered fabrics. The two ages from the top of the stalagmite were close in age to each other (but not within error), and older than expected (i.e. older than the ages from the lower region of primary aragonite). There is a change to calcite at the top of the stalagmite; it is possible that again these samples were collected from too close to the zone of recrystallisation.

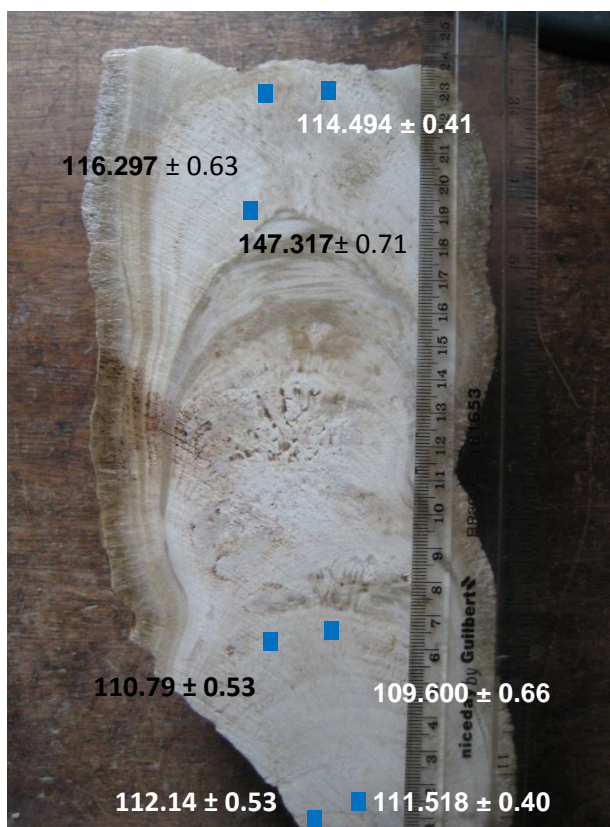


**Figure 4.23** Location and ages of U/Th samples from DIM-2

### 4.3.3 Stable Isotope Measurements

#### 4.3.3.1 Hendy Tests

Hendy tests (Hendy, 1971) were performed on 3 laminae in DIM-1, (Figures 4.24 A, 4.25 A-C, 4.26 A-C), of which one was above the hiatus, one below and one within the aragonite region. After sampling the Hendy Test in the upper section of DIM-1, it became apparent that the layer that had been followed may in fact have been a micro-hiatus. This may have had an effect on the isotopes. One Hendy test was carried out on DIM-3 (Figure 4.24 B, 4.25 D, Figure 4.26 D). Three Hendy Tests were carried out on DIM-2 (Figure 4.24 C, 4.27, 4.28), one across a change in mineralogy, where the change from aragonite to calcite had not occurred across full layers, so that layers cut across differing mineralogies; one in the lower section of aragonite and one in the upper section of aragonite.

The three Hendy tests in DIM-1 show low covariation between  $\delta^{18}\text{O}$  and  $\delta^{13}\text{C}$ , as well as low variation in  $\delta^{18}\text{O}$  along the layer (all 3 layers vary by up to approximately 0.5‰). The aragonite layer showed the lowest covariation between  $\delta^{18}\text{O}$  and  $\delta^{13}\text{C}$ , and the lowest variation in  $\delta^{18}\text{O}$  along the layer, which is to be expected as it is the primary mineral whereas the other 2 Hendy tests were taken from parts of the stalagmite which appear to be recrystallised. However, even the recrystallised layers returned good Hendy tests. This may indicate that the recrystallisation did not cause a large change in the stable isotopes of DIM-1.

The sample from DIM-2 that passes through the change in mineralogy shows high covariance between  $\delta^{18}\text{O}$  and  $\delta^{13}\text{C}$ , and large variation in  $\delta^{18}\text{O}$ , especially at the intersections between the two minerals. Thus, the recrystallisation of aragonite to calcite in DIM-2 has clearly led to a shift in the isotope ratios of oxygen and carbon. In contrast, the two layers from the primary aragonite regions returned Hendy tests that were low in  $\delta^{18}\text{O}$  variation and  $\delta^{18}\text{O}$ - $\delta^{13}\text{C}$  covariation (Figure 4.27C shows one data point which is very different to the others; this may be a measurement error, which would benefit from reanalysis in further work.

The Hendy test from DIM-3 shows much higher covariation between  $\delta^{18}\text{O}$  and  $\delta^{13}\text{C}$ , as well as slightly higher variation in  $\delta^{18}\text{O}$  along the layer (ca. 0.9 ‰). Therefore, it is likely that the stable isotope system of DIM-3 was not in isotopic equilibrium. Any slight change in sampling point laterally along a layer could produce a large difference in oxygen or carbon isotopes, especially as DIM-3 is so narrow, causing sampling troughs to correspond to a greater proportion of the layer laterally.

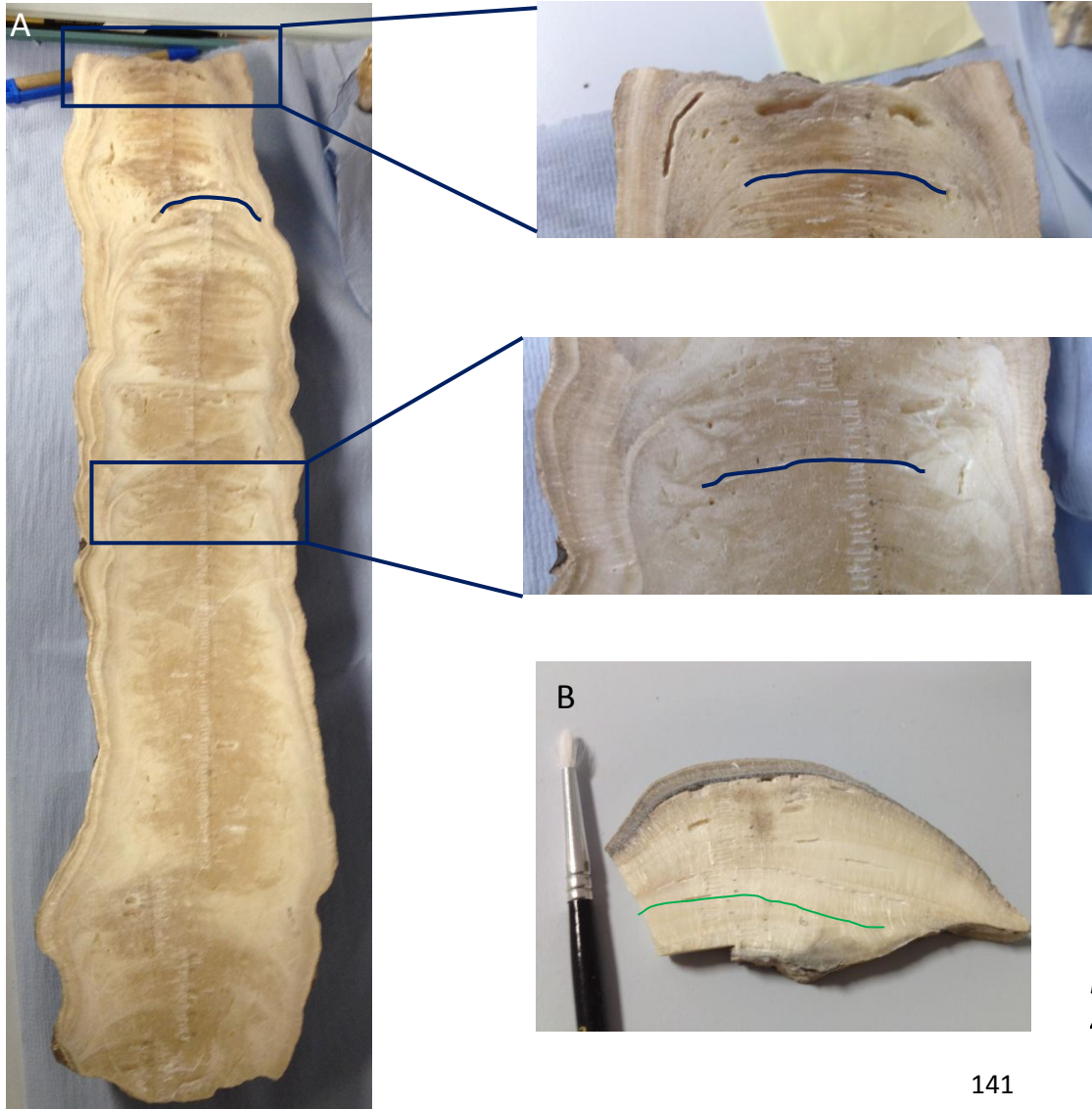


**Figure 4.24** Locations of Hedy Tests in the Dim Stalagmites  
 A) DIM-1, B) DIM-3, C) DIM-2

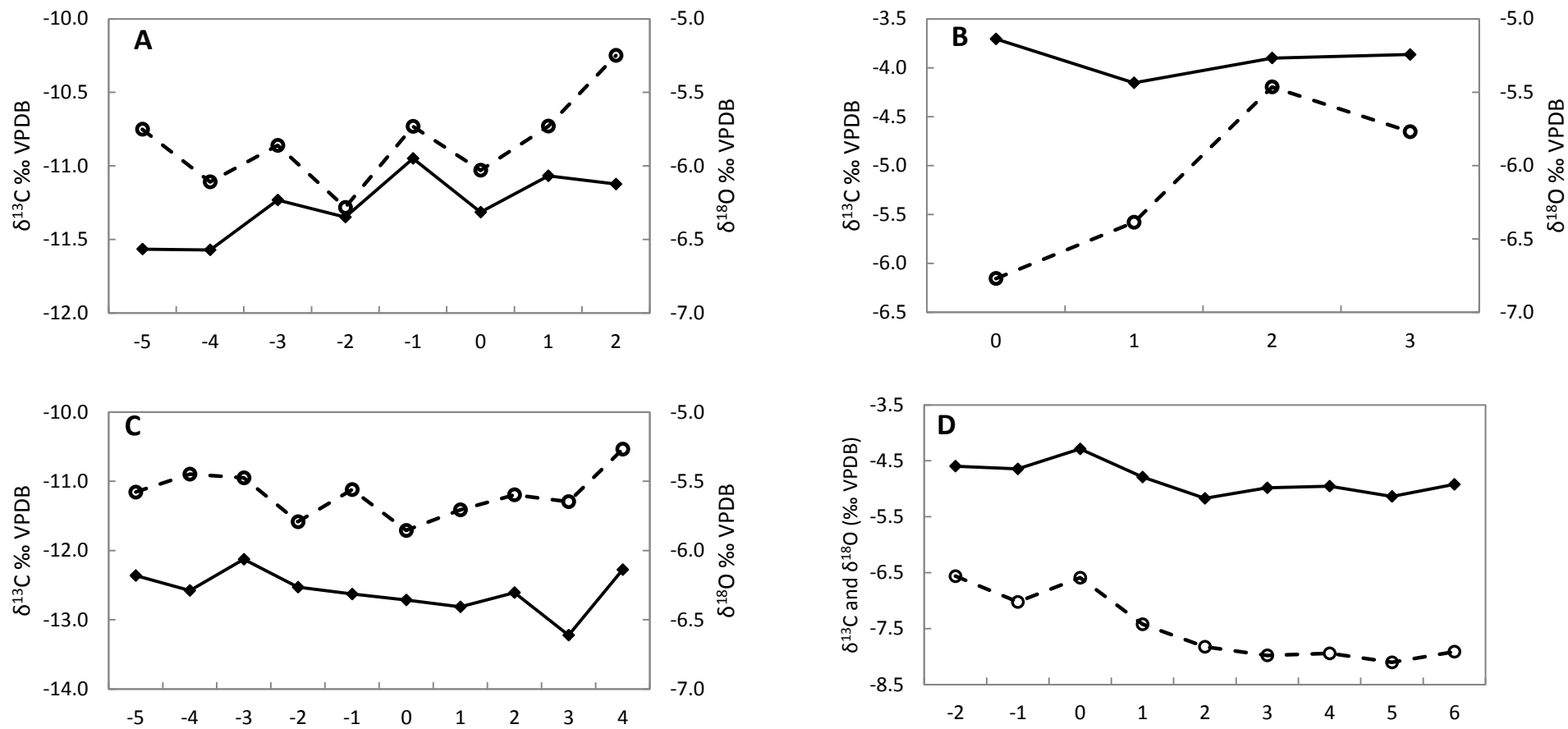


**Figure 4.25**

*Hendy tests for stalagmite DIM-1 (A-C) and DIM-3 (D),  $\delta^{18}\text{O}$  and  $\delta^{13}\text{C}$  variations along a single lamina.*

*Distance from base of stalagmite: A = 291mm, B = 474mm, C = 546mm, D = DIM-3*

*Filled diamonds = oxygen isotopes, open circles, dashed line = carbon isotopes.*

*Horizontal axis labels indicate relation to growth axis (denoted by 0).*

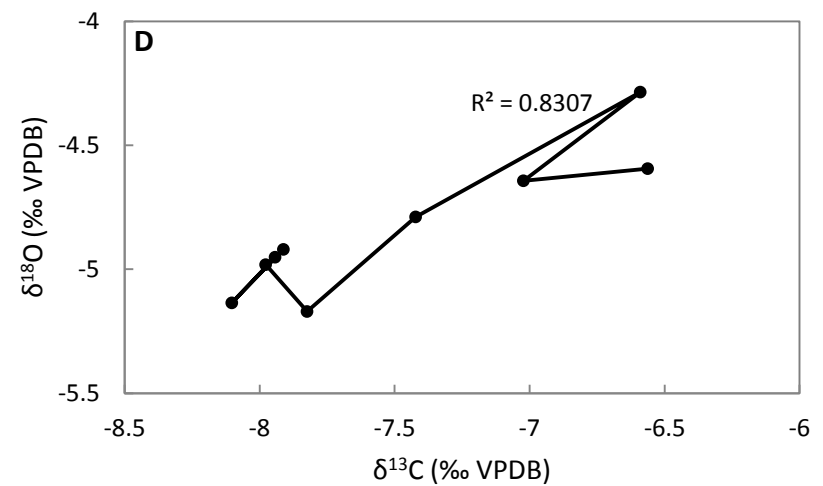
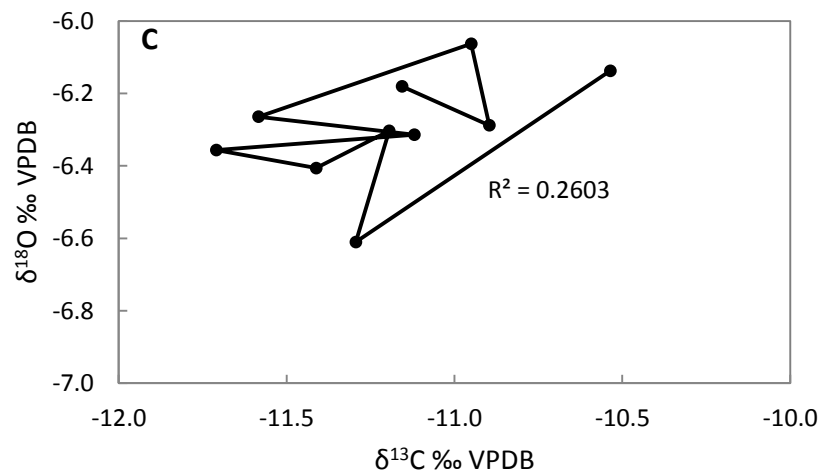
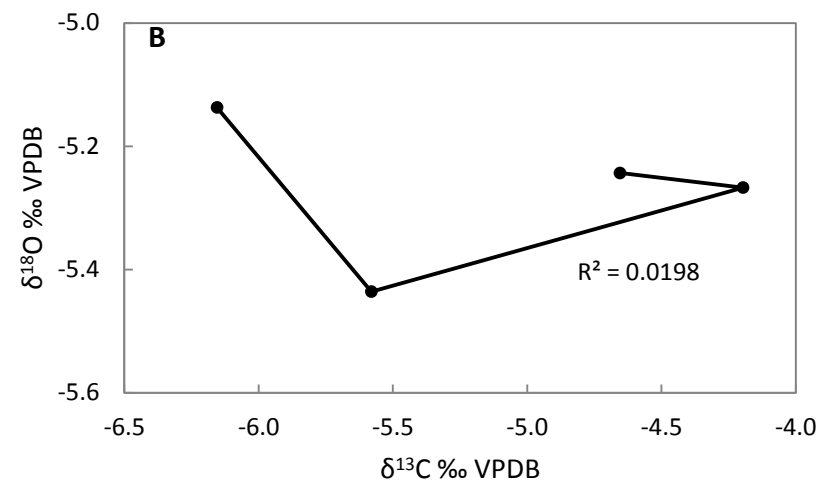
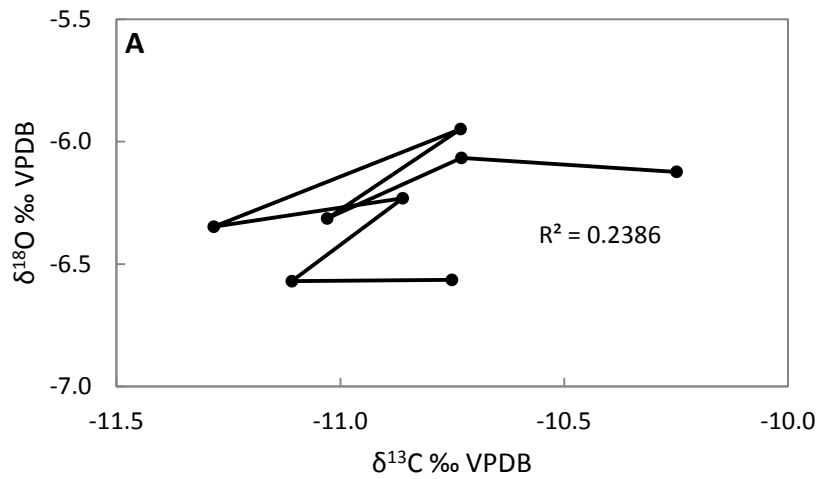


**Figure 4.26**  
**Hendy tests for stalagmite DIM-1(A-C) and DIM-3 (D), covariation between  $\delta^{18}\text{O}$  and  $\delta^{13}\text{C}$ .**  
**Distance from base of stalagmite: A = 291 mm, B = 474 mm, C = 546 mm, D = DIM3**  
 **$R^2$  values indicate amount of correlation between  $\delta^{18}\text{O}$  and  $\delta^{13}\text{C}$**

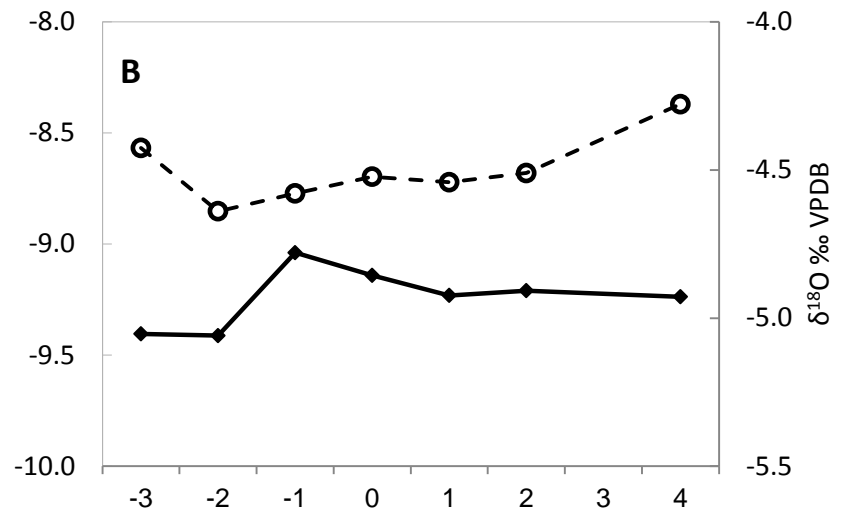
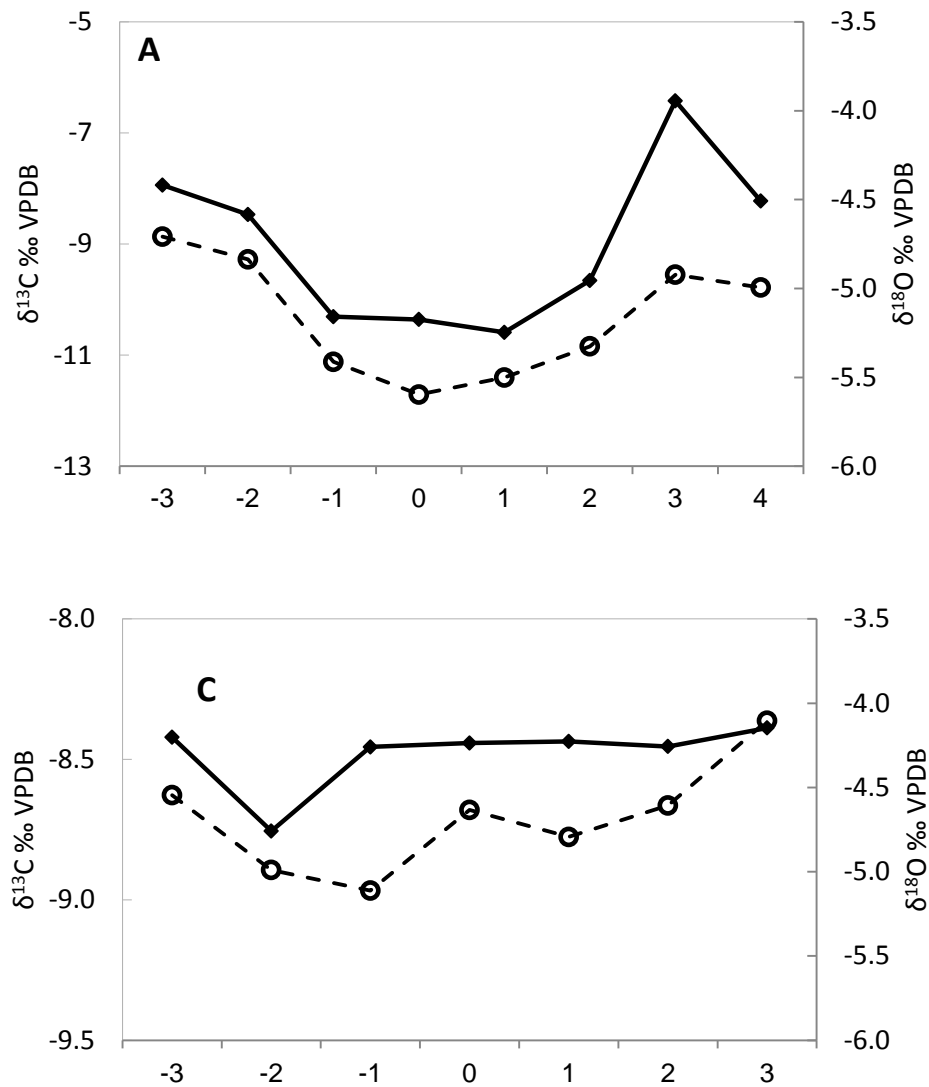


**Figure 4.27**

*Hendy tests for stalagmite DIM-2,  $\delta^{18}\text{O}$  and  $\delta^{13}\text{C}$  variations along a single lamina.*

*Distance from base of stalagmite: A) 180 mm, passing through the change from calcite to aragonite. B) In lower aragonite C) In upper aragonite*

*Filled black diamonds = oxygen isotopes, open circles = carbon isotopes.*

*Horizontal axis labels indicate relation to growth axis (denoted by 0).*

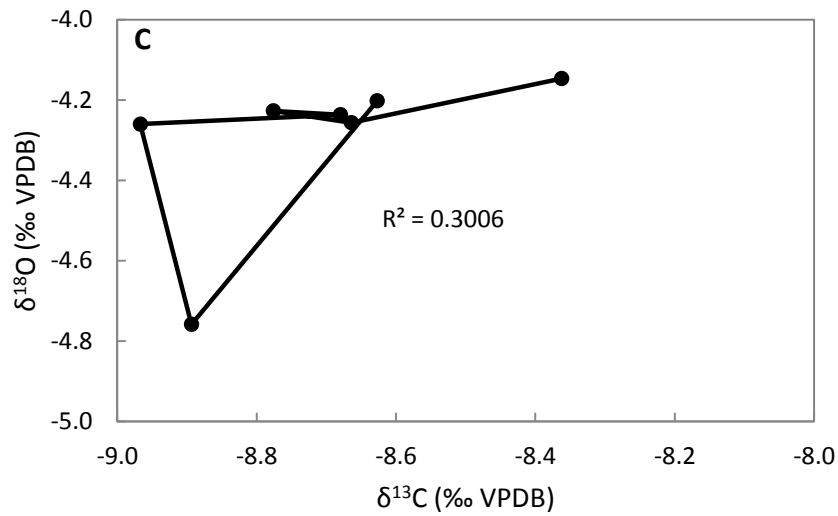
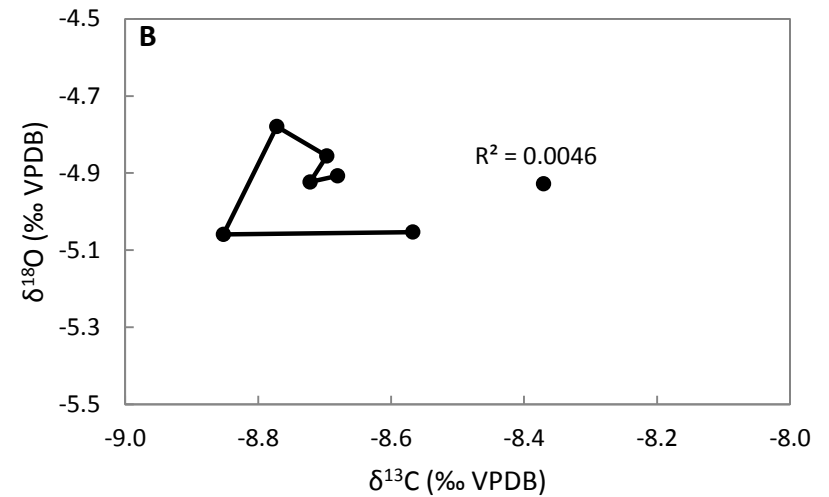
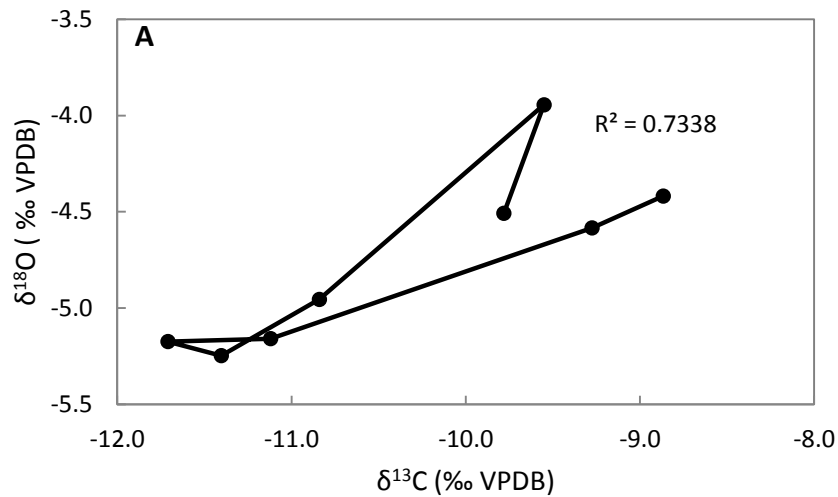


**Figure 4.28**

*Hendy tests for stalagmite DIM-2, covariation between  $\delta^{18}\text{O}$  and  $\delta^{13}\text{C}$ . Distance from base of stalagmite: A) 180 mm, passing through the change from calcite to aragonite. B) In lower aragonite C) In upper aragonite Lines join measurements in order of progression along lamina.*

### 4.3.3.2 Axial Profile Stable Isotope Results

#### 4.3.3.2.1 Sampling Strategy

Axial stable isotope samples were taken at 1-2 mm resolution in DIM-1, at 1 mm resolution in DIM-3 and at 1-5 mm resolution in DIM-2. DIM-2 was not sampled at as high resolution as DIM-1 and DIM-3 due to the fact that it was clearly recrystallised and therefore unlikely to be useful as a palaeoclimate proxy. The aim of sampling was instead to characterise the isotopic signature of recrystallised fabrics in DIM-2.

#### 4.3.3.2.2 DIM-1

##### 4.3.3.2.2.1 Oxygen Isotopes

The oxygen isotope variations through DIM-1 are plotted against time in Figure 4.29. The most striking part of the record is the rapid excursion to less negative values immediately before the aragonite layer, and the equally rapid return to more negative values with the return to calcite fabric. There is also a noticeable trend to more negative values beginning at ca. 129 kyr BP, which also coincides with an increase in the variability of the data.

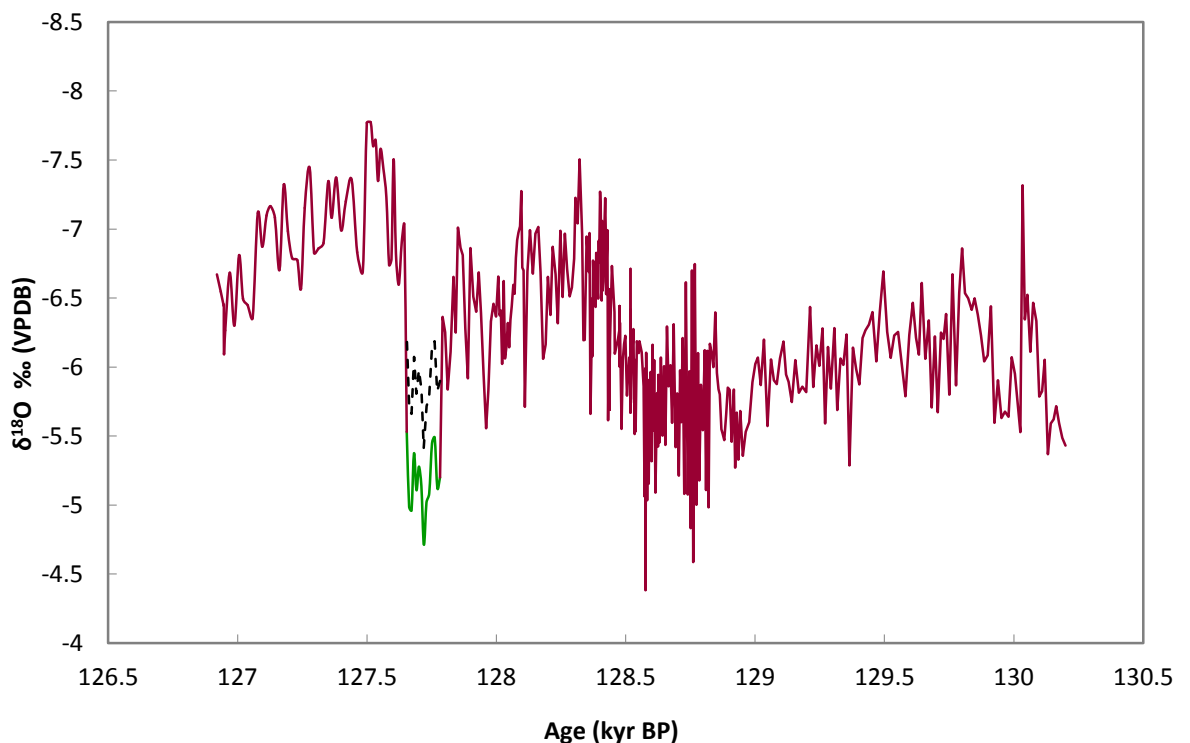


**Figure 4.29**  $\delta^{18}\text{O}$  variations in DIM-1 through time. Red line = calcite, green line = aragonite. Dashed black line = theoretical aragonite signal with equilibrium separation factor between calcite and aragonite removed. Separation factor of 0.7‰ used, as appropriate for temperatures of 3-19°C (Grossman and Ku, 1981). Dim Cave air temperature is currently quite stable at ca 18-19°C.

#### 4.3.3.2.2 Carbon Isotopes

Carbon isotopes for DIM-1 are plotted against time in Figure 4.30.  $\delta^{13}\text{C}$  shows similar variations to  $\delta^{18}\text{O}$ , with a trend to more negative values occurring at ca. 129 kyr BP, following by a pronounced trend to less negative values immediately preceding the aragonite layer, and a return to more negative values seen in the values for the aragonite layer and the calcite immediately above it. These more negative values are the most negative of the entire speleothem.

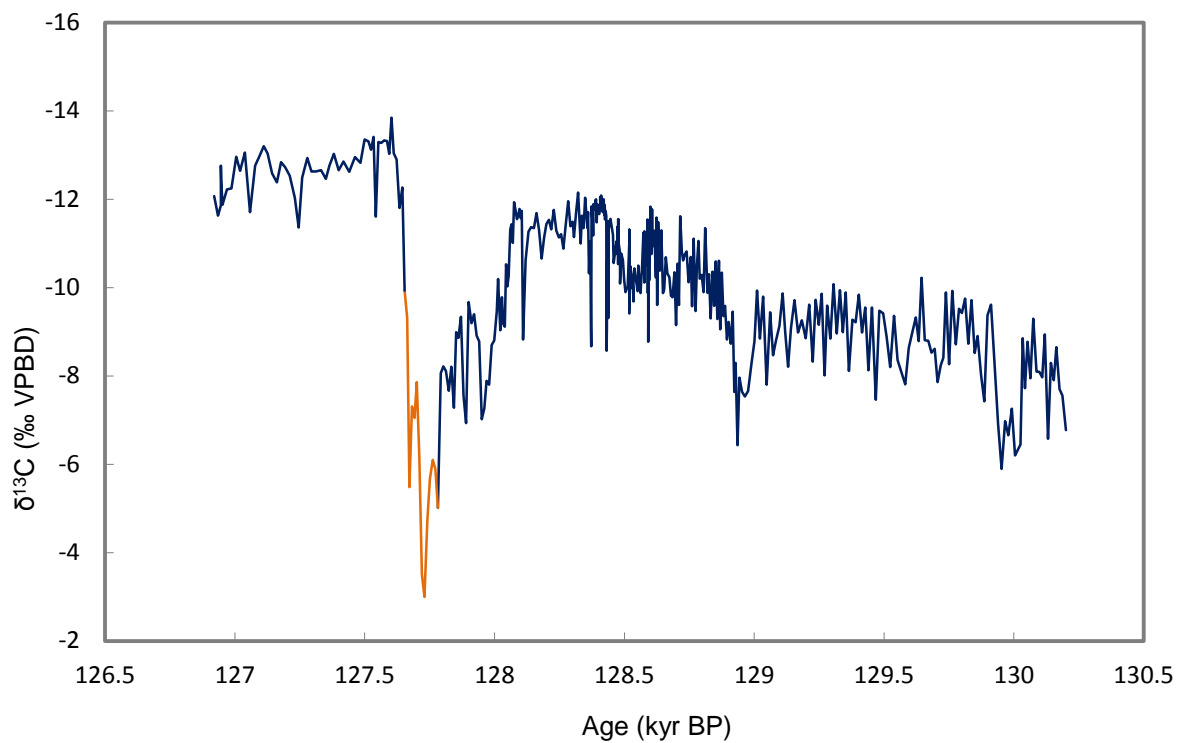


**Figure 4.30**  $\delta^{13}\text{C}$  variations in DIM-1 through time. Navy = calcite, orange = aragonite.

#### 4.3.3.2.2.3 *Oxygen and Carbon Isotope Variations*

A crossplot of oxygen and carbon isotope data is shown in Figure 4.31. There is a moderate positive covariation (0.3677) between the two isotopes, indicating that a common variable or set of variables may have been influencing both isotopes, but as the covariance is not very high they may still be interpreted separately. Positive covariance between  $\delta^{18}\text{O}$  and  $\delta^{13}\text{C}$ , which was also seen in records from Villars Cave (Genty et al., 2003) and Bourgeois-Delaunay, La Chaise de Vouthon, SW France (Couchoud et al., 2009).

The issue of the overlapping errors on the age model becomes apparent when the U/Th dates are plotted against  $\delta^{18}\text{O}$  and  $\delta^{13}\text{C}$  (Figure 4.32), and makes it difficult to pinpoint accurately when climatic or environmental changes may have happened in the region of Dim Cave. If a contemporaneous speleothem from Dim Cave had been recovered, comparing the 2 records would have been a possible way to anchor events in the DIM-1 isotope record to more certain dates. As this was not possible, the next alternative is to compare DIM-1 with contemporaneous records from caves (or other proxies) in the Mediterranean region. This will be performed in the palaeoclimatic interpretation (Section 4.4.6.1.)

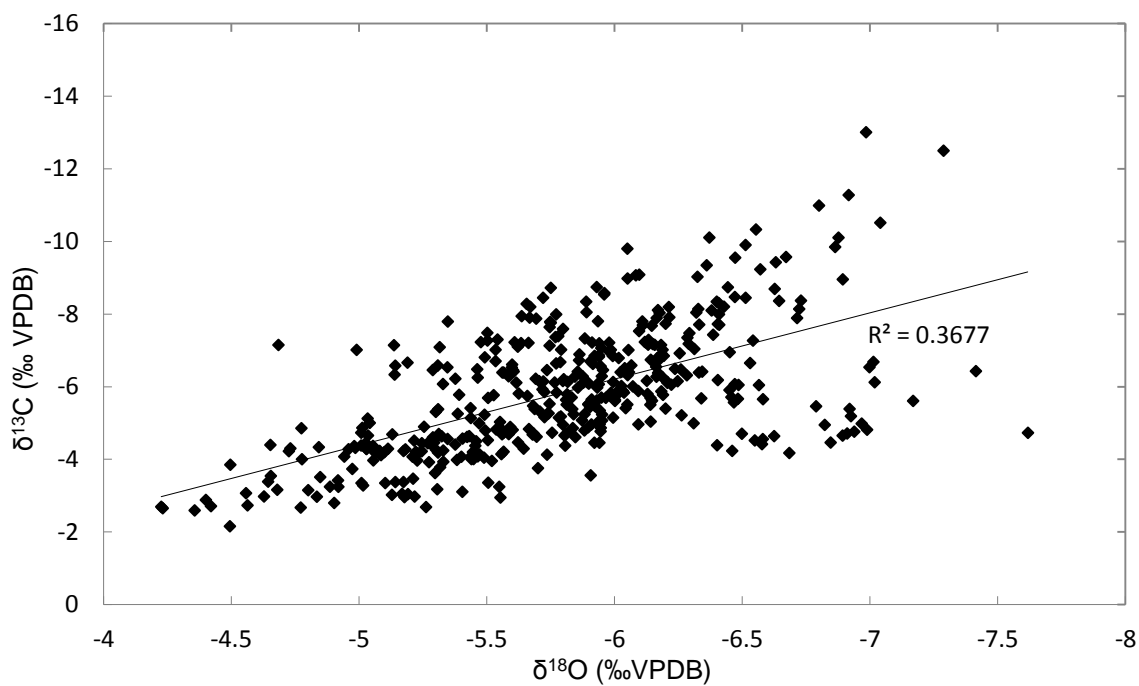


**Figure 4.31**  $\delta^{18}\text{O}$  and  $\delta^{13}\text{C}$  cross plot for isotopic axial profile of DIM-1. The  $R^2$  value for the line of best fit is displayed (0.3677).

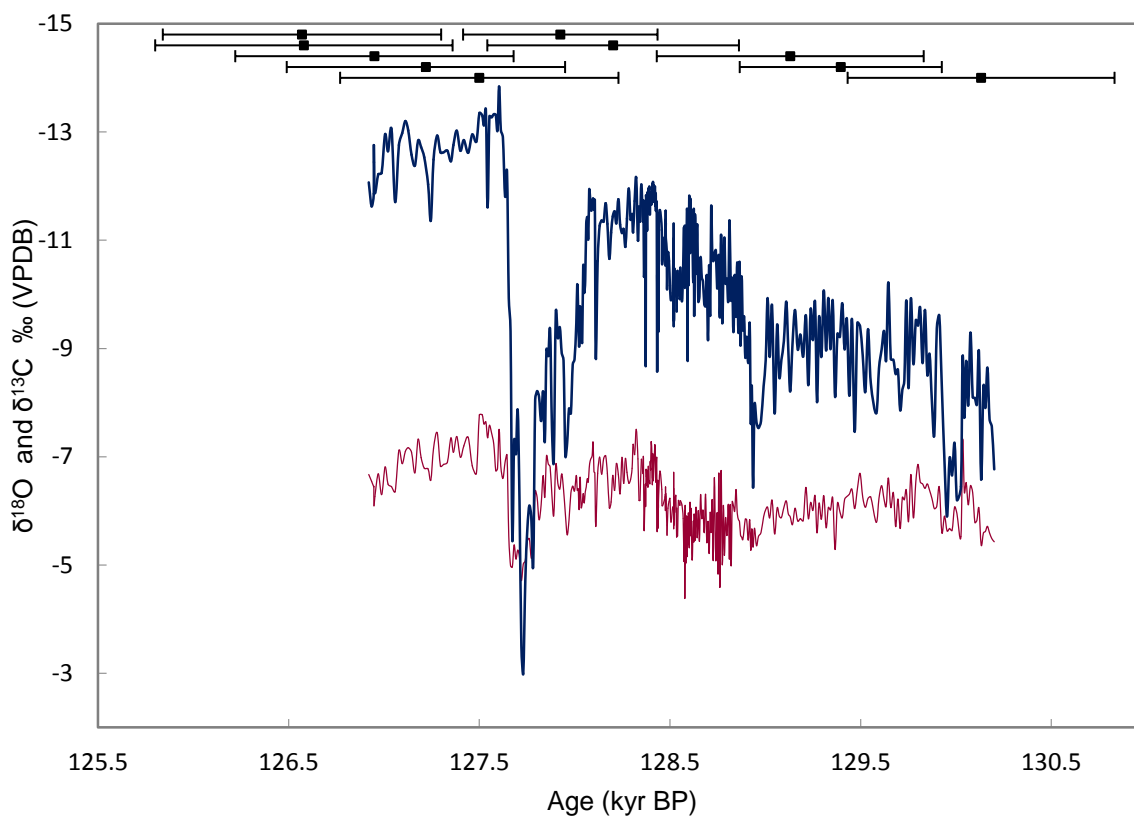


**Figure 4.32**  $\delta^{18}\text{O}$  (red) and  $\delta^{13}\text{C}$  (navy) variations in DIM-1 through time. U/Th dates shown at top, with errors.

#### 4.3.3.2.3 DIM-3

$\delta^{18}\text{O}$  and  $\delta^{13}\text{C}$  variations in DIM-3 (Figure 4.33) show much less variability than in DIM-1, which is not unexpected due to the fact that the record is much shorter, and DIM-3 is only comprised of aragonite.  $\delta^{18}\text{O}$  especially shows no discernible trend, with values oscillating within a 1‰ range for the length of the record and eventually reaching a plateau at higher values before growth ceases.  $\delta^{13}\text{C}$  shows more variability; the oscillating cycles are present in this record also, and of slightly bigger magnitude, and at the time that  $\delta^{18}\text{O}$  forms a plateau,  $\delta^{13}\text{C}$  shows a positive excursion of approximately 3.5‰. As the  $\delta^{18}\text{O}$  plateau and  $\delta^{13}\text{C}$  excursion occur immediately before the end of growth, all three events may be caused by the same set of climatic variables. This will be discussed further in Section 4.3.6.2.

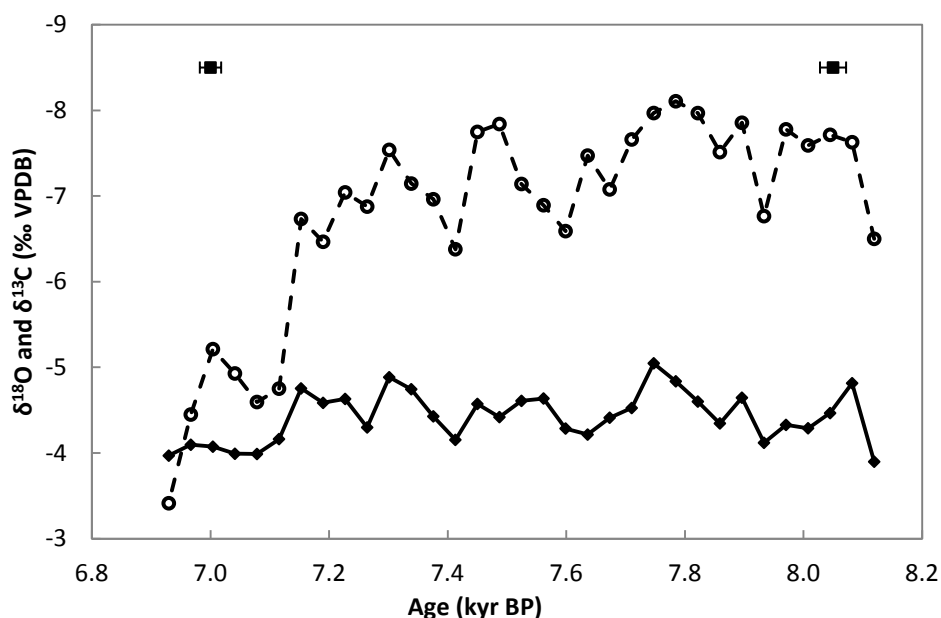


**Figure 4.33**  $\delta^{18}\text{O}$  and  $\delta^{13}\text{C}$  variations for DIM-3 through time  
Filled diamonds = oxygen isotopes, open circles, dashed line = carbon isotopes.  
U/Th dates shown at top as filled squares with error bars.

#### 4.3.3.2.4 DIM-2

The most prominent oxygen and carbon isotopic variations in DIM-2 (Figure 4.34) correspond to the changes in mineralogy.  $\delta^{13}\text{C}$  shows much larger variation than  $\delta^{18}\text{O}$ , with the most noticeable shift at a calcite-aragonite boundary occurring at the change located at approximately 185 mm, where  $\delta^{13}\text{C}$  shifts by ca. 4.5‰ and  $\delta^{18}\text{O}$  by ca. 2‰. In Figure 4.34, the calcite above this boundary is marked by a green bracket, and the aragonite below it is

marked by a red bracket. Due to the large difference in isotopic composition at this boundary, and the consistency of values within the  $\delta^{13}\text{C}$  record in these two sections, these sections are selected as likely representative values for primary aragonite and secondary calcite in DIM-2. The fact that the aragonite section marked by the brown bracket has similar  $\delta^{13}\text{C}$  values to the red bracketed aragonite strengthens this hypothesis.

The remaining bracketed section, identified by the purple bracket, contains three previously identified regions (calcite, aragonite and mixed mineralogy). This entire bracketed section contains  $\delta^{13}\text{C}$  values which vary between values similar to the brown/red bracketed aragonite areas, to values similar to the green bracketed calcite area. This suggests that it is not only the previously identified mixed mineralogy section which contains both calcite and aragonite, but that both the other two regions identified as aragonite and calcite respectfully are in fact of mixed mineralogy.

Using the aforementioned areas of DIM-2, primary aragonite and secondary calcite in DIM-2 can be characterised (Table 4.9). These ranges are representative; not every data point in each section falls into this range.

Carbonate Form	Representative $\delta^{18}\text{O}$ range	Representative $\delta^{13}\text{C}$ range
Primary Aragonite	-3.8‰ to -5.2‰	-8‰ to -10‰
Secondary Calcite	-4.5‰ to -5.5‰	-11‰ to -12‰

**Table 4.9** *Representative  $\delta^{18}\text{O}$  and  $\delta^{13}\text{C}$  of primary aragonite and secondary calcite in DIM-2*

There is little difference in the  $\delta^{18}\text{O}$  of primary aragonite and secondary calcite in DIM-2, although the calcite values are slightly more negative.  $\delta^{13}\text{C}$  offers a greater degree of confidence in distinguishing between the two minerals, as the two ranges do not overlap, with calcite values again more negative, as they were with  $\delta^{18}\text{O}$ .

The fact that the aragonite and calcite sections in the purple bracketed section appear to be of mixed mineralogy highlights the problems of using a small number of XRD samples to characterise areas defined by visible changes, and suggests that carbon and oxygen isotopes may be able to help define boundaries in mineralogies in some speleothems, provided the different mineralogies show distinct stable isotope signatures.

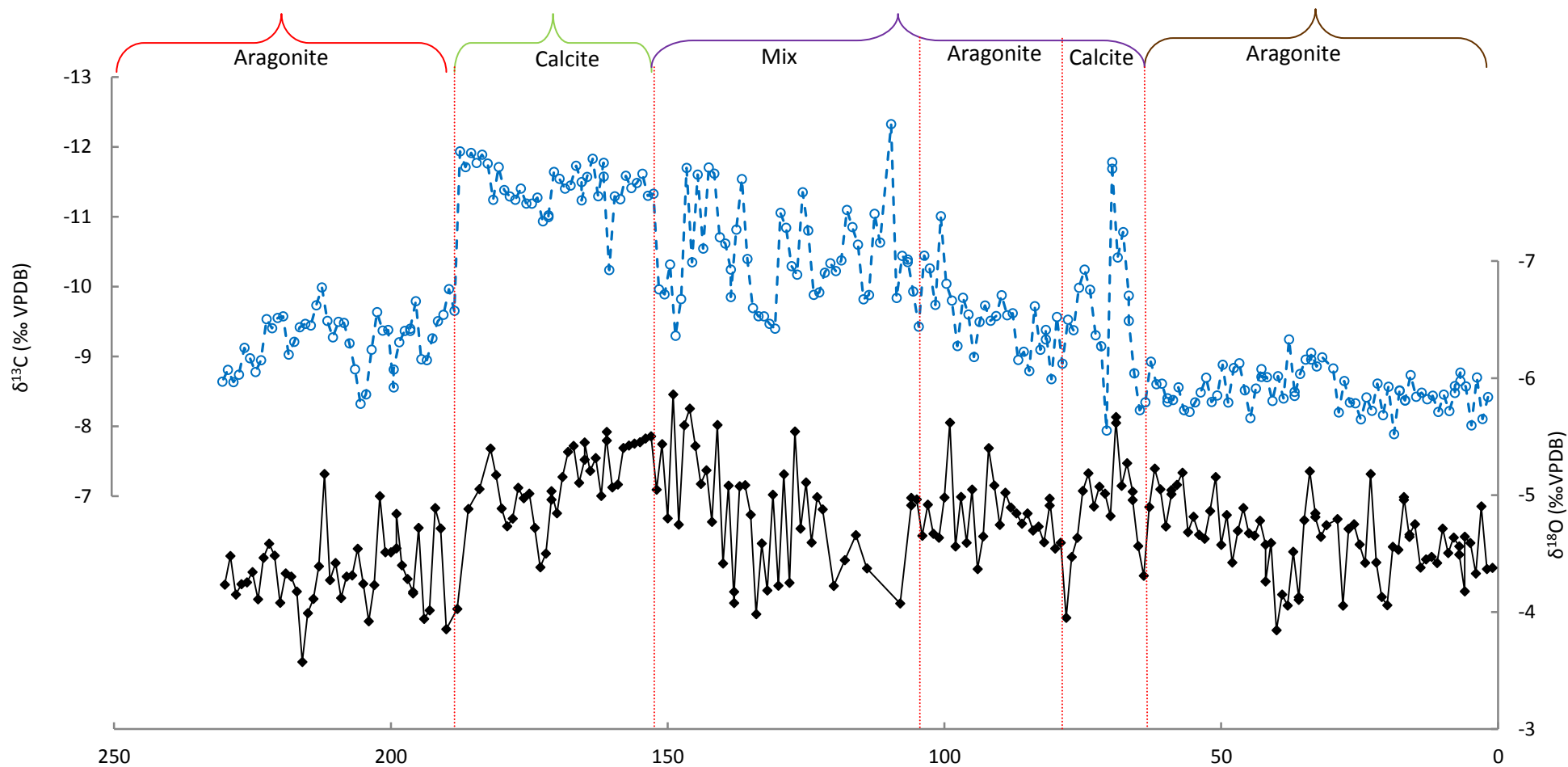


**Figure 4.34**

***δ<sup>18</sup>O (black diamonds) and δ<sup>13</sup>C (open circles and dashed line) variations for DIM-2 expressed against mm from the base of the stalagmite. Vertical red lines and labels at top indicate changes in mineralogy. Coloured brackets separate the record into sections discussed in the text.***

#### 4.3.4 Strontium Isotope Measurements

##### 4.3.4.1 Sampling Strategy

20 samples were selected throughout DIM-1, to represent the physical, mineralogical and isotopic changes in the stalagmite. Only 4 samples were selected from DIM-3 due to its small size. 8 samples were selected from DIM-2 in order to investigate the effect of recrystallisation on strontium isotopes. One sample each were analysed for a modern aragonite from Dim Cave collected from an actively precipitating soda straw, bedrock and soil above Dim Cave.

##### 4.3.4.2 Results

$^{87}\text{Sr}/^{86}\text{Sr}$  data for the Dim stalagmites and components of the cave system are presented in Table 4.10. The Dim Cave host carbonate has an  $^{87}\text{Sr}/^{86}\text{Sr}$  value of  $0.707162 \pm 0.000005$ . This limestone is believed to be of Palaeozoic age (Oruç Baykara, 2009, pers. comm.), which is in line with the  $^{87}\text{Sr}/^{86}\text{Sr}$  value as such seawater  $^{87}\text{Sr}/^{86}\text{Sr}$  values occurred during the Permian (McArthur et al., 2001). The acetic acid leach of the soil gave an  $^{87}\text{Sr}/^{86}\text{Sr}$  value of  $0.708455 \pm 0.000006$ . Speleothem  $^{87}\text{Sr}/^{86}\text{Sr}$  values vary between 0.708137 and 0.708338. Thus, all speleothem values were more radiogenic than the host rock and less radiogenic than the soil values, with the exception of DIM-2, which is slightly more radiogenic than soil values. All speleothem values were also less radiogenic than the value for modern seawater, which is  $0.70906 \pm 0.00033$  (Goede et al., 1998). All of these components are shown in Figure 4.35.

Stalagmite	Sample ID	Mm from base	Sample Type	$^{87}\text{Sr}/^{86}\text{Sr}$
DIM-1	DIM-1 BASE	8	acetic leach	0.708315 ± 0.00004
DIM-1	DIM-1 BASE	8	1% acetic preleach	0.708320 ± 0.000007
DIM-1	DIM1-90	90	acetic leach	0.708289 ± 0.000005
DIM-1	DIM1-98	98	acetic leach	0.708294 ± 0.000005
DIM-1	DIM1-105	105	acetic leach	0.708301 ± 0.000006
DIM-1	DIM1-106	106	acetic leach	0.708297 ± 0.000005
DIM-1	DIM-1 AS	124	acetic leach	0.708336 ± 0.000109
DIM-1	DIM1-200	200	acetic leach	0.708338 ± 0.000007
DIM-1	DIM-1 MID	304	acetic leach	0.708217 ± 0.000024
DIM-1	DIM-1 MID	304	1% acetic preleach	0.708200 ± 0.000015
DIM-1	DIM1-370	370	acetic leach	0.708205 ± 0.000008
DIM-1	DIM-1 BH	416	acetic leach	0.708201 ± 0.000025
DIM-1	DIM-1 BH	416	1% acetic preleach	0.708269 ± 0.000022
DIM-1	DIM1-430	430	acetic leach	0.708259 ± 0.000027
DIM-1	DIM1-438	438	acetic leach	0.708217 ± 0.000007
DIM-1	DIM-1 BH2	454	acetic leach	0.708110 ± 0.000011
DIM-1	DIM-1 BH2	454	1% acetic preleach	0.708163 ± 0.000017
DIM-1	DIM-1 ARAG	470	acetic leach	0.708152 ± 0.000007
DIM-1	DIM-1 ARAG	470	1% acetic preleach	0.708159 ± 0.000008
DIM-1	DIM1-474	474	acetic leach	0.708177 ± 0.000005
DIM-1	DIM1-478	478	acetic leach	0.708225 ± 0.000006
DIM-1	DIM-1 AH	482	acetic leach	0.708282 ± 0.000001
DIM-1	DIM-1 AH	482	1% acetic preleach	0.708253 ± 0.000011
DIM-1	DIM1-486	486	acetic leach	0.708214 ± 0.000007
DIM-1	DIM1-514	514	acetic leach	0.708251 ± 0.000018
DIM-1	DIM-1 TOP	560	acetic leach	0.708273 ± 0.000011
DIM-1	DIM-1 TOP	560	1% acetic preleach	0.708253 ± 0.000012
DIM-3	DIM3-BASE	2	acetic leach	0.708209 ± 0.000009
DIM-3	DIM-3	18	acetic leach	0.708248 ± 0.000011
DIM-3	DIM3-28	28	acetic leach	0.708201 ± 0.000006
DIM-3	DIM3-TOP	34	acetic leach	0.708278 ± 0.000008
DIM-2	DIM-2 BASE	10	acetic leach	0.708475 ± 0.000016
DIM-2	DIM2-65	65	acetic leach	0.708485 ± 0.000006
DIM-2	DIM2-70	70	acetic leach	0.708461 ± 0.000006
DIM-2	DIM-2 INV	100	acetic leach	0.708509 ± 0.000001
DIM-2	DIM-2 INV2	132	acetic leach	0.708516 ± 0.000006
DIM-2	DIM-2 CALC	170	acetic leach	0.708520 ± 0.000011
DIM-2	DIM2-190	190	acetic leach	0.708536 ± 0.000006
DIM-2	DIM-2 TOP	220	acetic leach	0.708561 ± 0.000007
DIM SOIL	-	-	acetic leach	0.708455 ± 0.000006
DIM SOIL	-	-	Silicate residue	0.716712 ± 0.000004
DIM SODA STRAW	-	-	acetic leach	0.708415 ± 0.000008
DIM BEDROCK	-	-	acetic leach	0.707162 ± 0.000005

**Table 4.10** *Strontium Isotope data for the Dim Cave stalagmites and environmental components.*

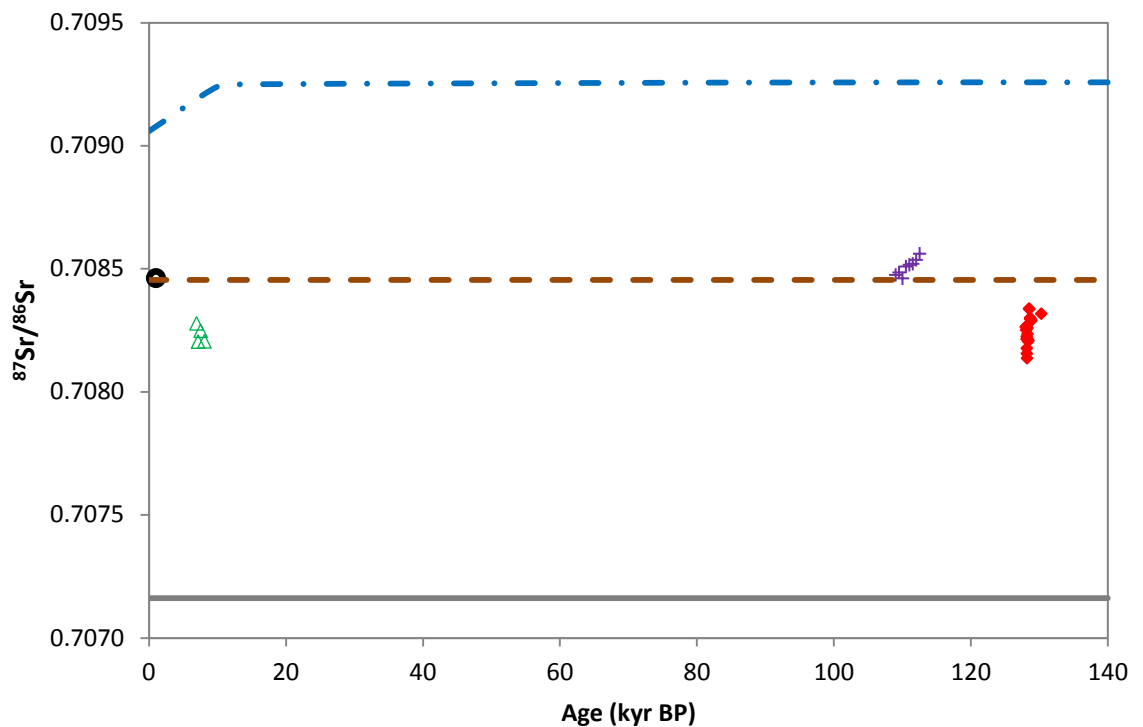


**Figure 4.35**

***$^{87}\text{Sr}/^{86}\text{Sr}$  of DIM-1 (filled red diamonds), DIM-2 (purple crosses), DIM-3 (unfilled green triangles), modern aragonite from a Dim cave soda straw (black ring), bedrock above Dim Cave (solid grey line), a soil acetic leach (dashed brown line) and modern seawater (dot-and-dashed blue line; data from Capo et al. (1990) and Goede et al. (1998)). DIM-2 samples are plotted at the age of the lower portion of primary aragonite.***

The host rock provides one of the most important sources of speleothem Sr, with other sources including the overlying soil layer, sea spray, and atmospheric dust (Banner et al., 1996, Goede et al., 1998, Ayalon et al., 1999, Bar-Matthews et al., 2000, Verheyden et al., 2000, Frumkin and Stein, 2004, Li et al., 2005, Zhou et al., 2009, Capo et al., 1998). The simplest explanation for variations in stalagmite  $^{87}\text{Sr}/^{86}\text{Sr}$  may be varying contribution from soil and host-rock sources above the cave (Oster et al., 2010). This can be assumed if dripwater  $^{87}\text{Sr}/^{86}\text{Sr}$  falls between the values for host rock and soil leachates (Zhou et al., 2009). And as there is little fractionation between dripwater and calcite (Banner and Kaufman, 1994), we will use the speleothem values. All the Dim speleothems are more radiogenic than the host rock, so there must be at least one other input of Sr to the drip water. As suggested above, soil may provide the exogenic input; alternatively the proximity of Dim Cave to the coast makes sea spray a possibility. Aeolian dust typically has  $^{87}\text{Sr}/^{86}\text{Sr}$  of ca. 0.7200, significantly higher than any other the Dim Cave system components, so it is less likely to be part of the exogenic component.

If the system is a simple two-component mixing arrangement, a linear mixing line will be created on an  $^{87}\text{Sr}/^{86}\text{Sr}$  vs.  $1/\text{Sr}$  diagram (Goede et al., 1998). A  $1/[\text{Sr}]$  (with units  $(\mu\text{g} / \text{g})^{-1}$ ) against  $^{87}\text{Sr}/^{86}\text{Sr}$  can be used to estimate the maximum isotopic composition of the exogenic source by extrapolating the line of best fit to  $1/\text{Sr} = 0$  (Goede et al., 1998). This is attempted in Figure 4.36. The calcite parts of DIM-1 are plotted separately to the aragonite samples from DIM-1 and DIM-3, but both data sets produce linear mixing lines which extrapolate to approximately the same point, 0.70865. This is therefore the maximum isotopic composition of the exogenic source. This exogenic value is then added to a replica of Figure 4.35 in Figure 4.37. The exogenic component is more radiogenic than the soil value, but less radiogenic than the seawater value. Therefore it is likely that the exogenic component is a combination of the two, with a potential small input from aeolian dust, but this could only be a small addition, as the  $^{87}\text{Sr}/^{86}\text{Sr}$  of a speleothem can change dramatically even if only a very small amount of material with a very different  $^{87}\text{Sr}/^{86}\text{Sr}$  to that of the normal source is added (Banner et al., 1996). Each speleothem can now be interpreted separately in terms of the relative inputs of Sr from the bedrock and exogenic sources. This will be done in the following sections.

In other carbonate systems, recrystallised carbonates may preserve the  $^{87}\text{Sr}/^{86}\text{Sr}$  value of the fluids that interact with them, causing recrystallisation (Banner, 1995). The fact that the recrystallised calcite of DIM-1 produced the same  $^{87}\text{Sr}/^{86}\text{Sr}$  vs.  $1/\text{Sr}$  solution to the exogenic Sr component, suggests that while the  $^{87}\text{Sr}/^{86}\text{Sr}$  may have been reset to the value of the percolating water, it is still in equilibrium with the system, and simply records the conditions at a later time (in the case of DIM-1, not much later, but perhaps longer in the case of DIM-2).

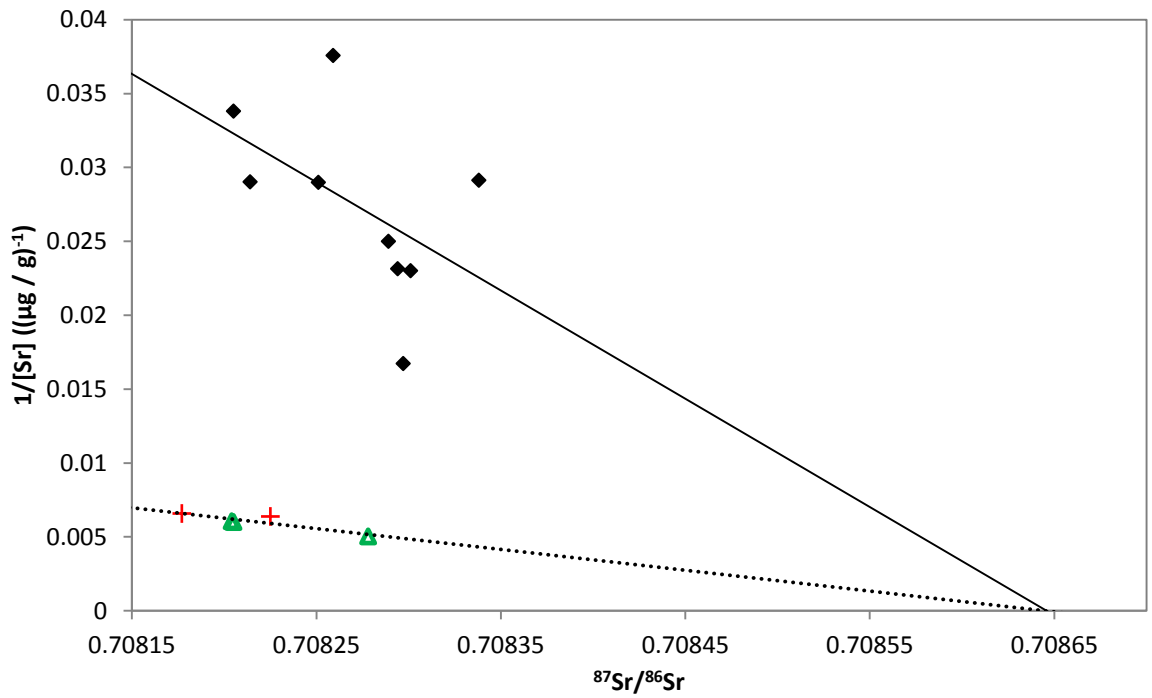


**Figure 4.36**  
 $^{87}\text{Sr}/^{86}\text{Sr}$  vs.  $1/[\text{Sr}]$  plot for DIM-1 (calcite= filled black diamonds, aragonite = red crosses) and DIM-3 (unfilled green triangles). DIM-2 is excluded due to the absence of  $[\text{Sr}]$  data at this time.

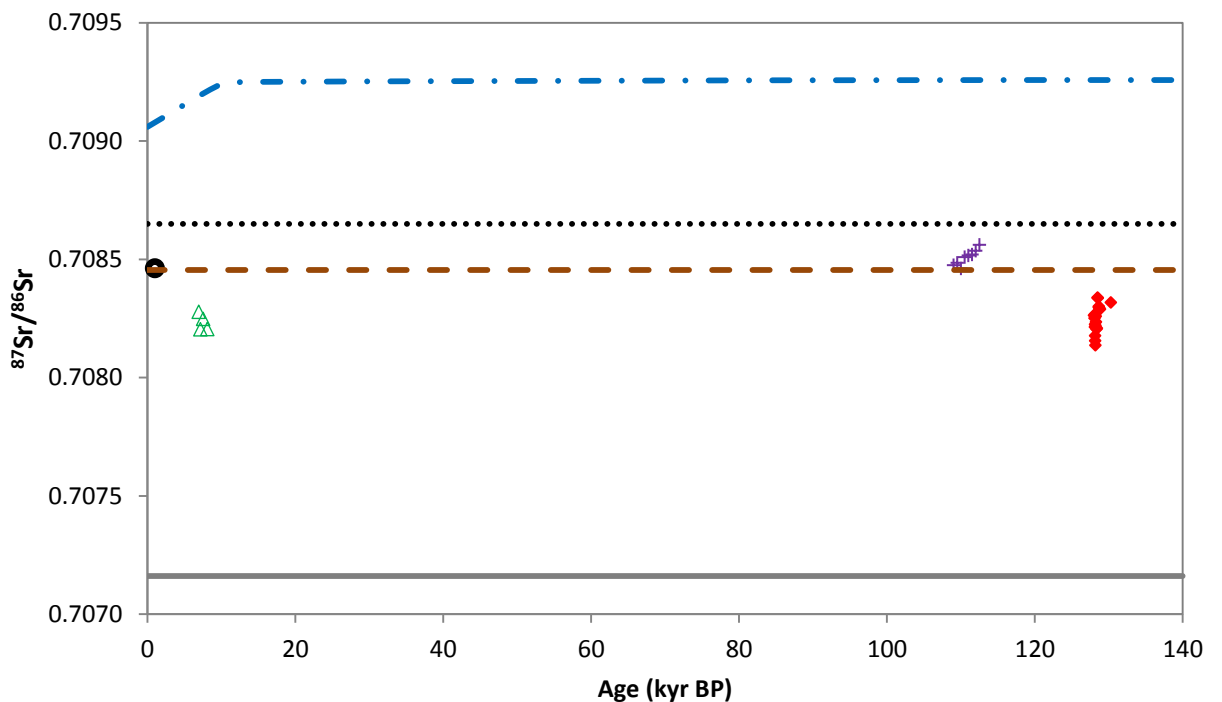
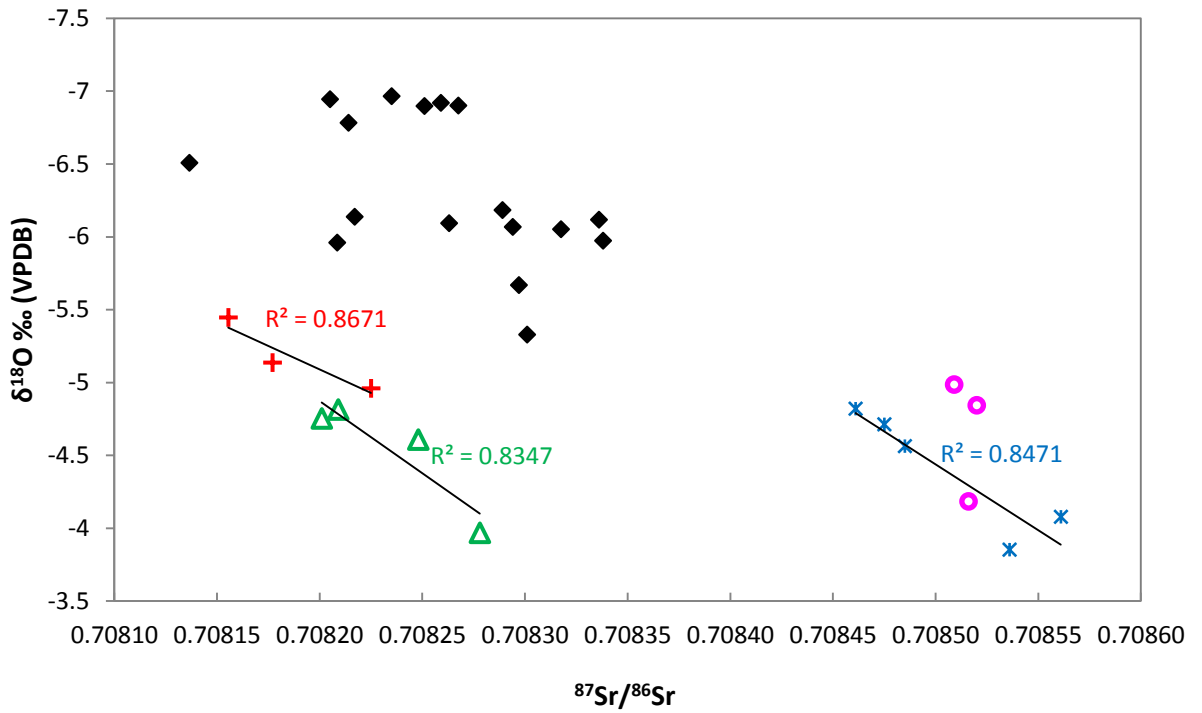


**Figure 4.37**  
 Exogenic source of Sr (dotted black line) added to plot of  $^{87}\text{Sr}/^{86}\text{Sr}$  of DIM-1 (filled red diamonds), DIM-2 (purple crosses), DIM-3 (unfilled green triangles), modern aragonite from a Dim cave soda straw (black ring), bedrock above Dim Cave (solid grey line), a soil acetic leach (dashed brown line) and modern seawater (dot-and-dashed blue line; data from Capo et al. (1990) and Goede et al. (1998)). DIM-2 samples are plotted at the age of the lower portion of primary aragonite.

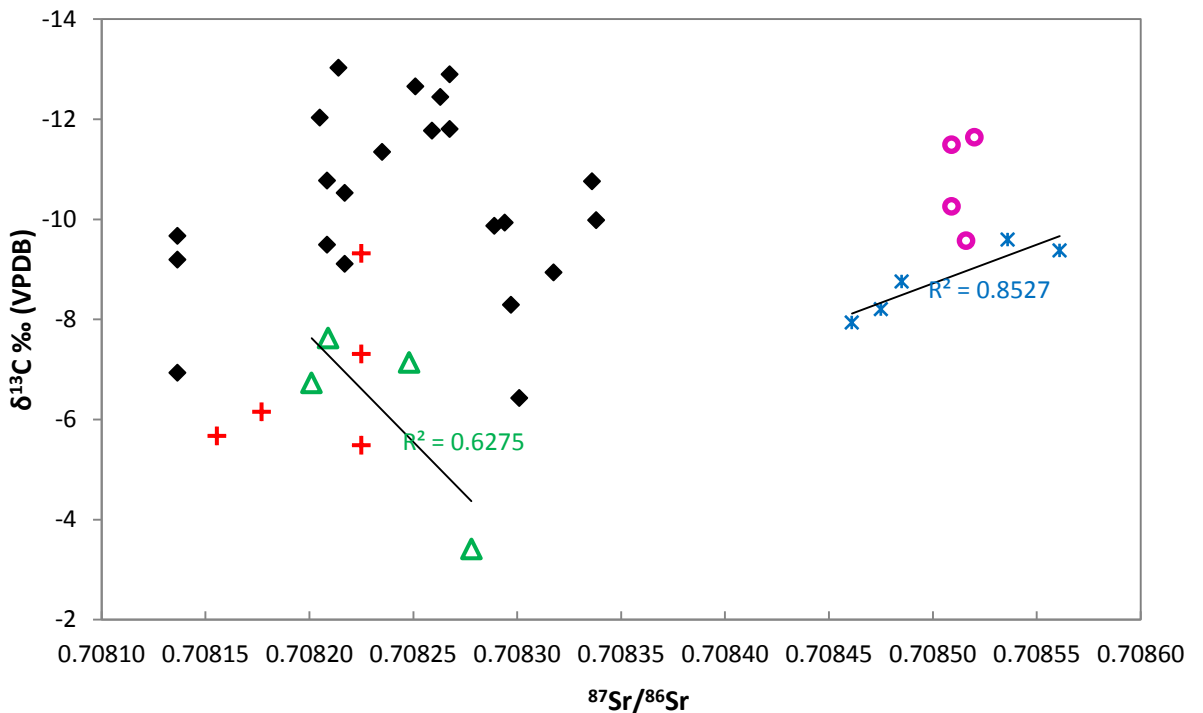
Figure 4.38 depicts the covariation between  $^{87}\text{Sr}/^{86}\text{Sr}$  and  $\delta^{18}\text{O}$  in the 3 Dim Cave speleothems. Aragonite and calcite are separated, with the result that aragonite samples show very high positive covariance between  $^{87}\text{Sr}/^{86}\text{Sr}$  and  $\delta^{18}\text{O}$  ( $R^2 = 0.8671$  for DIM-1 aragonite, 0.8347 for DIM-3 aragonite and 0.8471 for DIM-2 aragonite), while calcitic samples show low positive covariance ( $R^2 = 0.2297$  for DIM-1 calcite, 0.1008 for DIM-2 calcite [not shown on chart]). It is inconclusive whether this difference is due to the differing minerals themselves, or the effect of recrystallisation. If recrystallisation has resulted in a loss of covariance between  $^{87}\text{Sr}/^{86}\text{Sr}$  and  $\delta^{18}\text{O}$ , it is unclear which isotopic system has been changed. It is also possible that neither system changed; and that climatic conditions only caused covariance between  $^{87}\text{Sr}/^{86}\text{Sr}$  and  $\delta^{18}\text{O}$  at times when original aragonite was not being recrystallised as calcite shortly after (i.e. drier periods).

Figure 4.39 depicts the covariation between  $^{87}\text{Sr}/^{86}\text{Sr}$  and  $\delta^{13}\text{C}$  in the 3 Dim Cave speleothems, with calcite and aragonite separated. There is less covariance between  $^{87}\text{Sr}/^{86}\text{Sr}$  and  $\delta^{13}\text{C}$  compared to that between  $^{87}\text{Sr}/^{86}\text{Sr}$  and  $\delta^{18}\text{O}$ . This partly because such large changes occur in the  $\delta^{13}\text{C}$  of the DIM-1 record, so that there may be a difference of several per mil in only 2-3 mm, so that as the  $^{87}\text{Sr}/^{86}\text{Sr}$  samples taken were larger, they may have spanned more than one  $\delta^{13}\text{C}$  sample. There is a difference in the direction of covariation (i.e. positive or negative) between different aragonite datasets; DIM-3 shows a positive correlation, while the DIM-2 data is negatively correlated. The problematic DIM-1 aragonite dataset has 3  $\delta^{13}\text{C}$  points for one  $^{87}\text{Sr}/^{86}\text{Sr}$  value, and so shows a very low degree of covariation; however if the middle  $\delta^{13}\text{C}$  was taken as the correct value, the data would then show a very high degree of negative correlation.

As both the secondary calcite datasets plot within the  $^{87}\text{Sr}/^{86}\text{Sr}$  range of the corresponding primary aragonite (i.e. from the same speleothem), while the  $\delta^{18}\text{O}$  and  $\delta^{13}\text{C}$  values are more negative, it seems more likely that the  $\delta^{18}\text{O}$  and  $\delta^{13}\text{C}$  systems have been disturbed and the  $^{87}\text{Sr}/^{86}\text{Sr}$  values have remained unchanged (or only slightly changed).



**Figure 4.38**  $\delta^{18}\text{O}$  vs.  $^{87}\text{Sr}/^{86}\text{Sr}$  for the Dim Stalagmites: DIM-1 calcite (filled black diamonds), DIM-1 aragonite (red crosses), DIM-2 calcite (pink rings), DIM-2 aragonite (blue asterisks), DIM-3 aragonite (green triangles). Best-fit lines with associated  $R^2$  values are shown for the 3 aragonite data sets, to illustrate the high level of covariance compared with the calcite data sets.



**Figure 4.39**  $\delta^{13}\text{C}$  vs.  $^{87}\text{Sr}/^{86}\text{Sr}$  for the Dim Stalagmites: DIM-1 calcite (filled black diamonds), DIM-1 aragonite (red crosses), DIM-2 calcite (pink rings), DIM-2 aragonite (blue asterisks), DIM-3 aragonite (green triangles). As  $\delta^{13}\text{C}$  for the Dim Cave stalagmites is much more variable than  $\delta^{18}\text{O}$ , and  $^{87}\text{Sr}/^{86}\text{Sr}$  samples were in some cases selected specifically from areas of the stalagmites which showed high isotopic variability, selecting the corresponding data point for each  $^{87}\text{Sr}/^{86}\text{Sr}$  sample was not as simple. Therefore, in some cases more than one  $\delta^{13}\text{C}$  value has been plotted against an  $^{87}\text{Sr}/^{86}\text{Sr}$  point.

#### 4.3.4.2.1 DIM-1

27 analyses were performed on samples from DIM-1, some of which were replicates, with one analysis being on a 1% acetic leach, and one analysis performed on the “preleach”, in case too much Sr was stripped during the acetic leach step. Results were averaged to produce the plot in Figure 4.40 (insert), a 20 sample data set. One sample has a clearly much larger error than the others; as this sample essentially failed, it was removed, to produce the main plot of Figure 4.40. As is evident, removal of this point has only changed the shape of the data very slightly, while reducing the uncertainty considerably.

$^{87}\text{Sr}/^{86}\text{Sr}$  shows a similar trend to  $\delta^{18}\text{O}$ , as shown in Figure 4.40. As with the stable isotope data, the most prominent feature of the record occurs around the aragonite region and hiatus, although the strontium isotope values begin the negative excursion which brings them closer to the bedrock value earlier than the  $\delta^{18}\text{O}$  values begin the trend to more positive values associated with the aragonite region, and the return to more radiogenic  $^{87}\text{Sr}/^{86}\text{Sr}$  values which signals a higher exogenic component therefore occurs while the  $\delta^{18}\text{O}$  data is becoming more positive.

$^{87}\text{Sr}/^{86}\text{Sr}$  also falls to less radiogenic values before the aragonite region, beginning at ca. 128.5 kyr. This trend does not have an analogous change in the  $\delta^{18}\text{O}$  record, although the  $\delta^{18}\text{O}$  data appears to be much more variable at this time.

#### 4.3.4.2.2 DIM-3

The much lower  $^{87}\text{Sr}/^{86}\text{Sr}$  sampling resolution in DIM-3 compared to DIM-1 results in the possibility that the true changes may not be seen, if the areas where variations occurred were not sampled. From the four sampled points, there appears to be an oscillatory pattern to the values, with values beginning less radiogenic and becoming more radiogenic, returning to less radiogenic and finally becoming their most radiogenic at the end of growth. This last trend to more radiogenic occurs in approximately the same timeframe as the clear trend to less negative values in the  $\delta^{13}\text{C}$  data, thus for this part of the record,  $^{87}\text{Sr}/^{86}\text{Sr}$  and  $\delta^{13}\text{C}$  are positively correlated.

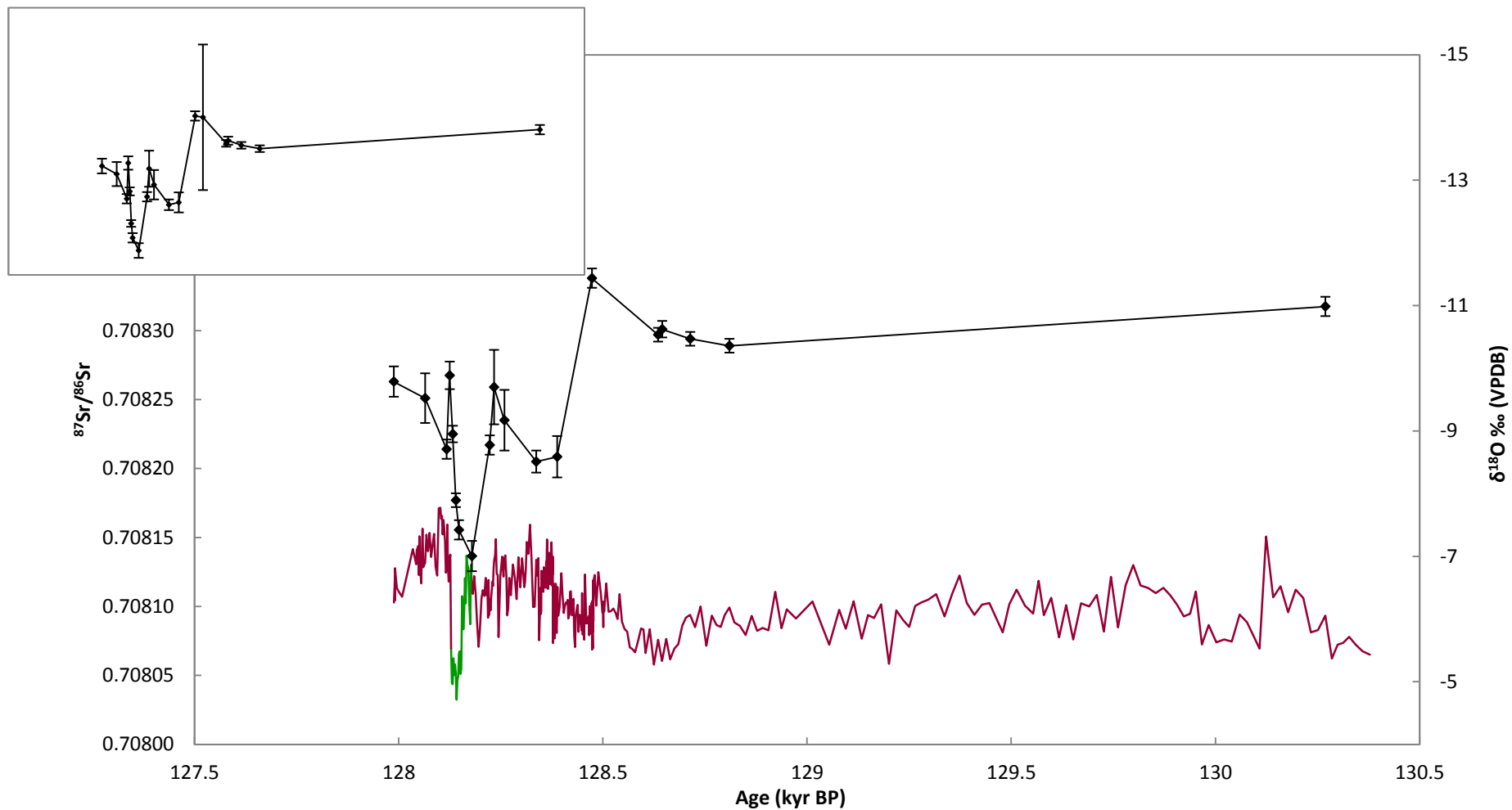


**Figure 4.40**  
 $^{87}\text{Sr}/^{86}\text{Sr}$  profile for DIM-1 (black filled circle with error bars, which represent internal precisions at the 2SE level), shown in comparison to  $\delta^{18}\text{O}$  (red line = calcite, green line = aragonite). Inset shows shape of profile before removal of the anomalous point.

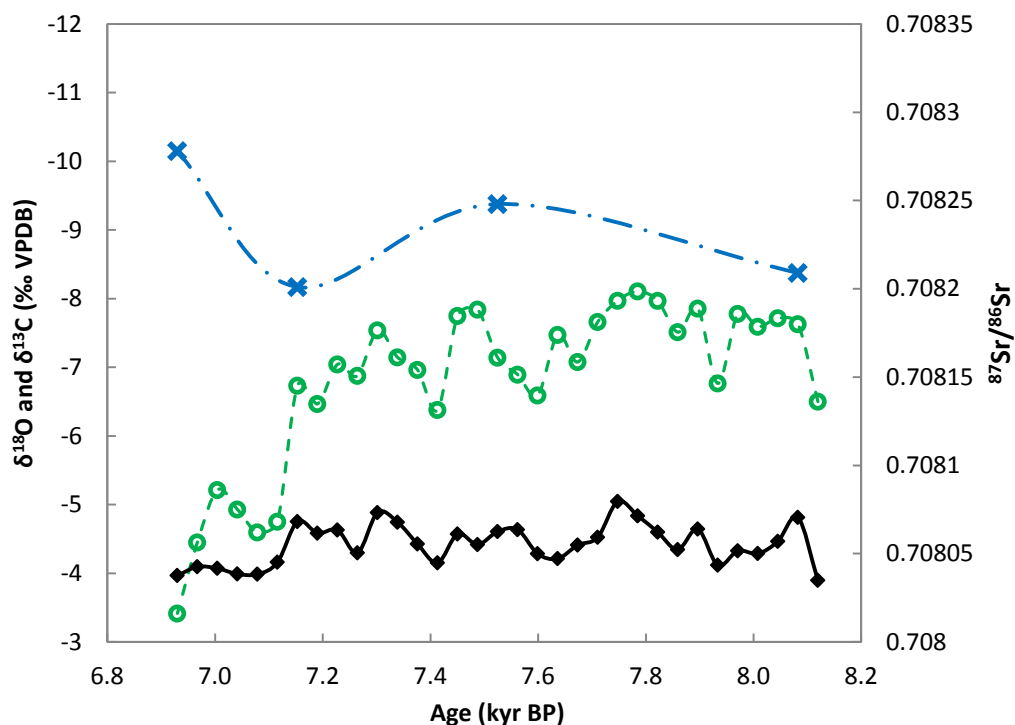


**Figure 4.41**  
 $^{87}\text{Sr}/^{86}\text{Sr}$  (blue crosses, dotted and dashed line) variations in DIM-3, compared with  $\delta^{18}\text{O}$  (black filled diamonds) and  $\delta^{13}\text{C}$  (green open circles and dashed line) profiles.  $^{87}\text{Sr}/^{86}\text{Sr}$  axis uses same values as Figure 4.37, to allow comparison of magnitude of variations with DIM-1.

#### 4.3.4.2.3 DIM-2

The  $^{87}\text{Sr}/^{86}\text{Sr}$  data for DIM-2 are shown in Figure 4.42 where they are compared to the oxygen and carbon data, and Figure 4.43, where they are compared to mineralogy. The general trend of  $^{87}\text{Sr}/^{86}\text{Sr}$  values in DIM-2 is from less radiogenic (0.708475) at the base of the stalagmite, to more radiogenic (0.708561) at the top. This general trend is interrupted by an excursion to less radiogenic values (0.708461) approximately 70 mm above the base of the stalagmite. This excursion occurs in a recrystallised section of the stalagmite. Figures 4.38 and 4.39 demonstrate that the covariation between  $^{87}\text{Sr}/^{86}\text{Sr}$  and both  $\delta^{13}\text{C}$  and  $\delta^{18}\text{O}$  that is seen in the primary aragonite is not present in the recrystallised calcite, presumably because one or both systems was altered during recrystallisation. Therefore, the  $^{87}\text{Sr}/^{86}\text{Sr}$  data from the recrystallised and mixed mineralogy sections may not be viable. The data from the aragonite region agrees with the general trend produced by all the data however; over time the data progresses from less radiogenic values which contain a high bedrock component to more radiogenic values which contain a higher relative input from the exogenic source.

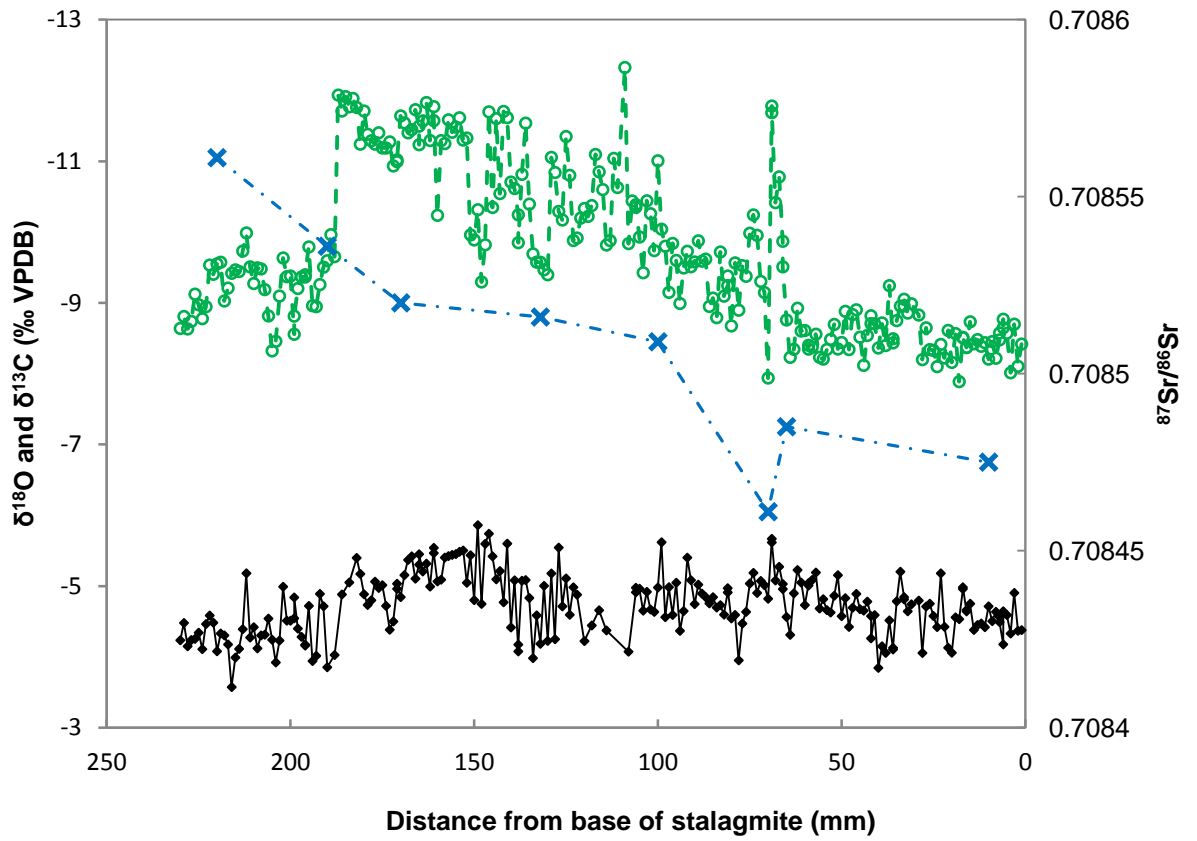


**Figure 4.42**  
 $^{87}\text{Sr}/^{86}\text{Sr}$  (crosses, dotted and dashed line) profile for DIM-2 shown in comparison to the  $\delta^{18}\text{O}$  (black diamonds) and  $\delta^{13}\text{C}$  (open circles and dashed line) profiles

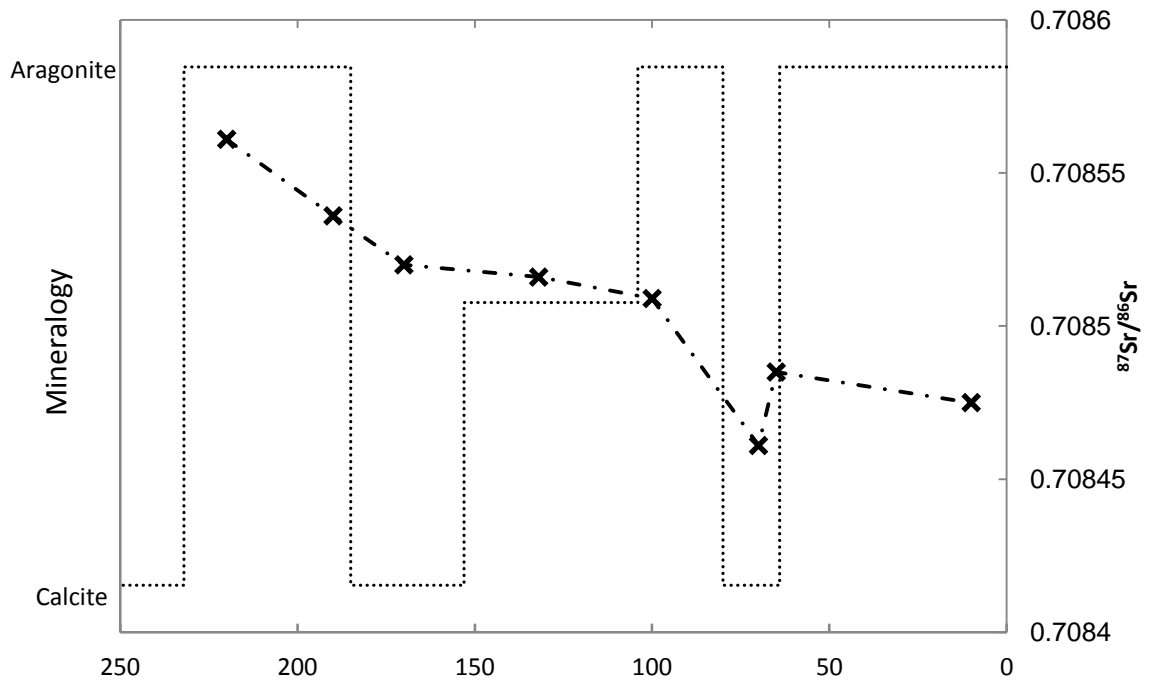


**Figure 4.43**  
 $^{87}\text{Sr}/^{86}\text{Sr}$  (crosses, dotted and dashed line) profile for DIM-2 shown in comparison to mineralogy (dotted line).

## 4.3.5 Trace Element Measurements

### 4.3.5.1 DIM-1

#### 4.3.5.1.1 Sampling Strategy

A suite of trace elemental data was collected via laser ablation. Not all elements will be presented here; only those data which were above detection limits and had discernible trends are mentioned.

It was not possible to analyse the whole of DIM-1 using laser ablation, due to the size of stalagmite, the limit of the size of piece which can fit in the laser stage, and the length of time taken for each analysis. Therefore, four sections were selected for analysis: the aragonite region (including a portion of calcite either side), the period at approximately 128.44 kyr BP, where Sr isotopes decrease greatly prior to the decrease associated with the aragonite region, a section from just above the shift in growth axis near the bottom of the stalagmite at approximately 128.9 kyr BP, which coincides with an increase in growth rate and the beginning of the trend to more negative values in the stable isotopes, and a section from the point at which oxygen isotopes begin to truly decrease, at approximately 128.52 kyr BP. For clarity in coming figures, these will be named Aragonite Region,  $^{87}\text{Sr}/^{86}\text{Sr}$  Collapse, Above Shift, and  $\delta^{18}\text{O}$  Change, respectively.

#### 4.3.5.1.2 Trace Element Results

Trace element data for DIM-1 is presented in Figures 4.44 - 4.49. The aragonite region (Figure 4.44 A) shows high Sr and low Mg, which is in accordance with the partition coefficients of Sr and Mg into aragonite (Kinsman and Holland, 1969, Oomori et al., 1987). The “ $^{87}\text{Sr}/^{86}\text{Sr}$  Collapse” region shows a large decrease in Mg, Sr and Ba, and high covariation in these elements. These collapses are not coeval with the  $^{87}\text{Sr}/^{86}\text{Sr}$  Collapse, as the laser tracts only covered a very short period of time. What they do seem to show, is that climate (especially precipitation) may have been very variable at this time, leading to large shifts in drip water trace elements.

The  $\delta^{18}\text{O}$  Change region (Figure 4.47), and the Above Shift region (Figure 4.49) do not show any important trends, but they are included here for comparison with the more variable time periods.

In Section 4.1.2.2, dripwaters for Dim Cave were presented and the theoretical ranges of Mg/Ca and Sr/Ca which should precipitate from them were calculated. These values can be compared with values for DIM-1. The predicted range of values for Mg/Ca \* 1000 of calcites precipitated from the Dim Cave drip waters is 11.252 – 134.082. This is in good agreement with the observed values of calcite in DIM-1, which ranged from 13.737 to 79.811. The predicted range of values for Sr/Ca \* 1000 of calcites precipitated from the Dim Cave dripwaters is 0.0417 to 0.129. The observed range for calcite in DIM-1 is 0.0253 – 0.203, which is a slightly larger range but only by a small margin. These similar values for Mg/Ca and Sr/Ca of calcites in DIM-1 to the predicted values of calcite precipitated from the Dim Cave drip waters suggests that drip water chemistry is similar today to at the time that DIM-1 was precipitated.

Sr/Ca values for aragonite in DIM-1 are also similar to those predicted, although of a larger range. The theoretical Sr/Ca \* 1000 range calculated using a distribution coefficient of 1.13 was 0.314 – 0.534, while the actual range in DIM-1 was 0.188 – 0.500.

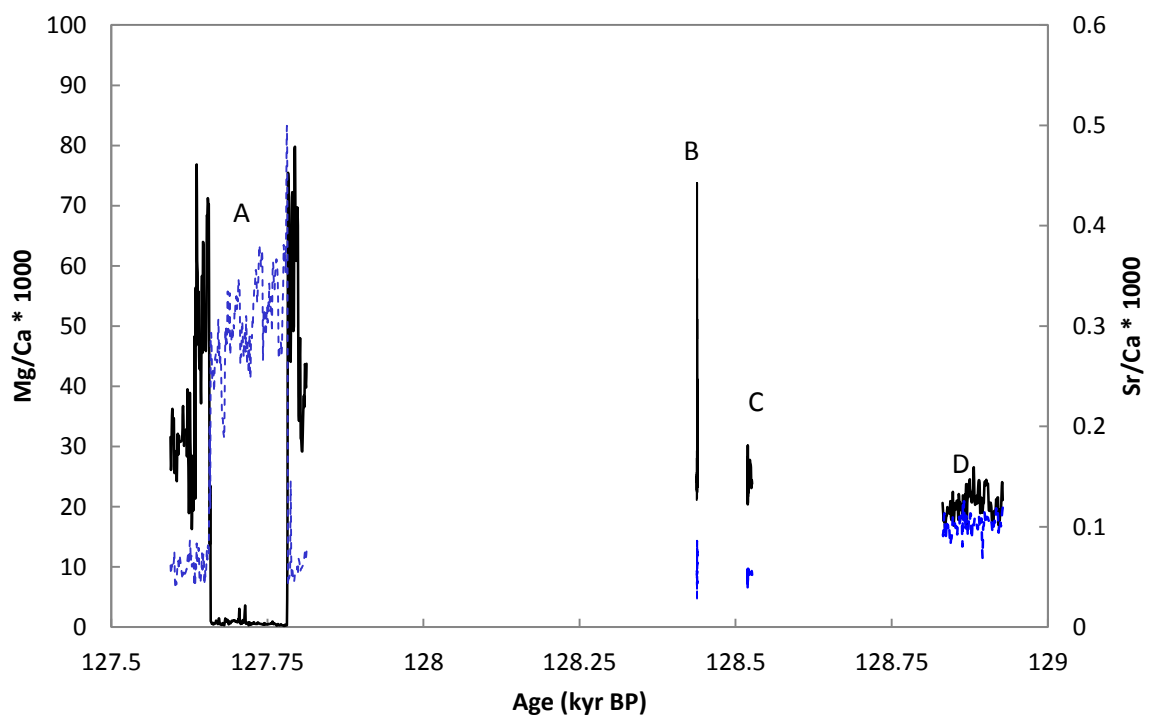


**Figure 4.44**  
**Mg/Ca \* 1000 (black line) and Sr/Ca \* 1000 (blue dotted line) variations for the sections of DIM-1 outlined above. Aragonite Region (A), <sup>87</sup>Sr/<sup>86</sup>Sr Collapse (B),  $\delta^{18}\text{O}$  Change (C), Above Shift (D).**

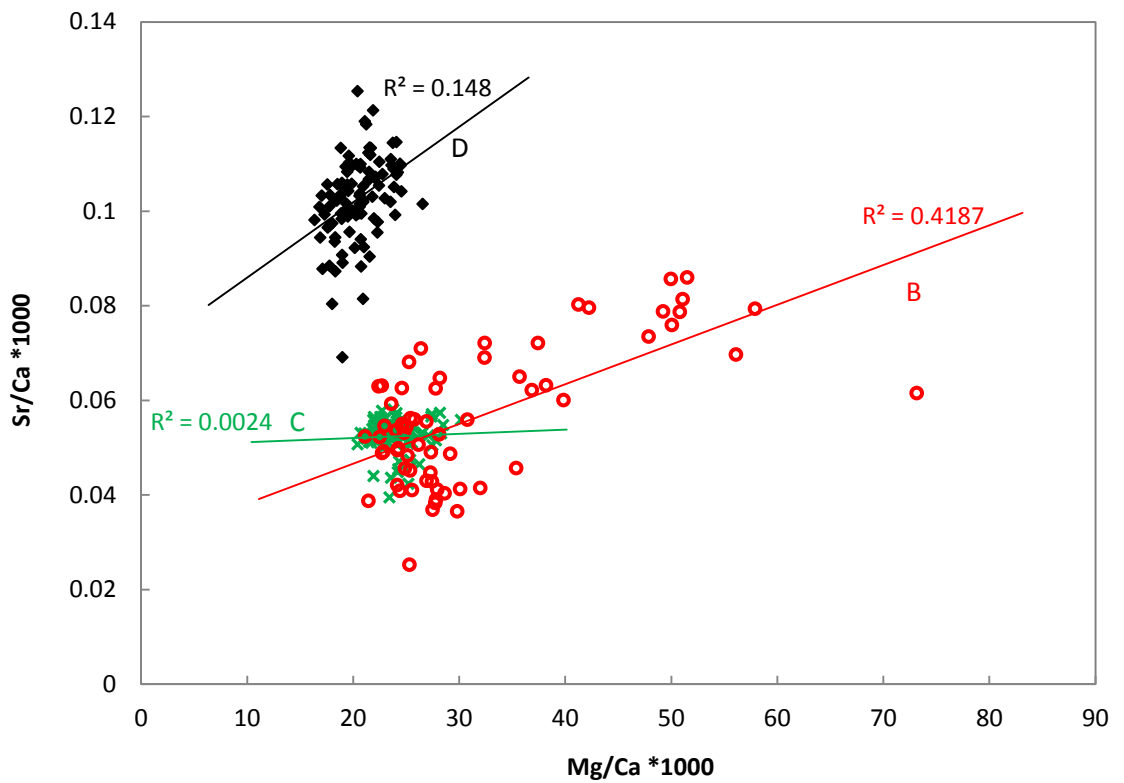


**Figure 4.45**  
**Crossplot of Mg/Ca \* 1000 vs. Sr/Ca \* 1000 for the sections of DIM-1 outlined above:  $^{87}\text{Sr}/^{86}\text{Sr}$  Collapse (red unfilled circles, B in Figure 4.44),  $\delta^{18}\text{O}$  Change (green crosses, C), and Above Shift (black diamonds, D) regions. The aragonite region is excluded as the near exclusion of Mg from aragonite would affect the correlation.**

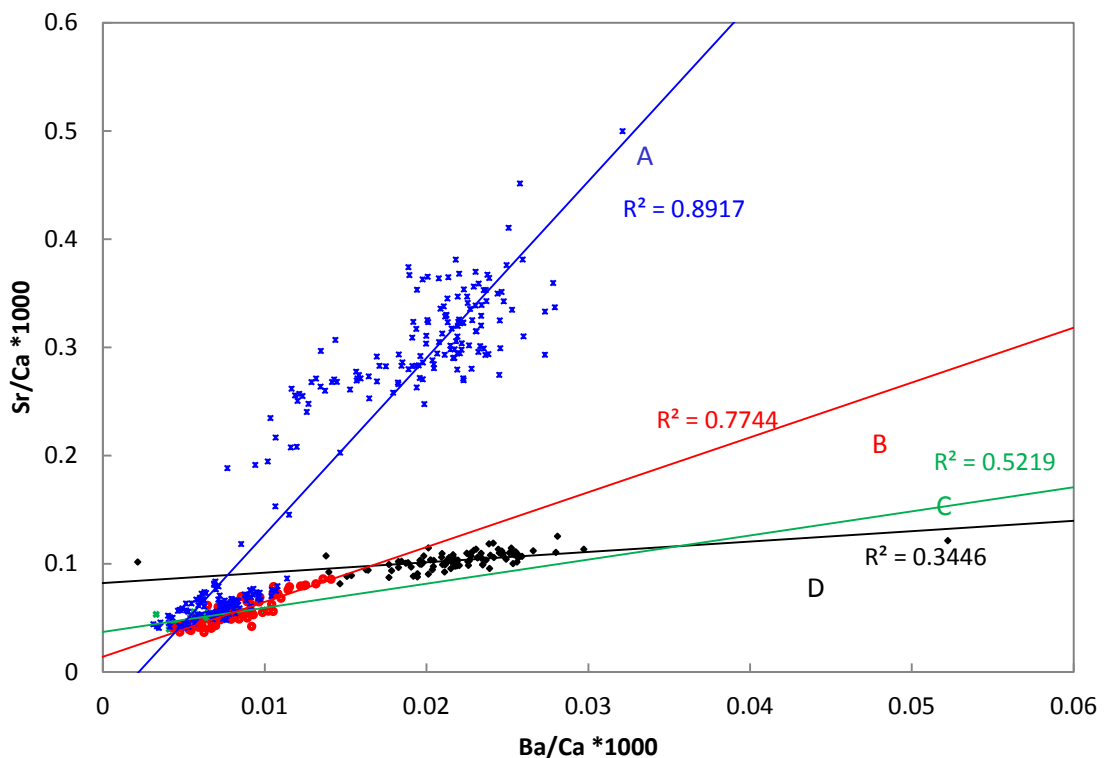


**Figure 4.46**  
**Crossplot of Sr/Ca \* 1000 vs. Ba/Ca \* 1000 for the sections of DIM-1 outlined above: the Aragonite Region (blue x's, A in Figure 4.44),  $^{87}\text{Sr}/^{86}\text{Sr}$  Collapse (red unfilled circles, B),  $\delta^{18}\text{O}$  Change (green crosses, C), and Above Shift (black diamonds, D) regions.**

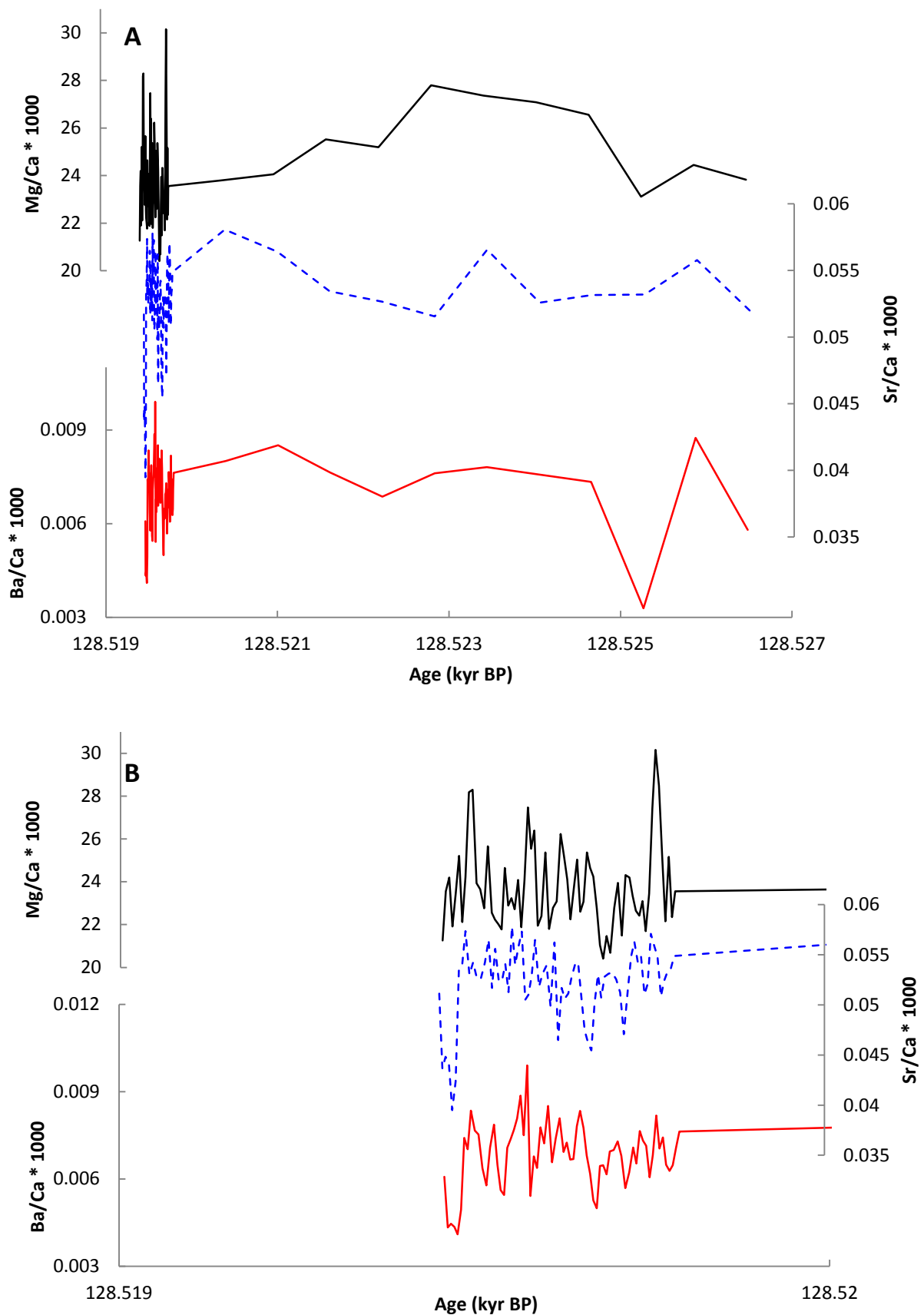


**Figure 4.47** Mg/Ca \* 1000 (black line), Sr/Ca \* 1000 (blue dotted line) and Ba/Ca \* 1000 (red line) variations for the  $\delta^{18}\text{O}$  Change region of DIM-1  
**A)** The entire record for this piece  
**B)** Higher resolution plot of the later part of this record, to enable trends to be viewed more clearly.

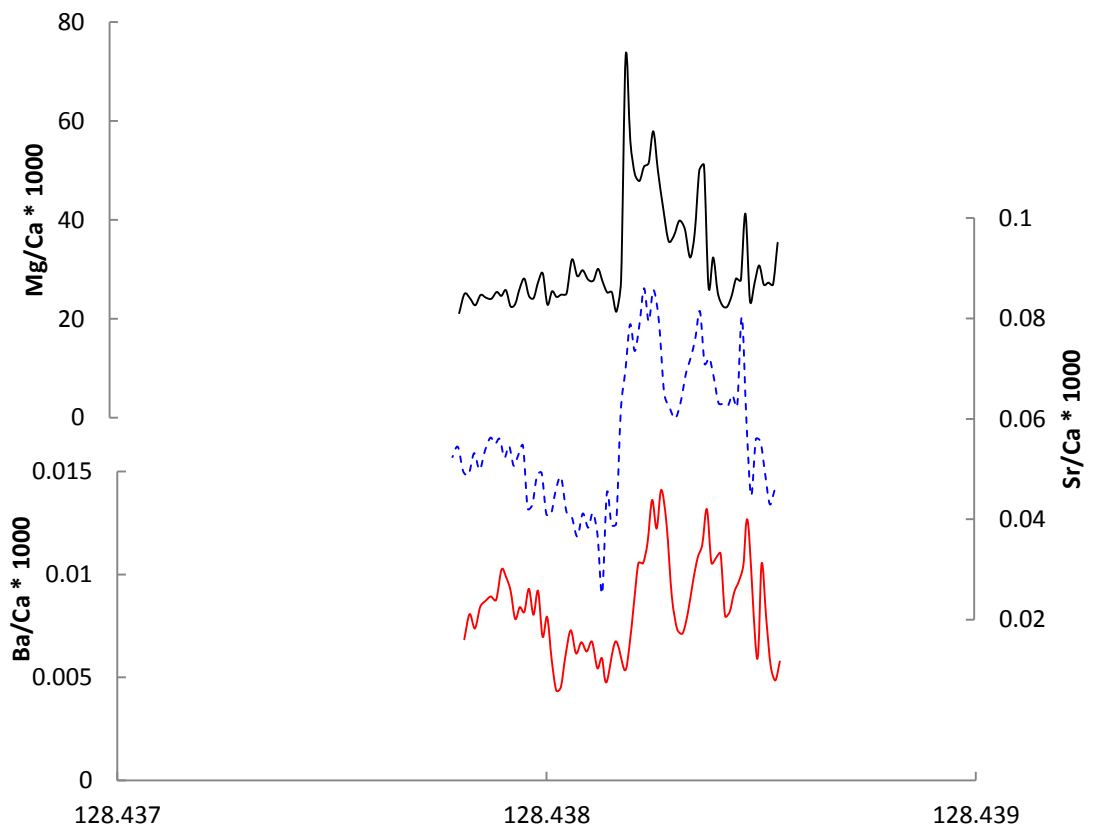


**Figure 4.48**  
*Mg/Ca \* 1000 (black line), Sr/Ca \* 1000 (blue dotted line), and Ba/Ca \* 1000 (red line) variations for the  $^{87}\text{Sr}/^{86}\text{Sr}$  Collapse region of DIM-1.*

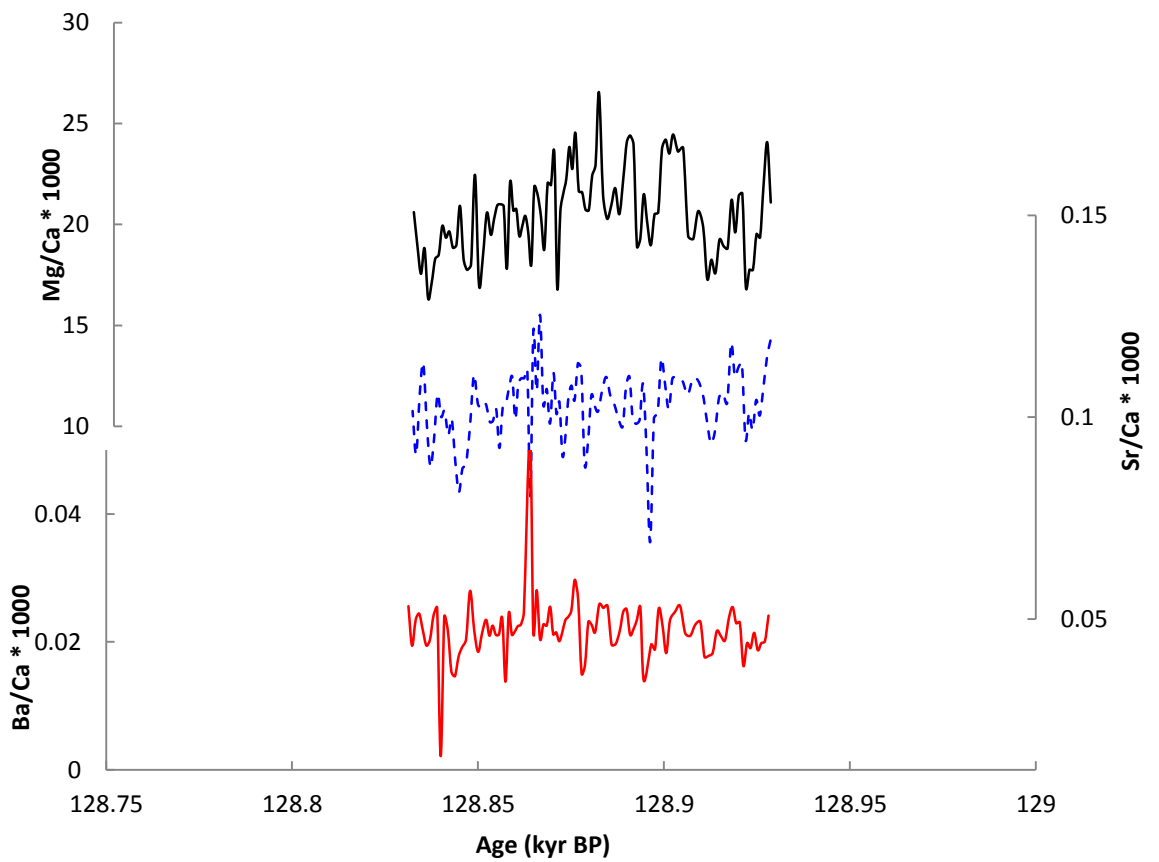


**Figure 4.49**  
*Mg/Ca \* 1000 (black line), Sr/Ca \* 1000 (blue dotted line), and Ba/Ca \* 1000 (red line) variations for the Above Shift region of DIM-1.*

#### 4.3.5.2 DIM-2

LA-ICP-MS was used to measure changes in trace element composition across two mineralogical changes in DIM-2 (Figures 4.50-4.51). These analyses were originally intended as screening runs; producing datasets of raw, uncorrected data over large transects quickly to pinpoint areas of interest. The data was then corrected to absolute elemental ratios using data from NIST glass standard scans.

The upper section analysed shows the expected compositions for both elements as the mineralogy changes: High Mg, low Sr in calcite, low Mg, high Sr in aragonite. This suggests that in DIM-2, trace element concentrations in recrystallised calcite were inherited from the reprecipitating water and not retained from the primary aragonite.

The lower transect does not show an abrupt change between minerals, with values oscillating between the two styles of geochemical content described above. This region falls within the area identified by the stable isotope data as being of mixed mineralogy, in contrast to the (low resolution) XRD boundaries. Therefore, the trace element data support the stable isotope data, in that the mineralogical change is not clearly defined at the lower boundary. It would seem that although this region appeared to give the most reliable U/Th dates, if a chronology were to be attempted, the upper region of aragonite is more likely to produce ages that have not been affected by open system behaviour.

Representative Mg/Ca \* 1000 and Sr/Ca \* 1000 values for primary aragonite and secondary calcite in DIM-2 are shown in Table 4.11. These values are in reasonably good agreement with the values expected to precipitate from the Dim Cave drip waters (calcite with Mg/Ca\*1000 of 11.3 - 134 and Sr/Ca\*1000 of 0.0417 – 0.129, aragonite with Sr/Ca\*1000 of 0.314 – 0.975).

Carbonate Form	Representative Mg/Ca * 1000 range	Representative Sr/Ca * 1000 range
Primary Aragonite	0-50	0.75-1.25
Secondary Calcite	75-100	0.1-0.3

**Table 4.11** *Representative Mg/Ca \* 1000 and Sr/Ca \* 1000 of primary aragonite and secondary calcite in DIM-2*

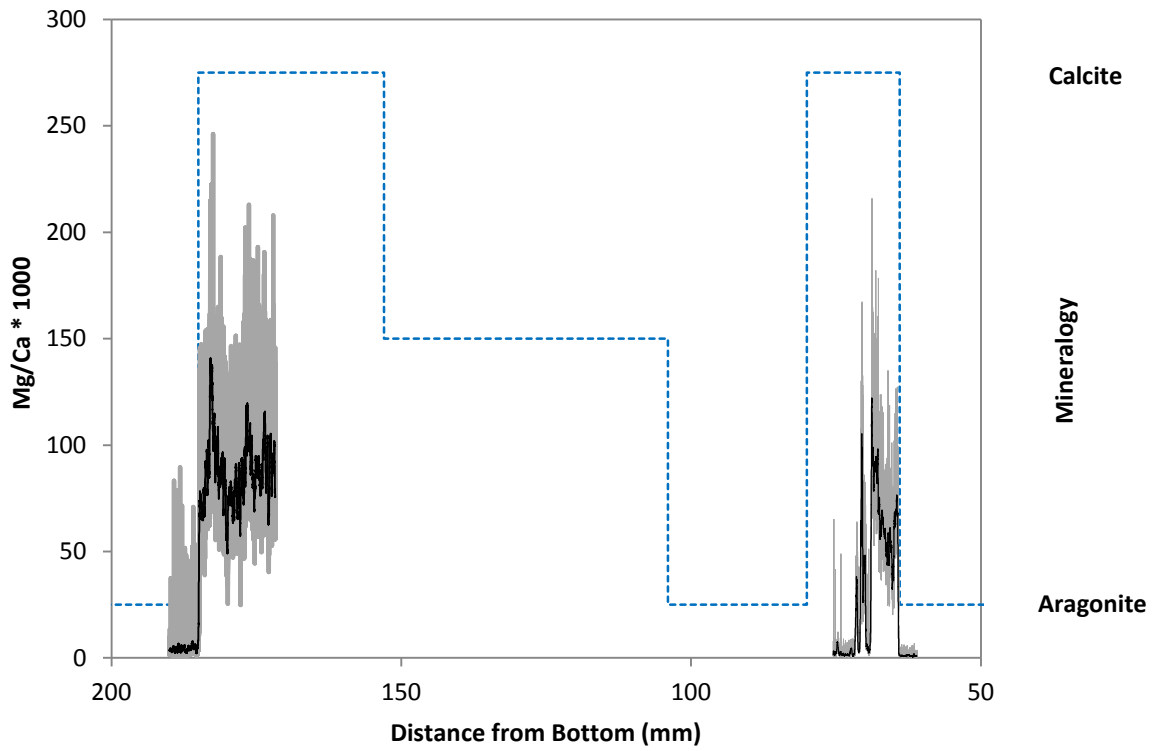


**Figure 4.50** *Mg/Ca \* 1000 data for DIM-2 (grey line). Black line represents a 50-point moving average. Mineralogy is represented by dashed blue line.*

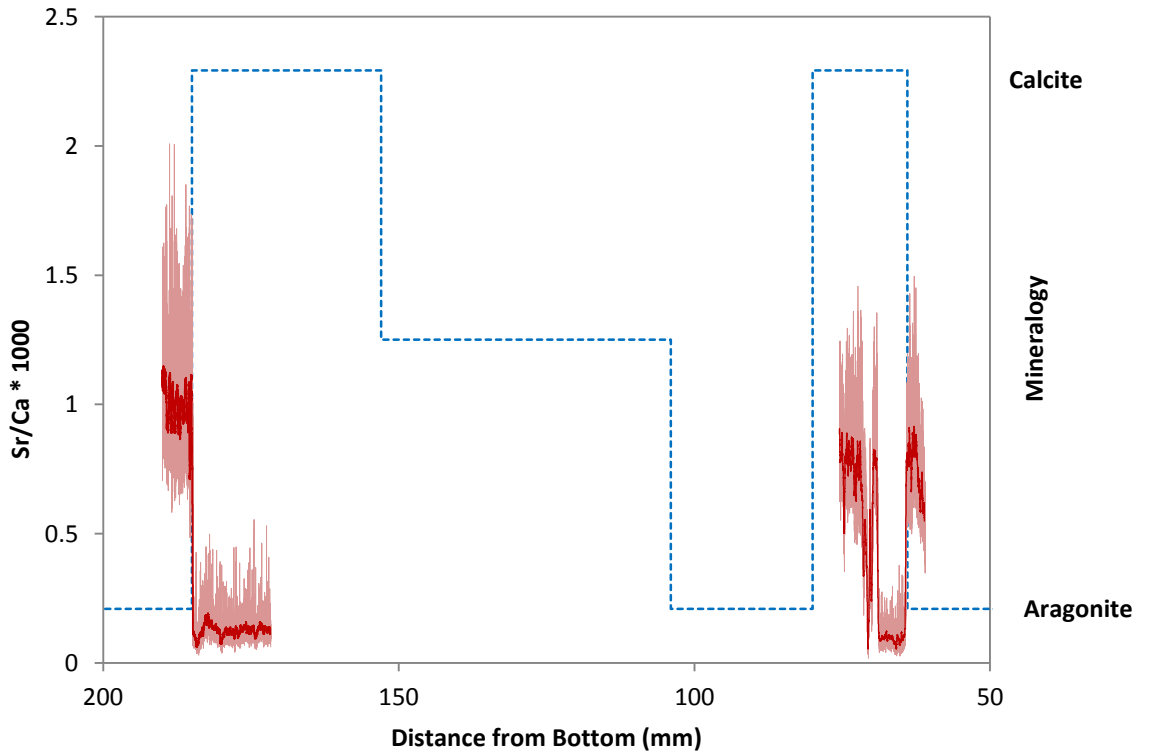


**Figure 4.51** *Sr/Ca \* 1000 data for Dim-2 (pink line). Red line represents a 50-point moving average. Mineralogy is represented by dashed blue line.*

## 4.3.6 Palaeoclimatic and Palaeoenvironment Interpretations

### 4.3.6.1 DIM-1

#### 4.3.6.1.1 *The Growth of DIM-1 and Subsequent Diagenesis*

DIM-1 began growth at approximately 130.2 kyr BP. This is approximately the time at which Vostok temperatures increased to as much as 3°C higher than today (Petit et al., 1999), and due to large errors on the DIM-1 age model, the start of accretion could also be related to the Asian Monsoon Termination at ca.  $129.3 \pm 0.8$  kyr BP (Yuan et al., 2004), and the Eemian interglacial, as will be discussed in section 4.3.6.1.2.

DIM-1 is comprised mostly of calcite, with a change to aragonite occurring immediately below a hiatus, followed by a continuation of calcite mineralogy to the (broken) top of the stalagmite. A small, post DIM-1 Holocene growth on the outside of DIM-1, named DIM-3, and actively precipitating speleothems in Dim Cave are formed of aragonite. Interpretation of these changing mineralogies is clearly crucial to the interpretation of the climatic signal within DIM-1, and pivotal to this process is confirming that all fabrics are primary. As explained in Section 4.4.1.4, the central axis of DIM-1 does not show signs of recrystallisation that are immediately obvious. The outer regions of the stalagmite have a different structure. Aragonite, as confirmed by XRD exists in places but when these layers are traced to the central growth axis the mineralogy is calcite. In thin section, small euhedral calcite crystals are common in the calcite parts of DIM-1 (Figure 4.12A), which is indicative of reprecipitation (Martín-García et al., 2009).

Therefore, the interpretation which best fits the evidence is that most, if not all, of the calcite in DIM-1 is secondary, having recrystallised from an original aragonite mineralogy. This primary aragonite is preserved in one axial region, immediately below the hiatus.

#### 4.3.6.1.1.1 *Aragonite as the Primary Mineral of DIM-1*

Aragonite speleothems have been found in hundreds of ambient temperature caves throughout the world (Moore, 1956, Cabrol, 1978, Hill and Forti, 1997, Bar-Matthews et al., 1991, Frisia et al., 2002, Woo and Choi, 2006). Aragonite tends to form in warmer caves, for example temperatures greater than  $>12^{\circ}\text{C}$  have been suggested (Moore, 1956, Cabrol, 1978, Cabrol and Coudray, 1982, Martín-García et al., 2009, Alonso-Zarza et al., 2011), although both polymorphs were able to form at  $14.5^{\circ}\text{C}$  in the Grotte de Clamouse, SW France (Frisia et al., 2002).

Many researchers have investigated the controlling factors of aragonite growth, such as temperature, drip water Mg/Ca ratios, phosphate, sulphate, organics and saturation (Moore, 1956, Kitano, 1962, Fyfe and Bischoff, 1965, Berner, 1966, Folk, 1974, Given and Wilkinson, 1985, González and Lohmann, 1988, Zhong and Mucci, 1989, Frisia et al., 2002, De Choudens-Sánchez and González, 2009, Bar-Matthews et al., 1991, Railsback et al., 1994). Aragonite has also been found to precipitate at high pH (Kim et al., 2006), and under very fast precipitation rates (Kitano et al., 1962, Kitano and Hood, 1965). Aragonite is sometimes able to precipitate from waters that the carbonate saturation state data dictate that only calcite should be able to form (Frisia et al., 2002), indicating that there may be threshold effects or interplay of several factors controlling which polymorph of calcium carbonate precipitates. The most important factors in controlling mineralogy appear to be temperature, Mg content and  $\text{CO}_3^{2-}$ -controlled kinetics, with equilibrium thermodynamics being of little importance (De Choudens-Sánchez and González, 2009). The interplay of these factors will be discussed in Section 4.3.6.1.3, in reference to the persistence of the aragonite region in DIM-1.

Aragonite may nucleate at clastic layers and corrosion surfaces in speleothems (Craig et al., 1984), with clastic layers perhaps occurring when there was insufficient water flow to wash them off the speleothem surface (Railsback et al., 1994). This is unlikely to have been the cause for DIM-1 aragonite, as aragonite is interpreted as being the primary mineral for the whole of the speleothem, not only the layer which remains now. Organic macromolecules may also act as templates for aragonite precipitation (Hou and Feng, 2005). This process may be of importance, as SLPL imaging revealed that the original aragonite parts of DIM-1 had high concentrations of fluorescent material, which is most likely to be organics, while the recrystallised calcite regions had lost most of this fluorescence. It is not yet clear why fluorescent material was not retained in the secondary calcite.

#### *4.3.6.1.1.2 Replacement of DIM-1 Aragonite by Calcite*

The replacement of aragonite by calcite is a dissolution-precipitation reaction, which occurs due to the difference in solubility of aragonite and calcite: At 25°C and one atmosphere, the solubility product of aragonite ( $k_{sA}$ ) is  $10^{-8.22}$ , while the solubility product of calcite ( $k_{sC}$ ) is  $10^{-8.35}$  (Garrels et al., 1960, 1961), and the more soluble polymorph will be the less stable (Fyfe and Bischoff, 1965). Therefore, recrystallization of aragonite may occur if the speleothem is open to water infiltration (Frisia et al., 2002), for example if the

speleothem is porous (Frisia et al., 2000) with evidence for dissolution phenomena (Frisia, 1996). Replacement occurs at the microscale, and occurs when waters are undersaturated in aragonite and saturated in LMC (Maliva et al., 2000, Frisia et al., 2002, Hopley et al., 2009, Alonso-Zarza et al., 2011). If waters are just below the saturation point of either mineral, micritization will occur, and waters undersaturated with respect to both minerals will cause dissolution (Martín-García et al., 2009). Thus, partial replacement of aragonite by the subsequently precipitating calcite indicates dissolution due to variations in solution composition (Spötl et al., 2002b).

Only a thin film of water (<100 Å) may be necessary to initiate the transformation from aragonite to calcite, or neomorphism, in a closed system (Pingitore, 1976, Perdikouri et al., 2008). In this process, aragonite dissolves on one side of the film, while calcite spontaneously precipitates on the other (Folk, 1965, Kinsman, 1969, Folk and Assereto, 1976, Pingitore, 1982, Bathurst, 1964, Dodd, 1966, Hopley et al., 2009). This process is known as calcitisation, which is more likely in a closed system, and in which aspects of the original aragonite are preserved (Hopley et al., 2009, Woo and Choi, 2006). A second possible method was suggested by Al-Aasm and Veizer (1986b, a), in which two stages occur, first dissolution of the aragonite and then cementation of the secondary calcite, which destroys all remnants of the original aragonite (Hopley et al., 2009, Woo and Choi, 2006).

It is assumed here that it was contact with waters that were undersaturated with respect to aragonite that led to dissolution of the aragonite and reprecipitation as calcite, but there are other possible causes. For example, aragonite speleothems which formed in caves that subsequently experienced an increase in humidity may undergo calcitisation (Woo and Choi, 2006), or changes in the composition and alkalinity of the infiltration water may be a cause of recrystallisation (Alonso-Zarza et al., 2011). The saturation state of drip waters is deemed to be the most likely cause, as it accounts for how some of the outer parts of the stalagmite could have remained as aragonite while the corresponding central parts of the stalagmite were recrystallised, due to the fact that the waters became saturated while flowing over the surface.

The rate of the transformation from aragonite to calcite is dependent on nucleation and growth rate of the replacing calcite, not on the dissolution rate of the aragonite (Morse and Mackenzie, 1990). During calcitisation, migration of ions towards incorporation into neomorphic calcite is controlled to a large degree by ionic diffusion rates, and not to such

an extent by concentrations of such ions in the pore waters (Pingitore, 1982, Woo and Choi, 2006). This may mean that trace elements in DIM-1 are not recording the concentration of the waters which lead to recrystallisation, but retain information from the primary aragonite. This trend will be modulated by uptake rates; for example as calcite grows it tends to preferentially accept ions smaller than  $\text{Ca}^{2+}$ , while aragonite will accept divalent cations the size of  $\text{Ca}^{2+}$  or larger, such as  $\text{Sr}^{2+}$  (Fyfe and Bischoff, 1965, Speer, 1983). Indeed strontium substitutes ideally for calcium in aragonite (Finch and Allison, 2007), leading to high concentration of Sr in aragonite (Bar-Matthews et al., 1991, Spötl et al., 2002b, Ortega et al., 2005). Sr concentration will thus be much lower in the reprecipitated calcite, in line with other speleothem records such as that of Cabrol (1978).

As the U/Th ages for calcitic samples of DIM-1 appear to be only slightly too old (as a percentage of the true age), it appears that recrystallisation of the primary aragonite may have happened soon after it was initially precipitated, perhaps within the same wet season or at the beginning of the next. The most likely cause of this diagenetic process is periods of high infiltration, similar to the “flushing” model suggested by Lachniet et al. (2012). DIM-1 formed of primary aragonite at a time when its feeding drip water was saturated with respect to aragonite. At some time afterwards (probably soon afterwards, as the U/Th system is in places only slightly disturbed), a rapid “flushing” of dripwater into the aquifer due to increased precipitation led to lower water/rock interaction times in the aquifer, thus producing cave waters which were undersaturated with respect to aragonite. When these waters reached the tip of DIM-1, they dissolved the metastable aragonite, after which they became saturated with respect to calcite but not aragonite, thus favouring recrystallisation as calcite, the stable polymorph, in the same location.

Mg/Ca of the dripwater would have had to have been low at this time, as  $\text{Mg}^{2+}$  inhibits calcite growth. At low Mg/Ca ratios and low supersaturation values, calcite is able to compete with aragonite for reactants due to its higher growth rate (De Choudens-Sánchez and González, 2009). Increased precipitation could result in low dripwater Mg/Ca, through the mechanisms of decreased water/rock reaction times, which would be further decreased if flushing events led to a change in hydrological routing so that conduit flow dominated (Cruz et al., 2007, Fairchild and Treble, 2009), a reduction in the amount of PCP occurring in the epikarst, as this would reduce the amount of Ca removed while Mg stayed in the groundwater (Fairchild et al., 2006, Cruz et al., 2007), and a reduction in the amount of dolomite dissolution relative to that of calcite in the epikarst due to its slower

dissolution (Fairchild and Treble, 2009). Once calcite has achieved nucleation, presence of  $Mg^{2+}$  in the solution will have little or no effect on the progress of transformation to calcite (Morse and Mackenzie, 1990).

This process of primary aragonite being precipitated by waters saturated with respect to aragonite, then subsequently dissolved by waters undersaturated with respect to aragonite during a period of high rainfall, and recrystallised as calcite, is interpreted as the mode of formation for the majority of DIM-1, and is summarised in Figure 4.52 (T0-T2). However, aragonite was able to persist in the region preceding the hiatus (and also above the hiatus in outer portions of the stalagmite). For this to happen, it is necessary that arid conditions continued after the precipitation of the aragonite layer which still remains, so that the stage of dissolution by waters undersaturated with respect to aragonite was delayed. The hiatus occurs at this point, supporting the view that there was a reduction in drip rate at this time. When waters became undersaturated with respect to aragonite again, and dissolution of the aragonite and recrystallisation as calcite recommenced, the percolating waters could not penetrate deep enough to dissolve all of the aragonite which had been deposited since the last phase of recrystallisation had occurred. Therefore, the aragonite region was protected, and the previous growth mode of precipitation-dissolution-recrystallisation continued above it. The survival of some aragonite above the hiatus, but not as complete layers and only in outer portions of the stalagmite, indicates that the waters that recrystallised this depth of DIM-1 were only slightly undersaturated with respect to aragonite, and that they quickly gained saturation with respect to aragonite as they flowed over the stalagmite surface. This process is summarised in Figure 4.52 (T3-T7).

Diagenetic alteration has important implications for interpretation of the stable isotopes in DIM-1, as the oxygen isotope fractionation factors for aragonite and calcite as they precipitate from fluids are different (Lachniet, 2009).

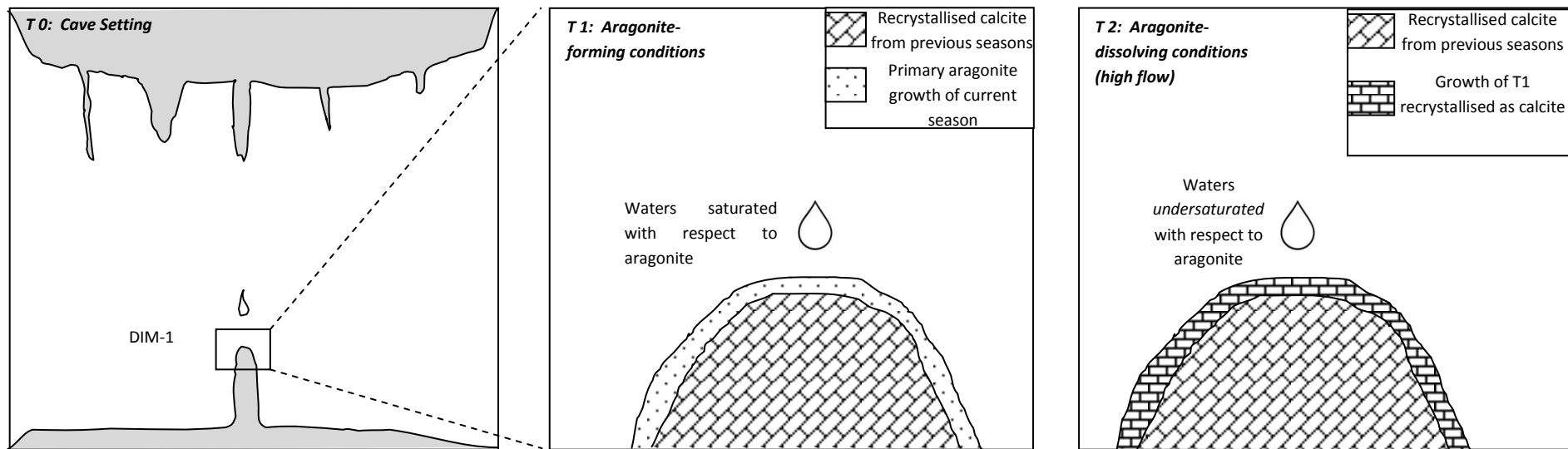


**Figure 4.52** This page and following page  
 The growth and recrystallisation of DIM-1. Not to scale. Processes and geometry are simplified.

**T0:** DIM-1 as it would have grown in the cave setting.

**T1:** A layer of primary aragonite is precipitated during the wet season from dripwaters that are saturated with respect to aragonite.

**T2:** Either later in the same wet season, or at the beginning of the next year's, water flow is higher than in T1, leading to waters that are undersaturated with respect to aragonite. These waters dissolve the aragonite precipitated during T1 as they flow over the speleothem surface, and the layer is reprecipitated as secondary calcite.

**T3:** Flow returns to conditions which promote waters saturated with respect to aragonite, resulting in another layer of primary aragonite.

**T4:** Conditions become more arid, so that there is no period of high flow producing dripwaters undersaturated with respect to aragonite that would recrystallise the aragonite layer formed in T3. Instead, waters saturated with respect to aragonite form another layer of aragonite on the speleothem surface.

**T5:** As conditions start to return to wetter conditions, waters slightly undersaturated with respect to aragonite dissolve the aragonite precipitated in T4 at the tip of the stalagmite. As they do so, because they are only slightly undersaturated with respect to aragonite, they become saturated before they reach the flanks of the stalagmite. Thus, the aragonite formed during T4 on the flanks of the stalagmite remains.

**T6:** A period of waters saturated with respect to aragonite results in a new layer of aragonite being deposited.

**T7:** Higher flow leads to dripwaters undersaturated with respect to aragonite, which dissolve and recrystallise the aragonite layer deposited during T6 as calcite. The aragonite layer deposited during T3, and the aragonite sections created on the flanks during T4-5, are preserved and protected by the surrounding calcite, and therefore persist as the rest of the speleothem is formed by an alternating cycle of aragonite layer precipitation and subsequent dissolution and recrystallisation of that layer as calcite.

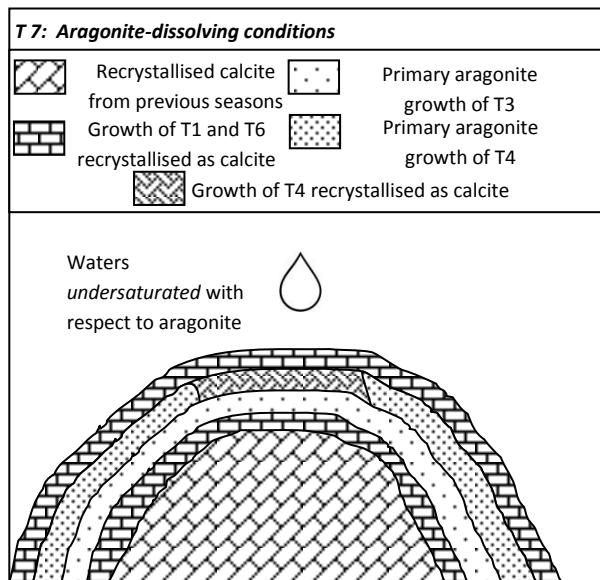
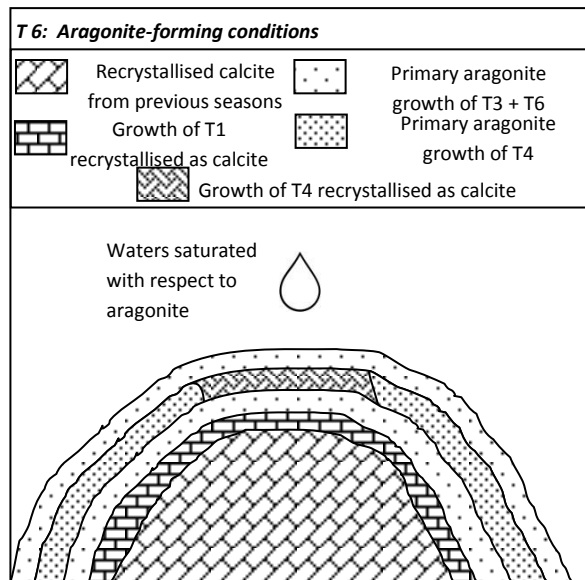
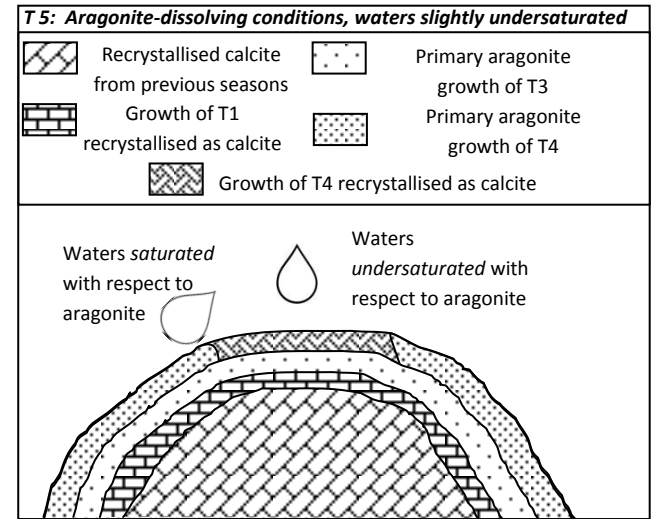
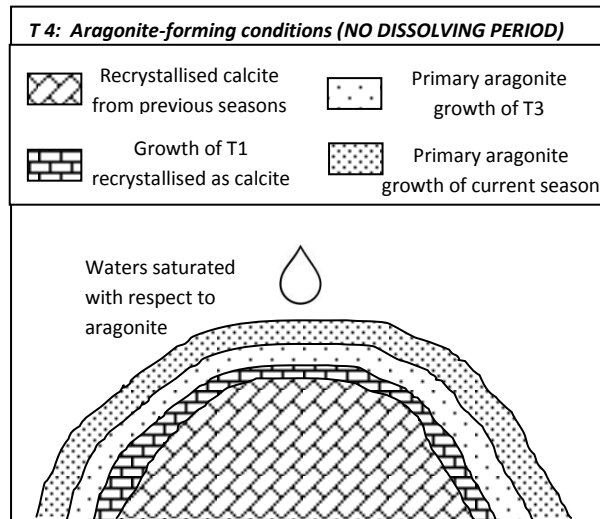
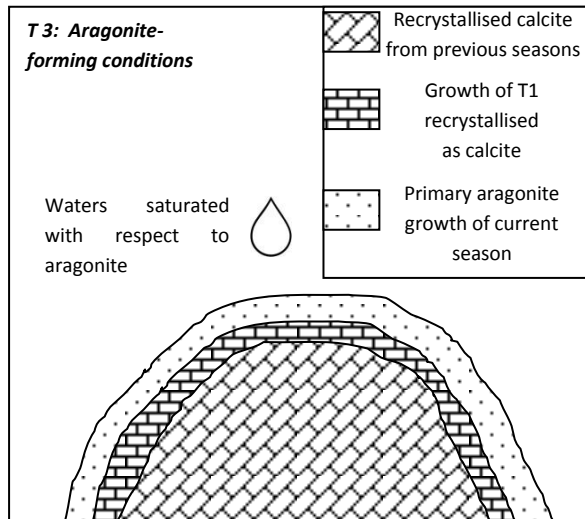


Figure 4.52 Continued. Figure description on previous page.

#### 4.3.6.1.2 The Eemian Record in DIM-1

Figure 4.53 A shows DIM-1  $\delta^{18}\text{O}$  with a 10-point running mean to make identification of trends easier. At approximately  $128.6 \pm 0.7$  kyr BP,  $\delta^{18}\text{O}$  began a trend to more negative values, with the culmination of the trend occurring at  $128.4 \pm 0.7$  kyr BP. This trend most likely reflects an increase in precipitation. Figure 4.53 B shows DIM-1  $\delta^{13}\text{C}$  with a 10-point running mean.  $\delta^{13}\text{C}$  data for DIM-1 suggests that warm, wet conditions may have been reached slightly earlier, with the trend to more negative values beginning at ca  $128.9 \pm 0.7$  kyr BP, and reaching a plateau of low values at ca  $128.7 \pm 0.7$  kyr BP. This date for the onset of warm-wet conditions is very similar to the chronology suggested by a speleothem from Antro del Corchia, Italy, in which the change occurred at  $128.6 \pm 0.7$  (Drysdale et al., 2005) (Figure 4.54).

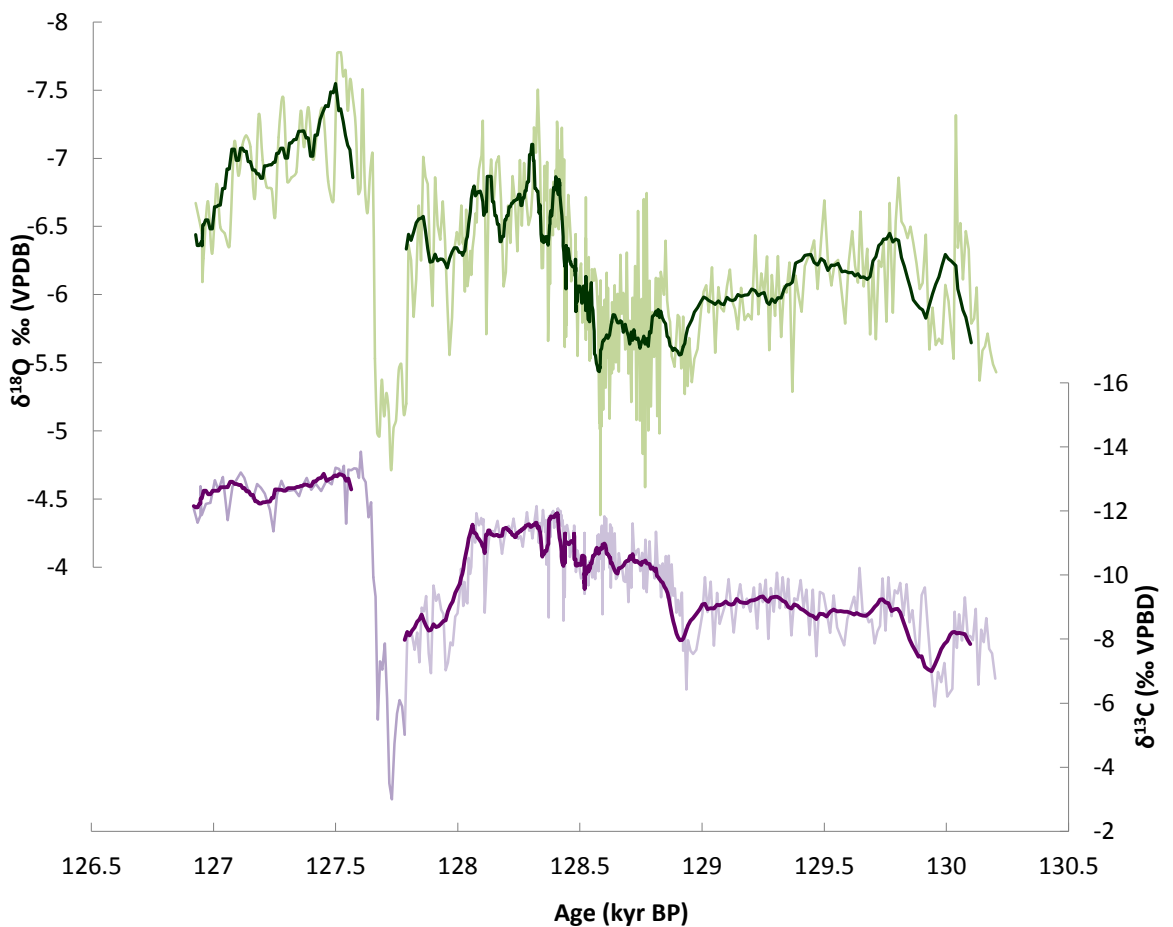


Figure 4.53  $\delta^{18}\text{O}$  (green line) and  $\delta^{13}\text{C}$  (purple line) data for DIM-1 with 10-point running mean.

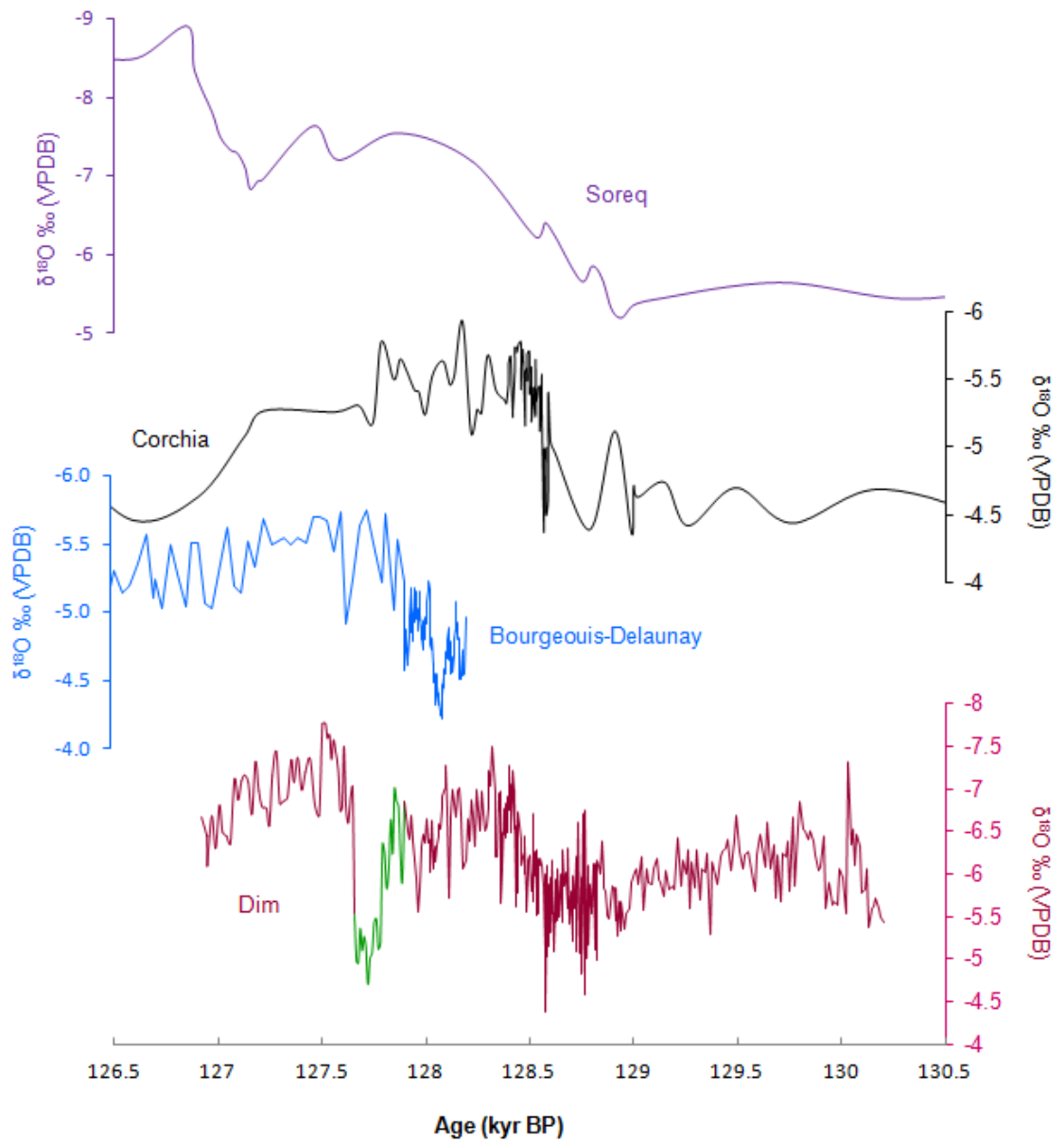


Figure 4.54: Comparison of  $\delta^{18}\text{O}$  record of DIM-1 (red and green lines) with several other records from MIS 5e; Purple line = Soreq Cave, Israel (Grant et al., 2012), Black line = Corchia Cave, Italy (Drysdale et al., 2009), Blue line = Bourgeois-Delaunay Cave, France (Couchoud et al., 2009).

Soreq Cave in Israel experienced intense rainfall associated with sapropel S5 at ca. 128-121 kyr BP (Bar-Matthews et al., 2003, Grant et al., 2012). Sapropel S5 occurred at ca. 125 kyr BP, at which time climate in the eastern Mediterranean favoured forest growth (Cheddadi and Rossignol-Strick, 1995). Orbital tuning gives S5 an age of ~120 kyr BP (Hilgen, 1991), while dating via the Monsoon Index gives an age of ca. 127 kyr BP (Rossignol-Strick and Paterne, 1999). At the time of S5, it appears that the west-east atmospheric gradients changed in the Mediterranean (Plagnes et al., 2002). Sapropel S5 occurred after the deglaciation, and therefore could not have been caused by increased melt water discharge, thus increased precipitation is a possible candidate, especially as north-eastern Mediterranean pollen data support the proposal of a wet climate at the time of Sapropel S5 (Bar-Matthews et al., 2003, Cheddadi and Rossignol-Strick, 1995).

The positive covariation between  $\delta^{18}\text{O}$  and  $\delta^{13}\text{C}$  in DIM-1 is unlikely to have been caused by a change in the seasonal pattern of rainfall, as this would produce anti-correlated  $\delta^{18}\text{O}$  and  $\delta^{13}\text{C}$  in cases of both winter-to-summer-dominated and summer-to-winter-dominated regime changes (Couchoud et al., 2009).

#### 4.3.6.1.3 *The Aragonite Region and Hiatus*

The section of DIM-1 which incorporates the primary aragonite region and the hiatus is interpreted as recording an arid phase. There are several reasons for this, derived from multiple proxies. Figure 4.55 shows variations in Mg/Ca, Sr/Ca,  $\delta^{13}\text{C}$ ,  $\delta^{18}\text{O}$  and  $^{87}\text{Sr}/^{86}\text{Sr}$  for the time period 128.5 kyr BP – 127.5 kyr BP. Aragonite has previously been used as an indicator for aridity (Denniston et al., 2000, McMillan et al., 2005), although in these cases aridity caused a switch in primary mineralogy from calcite to aragonite. Similar principles apply in the case of DIM-1 however, despite the fact that it is persistence of the primary aragonite that is the indicator for aridity. This conclusion assumes that recrystallisation in others parts of the speleothem is only due to increased precipitation soon after the original aragonite growth, which may be over-simplistic as recrystallisation may happen long after the original growth if the recrystallising waters can penetrate deep enough into the speleothem.

There is also a possibility that some of the calcite may be primary, as the Mg/Ca and Sr/Ca values are within the expected ranges of primary calcite precipitation from the Dim Cave drip waters. If this were the case, the aragonite layer would be interpreted as being caused by an arid interval for the simpler reason that longer residence times would raise Mg/Ca values in the drip waters, restricting calcite growth and encouraging aragonite growth. An

increase in Mg/Ca that occurs immediately before the hiatus could then be interpreted in terms of PCP, which would also indicate increased aridity. High resolution petrographic analysis of the calcite of DIM-1, particularly immediately before and after the hiatus, would be a vital next step to determine the cause of the aragonite layer in DIM-1.

The start of the arid interval occurs at ca. 128.1 kyr BP, as shown by the beginning of a trend to less radiogenic values in the  $^{87}\text{Sr}/^{86}\text{Sr}$  data, a trend to more positive values in the  $\delta^{13}\text{C}$  data and a reduction in stalagmite width by approximately 50%. Less radiogenic  $^{87}\text{Sr}/^{86}\text{Sr}$  values indicate that there is a larger contribution of bedrock-derived Sr, which would result from increased residence times arising from reduced precipitation. This interpretation is the same as that reached by Banner (1996), who suggested that where there is a climatic control on fluctuations between soil and host-rock contributions to groundwater Sr, during periods of high E/P (i.e. low recharge) cave waters (and so speleothems) will carry more of a bedrock  $^{87}\text{Sr}/^{86}\text{Sr}$  signature, due to long residence time (leading to increased water-rock interaction time) and predominantly conduit pathway flow.

More positive  $\delta^{13}\text{C}$  values also indicate a reduction in rainfall, as either a reduction in soil microbial activity or vegetation density, or a shift to a higher proportion of C4 plants, which thrive in drier conditions, would lead to an increase in  $\delta^{13}\text{C}$  (Dorale et al., 1992, Bar-Matthews et al., 1997, Baldini et al., 2005, Fairchild et al., 2007, Baker et al., 1997, Genty et al., 2003, Fleitmann et al., 2009). This shift occurs very rapidly, but this does not exclude vegetation change as a possible cause, as Fleitmann et al. (2009) inferred that large shifts in vegetation occurred in Northern Turkey in only a few decades to centuries during Holocene Greenland interstadials. The high  $\delta^{13}\text{C}$  in the DIM-1 aragonite layer also occurs at a time of high  $\delta^{18}\text{O}$ , which may indicate kinetic effects such as prolonged degassing or evaporation, which would contribute to the high  $\delta^{13}\text{C}$  values. This process was previously suggested by Frisia et al. (2002), although other caves which might be expected to show highly evaporative conditions do not always show coenrichment of  $\delta^{13}\text{C}$  and  $\delta^{18}\text{O}$  (Bar-Matthews et al., 1991, Hopley et al., 2009).

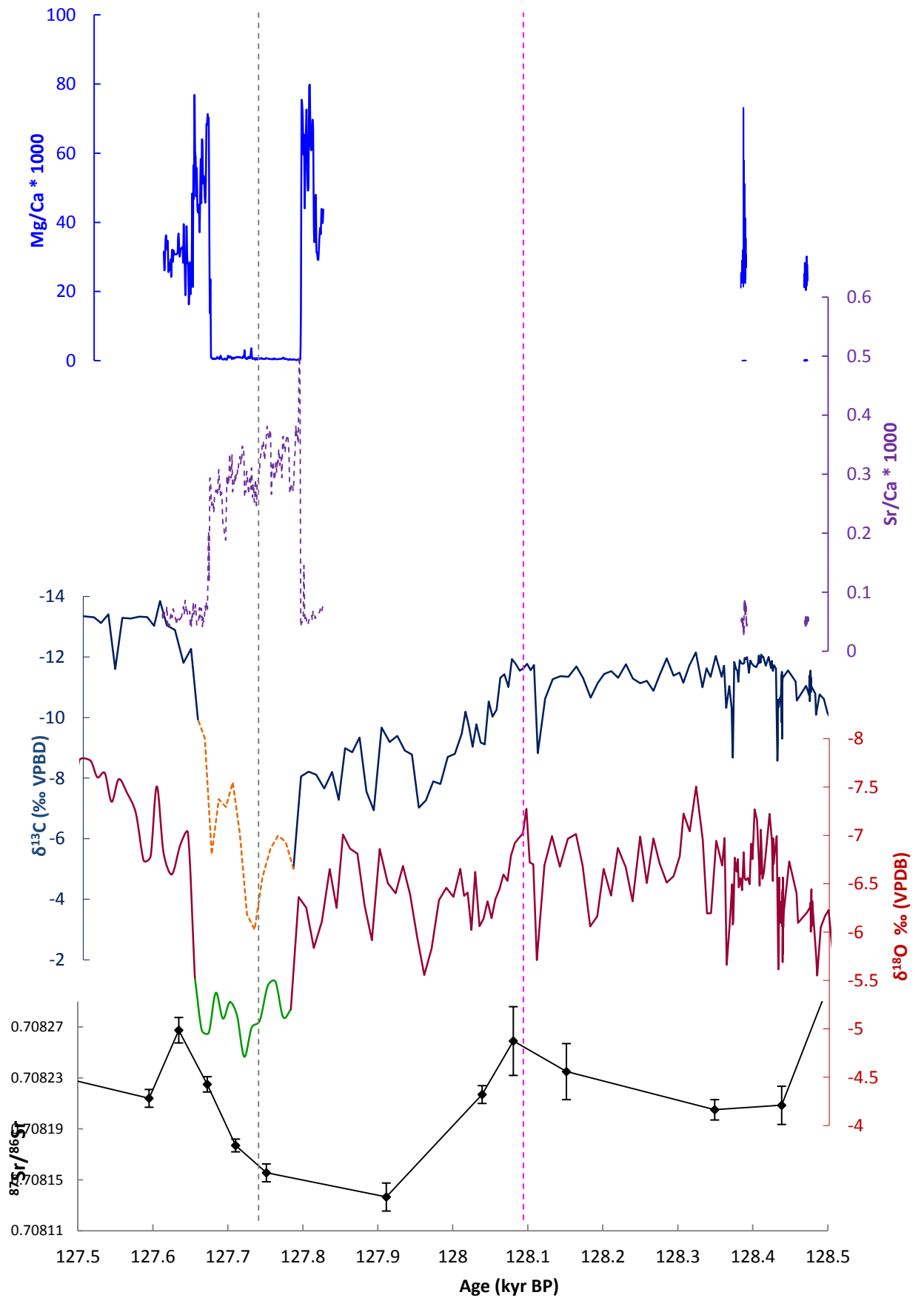


**Figure 4.55**  
*The expression of an arid phase in DIM-1 in multiple proxies: Mg/Ca (royal blue line), Sr/Ca (dashed purple line),  $\delta^{13}\text{C}$  (navy line, with aragonite region in orange),  $\delta^{18}\text{O}$  (red line, with aragonite in green),  $^{87}\text{Sr}/^{86}\text{Sr}$  (black line). Pink dashed vertical line indicates the beginning of aridity; gray dashed vertical line indicates the beginning of the return to wetter conditions.*

Previous studies have shown that speleothem growth rate decreases as a result of cold/arid intervals (Baker et al., 1993b, Asrat et al., 2007), due to reduction in biomass/bioproductivity above the cave (Baldini et al., 2005). Therefore the reduction in width of DIM-1 leading up to the aragonite region also supports aridity.

At the time this increased aridity trend began, the aragonite which was being precipitated was still subsequently being recrystallised as calcite. However, as aridity intensified, prior precipitation of aragonite would have increased upflow of DIM-1. Prior precipitation is enhanced during times of low water recharge, as water-rock contact times are increased (Fairchild et al., 2000, Fairchild and McMillan, 2007). Prior precipitation causes cations to be removed from the precipitating solution in the proportion they are incorporated into calcite (Holland et al., 1964). As distribution coefficients for trace elements are typically far less than 1, following prior precipitation Ca will be reduced to a much greater degree than trace elements such as Mg. Therefore, as aridity progresses, Mg concentration in the drip waters will have increased. Increased drip-water Mg concentration has previously been shown to arise as result of low water availability (e.g. Bar-Matthews et al., 1991, Frisia et al., 2002, Polyak and Asmerom, 2001, Railsback et al., 1994). Prior calcite precipitation can increase Mg/Ca to the point at which aragonite is the favoured polymorph (Frisia et al., 2002, Spötl et al., 2002b). This is important because it has been previously shown that wetted aragonite speleothems may not undergo recrystallisation to calcite, if aragonite-forming conditions persist, such as high fluid  $Mg^{2+}$  (Frisia et al., 2002).

Incorporation of  $Mg^{2+}$  into the calcite crystal lattice increases as solution  $Mg^{2+}$  increases (Davis et al., 2000). High levels of  $Mg^{2+}$  in the lattice then inhibit calcite nucleation.  $Mg^{2+}$  directly modifies calcite surface morphology, by altering the orientation of steps on the growth surface (Davis et al., 2004), leading to a reduction in the rate of step growth via an increase in solubility (Davis et al., 2000). The increase in solubility prevents the growth of calcite nuclei beyond subcritical size (Reddy and Wang, 1980).

While calcite growth is reduced, the presence of high Mg does not inhibit aragonite precipitation as Mg incorporation into aragonite is much lower than in calcite (Fyfe and Bischoff, 1965, Berner, 1975, Mucci and Morse, 1983, Davis et al., 2000). High  $Mg^{2+}$  content in fact promotes aragonite precipitation (Murray, 1954, Fyfe and Bischoff, 1965, Davis et al., 2000, Lippmann, 1973, Gutjahr et al., 1996), allowing aragonite precipitation to occur even if the water was at low saturation, or in fact undersaturated with aragonite (Frisia et al., 2002).

However, high Mg/Ca is insufficient to initiate aragonite nucleation on its own, although it is accepted as being the prime factor (Hill and Forti, 1997); other factors such as drip rate, growth rate, degassing, temperature, salinity, presence of  $\text{SO}_4^{2-}$ ,  $\text{HPO}_4^{2-}$ , organics, evaporation and ion transport mechanism, must be considered (Cabrol, 1978, Given and Wilkinson, 1985, Frisia et al., 2002, Zhong and Mucci, 1989). The existence of at least one other controlling factor is supported by the fact that studies seeking to pinpoint the dripwater Mg/Ca value at which aragonite will outcompete calcite have returned very different values. Solution Mg/Ca may only need be as high as 0.4 for aragonite to precipitate under certain conditions, such as 10°C, pH 7 (Filipov, 1990), while as a general rule, in order for aragonite to be precipitated, drip water Mg/Ca must be in excess of 1.0 (Folk, 1994, Morse et al., 1997, González and Lohmann, 1988). There is also disagreement about whether there is an upper limit; Frisia et al. (2002) found that in the Grotte de Clamouse, France, aragonite precipitated from fluids with Mg/Ca higher than 1.1, but lower than 2.06 as above this no aragonite was found to precipitate. This is contradicted by Fischbeck and Müller (1971), who found that aragonite was the main polymorph to form at Mg/Ca of 2.91, and at 4.36 it was the only polymorph.

Further aragonite precipitation will raise solution Mg/Ca further still, as  $\text{Mg}^{2+}$  is adsorbed up to 40 times less in aragonite than in calcite (Mucci and Morse, 1985) due to the different partitioning behaviour of aragonite (Morse and Mackenzie, 1990, Hill and Forti, 1997, Spötl et al., 2002b, McMillan et al., 2005), unless the aragonite structure is significantly relaxed, or nanodomains contain an Mg-rich phase (Finch and Allison, 2007). As a result, aragonite speleothems are found to contain little or no Mg (McMillan et al., 2005, Martín-García et al., 2009). Aragonite precipitation also lowers the saturation of the waters, until calcite growth is no longer possible, whereas high supersaturation could have allowed calcite precipitation at high levels of drip water Mg/Ca (Mg/Ca >1) by elevating growth rates beyond the influence of calcite nuclei inhibition by  $\text{Mg}^{2+}$  (Fernández-Díaz et al., 1996, De Choudens-Sánchez and González, 2009).

This indicates that the degree of solution supersaturation exerts a strong control over speleothem mineralogy by controlling mineral growth rates (De Choudens-Sánchez and González, 2009), and in fact a combination Mg/Ca ratio and supersaturation of dripwaters have been shown to essentially control mineralogy (Given and Wilkinson, 1985, Fernández-Díaz et al., 1996, De Choudens-Sánchez and González, 2009). Importance of saturation is

so strong that while calcite can compete with aragonite for reactants at low Mg/Ca and low supersaturation (De Choudens-Sánchez and González, 2009), aragonite may precipitate from waters with low/no Mg under conditions of very high supersaturation (González and Lohmann, 1988), or if sudden loss of CO<sub>2</sub> results in instantaneous aragonite supersaturation (Chafetz et al., 1991). Hydrochemical conditions within Vinschgau Valley, NW Italy led to differing saturation states at different sites, so that both calcite and aragonite could form synchronously within the same valley (Spötl et al., 2002b). Saturation was also found to affect the threshold at which Sr becomes an inhibitor to calcite growth (Wasylenki et al., 2005).

During the period of time that the surviving aragonite region was precipitated, dripwater Mg/Ca remained high due to the prolonged aridity, and so aragonite was able to continue precipitating and not undergo recrystallisation even though the speleothem may have become wetted. However, it does appear that soon after the beginning of the aragonite region's growth, precipitation began to increase. This is indicated by the fact that <sup>87</sup>Sr/<sup>86</sup>Sr began increasing away from bedrock values at approximately 127.75 kyr BP, indicating an increase in water-rock interaction due to increased residence times. Almost synchronously, δ<sup>13</sup>C began to return to more negative values, indicative of an increased density of vegetation and the soil layer, and a higher proportion of C3 vegetation. Sr/Ca began to reduce slightly at this time also. Despite these signals of reduced aridity, primary aragonite continued to persist. This is due to the fact that Mg/Ca levels in the dripwater were still high enough following the initial aridity, compounded by removal of Ca with only small amounts of Mg as aragonite precipitated, that calcite growth was not possible, even as Mg/Ca levels began to be lowered as a result of the increased precipitation flux. This suggests that there may be lags involved with the response of crystallography to precipitation variations due to threshold effects, as also found by McMillan et al. (2005) in the Grotte de Clamouse, S France. As a result, other, more direct proxies, should be used to interpret the exact timing of changes in rainfall amount.

By approximately 127.6 kyr BP, dripwater Mg/Ca had reduced enough to allow calcite precipitation, so recrystallisation of the aragonite resumed. The δ<sup>13</sup>C equilibrium separation factor between aragonite and calcite is 1.7 ± 0.4‰, and is independent of temperature between 10 and 40°C (Romanek et al., 1992). The decrease in δ<sup>13</sup>C at the change is greater than this, indicating that it is not only the differing mineralogy that caused the large difference. There may also be some change associated with the

recrystallisation process, but as values of the secondary calcite are likely to be somewhere between the values of the original mineral and the recrystallising fluid, the values should still be representative of conditions during the period of speleothem growth and recrystallisation.

Before the return to the cycle of recrystallisation took place, however, a growth hiatus occurred. Both  $\delta^{13}\text{C}$  and  $^{87}\text{Sr}/^{86}\text{Sr}$  show no record of a reversal in the trend to increased precipitation, but it is extremely likely that an arid event of some kind occurred to cause the hiatus. As the length of time in which the aragonite region was precipitated was ca. 120 years according to the age model, and the sample resolution of  $\delta^{13}\text{C}$  is only 1 sample per approximately 10 years (and far coarser resolution for  $^{87}\text{Sr}/^{86}\text{Sr}$ ), it is possible that the event was of such short duration it was not picked up in the proxies. High resolution analysis of the section of growth immediately preceding the hiatus could potentially shed some light on this, so would be an interesting direction for further work.

Above the hiatus, recrystallisation of the aragonite as calcite continued to the (broken) top of the stalagmite, with the exception of the surviving areas of aragonite in the outer regions of the stalagmite, as discussed above.

The existence of the arid phase in DIM-1 suggests climate instability in SW Turkey during early MIS 5e. The Last Interglacial is now known to have shown climatic variability, rather than stability (Seidenkrantz et al., 1995, Guiot et al., 1993, Field et al., 1994, McManus et al., 1999, Muller et al., 2005, McManus et al., 1994, An and Porter, 1997, Grootes et al., 1993). At least two oscillations of sea water cooling to ca. 2°C cooler than today occurred during MIS 5e (Knudsen et al., 2002). These events were associated with the repeated southward expansion of polar waters, implying repositioning of an oceanic front at the boundary between surface currents which originated in the subtropical Atlantic and Arctic (McManus et al., 1994). These episodes correlate with previously identified changes on the Greenland ice sheet (Dansgaard et al., 1993, Grootes et al., 1993). There is also evidence for SST fluctuations in the Nordic seas at ca. 127-126 ka, 122-121 ka and 117 ka BP (Fronval and Jansen, 1996). A combined isotopic and palynological record from Ioannina, Greece indicates a change to wetter conditions at 127.3 ka BP, warmer/drier conditions occurring at 126.8 and 125.7 ka BP, a change to cooler/wetter conditions at 123.6 and 120.3 ka BP and colder/drier conditions at 114.2ka BP (Tzedakis et al., 2003a).

Speleothem records from SW France and Italy also display suborbital climate variability during MIS5e (Couchoud et al., 2009, Drysdale et al., 2009). Millennial-scale fluctuations in  $\delta^{18}\text{O}$  were found to be closely matched but lagged by changes in  $\delta^{13}\text{C}$  in a speleothem record of MIS 5e from Bourgeois-Delaunay, La Chaise de Vouthon, SW France (Couchoud et al., 2009). The lags were interpreted as responding to the fact that a rainfall  $\delta^{18}\text{O}$  signal is transported to a speleothem far faster than soil and vegetation above a cave respond to climatic change and transmit a corresponding change in  $\delta^{13}\text{C}$  to the dripwater and subsequently the speleothem (Couchoud et al., 2009). Warm-wet conditions persisted at Antro del Corchia, Italy, during the period  $\sim 128.3 - 126.5$  kyr BP, with a dry episode  $\sim 126.5 - 125.2$  kyr BP. (Drysdale et al., 2005, Drysdale et al., 2009). A dry episode in the French record at  $\sim 128.2 - 127.9$  kyr BP appears to very closely match the arid phase recorded in DIM-1, which is interpreted as beginning at 128.1 kyr BP. However, the errors in the DIM-1 age model are large enough that matching the arid interval recorded by DIM-1 to any specific arid interval in the Bourgeois-Delaunay record is over optimistic; therefore it is more realistic to infer that DIM-1 responded to millennial scale variability during MIS 5e, as seen by other authors. Similarly, it is tempting to relate a reversal in the trend towards more negative values at Soreq Cave (Grant et al., 2012) at ca. 127 kyr BP to the arid interval in DIM-1, however again the age errors preclude such exact matches (especially as at this point of the Soreq chronology, the errors on the ages are of the order of 2kyr).

#### **4.3.6.2 DIM-3**

##### *4.3.6.2.1 Absence of the 8.2 kyr Event*

Low  $\delta^{18}\text{O}$  values are recorded during the period ca. 8.1 – 8.5 kyr BP in speleothems from Ernesto Cave (McDermott et al., 1999) and Savi Cave (Frisia et al., 2005) in Italy, and Soreq Cave (Bar-Matthews et al., 1999, 2000, 2003) in Israel. This time period corresponds to the 8.2 kyr Event and cooling caused by fluctuations in solar output (Street-Perrott and Perrott, 1990, Goodfriend, 1991, Rohling and Palike, 2005). However, not all records from the eastern Mediterranean show this event; for instance there is no clear evidence for it in a speleothem record from Jeita Cave, Lebanon (Verheyden et al., 2008) Although DIM-3 doesn't cover this interval, the fact that growth began approximately when this period ended may suggest that conditions were also too dry for speleothem precipitation at Dim Cave. This assumes that DIM-1 had already toppled, and was positioned underneath the drip that DIM-3 precipitated from, but this can't be proven. It is also possible that some

growth occurred during the early Holocene on DIM-1, but that this growth was lost when the stalagmite was broken.

#### 4.3.6.2.2 *The Growth of DIM-3*

The entirety of DIM-3 is primary aragonite, whereas DIM-1 precipitated as aragonite which was then subsequently reprecipitated as calcite in the majority of the speleothem. As detailed above, this recrystallisation is interpreted as indicating that the rainy season was sufficiently wet, as the presence of a fluid undersaturated with aragonite is necessary for recrystallisation of aragonite. Therefore we can infer that conditions in SW Turkey were drier during the early Holocene than the early last interglacial. This is supported by reduced growth rate in DIM-3 compared to DIM-1, and the fact that  $\delta^{18}\text{O}$  values in DIM-3 are more positive (-3.9 to -5 ‰) than the primary aragonite in DIM-1 (-4.7 to -5.5 ‰).

Although the early Holocene appears to have been drier than early MIS 5e, it also may have been wetter than the rest of the Holocene. As discussed above, it cannot be proven that DIM-1 fell in time for DIM-3 to record the earliest Holocene, and it also cannot be proven that tectonic activity did not cause DIM-1 to roll out of the path of the drip that precipitated DIM-3. However, for the purposes of this interpretation we will assume that DIM-3 was underneath its feeding drip for the entirety of the Holocene, and therefore that the period of growth of DIM-3 represents a pluvial period within a more arid Holocene. This time period correlates with a pluvial period documented across the eastern Mediterranean known as the Early Holocene Wet Period.

##### 4.3.6.2.2.1 *The Early Holocene Wet Period*

The early Holocene in the eastern Mediterranean and Levant region was a wet period, and appears to have been the wettest phase of the last 25,000 years in the region (Robinson et al., 2006; their Fig 15D and references therein). This period is sometimes referred to as the 'Holocene Optimum' (e.g. Peyron et al., 2011). A substantial increase in precipitation over the Mediterranean basin would likely have been associated with a reorganization of regional atmospheric circulation, (e.g. Zanchetta et al., 2007).

Speleothem records indicate that conditions were wet during the early Holocene in Israel at Jerusalem cave (Frumkin et al., 2000) and from 8.5 – 7 kyr BP at Soreq Cave (which experienced rainfall double that of today) (Bar-Matthews et al., 1997, 1999, 2000, 2003, Ayalon et al., 1999), from 9.2 - 6.5 kyr BP at Jeita Cave in Lebanon (Verheyden et al., 2008), from 8.9 – 7.3 kyr BP at Antro del Corchia, Italy (Zanchetta et al., 2007), from 8.2 – 7.1 kyr BP at Renella Cave in central Italy (Zhornyak et al., 2011), approximately 8.9 kyr BP in NW

Italy (Spötl et al., 2002b), and from ~8.5 – 7.5 kyr BP in Sicily (Frisia et al., 2006). In Oman, there is evidence for a pluvial period from 10.5 – 6 kyr BP from speleothems (Burns et al., 1998, Fleitmann et al., 2003b) and travertines and fracture calcites (Clark and Fontes, 1990). A pluvial period also occurred in the nearby Arabian Peninsula during the period ca. 9 – 6 kyr BP (McClure, 1976).

In addition to speleothem records, several other proxies indicate more pluvial conditions in the eastern Mediterranean and Middle East during the early Holocene, such as pollen records from SW Turkey (Vermoere et al., 1999), Syria and Israel (Rossignol-Strick, 1995), the Tenaghi Philippon in Greece and Lake Accesa in Italy (Peyron et al., 2011), Sicily (Sadori and Narcisi, 2001), the Zagros Mountains, Iran (Wright et al., 1967, Van Zeist and Bottema, 1977, Stevens et al., 2001) and the African tropics (Gasse, 2000); high lake stands in North Africa (Street and Grove, 1979, COHMAP Members, 1988, Magny et al., 2002), East Africa (Butzer et al., 1972), and SW Libya (Armitage et al., 2007); lacustrine records from Turkey (Van Zeist and Woldring, 1978, Lemcke and Sturm, 1997, Leng et al., 1999, Wick et al., 2003, Roberts et al., 2001) the Yammouneh basin, Lebanon (Develle et al., 2010), the Arabian Peninsula (McClure, 1976), the Balkan Peninsula (Leng et al., 2010), and Lake Lisan and the Dead Sea (Neev and Hall, 1979, Frumkin et al., 1991, Migowski et al., 2006); southward migration of the desert boundary in Israel (Goodfriend, 1991, Goodfriend, 1999); palaeostream deposits in the Wadi Faynan, Jordan (McLaren et al., 2004); and palaeosols on the Israeli coastal plain (Gvirtzman and Wieder, 2001).

This pluvial period did not necessarily prevail over the entire Mediterranean region, as (Jalut et al., 2009) explained; various regional climates were able to prevail during the period, such as an attenuated oceanic type in the Western and Central Mediterranean. For instance, in Morocco the early Holocene was a dry period (Cheddadi et al., 1998), and isotopic and pollen data from Lake Gölhisar, southwest Turkey (further west than Dim Cave), suggest that the period 8.9 – 6.8 kyr BP was an arid interval in the area (Eastwood et al., 2007). However, the authors also indicate that isotopic fluctuations during the period 8800-5100 cal. yr BP suggest oscillations between aridity and humidity. It is possible that DIM-3 also records fluctuations in aridity, as both the  $\delta^{18}\text{O}$  and  $^{87}\text{Sr}/^{86}\text{Sr}$  data oscillate.

The deposition of sapropel 1 (S1) in the Eastern Mediterranean basin also suggests increased regional runoff at this time (Kallel et al., 1997b, Melki et al., 2010). A sapropel is a thin, black, often laminated, discrete layer of organic-rich sediment devoid of benthic organisms, deposited at large scale (Eastern Mediterranean basin wide) in response to

enhanced rainfall and freshwater continental runoff (Bar-Matthews et al., 2000, Emeis et al., 2000). Sapropels were deposited at times when the eastern Mediterranean deep waters were anoxic, which is believed to have been induced by stratification of the water column driven by a low-salinity surface layer (Rossignol-Strick et al., 1982, Rossignol-Strick, 1985, Rohling and Hilgen, 1991, Rohling, 1994, Kallel et al., 1997b, Bosch et al., 1998, Passier et al., 1999). Sapropel intervals correlate closely with Northern Hemisphere insolation maxima, precession minima, and periods of decreasing ice volume, implying that deep water anoxia in the eastern Mediterranean Sea is linked to climate (Cita et al., 1977, Vergnaud-Grazzini et al., 1977, Rossignol-Strick, 1983, 1985, Hilgen, 1991, Lourens et al., 1996, Calvert and Fontugne, 2001).

The formation of S1 was the only time in the past 18 kyr BP that hydrological changes in the North Atlantic Ocean and Mediterranean Sea were not directly connected (Kallel et al., 1997b, Kallel et al., 1997a). Estimates for the length of S1 vary; analysis of ODP sites 969, 967 and 964 led Emeis et al. (2003) to suggest a duration of ca 9.5 – 7 Kyr, while a longer estimate of ca. 10.8 – 6.1 kyr BP was reached by De Lange et al. (2008) following analysis of a suite of cores covering the eastern Mediterranean basin. Bar-Matthews et al. (2000) suggest that eastern Mediterranean speleothem low  $\delta^{18}\text{O}$  events may bracket the maximum duration of sapropel events as they both reflect an increase in annual rainfall, and sapropel formation has a number of issues which affect interpretation of the length of the pluvial phase, such as diagenetic re-oxidation and mobilization processes (e.g. Wilson et al., 1985, Pruysers et al., 1991), and the fact that formation lags precipitation increase due to a critical threshold of flooding while speleothem  $\delta^{18}\text{O}$  has a much more immediate response (Bar-Matthews et al., 2000).

A brief return to deep-water ventilation is inferred from an interruption in S1 deposition, observed at many eastern and central Mediterranean marine sites (Rohling et al., 1997, De Rijk et al., 1999, Ariztegui et al., 2000, Myers and Rohling, 2000, Giunta et al., 2003). The reversal is believed to have lasted from ca. 500 – 150 years during the period ca. 8.0-7.5 kyr BP (Ariztegui et al., 2000), and may have been caused by a brief cooling event that allowed some deep and intermediate water circulation to resume (Myers and Rohling, 2000). Evidence for a short dry event on land at ca. 8 kyr BP has also been reported from Soreq Cave (Bar-Matthews et al., 1997, 1999), the Negev desert (Goodfriend, 1988, Goodfriend, 1991) and tropical locations in Africa and Arabia (Street-Perrott and Perrott, 1990). The fact that DIM-3 only begins deposition at approximately this time makes it very hard to

identify the imprint of a dry event in the DIM-3 record, however it is possible that the timing of initiation of growth is a reflection of the end of a dry period, as conditions only became suitable for speleothem growth after such an event. It is not clear whether growth did not occur before the arid event because conditions were not wet enough at Dim Cave to allow speleothem growth, or whether DIM-1 may have fallen over at this time.

#### *4.3.6.2.2.1.1 Causes of the Pluvial Period*

Wet conditions in the eastern Mediterranean may have been related to the enhanced African monsoon during a period of high insolation, or by a greater frequency of storms tracks into the area (Stevens et al., 2001), or due to the fact that the ITCZ shifted to the north by approximately 500 km at this time (McClure, 1976, Sirocko et al., 1993, Fontes et al., 1993) allowing the south-west monsoon to bring rainfall to the area.

S1 lasted longer than the period of increased precipitation in other records, and it has been suggested that in the Levantine basin, increased Nile discharge contributed to the increase in freshwater in the early and middle part of sapropels formation, as flow was believed to have been high during the period 9 – 5.6 kyr BP (Butzer et al., 1972), but it has recently been shown that discharge declined after ca. 8 kyr BP (Scrivner et al., 2004, Revel et al., 2010). (Zhornyak et al., 2011) tentatively suggest that increased Mediterranean precipitation over the entire basin may have sustained sapropel formation after 8 kyr BP, but admit that they are unable to test this theory with their data.

Evidence for movements in the ITCZ affecting rainfall in the eastern Mediterranean at this time includes the fact that north of the equator, tropical regions experienced increased precipitation during the early Holocene (Fleitmann et al., 2003a, 2007, Haug et al., 2001, Stott et al., 2004), while close to the equator, precipitation was increased during the mid Holocene (Partin et al., 2007), and south of the equator this pluvial period occurred in the late Holocene (Mayle et al., 2000, Baker et al., 2001, Wang et al., 2006).

This trend is likely due to a southward migration of the ITCZ during the Holocene in response to changes in the seasonality of the precession cycle (Haug et al., 2001, Stott et al., 2004, Wang et al., 2004, Partin et al., 2007). Seasonality of precession is dependent on which hemisphere is at perihelion/aphelion during summer/winter when the earth has an elliptical orbit (Williams et al., 1998). For instance, at present, southern hemisphere summer occurs at perihelion and northern hemisphere summer occurs at aphelion. This means that southern hemisphere summers receive stronger solar heating as the Earth is closer to the sun than at northern hemisphere summer, and that southern hemisphere

summers are shorter due to the higher speed revolution of the Earth around its orbit near perihelion(Williams et al., 1998).

Seasonality affects the position of the ITCZ because when Southern Hemisphere insolation becomes more seasonal the ITCZ will be more likely to be pulled to the Southern Hemisphere, and when Northern Hemisphere insolation becomes more seasonal, the ITCZ will be more likely to be pulled to the Northern Hemisphere with a more northerly position leading to more precipitation north of the equator, and vice versa (Berger and Loutre, 1991, Liu et al., 2000, Haug et al., 2001).

Pollen records from the Tenaghi Philippon in Greece and Lake Accesa in Italy indicate a 'Holocene Optimum' from 9.5 – 7.8 kyr BP, with pronounced seasonality causing mild, wet winters and warm, dry summers (possibly drier than today) (Peyron et al., 2011). Evidence for warm, dry summers include the fact that the summer drought in Iran was lengthened (Stevens et al., 2001). Increased winter precipitation was also recorded by speleothems at Carburangeli Cave in Sicily (Frisia et al., 2006) and a marine pollen record in the Aegean Sea (Kotthoff et al., 2008). Increased seasonality explains why some proxies from the region seem to suggest reduced rainfall, e.g. the lake level record for Lake Accesa, Italy (Magny et al., 2007) which was based on carbonate concretions which form during the summer. There appears to have also been increased seasonality during the early Holocene in Iran and eastern Anatolia, due to reduced or absent spring precipitation and wet winters (Stevens et al., 2001, Wick et al., 2003, Djamali et al., 2010).

#### 4.3.6.2.3 *Cessation of Growth*

The end of DIM-3's growth is approximately 7 kyr BP, suggesting that conditions may have become more arid at this time. This is supported by a slight decrease in speleothem width at the very top of DIM-3, an increase in  $\delta^{13}\text{C}$  values in of  $\sim 4\text{‰}$  at approximately 7.3 kyr BP, with the trend culminating in the cessation of growth and the precipitation of a non-pure overgrowth. However, it is also possible that DIM-1 may have moved in its position on the cave floor as it was no longer fixed in place, especially as Turkey is a tectonically active region. In this scenario, the drip that precipitated DIM-3 may have continued to feed speleothem growth, just not on to DIM-3.

$\delta^{18}\text{O}$  values do not show a corresponding increase; however a plateau occurs for approximately the last 0.2 kyr of growth, compared to the rest of the record which shows variation towards more negative values of up to  $1\text{‰}$ . This may therefore be the expression of the aridification in the  $\delta^{18}\text{O}$  record.

Strontium isotopes also do not show the trend which may be expected (values moving towards the bedrock values due to increased water-rock interaction time as residence times are increased). However, it is possible that there was an increase in the contribution of Sr from aeolian dust at this time, as aeolian dust has been shown to be a considerable source of Sr to speleothems in arid and semi-arid regions (Goede et al., 1998). If increased aridity led to an increase in aeolian dust in the soil above Dim Cave, this could greatly affect the  $^{87}\text{Sr}/^{86}\text{Sr}$  of DIM-3, as aeolian dust typically has  $^{87}\text{Sr}/^{86}\text{Sr}$  of ca. 0.7200 (Capo et al., 1998). As this value is so much higher than the other components of the system affecting Dim Cave, only a small increase in the amount of dust in the soil above Dim Cave would be necessary to cause a large change in speleothem values. Increased dust mobilization may indicate arid conditions in the source region (i.e. the Saharan region) (Moulin et al., 1997, Frumkin and Stein, 2004). This is corroborated by the fact that the end of the period of growth of DIM-3, which coincides with the end of the pluvial period in the Mediterranean, was also found to coincide with increased aridity in North Africa and the Middle East due to the intensification of the African Monsoon (deMenocal et al., 2000). Thus it appears that when conditions are moderately wet, such as during the period of growth of DIM-1, Sr from the bedrock is able to compensate for the much higher  $^{87}\text{Sr}/^{86}\text{Sr}$  value of aeolian dust in the soil, while when dust levels increase as conditions become more arid, aeolian dust dominates the  $^{87}\text{Sr}/^{86}\text{Sr}$  signal in the dripwater that feeds Dim Cave. This necessitates a multi-proxy approach to interpreting  $^{87}\text{Sr}/^{86}\text{Sr}$  in Dim Cave.

The indication of an increase in aridity at Dim Cave at ca. 7.3 kyr BP suggested by DIM-3 supports evidence from other records in the eastern Mediterranean that conditions became more arid at this time. For example, from 7.5 – 6.5 kyr BP at Carburangeli Cave, Sicily, the prevalence of wet winters began to decrease, with multi-decadal long dry spells punctuating the wet periods (Frisia et al., 2006). This suggests that the mid-Holocene was a drier and unstable period. Several other records also support this conclusion. After 7.0 kyr BP, the isotopic signatures of a Soreq Cave speleothem return to similar to the present day, suggesting that Eastern Mediterranean climate became similar to present at this time, while many short, small isotopic excursions suggest that the Holocene climate was unstable (Bar-Matthews et al., 1999). A speleothem record from Jeita Cave, Lebanon also suggests that mid-Holocene climate was drier than the early Holocene and not stable, with the transition occurring at ca. 6.5 kyr BP at this location (Verheyden et al., 2008), approximately the time when natural vegetation patterns were established in south-western Turkey, indicating that the modern climate type had been reached (Van Zeist et al., 1975).

#### 4.3.6.2.4 *Archaeological Evidence and the Mesolithic to Neolithic Transition*

When considering ancient civilisations, disentangling the effect of climate from the effects of cultural and political change on a population's survival can be very difficult (Glueck, 1960, Raikes, 1967, Weiss and Bradley, 2001, Weninger et al., 2009). Despite this, speleothem records have been successfully used to help understand cultural change (e.g. Drysdale et al., 2006, Frisia et al., 2006, Webster et al., 2007, Bar-Matthews and Ayalon, 2011, Railsback et al., 2011, Drake, 2012), so it is important to ascertain whether DIM-3 can provide similar insights.

In central Anatolia, the large and well-established settlement at Catalhöyük-East was deserted abruptly during the 8.2 kyr event (Gokturk et al., 2002), which was likely due to irregularities in the water supply, as the success of agriculture in the area would have relied on the freshwater supply (Weninger et al., 2006). Following the 8.2 kyr event, a new settlement was established ca. 200m away across the River Carşamba (Catalhöyük-West) (Gokturk et al., 2002), marking the beginning of the Early Chalcolithic (*sensu strictu*) in Central Anatolia (Weninger et al., 2006). Several studies (e.g. Bar-Yosef Mayer et al., 2012) have sought to discover whether the cause of the abandonment of the settlement was related to climate.

The 8.2 kyr event seems to have had a hand in either the demise or creation of many settlements in the Eastern Mediterranean, with no sites showing clear stratigraphic evidence for continuous settlement during the event (Weninger et al., 2006). This points to the suggestion that settlements may have been abandoned during the event due to water shortage, by necessity due to crop failing and the threat of starvation, and new settlements were built when regions with more plentiful freshwater supplies were found, mostly through expansion of settlements into south-east Europe (Weninger et al., 2006, Berger and Guilaine, 2009). The moist period identified in DIM-3 suggests that on the SW Mediterranean coast of Turkey, wet conditions returned shortly after the 8.2 kyr event, allowing displaced civilisations to resettle on land which would be ideal for agriculture.

However, not all areas of the eastern Mediterranean may have shared in this period of increased precipitation. The Sofular cave record from northern Turkey doesn't appear to have an event corresponding to the growth of DIM-3, which may be because the dominant moisture source for this cave is the Black Sea (Fleitmann et al., 2009), while the moisture which supplied the increased precipitation to other parts of the eastern Mediterranean came from an Atlantic or Mediterranean source. The Dead Sea experienced a period of

prolonged low-level between 8.6 and 5.6 cal kyr BP due to a prolonged arid spell (Migowski et al., 2006). The island of Cyprus appears to have deserted for >1 kyr following the 8.2 kyr event (Weninger et al., 2006), but it is not clear if this was because precipitation remained too low to support farming during that period, or because the position of Cyprus as an island made it more difficult for displaced peoples to reach it, choosing instead to remain on the European landmass.

The Mesolithic to Neolithic transition appears to have occurred when conditions were becoming more dry in the Mediterranean region, at the transition from early Holocene pluvial phase to present-day climate mode, due to the fact that agricultural methods were more success for food accumulation (Frisia et al., 2006). Neolithisation is believed to have originated in the Fertile Crescent (Flannery, 1973), with the expansion into coastal Anatolia occurring by the 63<sup>rd</sup> century cal BC in a model created by Lemmen et al. (2011). From Anatolia, it appears that populations spread into south-east and central Europe, taking their Neolithic culture with them, as indicated by similarities in craniometric variables of ancient populations (Pinhasi and Pluciennik, 2004). The end of growth of DIM-3 at ca. 7 kyr BP is interpreted as resulting from increasingly arid conditions at Dim Cave which prevailed over much of the eastern Mediterranean. These arid conditions may have been the driver for ancient civilisations to adopt permanent settlements and farming as a means to gather food.

#### **4.3.6.3 DIM-2**

As DIM-2 is clearly a recrystallised speleothem, and appears to have recrystallised in a more pervasive way than DIM-1, it is unlikely to yield any usable palaeoclimatic information. However, useful information may be gleaned from the variation in chemical proxies between the primary aragonite and secondary calcite regions. As discussed above, DIM-1 is expected to have retained much of its geochemical character when recrystallised, due to the fact that recrystallisation occurred soon after precipitation, whereas DIM-2 appears to have recrystallised in a more pervasive manner, perhaps with large sections of aragonite being recrystallised at one time (e.g. the central recrystallised calcite zone), which may have been possible if the aragonite was very porous. As the surviving aragonite is of a very soft, porous nature, and the aragonite which was recrystallised is expected to be at least as if not more open to infiltration, this seems a likely pathway for recrystallisation. In comparison, the surviving aragonite of DIM-1 and DIM-3 is, while softer than the calcite in DIM-1, is harder and more compact than the primary aragonite of DIM-2.

The trace elemental composition of calcite and aragonite in DIM-2 is similar to that of DIM-1, in that both polymorphs exhibit the expected tendency to accept ions of a certain size; Mg substitutes for Ca in calcite but much less so in aragonite, and Sr substitutes for Ca in aragonite but less so in calcite. Therefore, the secondary mineral appears to be recording the geochemical signature of the reprecipitating fluids and not the primary mineral. Mg and Sr levels of secondary calcites have been found to be similar to primary calcites (Martín-García et al., 2009). Conversely, secondary calcites have also been found to have trace element compositions intermediate between primary aragonite and calcite, indicating a variation in the openness of the system, or a calcite-aragonite mixing trend, or both (Hopley et al., 2009). At this time no primary calcite from Dim Cave has been found, so it is not possible to compare the compositions of primary and secondary calcite. Therefore the compositions of secondary calcite in DIM-2 may contain a geochemical signature intermediate between primary calcite and aragonite.

# *Chapter 5*

*A Record of arid events  
during MIS 9-7 from Torang  
Cave, Southern Iran*

## 5.1 Torang Cave

Torang Cave (Figure 5.1) was visited previously by Dr Sa'ad Al-Omari and Dr Peter Rowe on 29/05/2005, at which stalagmite TG-6 and 5 other stalagmites not analysed here were collected. Torang Cave is located 70 km SE of Baft in Iran, at coordinates N 28° 45' 18.7"; E 56° 48' 43.4". As the cave was not visited during the current project, no cave monitoring or drip water data is presented here. Torang Cave is at an elevation of 1987 m.a.s.l., 25 m from the valley floor, and the overburden is 30 m thick. The cave is believed to be a fissure cave, most likely formed in a fault, and is approximately 50 m long and 20 m deep.

An online account published in a mountaineering magazine attests that Torang Cave is currently very wet, so much so that the author suggested the cave water could be trapped and used to alleviate the pressure put on water supplies by drought in the area (Salahi, 2005).

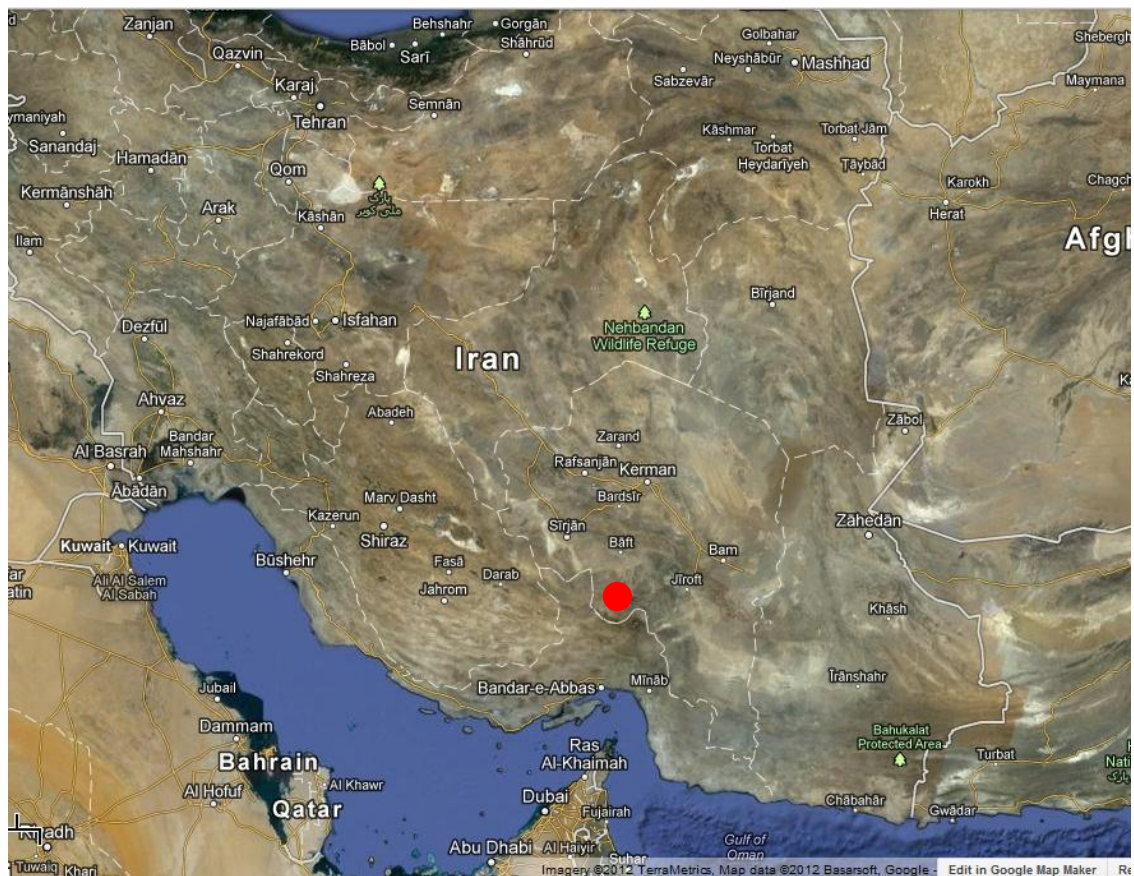


**Figure 5.1** Location of Torang Cave (red circle)

## 5.2 Isotopic Composition of Precipitation and Groundwater near Torang Cave

### 5.2.1 IAEA Weather Station Data

The closest IAEA station to Torang Cave with a large dataset is at Tehran (Figure 5.2, pink triangle). It is one of only 2 IAEA stations in Iran, both of which are located close to Tehran. Geographical data comparing the location of Torang Cave with the Tehran IAEA station is shown in Table 5.1.



**Figure 5.2**  
**Map of Iran showing location of Torang Cave (red circle) and Tehran IAEA station (pink triangle)**

Location	Latitude / Longitude (degrees)	Elevation (m.a.s.l)
Torang Cave	28.45N	1987
	56.48E	
Tehran IAEA Station	35.68N	1200
	51.32E	

**Table 5.1 Geographic data for Torang Cave and Tehran IAEA Station**

The monthly averages of several climate variables recorded at Tehran IAEA station are shown in Figure 5.3. Figure 5.3A shows average monthly air temperature and precipitation amount, and indicates that the region experiences a high seasonal contrast, with hot summers and cold winters, in which temperatures reach as low as 2.8°C on average. Rainfall is very low annually, with the heaviest rainfall occurring in the winter and spring. For comparison, the heaviest month by precipitation at Antalya IAEA station is December, in which average volumes are in excess of 250 mm, while at Tehran, the largest volume falls in January and is only ca. 35 mm on average. The summer season is very dry at Tehran, with the months June-September each receiving less than 10 mm on average. Figure 5.3 B and C compare monthly average weighted  $\delta^{18}\text{O}$  of precipitation with air temperature and precipitation amount and indicate that  $\delta^{18}\text{O}$  is in general positively correlated with air temperature and negatively correlated with precipitation amount (note that  $\delta^{18}\text{O}$  values on y-axis are in reverse order). The weighted means of  $\delta\text{D}$  and  $\delta^{18}\text{O}$  of precipitation are shown in Figure 5.3D; both isotopes follow similar patterns throughout the year, with an overall trend towards less negative values from Jan-June, and towards more negative values from Oct-Dec. The months of July and August are contrary to the trend, as they are more negative than the values for September. The intervening months show some variability, most likely due to the low number of samples due to years in which precipitation could not be collected, and the effects of intense rainfall events.

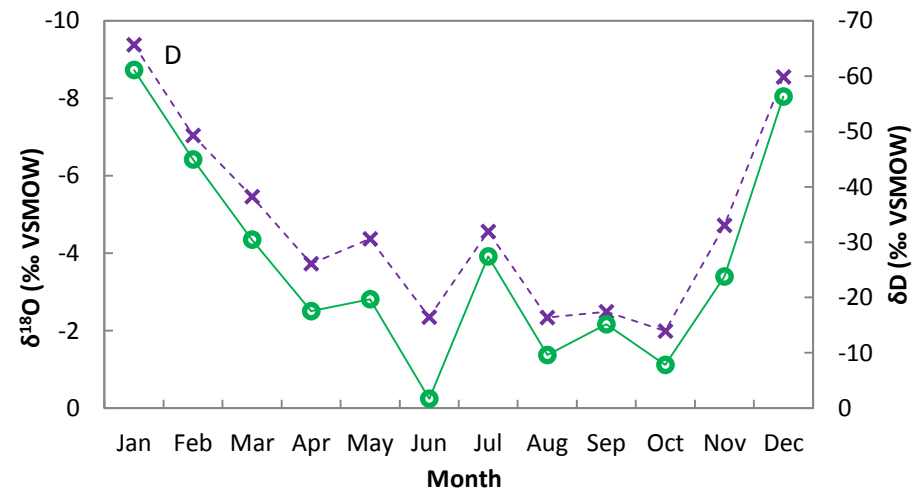
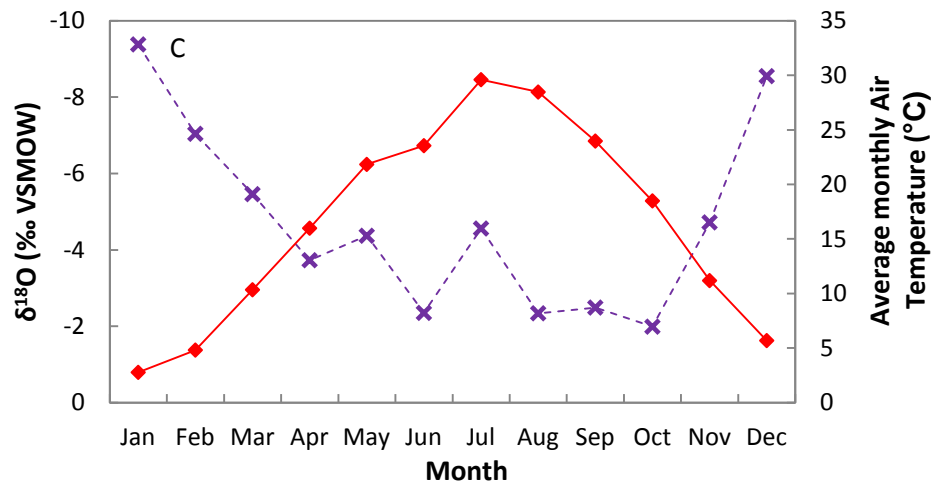
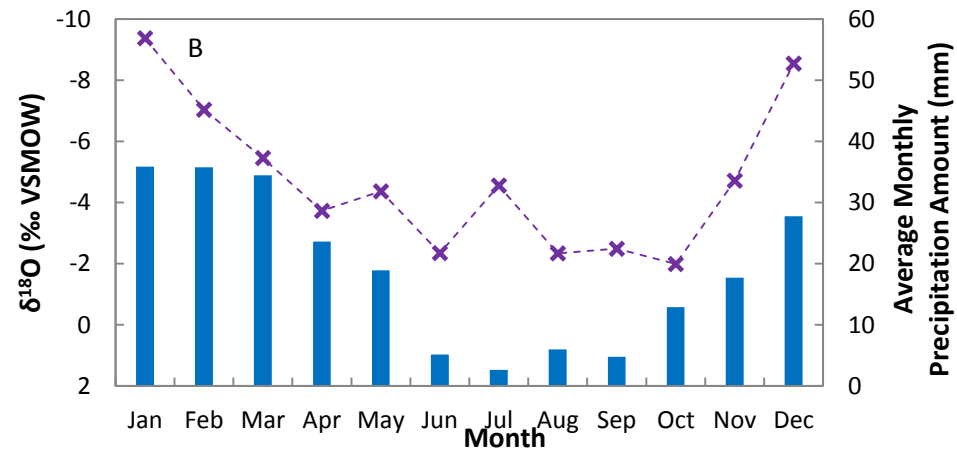
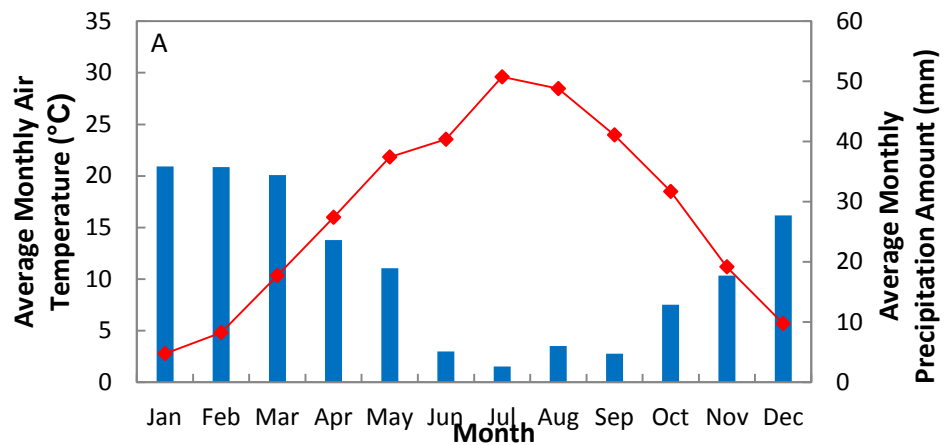
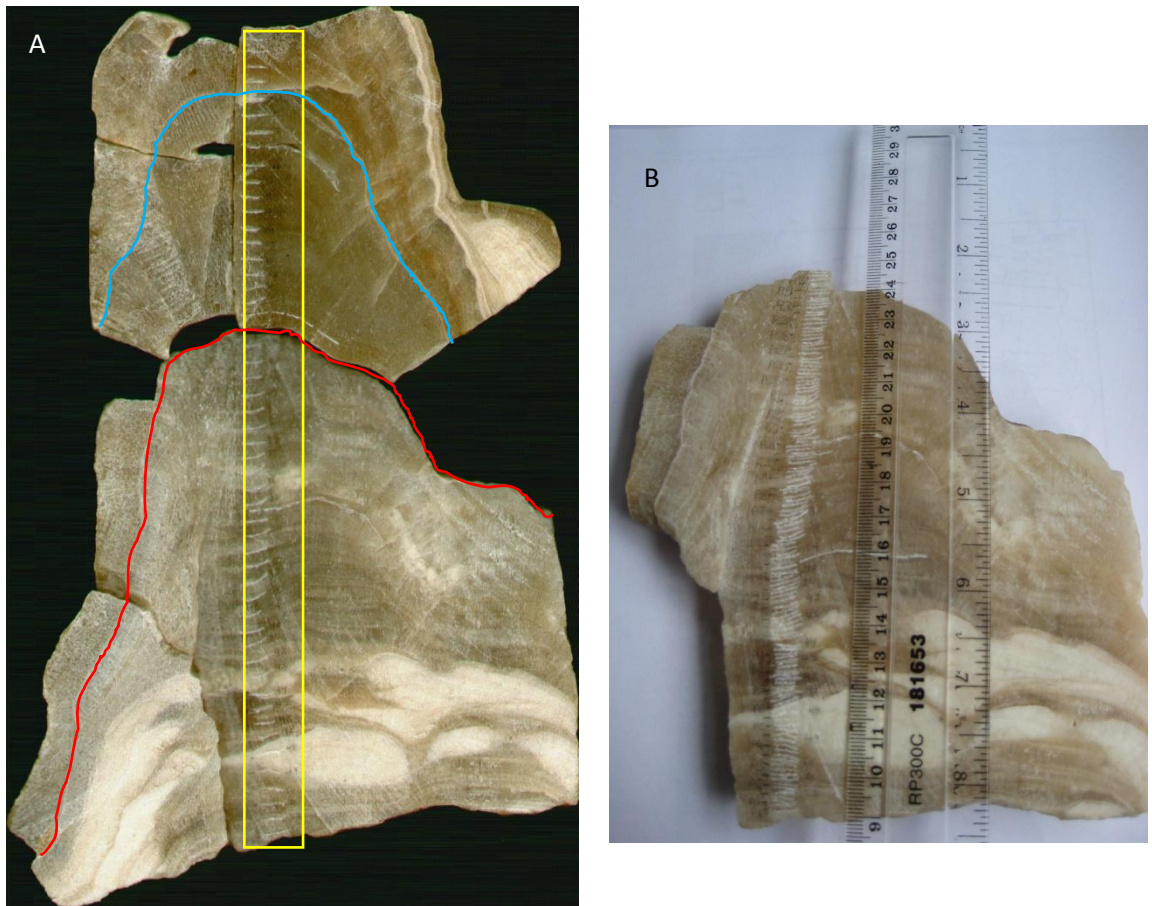


Figure 5.3 Average monthly precipitation amount (blue bars), air temperature (red diamonds and solid line), weighted  $\delta^{18}\text{O}$  of precipitation (purple crosses and dashed line) and weighted  $\delta\text{D}$  of precipitation (green open circles and solid line) at Teheran (IAEA and WMO, 2006), for the period 1960-1987. A) Precipitation amount and air temperature. B) Precipitation amount and  $\delta^{18}\text{O}$  of precipitation. C) Air temperature and  $\delta^{18}\text{O}$  of precipitation. D)  $\delta^{18}\text{O}$  of precipitation and  $\delta\text{D}$  of precipitation

### 5.3 Stalagmite TG-6

Stalagmite TG-6 (Figure 5.4) was collected 30 m from the cave entrance, and was clearly not actively growing at the time of collection. At the start of this project, the stalagmite had been cut into slabs previously, and the central slab had broken into several pieces. The stalagmite is not of the tall, conical shape seen in DIM-1 and DIM-2; it has a more squat morphology, although the fact that parts of the slab may be missing makes it harder to judge exactly what shape TG-6 was when it was precipitating in the cave. Two depositional hiatuses were visible, as shown in Figure 5.4, in fact the slab had broken along the weak point of the lower hiatus. The majority of TG-6 is a matt, brownish-yellow colour, but towards the bottom of the stalagmite, cream “cloud” shapes are interspersed across the width of the speleothem.



**Figure 5.4** Stalagmite TG-6.

**A)** TG-6 slab, as it existed at the time of the start of this project. Red line indicates position of a depositional hiatus along which the slab had broken after sawing. Blue line indicates a second depositional hiatus. Yellow box indicates low resolution stable isotope sampling along growth axis carried out by Sa'ad Al-Omari prior to this project.

**B)** Close up of large lower slab, to show resolution of stable isotope sampling with Sa'ad Al-

### 5.3.1 Uranium Series Dating

#### 5.3.1.1 Sampling Strategy

The majority of dating of TG-6 had been carried out prior to its use for this research, by Dr Sa'ad Al-Omari (Figure 5.5). This dating chronology contained an inversion, most likely associated with material sampled too close to a very clear depositional hiatus, at which detrital material had accumulated before growth resumed. Therefore 2 dates (yellow ovals in Figure 5.5) were resubmitted for analysis as part of this research; the suspected contaminated date below the lower hiatus and the date immediately above this hiatus, in case it has also been contaminated due to its proximity to the hiatus.

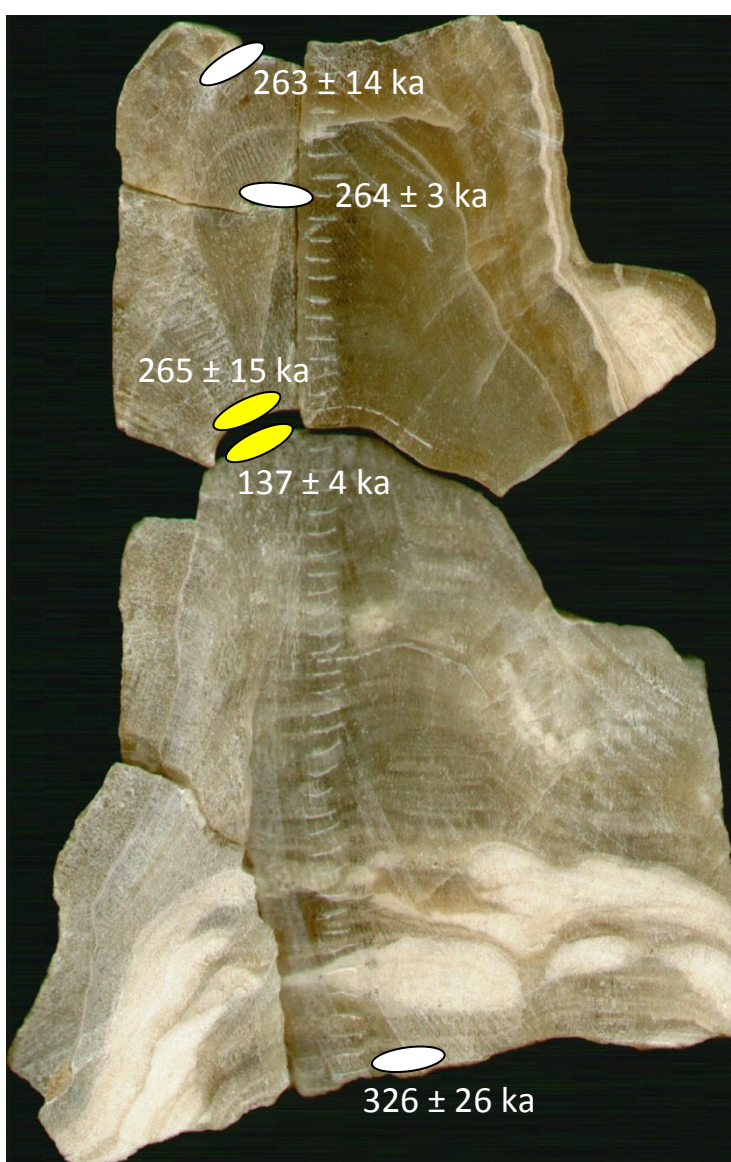


**Figure 5.5** Location of U/Th dates previously performed on TG-6 (ovals). Yellow ovals indicate the two dates that were selected to be reanalysed due to suspected contamination from the hiatus.

### 5.3.1.2 Results

Unfortunately, due to laboratory issues, the two resampled dates have not yet been returned. Therefore, in order to create an age model, the sample below the hiatus was excluded as it was not in stratigraphic order, but the sample from above the lower hiatus was used as it fits within the order of the other dates (Table 5.2).

Sample ID	$^{238}\text{U}$ (ppm)	$^{232}\text{Th}$ (ppb)	$[^{234}\text{U}/^{238}\text{U}]$	$[^{230}\text{Th}/^{234}\text{U}]$	$[^{230}\text{Th}/^{232}\text{Th}]$	Age (kyr)
NI7	0.617	0.292	$1.349 \pm 0.008$	$0.978 \pm 0.008$	8501	<b><math>263.391 \pm 14.182</math></b>
NI8	0.803	0.407	$1.406 \pm 0.098$	$0.987 \pm 0.123$	8348	<b><math>263.971 \pm 2.876</math></b>
NI9	1.244	1.122	$1.341 \pm 0.004$	$0.980 \pm 0.008$	4447	<b><math>265.816 \pm 14.606</math></b>
NI11	0.321	35.045	$1.351 \pm 0.004$	$1.031 \pm 0.009$	39	<b><math>326.128 \pm 26.062</math></b>

**Table 5.2** *U/Th Age Data for stalagmite TG-6.  $[^{234}\text{U}/^{238}\text{U}]$ ,  $[^{230}\text{Th}/^{238}\text{U}]$  and  $[^{230}\text{Th}/^{232}\text{U}]$  are activity ratios. Ages are corrected for detrital interference.*

An additional age was supplied by Dr Sa'ad Al-Omari, who carried out the original research on TG-6. This age is for the top of the stalagmite (coeval with sample NI7 in Table 5.2) and is  $223 \pm 4$  kyr BP. Unfortunately, no further geochemical information was supplied, however as the error far smaller than that for sample NI7, and the age is in stratigraphic order, this age was substituted for sample NI7 in the age model.

### 5.3.1.3 Age Model and Growth Rates

An age model was constructed for TG-6 (Figure 5.6) using the StalAge algorithm (Scholz and Hoffmann, 2011).

The age model (green line, Figure 5.6) suggests a nearly constant growth rate. This is very unlikely, as there two clear depositional hiatuses in TG-6. Without the date below the lower hiatus, it is impossible to determine how long the stalagmite did not precipitate at the time of the hiatus, and therefore impossible to accurately predict the growth rates of TG-6. Also, the age model produced does not place a high importance on the top age, so that the date for the cessation of growth is much older than 223 kyr BP. Other methods of constructing the age model will be looked into in section 5.3.6.

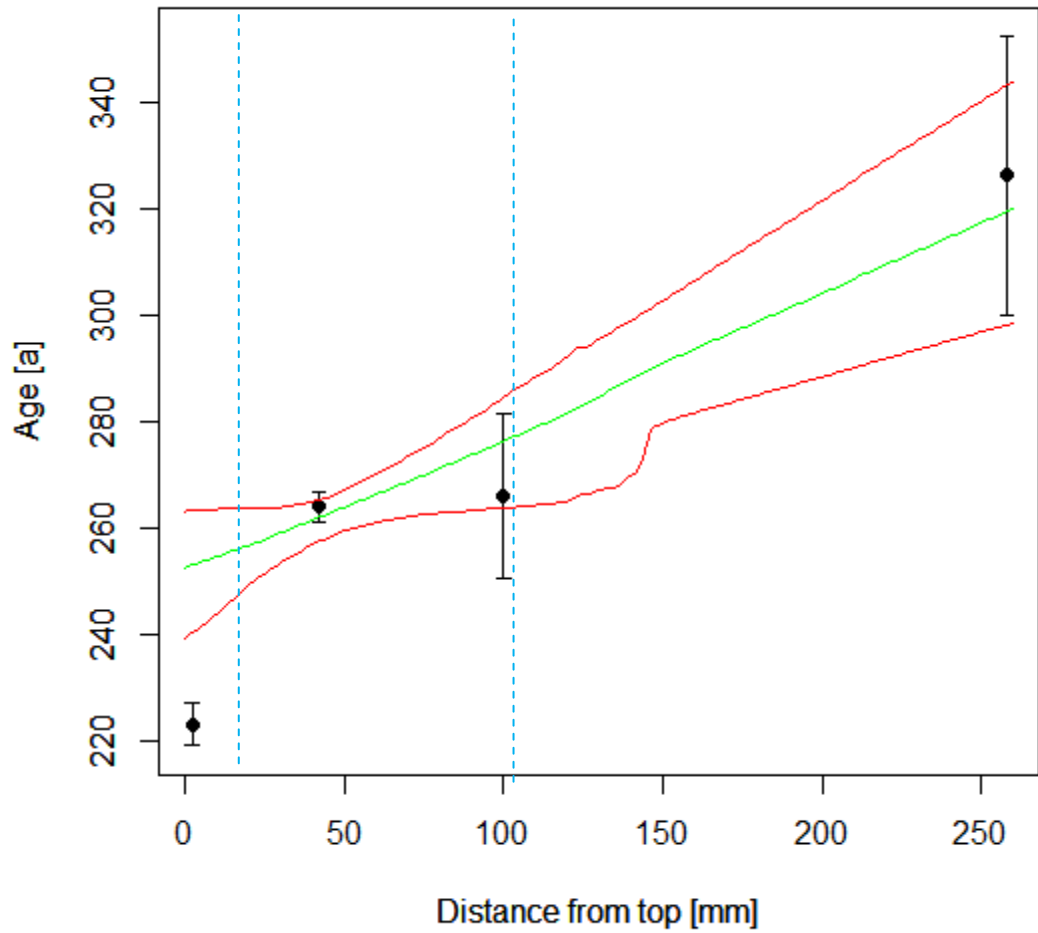


Figure 5.6 Age Model for TG-6. Green line indicates age model, red lines indicates error envelope. Blue dotted lines indicate positions of the hiatuses.

## 5.1.1 Physical Characteristics

### 5.1.1.1 Stalagmite Shape

It is hard to determine the exact shape of TG-6, as it had been sawn and broken into so many pieces; however it appears that it was not of a constant diameter, and so therefore may have been fed by a drip of variable discharge.

### **5.1.1.2 Crystallography**

The white curved forms within the fabric of TG-6 are a striking feature. To investigate the reason for this change in colouring, the transition at the edge of one of these shapes was analysed under the microscope in thin section (Figure 5.7). The mineralogy of the fabric which makes up the bulk of TG-6, the brownish coloured fabric (Figure 5.7A), appears to be calcite. The crystals that make up this calcite are equant, which may be indicative of recrystallisation. The fabric of the white shapes (Figure 5.7B) appears to be aragonite. The shapes of the aragonite regions are so undulous, and their spacing within the rest of speleothem so complex and unlike the “superposition” mode of speleothem growth in which layers build up vertically, that it seems unlikely that these changes in mineralogy are primary. Therefore, it is likely that TG-6 was originally aragonitic and has since recrystallised to calcite in the majority of the speleothem.

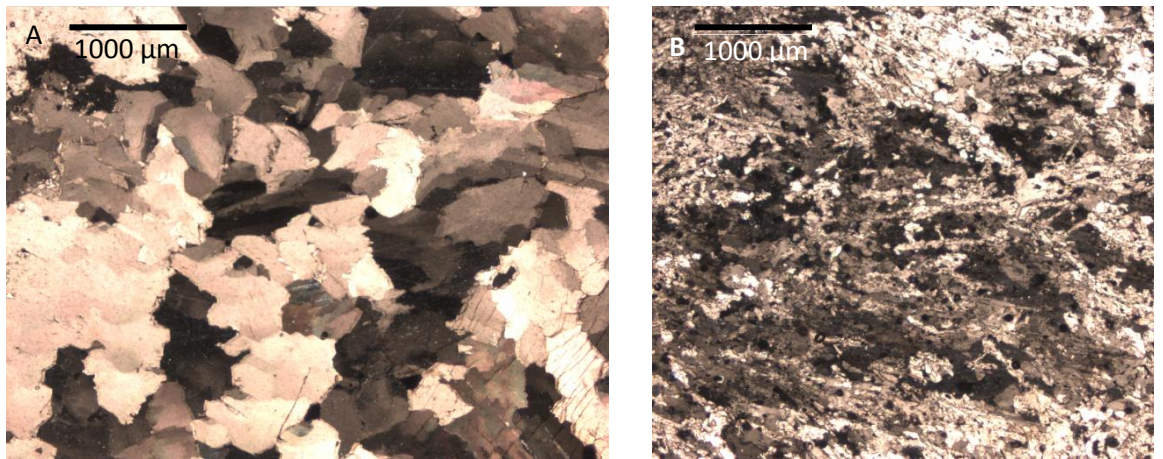


**Figure 5.7**      **Microscope images of TG-6**  
**A) The matte, brownish fabric which makes up the majority of the speleothem**  
**B) One of the white, cloud-like forms**

## 5.1.2 Stable Isotope Measurements

### 5.1.2.1 Sampling Strategy

Sampling for stable isotope measurements had already been carried out at coarse resolution by Dr Sa'ad Al-Omari (Figure 5.8A). Sampling was continued to increase the resolution to approximately 1 mm (Figure 5.8B)

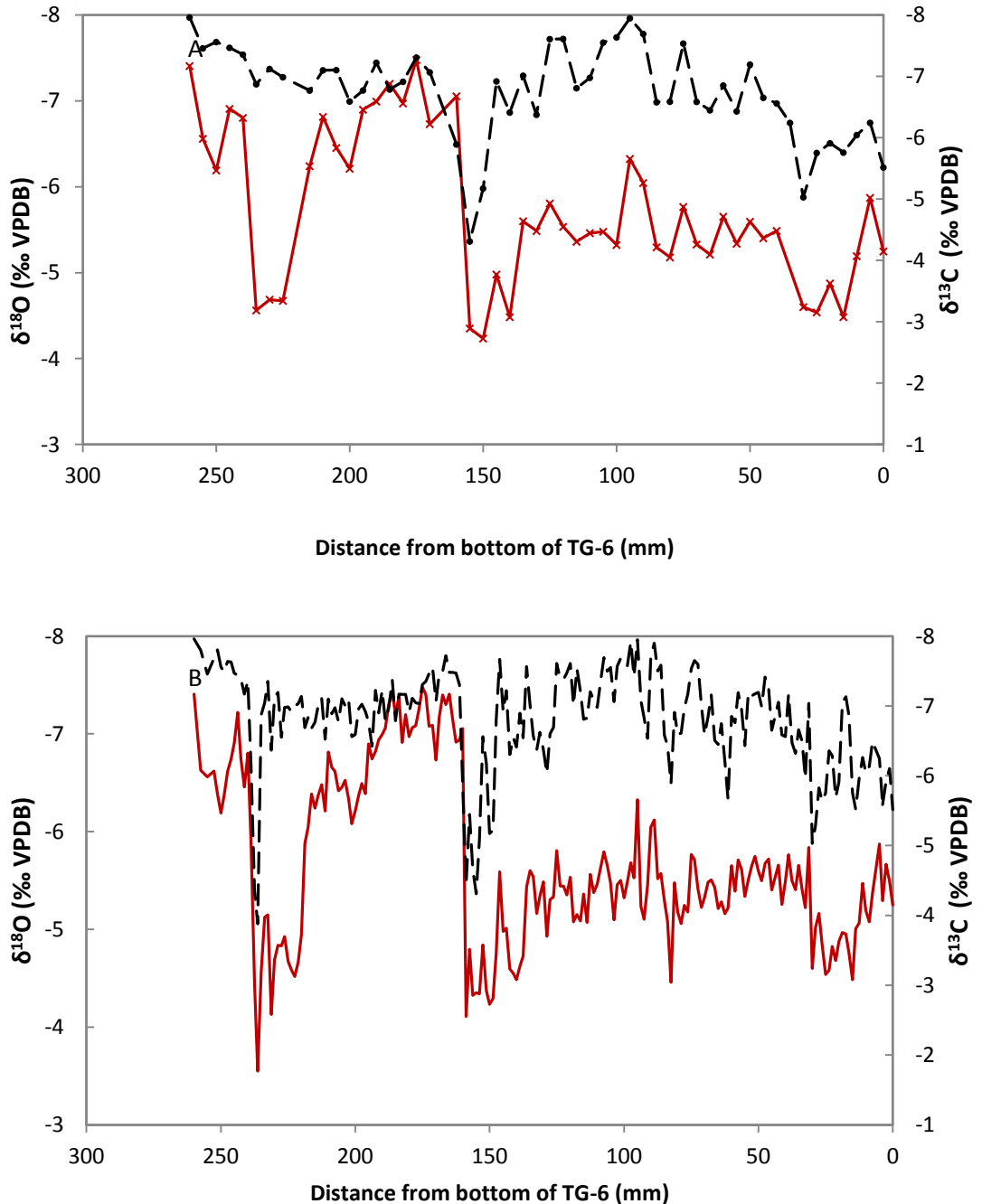


**Figure 5.8**  $\delta^{18}\text{O}$  (red lines) and  $\delta^{13}\text{C}$  (black dashed line) data for TG-6  
A) Original, low resolution data compiled by Dr Sa'ad Al-Omari  
B) Additional data to produce resolution of ~1 mm, this study.

### **5.1.2.2 Hendy Tests**

Hendy tests (Hendy, 1971) were performed on 3 lamina in TG-6 (Figure 5.9 and 5.10). The layers were chosen to represent the area below the lower hiatus (A), between the two hiatuses (B), and above the top hiatus (B).

The covariation between  $\delta^{18}\text{O}$  and  $\delta^{13}\text{C}$  increases with distance from the base of the stalagmite, indicating departure from equilibrium. This may be due to recrystallisation of the original aragonite; the lower areas have not completely recrystallised and so the original isotopic signature and equilibrium is retained; while nearer the top of the speleothem, recrystallisation to calcite is much further progressed, so that the stable isotope signature of the original aragonite may have been lost.

### **5.1.2.3 Axial Isotope Measurements**

A crossplot of  $\delta^{18}\text{O}$  and  $\delta^{13}\text{C}$  data is shown in Figure 5.11. As the covariation was not as high as expected, the data were separated into sections of growth, as explained in the figure caption. This process revealed that the degree to which kinetic processes affected the isotopic character of TG-6 was not constant through time. Specifically, covariation was lowest after each hiatus, perhaps due to reduced evaporation as conditions became more humid.

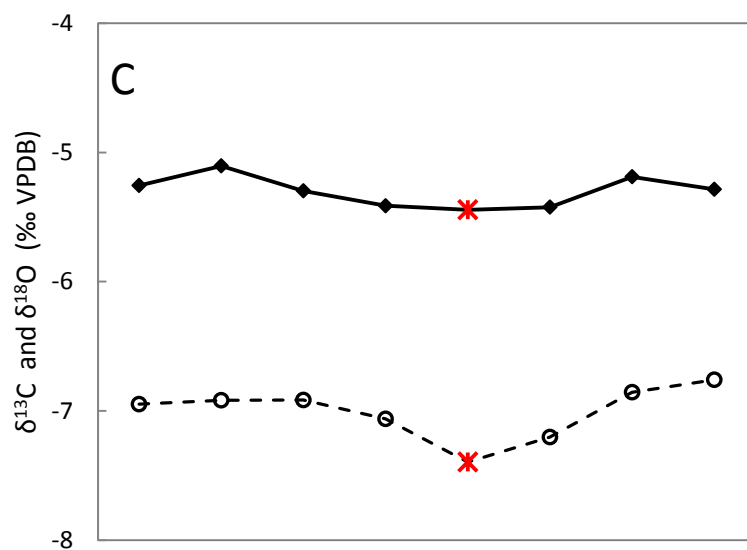
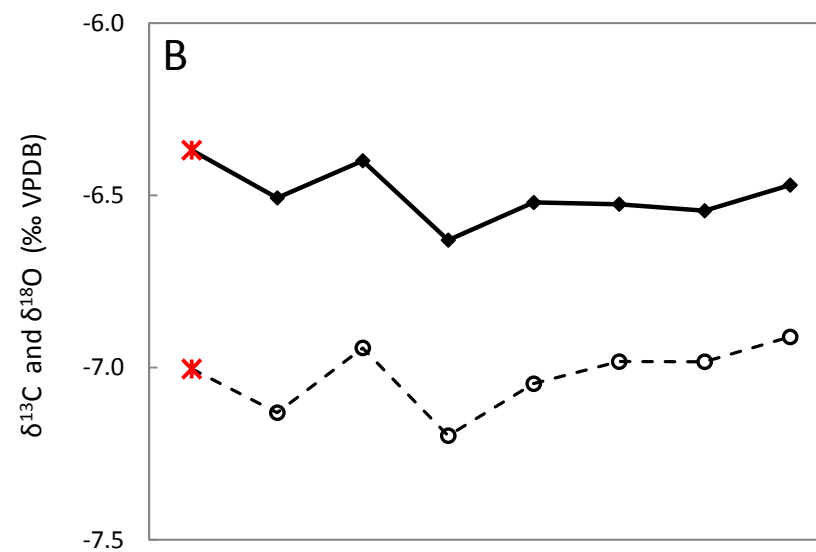
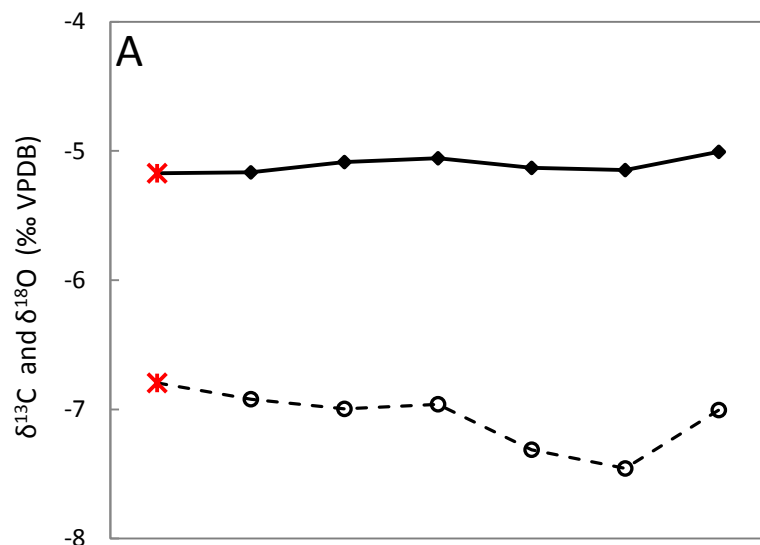


**Figure 5.9**

*Hendy tests for stalagmite TG-6,  $\delta^{18}\text{O}$  (black filled diamonds, solid line) and  $\delta^{13}\text{C}$  (unfilled circles, dashed line) variations along a single layer.*

*Distance from base of stalagmite: A) 104mm. B) 213.75mm. C) 247.5mm.*

*Red stars indicate growth axis.*

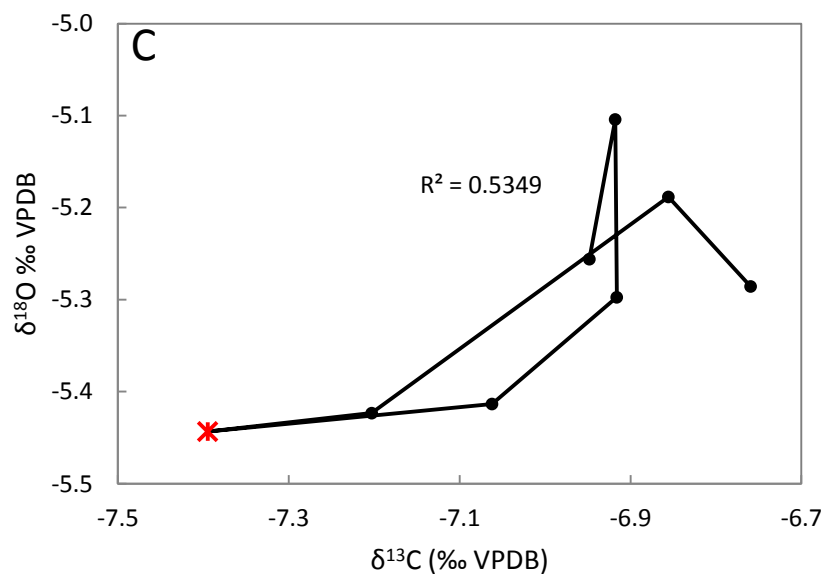
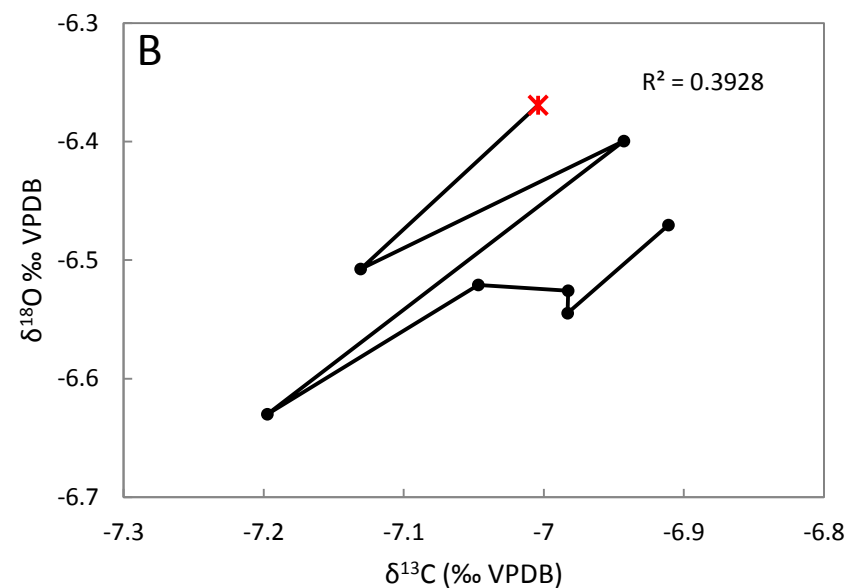
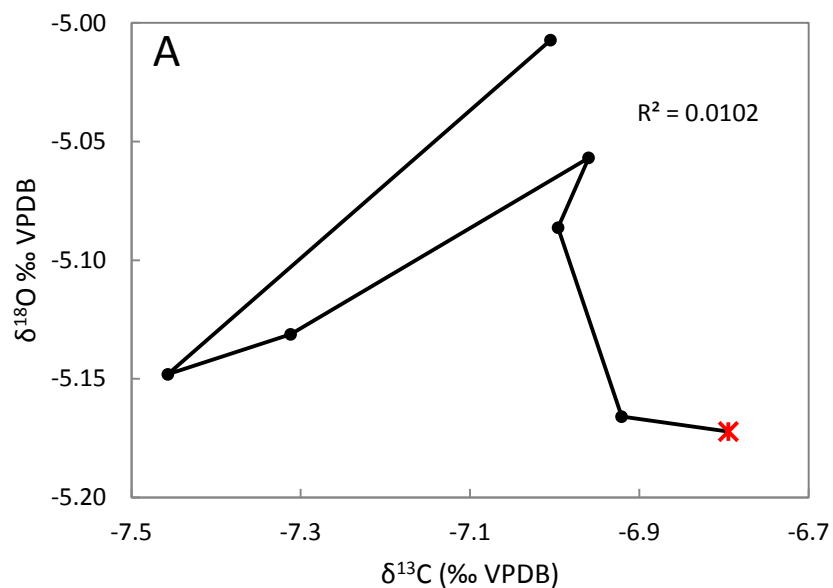


**Figure 5.10**

*Hendy tests for stalagmite TG-6, covariation between  $\delta^{18}\text{O}$  (black filled diamonds, solid line) and  $\delta^{13}\text{C}$  (unfilled circles, dashed line).*

*Distance from base of stalagmite: A) 104 mm. B) 213.75 mm. C) 247.5 mm.*

*Lines join measurements in order of progression along lamina. Red stars indicate growth axis.*

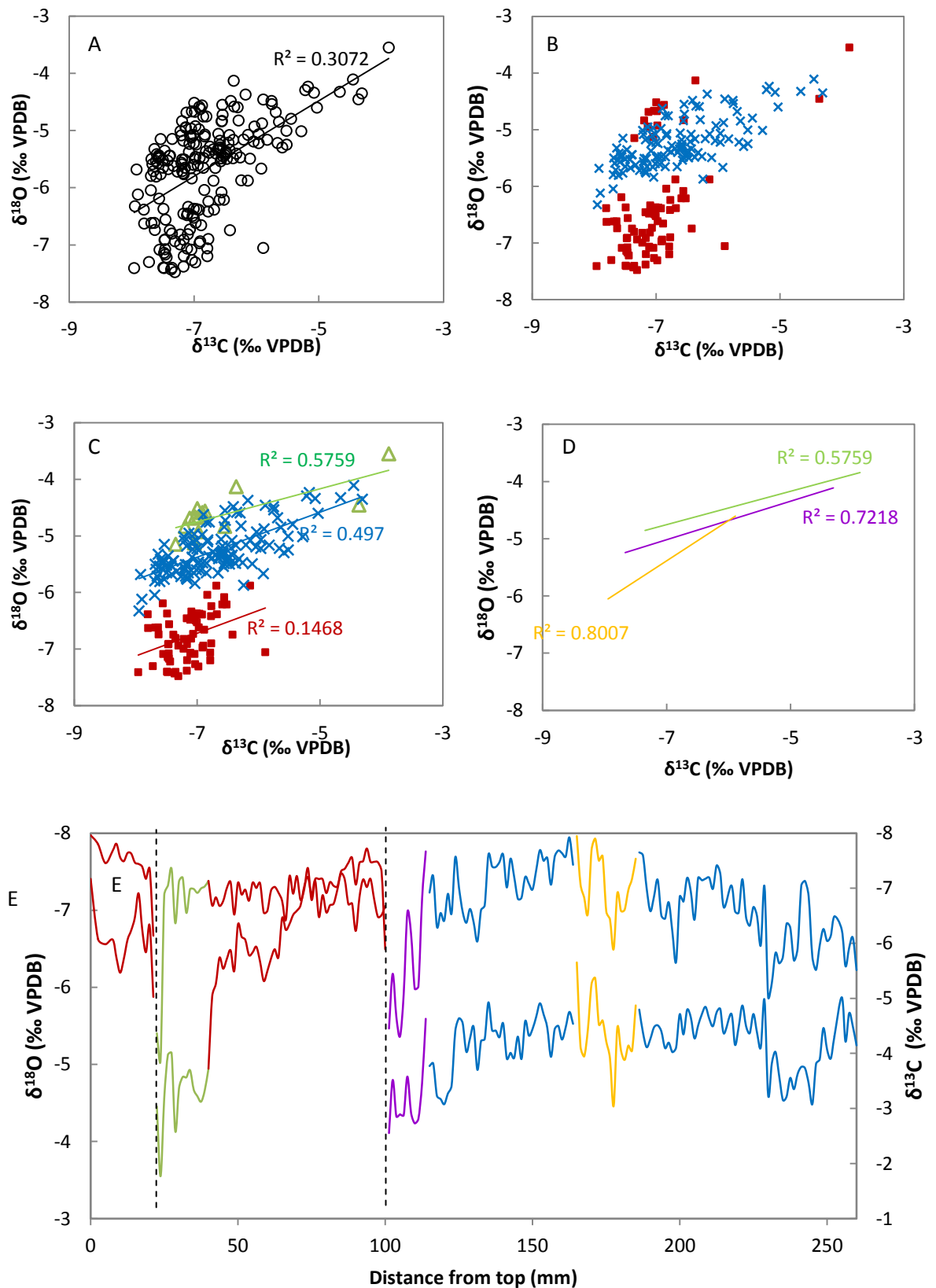


Figure 5.11: Crossplot of  $\delta^{18}\text{O}$  and  $\delta^{13}\text{C}$  data for TG-6

A: All data. Data show a positive correlation, but the relationship is not as strong as expected, given the clear similarities in the shapes of the  $\delta^{18}\text{O}$  and  $\delta^{13}\text{C}$  curves. For this reason, the profiles were split into regions of differing coherence between  $\delta^{18}\text{O}$  and  $\delta^{13}\text{C}$ , as in Meyer et al. (2009).

B: Data separated into samples from above the lower hiatus (red squares) and below this hiatus (blue crosses).

C: Data from B, with the data from above the hiatus further divided; so that data from the region 22.5-38.75 mm are separate (green triangles).

D) Lines of covariance and  $R^2$  values for 3 areas of high covariance in  $\delta^{18}\text{O}$  and  $\delta^{13}\text{C}$ . The colours of these lines correspond to the colours of E, which separates all the data into regions of similar covariance.

E:  $\delta^{18}\text{O}$  and  $\delta^{13}\text{C}$  data for TG-6, separated into regions of similar covariance. Colours correspond to groups plotted in C and D. Black vertical dashed lines indicate the position of the two hiatuses.

#### 5.1.2.4 Oxygen Isotopes

The  $\delta^{18}\text{O}$  record for TG-6 (Figure 5.12) begins with a reasonably stable plateau for ca. 40 kyr. Superimposed on this plateau are variations of up to  $\sim 1.5\text{‰}$ . At 277.3 kyr BP there is a large excursion of approximately  $3.5\text{‰}$  to more negative values. This change is associated with the lower hiatus. Values then begin to gradually increase until ca. 265.2 kyr BP, when an abrupt return to more positive values occurs, this excursion resulting in the most positive values of the speleothem. Following this at ca. 259.9 kyr BP, an abrupt negative excursion occurs, which is associated with the upper hiatus, and is of similar magnitude to the excursion associated with the lower hiatus.

#### 5.1.2.5 Carbon Isotopes

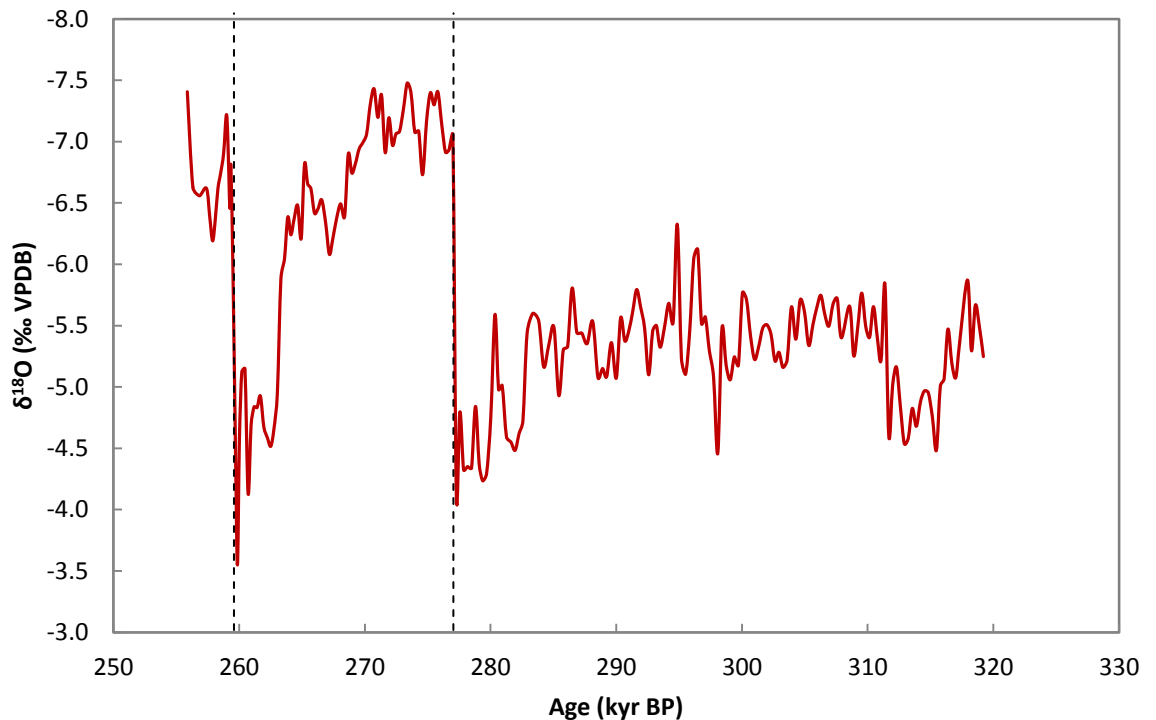


**Figure 5.12**  $\delta^{18}\text{O}$  data for TG-6. Dashed vertical lines indicate position of hiatuses.

The  $\delta^{13}\text{C}$  record for TG-6 is shown in Figure 5.13. From ca. 320 - 295 kyr BP, the data are variable and form a gradual decrease of ca.  $2.5\text{‰}$ . Superimposed on this trend are large variations of up to ca.  $2\text{‰}$ . From ca. 295 - 280 kyr BP, the trend plateaus, but there are still relatively large variations about the mean, up to approximately  $1\text{‰}$ . Between ca. 280 and 277 kyr BP, values become more positive by ca.  $3\text{‰}$ , with two short-lived reversals of ca.  $1\text{‰}$  superimposed on the excursion. At 277.3 kyr BP, there is an abrupt excursion to more negative values by ca.  $3\text{‰}$ . This excursion coincides with the lower hiatus, and the associated  $\delta^{18}\text{O}$  change. After growth resumes above the lower hiatus, values remain low

and show less variability than below the lower hiatus, until at ca. 260 kyr BP, values once again abruptly increase by ca 3‰, and then immediately decrease by the same amount. The abrupt decrease in values occurs at the upper hiatus, above which values appear to continue to become more negative, but this trend is interrupted by the fact that the top of the stalagmite is broken.

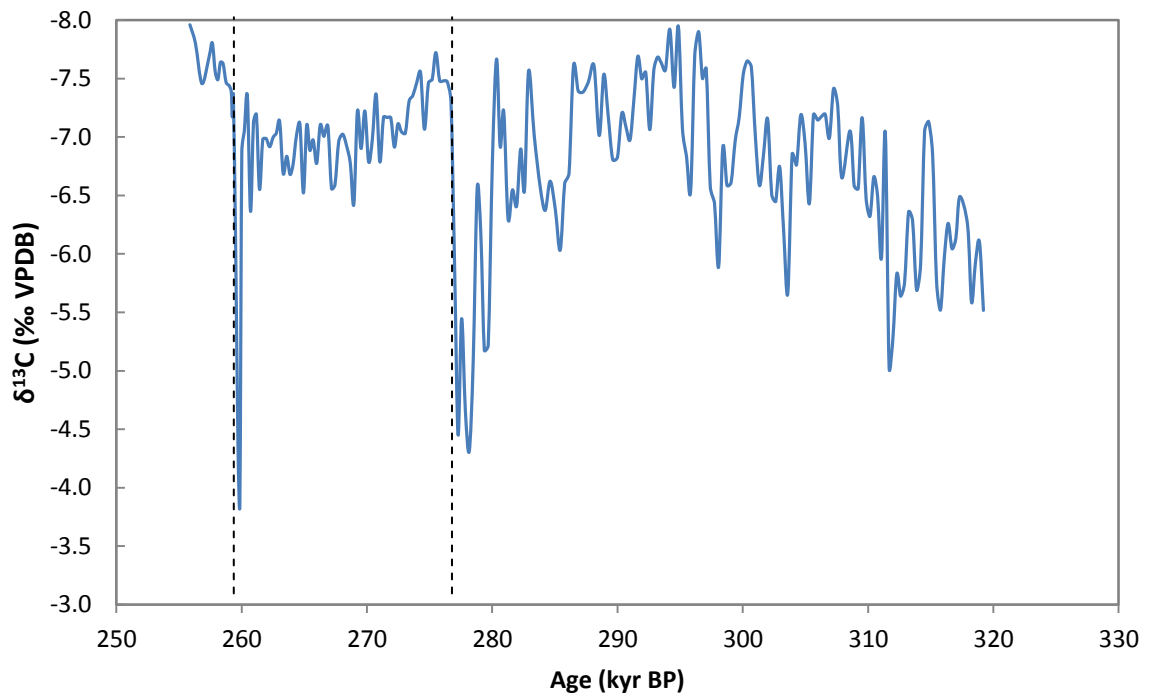


**Figure 5.13**  $\delta^{13}\text{C}$  data for TG-6. Dashed vertical lines indicate position of hiatuses.

### 5.1.3 Trace Element Measurements

#### 5.1.3.1 Sampling Strategy

A laser ablation transect was run across the lower hiatus, that is it incorporates the very top of the bottom slab of TG-6 and the very bottom of the top slab.

#### 5.1.3.2 Results

Mg/Ca (Figure 5.14) increases gradually over the region, with no large change at the hiatus. Sr/Ca (Figure 5.15) shows a large increase at the hiatus. Ba/Ca\*1000 (Figure 5.16) shows the most dramatic change; values increase at the hiatus by more than an order of magnitude.

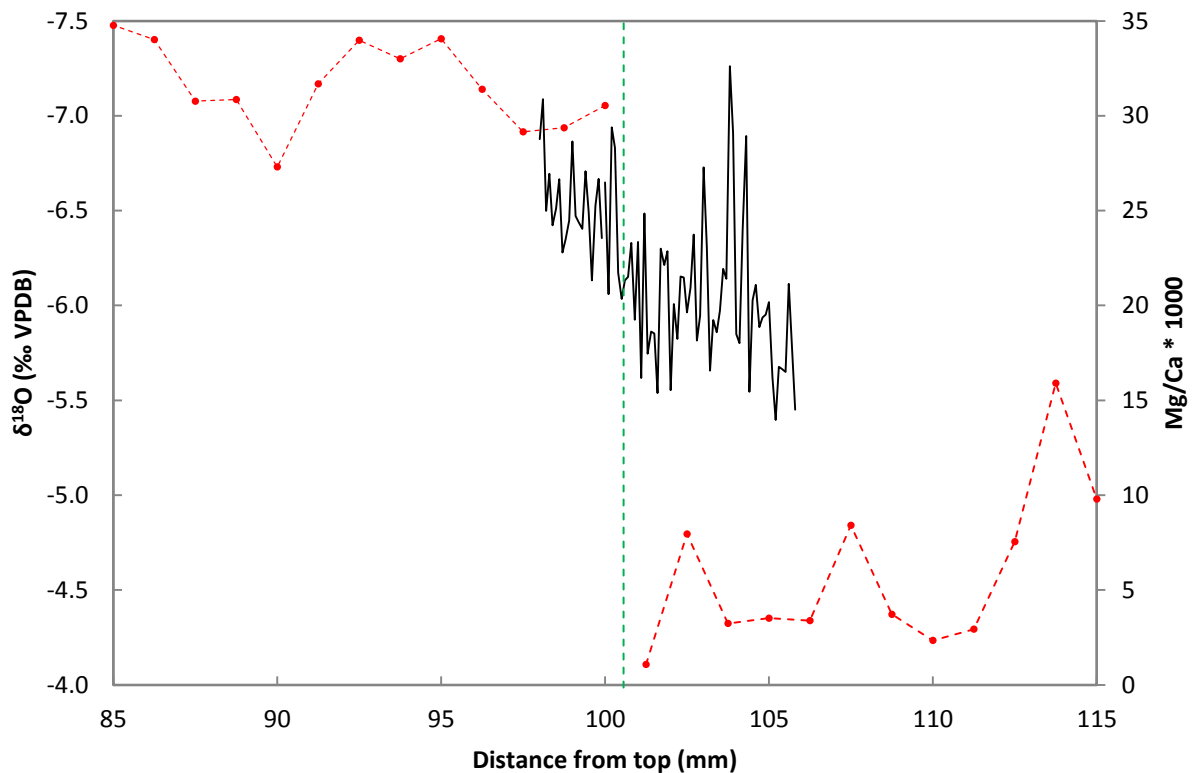


**Figure 5.14** Mg/Ca \* 1000 (black line) for the lower hiatus region, in comparison to  $\delta^{18}\text{O}$  (red line) Dashed green vertical line denotes location of hiatus.

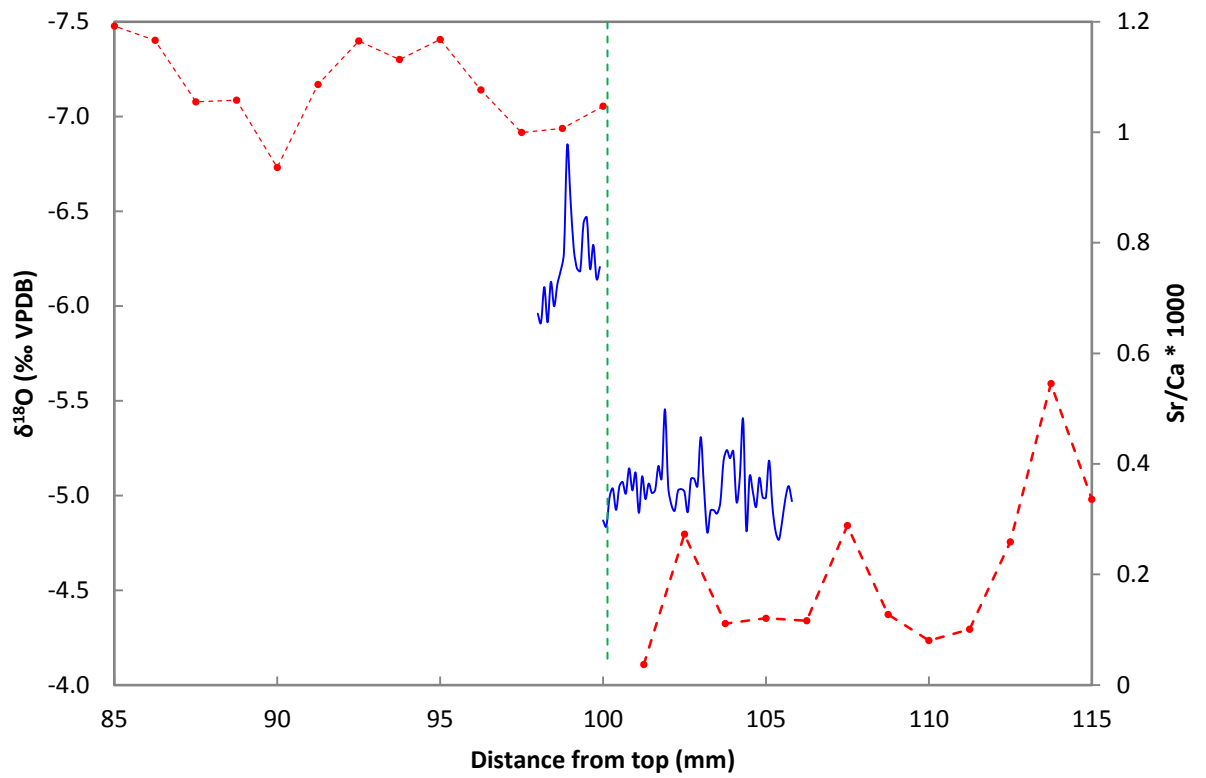


**Figure 5.15** *Sr/Ca \* 1000 (blue line) for the lower hiatus region, in comparison to  $\delta^{18}\text{O}$  (red dashed line). Dashed green vertical line denotes location of hiatus.*

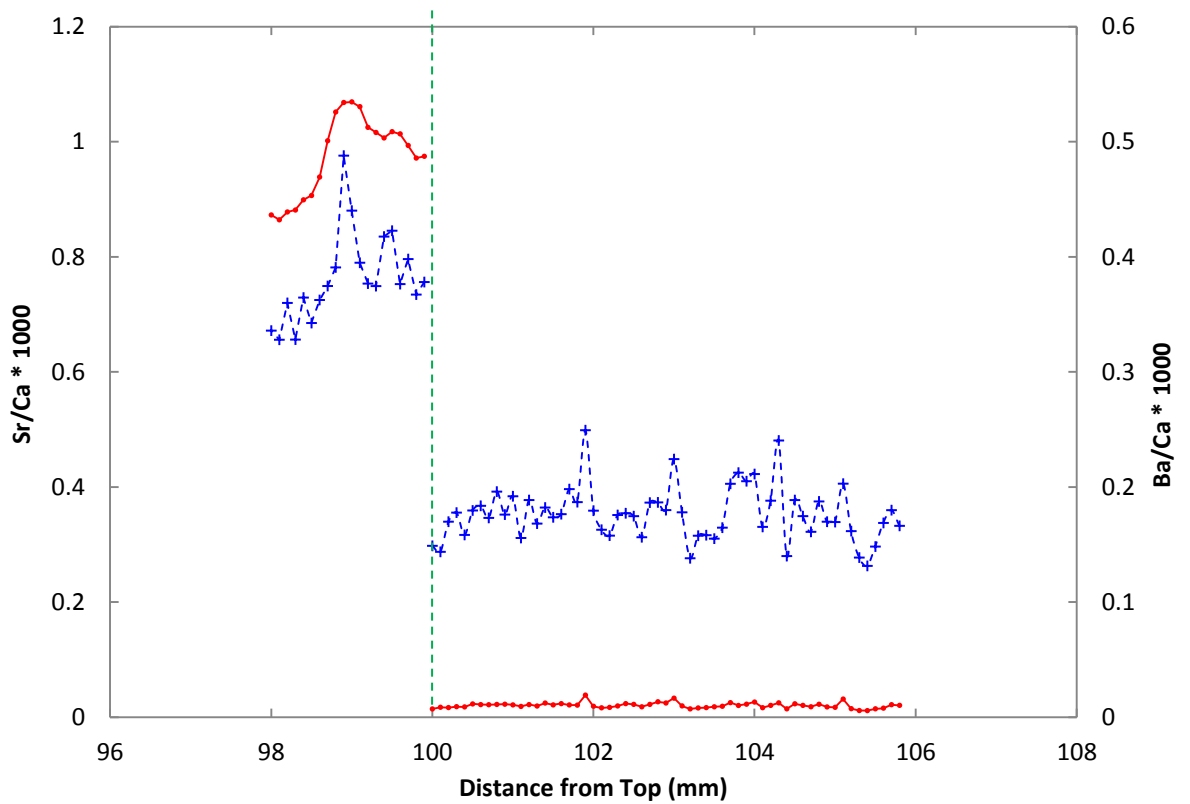


**Figure 5.16** *Ba/Ca\*1000 (red line) for the lower hiatus region, in comparison to Sr/Ca\*1000 (crosses and blue dotted line) Dashed green vertical line denotes location of hiatus.*

#### 5.1.4 Fluorescence Imaging

Fluorescence imaging of TG-6 (Figure 5.17) appears to show highly fluorescent areas in the light coloured, cloud-shaped forms which petrographic analysis indicates may be aragonite, while the rest of the speleothem is calcite. If the processes identified in DIM-1 occurred in TG-6 also (i.e. aragonite areas contain original fluorescence, then when recrystallised this fluorescence is lost), this data corroborates the recrystallisation of parts of TG-6.

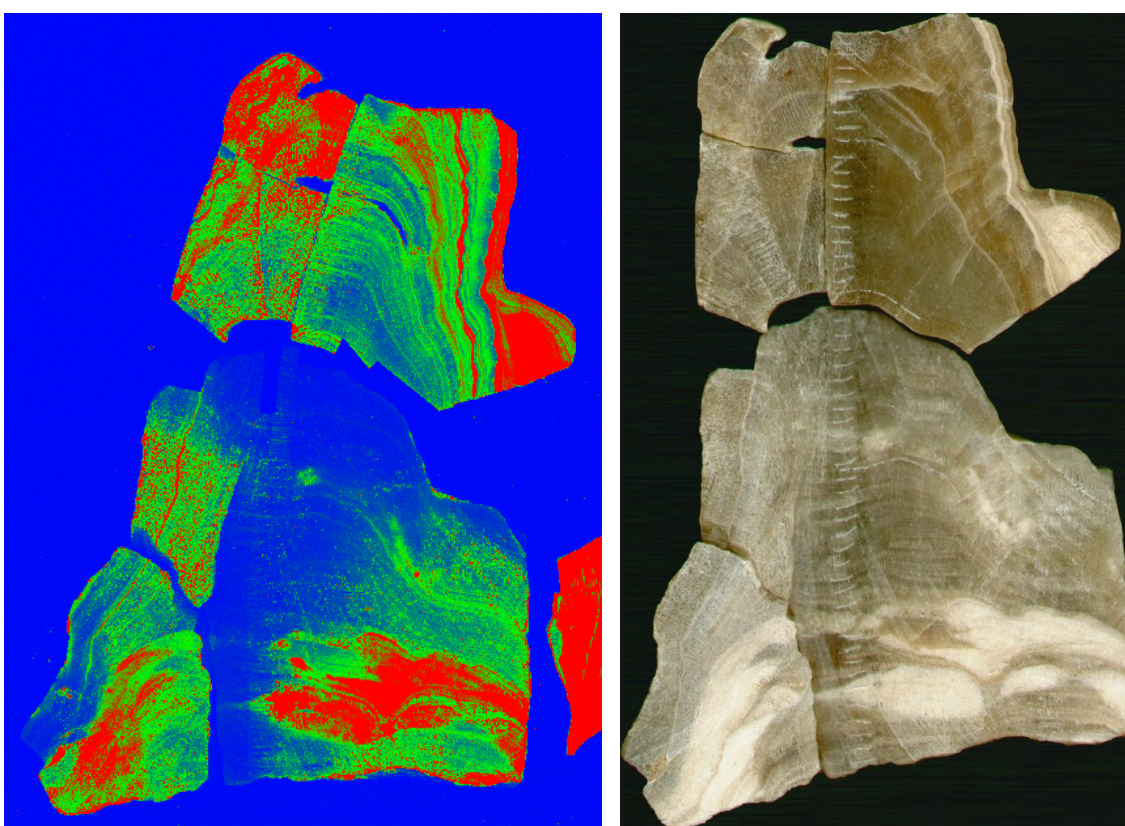


**Figure 5.17** *Fluorescence Imaging of TG-6, with true colour photograph for comparison. Blue colouring indicates low fluorescence, green indicates higher fluorescence and red colouring indicates highest fluorescence (levels are relative, not absolute).*

### 5.3.6 Palaeoclimatic Interpretation of TG-6

TG-6 grew between  $326 \pm 26$  kyr BP and  $223 \pm 4$  kyr BP with at least 2 major hiatuses. Only four dates form the age model for TG-6, of which 2 have large errors. Therefore, the age model for TG-6 is necessarily over- simplistic, due to the lack of dates. There is thus no constraint on the length of the either of the two hiatuses. The age model constructed using the 4 ages available produces an almost linear growth model and associated constant growth rate; an extremely unlikely scenario in a stalagmite with at least two depositional hiatuses. Also, microscope evidence suggests that recrystallisation may have occurred, with calcite replacing primary aragonite. If so, open system conditions may have led to U loss and reported may be older than the “true” ages of the original aragonite.

A series of approaches have been explored In order to attempt to assess some of the uncertainties in the TG-6 age model. First, an age model was created in which the ages were merely connected point-to-point, assuming constant growth between points, and no cessation of growth at the hiatuses. This age model is shown in Figure 5.18.

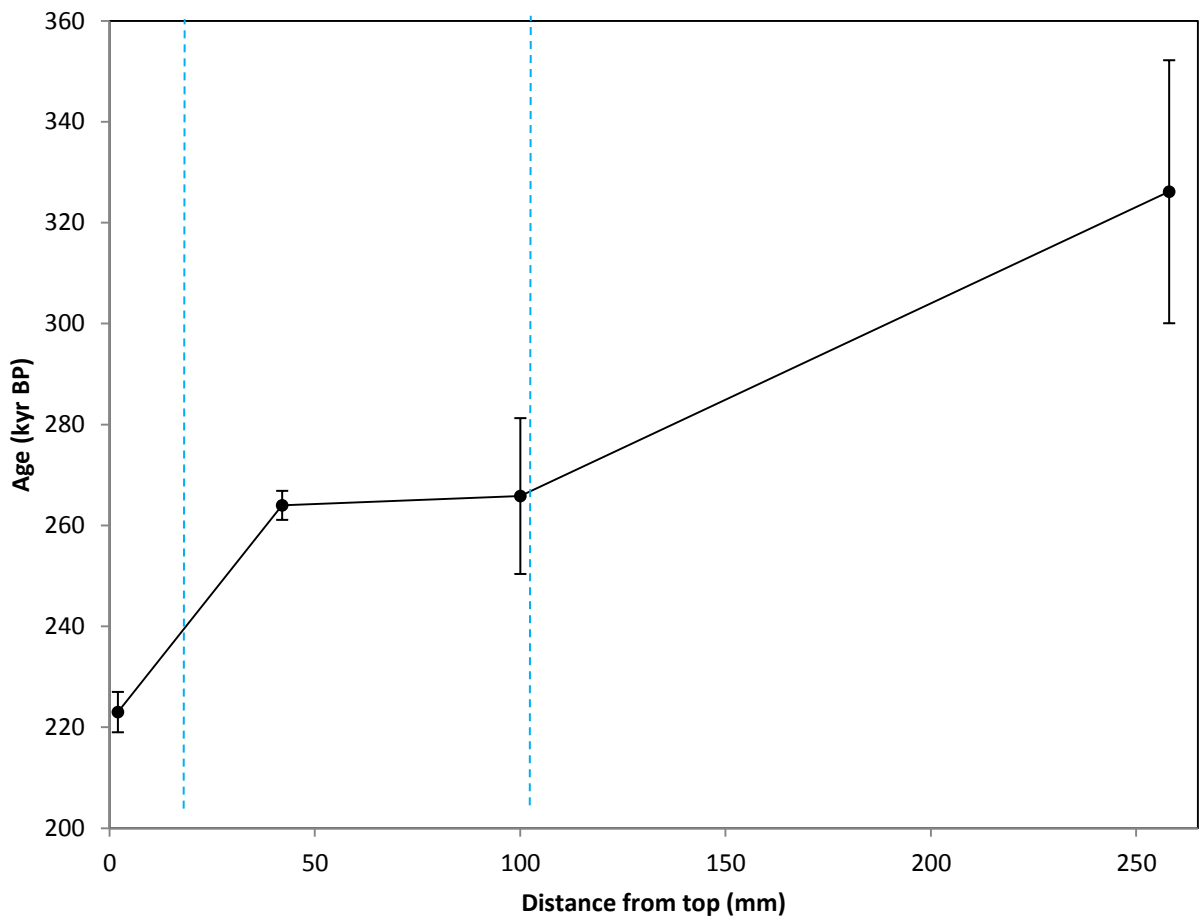


**Figure 5.18**  
**Point to point age model for TG-6. Dashed blue vertical lines represent the approximate position of the two hiatuses.**

The point to point age model shown in Figure 5.18 is very simplistic, due to its point to point nature, with a problematic issue being that it assumes no cessation of growth at the hiatuses. It is likely that growth ceased for some length of time at the hiatuses, although as the dates currently available do not provide limits to the length of the cessation of growth, the timing of these periods of inactivity can only be hypothesised. An attempt to do so follows.

The start of growth of TG-6 at  $326 \pm 26$  kyr BP falls within the early part of MIS 9, suggesting that the growth phases of TG-6 may be linked to interglacial conditions. This age is within error of a period of growth of a speleothem from Kana'im Cave in the Dead Sea area of Israel, which was growing at  $323.7 \pm 18.9$  kyr BP (Lisker et al., 2010). MIS-9 is interpreted as a particularly warm and wet interglacial in Siberia, with significantly more speleothem growth than during MIS 1, 5 or 7 (Vaks et al., 2013). In Northern Oman, the primary source of moisture during MIS 9 was monsoon rainfall, while Mediterranean-source precipitation was decreased or even absent (Fleitmann et al., 2003b). This strongly suggests that the ITCZ was located further to the north than at present (Fleitmann et al., 2003b), and it is possible that if the ITCZ was displaced far enough north, monsoonal rainfall could also have reached Torang Cave in southern Iran at this time. MIS 9 appears to have been a very wet interglacial, which may have been an important factor in allowing speleothem growth at Torang Cave, as today the region experiences low levels of rainfall.

The oldest date above the lower hiatus is  $265 \pm 15$  kyr BP, which is during MIS 8, at a time of high ice sheet extent (Petit et al., 1999). The increase in Mg/Ca (Figure 5.14), Sr/Ca (Figure 5.15) and Ba/Ca (Figure 5.16) across the hiatus, as well as the marked excursions in  $\delta^{18}\text{O}$  (Figure 5.12) and  $\delta^{13}\text{C}$  (Figure 5.13), indicate that conditions were drier during the deposition of growth above the lower hiatus compared to growth below the lower hiatus. This is compatible with the reduced precipitation levels during glacial periods compared to interglacial periods. Speleothems generally are more likely to grow in interglacial periods, but some have been known to grow during glacial periods, so growth of TG-6 during MIS 8 is not without precedent. For example, a speleothem from Kana'im Cave, Israel grew during the period  $259.8 \pm 7.1$  to  $247.9 \pm 6.3$  kyr BP (Lisker et al., 2010), and flowstone SPA 59 from Spannagel Cave, Austria, grew during the period ca. 261 – 249 kyr BP, (Holzkämper et al., 2005).

Therefore, from these two dates on TG-6 it can be deduced that the lower hiatus began sometime between  $326 \pm 26$  kyr BP and  $265 \pm 15$  kyr BP, and finished at  $265 \pm 15$  kyr BP or

shortly before. A collapse in arboreal pollen at the Tenaghi Philippon, NE Greece, began at ca. 280 kyr BP and recovered ca. 265 kyr BP (Tzedakis et al., 2003b). The similarity in the end point of the vegetation collapse and the age above the lower hiatus of TG-6 suggests that the two events may be linked to wider climate changes, as both a vegetation collapse and a cessation of speleothem growth may be caused by a reduction in precipitation, for example. Therefore, a duration of 280 – 265 kyr BP has been applied to the hiatus (Figure 5.19).

Similarly, the upper hiatus must occur between the top two dates; i.e. between  $264 \pm 3$  and  $223 \pm 4$  kyr BP. The growth of TG-6 during MIS 9, a particularly wet interglacial, and MIS 8, a glacial, suggests that effective precipitation may be the dominant factor in speleothem growth in Torang Cave, with growth able to occur when either temperature is low enough (MIS 8), or precipitation high enough (MIS 9), for effective precipitation to reach a threshold. Therefore, as conditions in MIS 7e were not as wet as during MIS 9 (Vaks et al., 2013), effective precipitation may not have been high enough to initiate speleothem growth. For this reason, the length of the upper hiatus has been correlated with the length of MIS 7e, which is ca. 237 – 228 kyr BP (Robinson et al., 2002), as shown in Figure 5.19. A speleothem record from Peqiin Cave, Israel, also displays a hiatus during the period 240 – 227 kyr BP (Bar-Matthews et al., 2003), although the authors attribute this to lack of sampling resolution rather than an actual cessation of growth. The remainder of growth of TG-6 above the upper hiatus to the broken top would then have grown during MIS 7d, when effective precipitation was once again high enough for speleothem growth.

These assumptions about the length of the two hiatuses have been applied to the point-to-point age model, to create the adapted age model shown below in Figure 5.19.

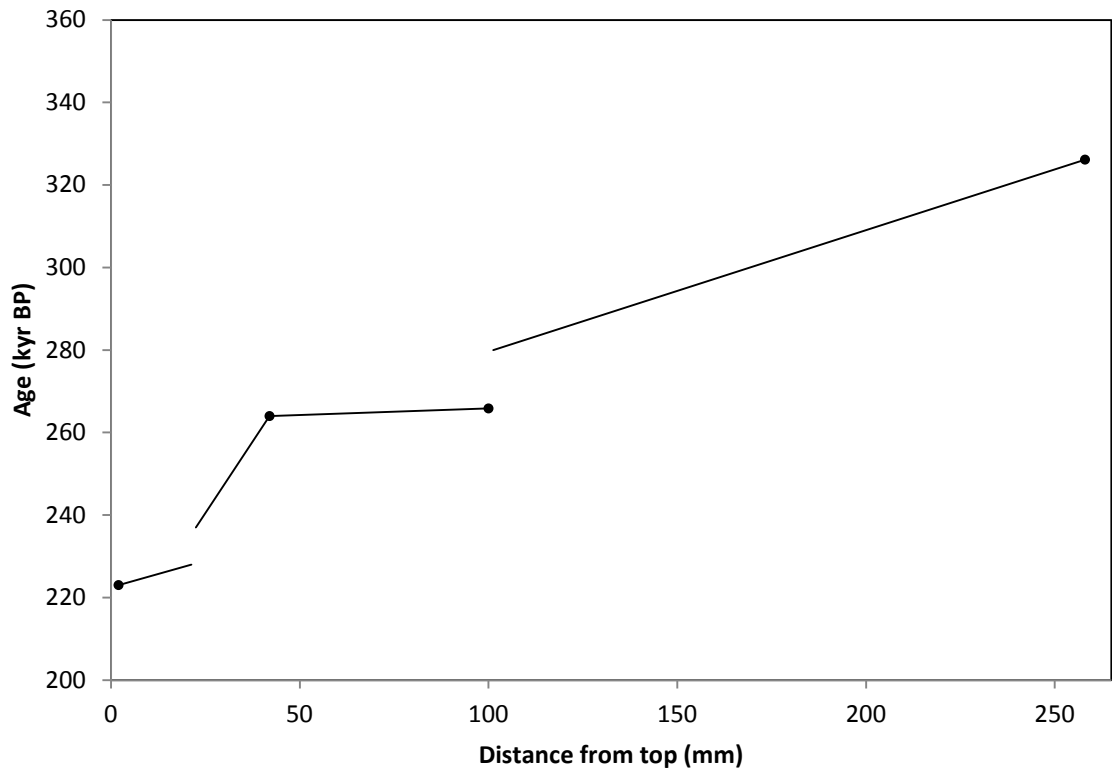


**Figure 5.19**  
**Point to point age model for TG-6, with hypothetical lengths of growth hiatuses included. The four ages are included as black circles.**

This adapted age model was then applied to the oxygen and carbon stable isotope data for TG-6 (Figure 5.20).

The  $\delta^{18}\text{O}$  and  $\delta^{13}\text{C}$  data shown in 5.20 support the interpretation of the growth of TG-6 being driven by precipitation availability. At ca. 284 kyr BP,  $\delta^{13}\text{C}$  began to increase by ca. 4‰, with the excursion ending as growth ceased at the lower hiatus. This trend indicates increasing aridity, which is in agreement with the position of a hiatus at the end of this trend, and the timing of the vegetation collapse in the Tenaghi Philippon record. At ca. 265 kyr BP, when growth resumed,  $\delta^{13}\text{C}$  values had returned to low values, indicating a return to wetter conditions, or an increase in effective precipitation.  $\delta^{18}\text{O}$  values were also more negative than below the hiatus by approximately 2‰, which suggests increased precipitation.

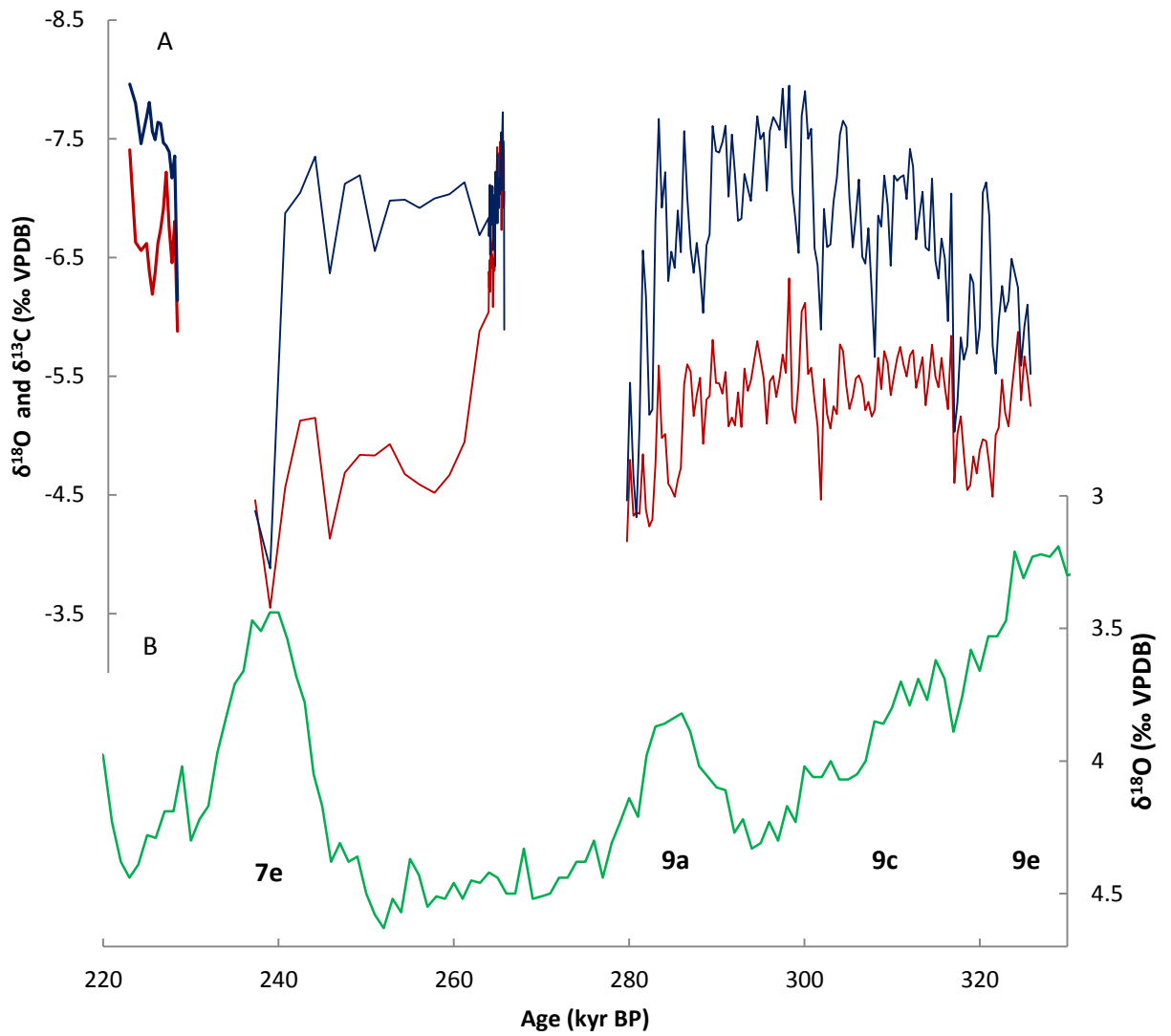


**Figure 5.20**

**A)  $\delta^{18}\text{O}$  (red line) and  $\delta^{13}\text{C}$  (blue line) data for TG-6, plotted against the amended age model described above.**

**B) Benthic  $\delta^{18}\text{O}$  record compiled from a stack of 57 global records (Lisiecki and Raymo, 2005). Terrestrial interglacial stages are indicated, after Tzedakis et al. (2003b).**

Furthermore, the first two dates above the lower hiatus ( $265.8 \pm 15$  and  $264.0 \pm 3$  kyr BP) indicate that approximately 58 mm of growth between these two sampling locations occurred in less than 2 kyr, giving a growth rate of  $0.032 \text{ mm yr}^{-1}$ . This is far faster than growth rates for the rest of the stalagmite, as below the lower hiatus the growth rate was  $0.0034 \text{ mm yr}^{-1}$ , and above the upper hiatus the growth rate was  $0.0038 \text{ mm yr}^{-1}$ , both an order of magnitude slower. The slowest growth appears to have occurred between the fast growth section and the upper hiatus, during the period 264 to 237 kyr BP, when the growth rate was just  $7.2 \times 10^{-4} \text{ mm yr}^{-1}$ . These growth rates have been approximated using only 4 dates and the estimated beginning and end points for the two hiatuses, so they are probably not completely accurate. However, it does appear that the fastest growth in TG-6 occurred just above the lower hiatus, which indicates increased effective precipitation as this would have facilitated faster carbonate precipitation.

Both oxygen and carbon isotopes return to more positive values by ca. 240 kyr BP, indicating low water availability, although  $\delta^{18}\text{O}$  began to increase sooner than  $\delta^{13}\text{C}$ . Following these isotopic excursions, the second major growth hiatus occurred, after which  $\delta^{18}\text{O}$  and  $\delta^{13}\text{C}$  returned to more negative values, signalling a return to higher effective precipitation levels.

With the age model of TG-6 as limited as it currently is, any palaeoclimatic interpretations drawn can only be hypotheses. Further dates would help to improve the precision and accuracy of the age model, allowing more certain conclusions about climate in SW Iran during MIS 9-7 to be drawn.

# Chapter 6

U/Pb dating of a  
Speleothem from Sehlak  
Cave, Iran

## 6.1 Sehlak Cave

Sehlak cave was previously visited by Dr Sa'ad Al-Omari and Dr Peter Rowe on 31.05.2005, at which time stalagmite SK-1 was collected, along with 6 other samples not analysed here. As the cave was not visited during this project, no modern dripwaters or calcite are presented here. Sehlak Cave is located near Baft in Southern Iran, at coordinates N 28° 33' 0"; E 55° 8' 95". The cave is at an elevation of 1990-2168 m.a.b.s.l., at a distance of 10 m from the valley floor, and has an overburden of approximately 50 m. The cave is 50 m long and 5-10 m deep. Sehlak's close proximity to Torang Cave enables use of the same IAEA data to determine modern precipitation patterns.



**Figure 6.1** Location of Sehlak Cave (white diamond) within Iran

## 6.2 Stalagmite SK-1

Stalagmite SK-1 (*Figure 6.1*) was collected from Sehlak Cave, Iran. SK-1 was collected 45 m from the cave entrance and was inactive when removed from the cave. The outside of the stalagmite was very corroded on one side. This is most likely due to a prevailing air movement through the cave with a large moisture content.

From the outside, the shape of SK-1 appears to be quite regular and conical, suggesting a constant drip. However, the inside revealed that although layer width remained relatively constant, the drip axis varied considerably.



**Figure 6.1** Stalagmite SK-1  
Red boxes indicate approximate location of pieces chosen for LA-ICP-MS analysis.

### **6.2.1 Previous Attempts to Date SK-1**

A previous attempt to date SK-1 using U/Th dating methods was carried out by Dr Sa'ad Al-Omari, the collector of the stalagmite. A piece from the very top of SK-1 was used, and was found to be outside the limits of the U/Th method (i.e. older than ~700 kyr). Therefore, in this project, U/Pb dating was proffered and attempted as an alternative method.

### **6.2.2 Preliminary Screening of Samples**

LA-ICP-MS was used as a tool for screening samples to find those areas most likely to yield material datable by isotope dilution thermal ionization mass spectrometry, i.e. areas with high U, low common lead and a high range of U/Pb ratios. The first scans used a NIST glass standard, but as this was not ideal due to coupling issues, a carbonate laser ablation standard was procured. This standard was donated to the NIGL laboratory at BGS, by Dr Troy Rasbury, and has been named the Rasbury standard. It is a paleosol from the late Permian of Texas, with a known age of 251 Ma and U content of 5 ppm, and appears to have a very homogenous composition.

Target areas of SK-1 were chosen to retrieve ages of the top and bottom of the stalagmite, and two prominent shifts in drip axis (Figure 6.2). However, preliminary scans of these pieces were in the main unsuccessful, with a low spread in U/Pb compositions leading to large errors (often 100% of the age). Therefore, the data for the bottom and the drip axis change piece are not shown here. However, analyses of the top yielded much more promising results (Figures 6.3 & 6.4). Ablation points were clustered in 3 lines; the top layer (A), the bottom layer (B), and a layer running through the middle which was of much lighter colouring than the rest of the piece (C) (Figures 6.3 and 6.4). The top and bottom analyses (A & B), gave very imprecise data, having too much common lead in them, while the lighter layer gave a much wider range of  $^{238}\text{U}/^{206}\text{Pb}$  data, and therefore a much more precise estimate of the age (C). Figure 6.3(D) shows how this layer was analysed further to ascertain whether the higher spread of  $^{238}\text{U}/^{206}\text{Pb}$  values characterised the whole layer. This process produced a wide spread of values, which anchored the isochron, therefore improving the error.

As aragonite is known to typically contain higher U concentrations than calcite, XRD was used to identify the mineral forming the light layer near the top of SK-1. The layer was proven to be aragonite, while the layers immediately above and below were calcite. The locations of these mineralogies are summarised in Figure 6.4.

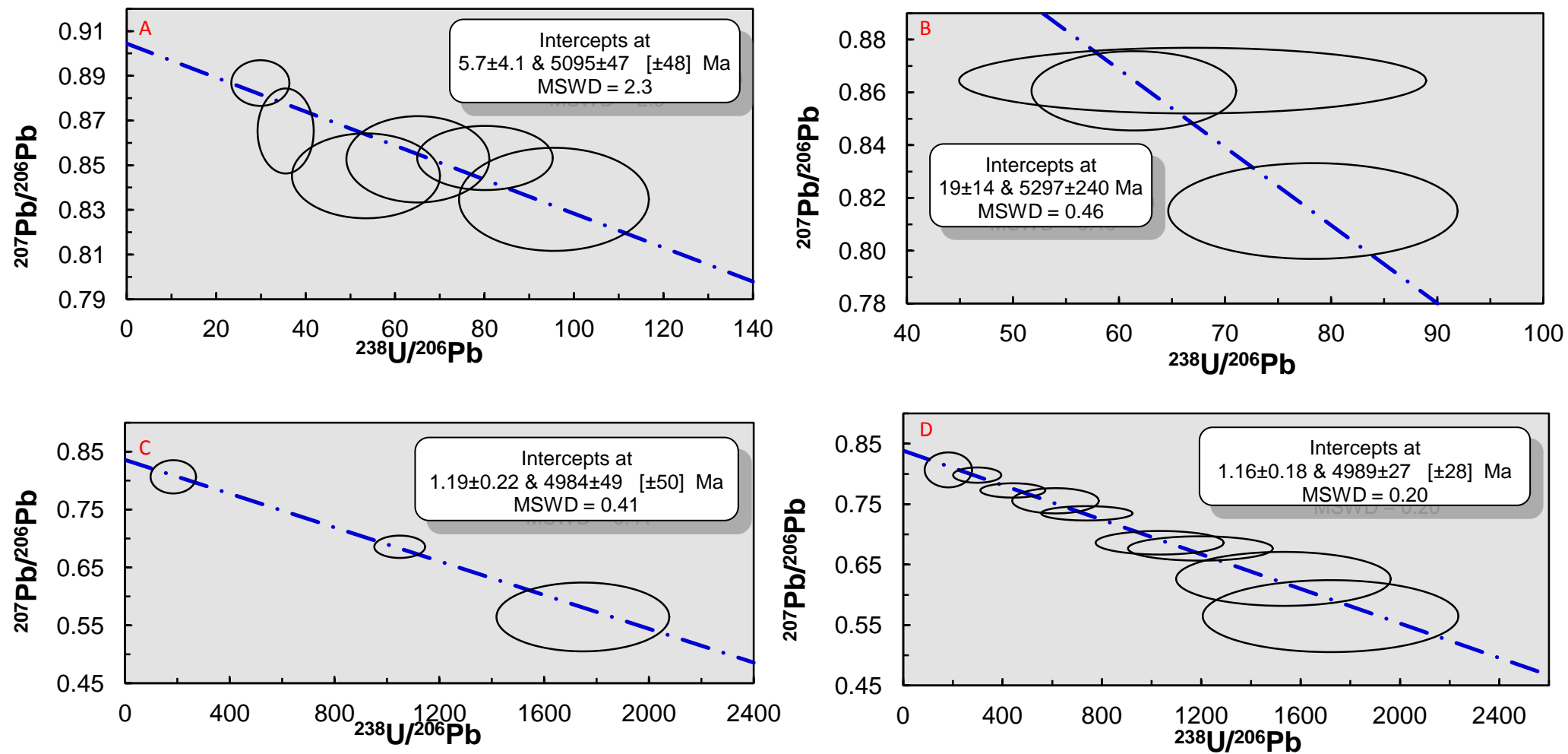


**Figure 6.3** Tera-Wasserburg diagrams for the top of SK-1. Data-point error ellipses are 2s. A) The top calcite layer. B) The next calcite layer below the aragonite layer. C) The aragonite layer, preliminary scan. D) The aragonite layer, additional data from extra laser scans

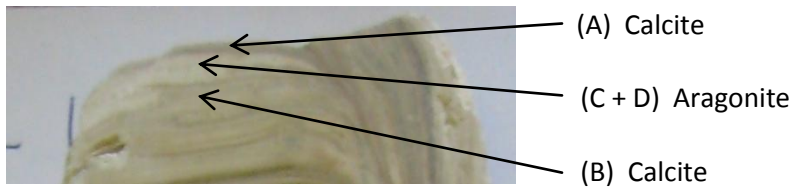


**Figure 6.4** *Mineralogy of the top of SK-1. Letters in parentheses refer to text description below and graphs in Figure 6.3.*

### 6.2.3 High Resolution Sampling by LA-ICP-MS

The data collected from the aragonite layer at the top of SK-1 were expanded upon in subsequent analyses, to produce as wide a range of  $^{238}\text{U}/^{206}\text{Pb}$  values as possible. The composite of these analyses, with the data normalised to the known age of the Rasbury standard, is shown in Figure 6.5. This method appears to have produced a reasonably precise age, with a 10% error. The fact that the age is precise, however, does not mean that it is accurate, and therefore comparison with an age reached by conventional dissolution of a chip of sample is necessary.

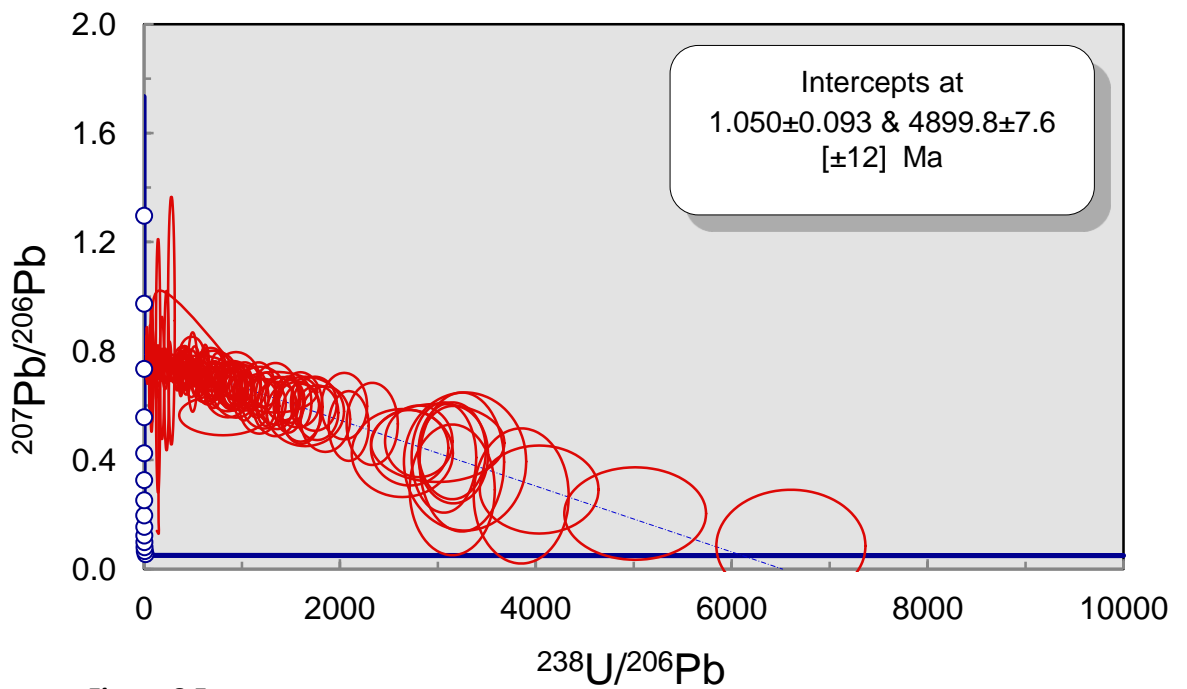


**Figure 6.5** *Tera-Wasserburg diagram of composite of several sets of LA-ICP-MS analyses of the aragonite layer in SK-1. Data have been normalised to the known age of the Rasbury standard. Error ellipses are 68.3% confidence.*

Following the success of LA-ICP-MS analysis of the aragonite layer, the logical next step would be to find any other aragonite layers in SK-1. Autoradiography was chosen as a non-destructive method to scan the whole face of the stalagmite for potential sampling locations.

#### **6.2.4 Digital Autoradiography and Fluorescence**

Digital autoradiography was used to identify areas of high radioactivity in SK-1, in the hope that they would contain high U and therefore be useful for U/Pb dating,. This approach has been used successfully by others, (e.g. Cole et al., 2003, Pickering et al., 2010). The method involved placing the flat, cut surface of SK-1 in contact with a Eu-doped BaClF digital storage phosphor imaging plate inside a box to protect the plate from being affected by background radiation for an extended period of time. Due to the quite low content of U in SK-1, a week was found to be necessary.

After the exposure period, the plate was scanned with red (635 nm) laser light on an Amersham Biosciences Scanner Storm 860 digital autoradiograph and fluorescence scanner. This scanning released the absorbed incident energy stored in the excited phosphor crystals by radioactive bombardment from SK-1 as a photostimulated luminescence signal, with an intensity proportional to the energy absorbed (Amemiya and Miyahara, 1988). The luminescence data was then translated into an image using Amersham Biosciences ImageQuant TL v2005 (*Figure 6.6*).

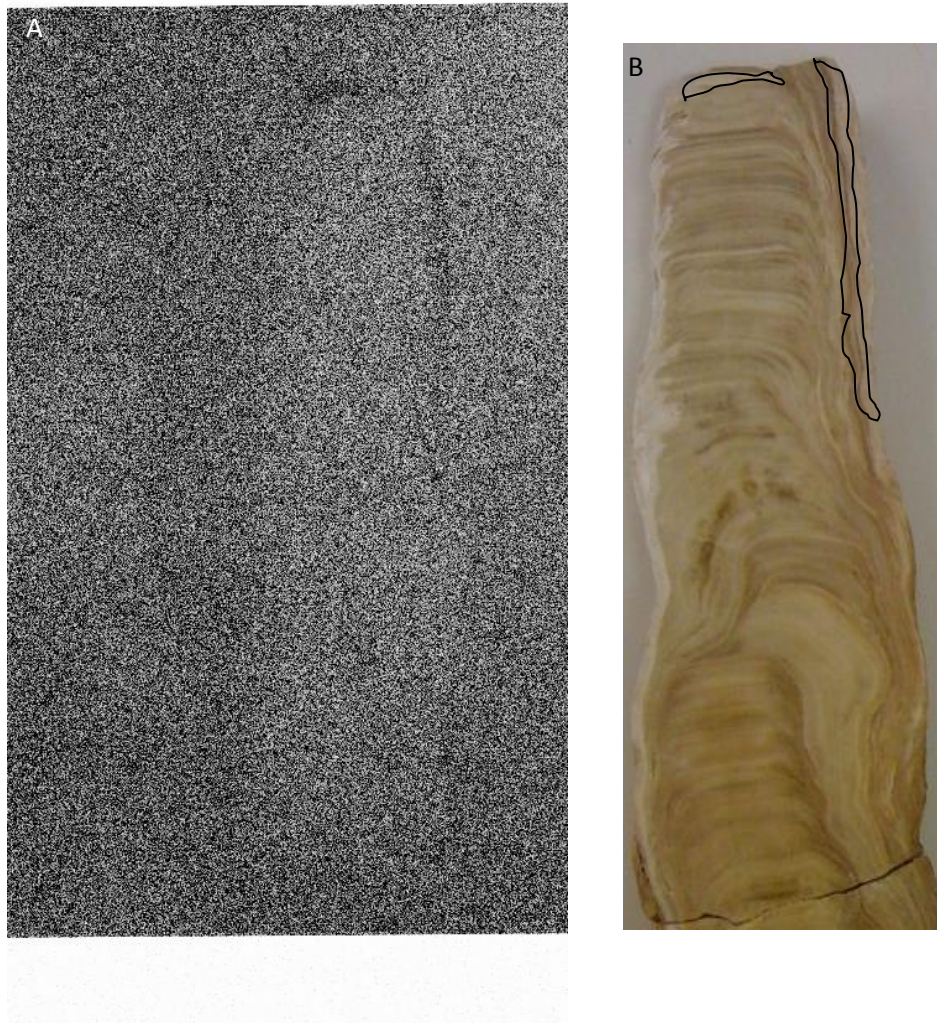


**Figure 6.6**

**A) Autoradiography image of SK-1. Dark areas indicate high radioactivity.**

**B) The corresponding visible areas in SK-1 (outlined in black) that are causing high radioactivity, assumed to be due to high U content.**

With the exception of an outer layer, which corresponds to an unknown position on the growth axis, the only area of high radioactivity identified in SK-1 by autoradiography was the previously identified top aragonite layer. It therefore appears that only this layer can be dated by U/Pb methods, negating the possibility of producing a full chronology, but nonetheless a useful exercise in comparing the results to the age calculated from the LA-ICP-MS data.

SK-1 was also scanned for fluorescence using the digital autoradiograph (Figure 6.7). The images produced are shown in Figure 6.7. The aragonite layer and outer layers that produced a high radioactivity signal in autoradiography analysis show as highly fluorescent areas (red), while an additional layer (identified by white box in A) also shows as high fluorescence but was not visible in the autoradiographic analysis. This layer was not further analysed in this study, but further work could include XRD analysis to identify whether the layer is calcite or aragonite, and if it is aragonite LA-ICP-MS screening would determine if further U/Pb work on this layer would be profitable.

The fluorescence data also show a similar situation to the Dim stalagmites, where areas of the stalagmite have almost no fluorescence, while others show higher fluorescence that also contains clear structure. This therefore may indicate that there has been replacement of primary aragonite by secondary calcite.

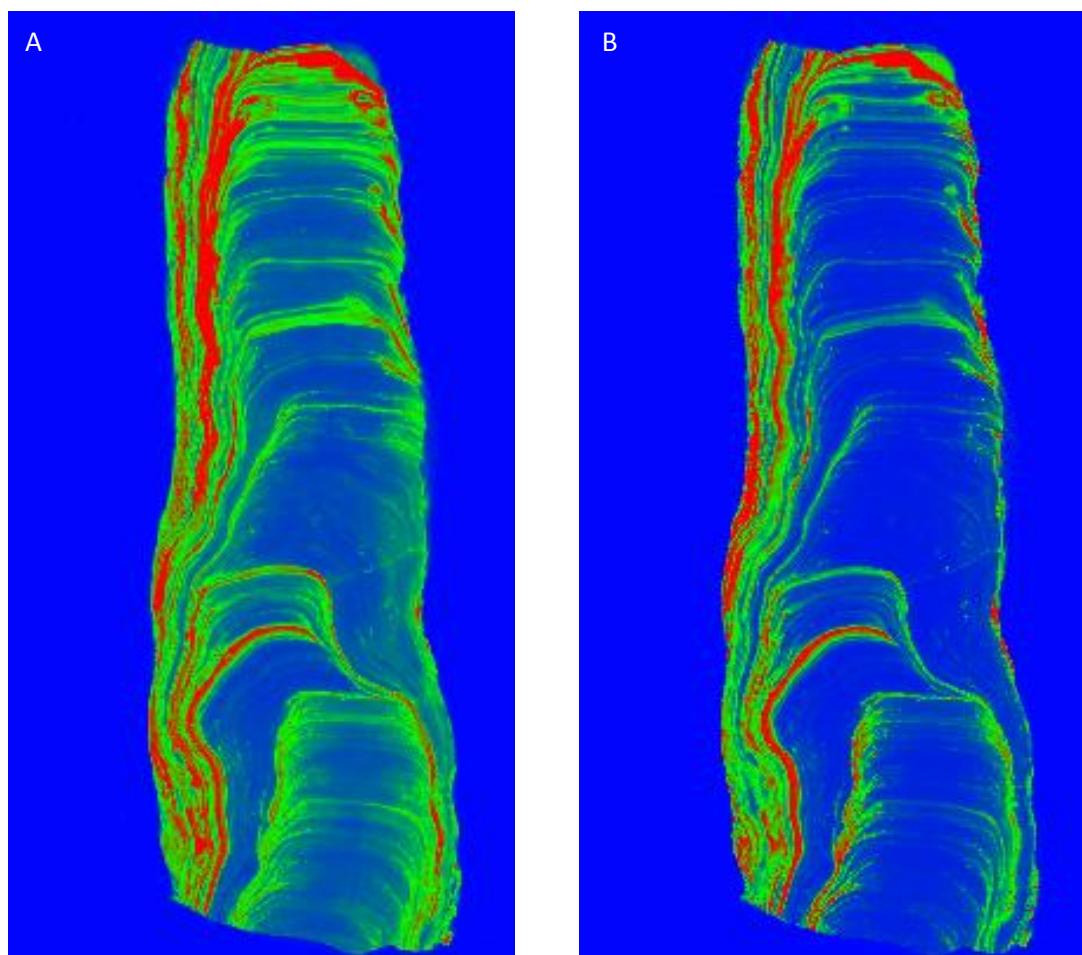


**Figure 6.7** Fluorescence intensity of SK-1. Blue colouring indicates low fluorescence, green indicates higher fluorescence and red colouring indicates highest fluorescence (levels are relative, not absolute). A) Blue (450 nm) laser light image; B) Red (635 nm) laser light image

## 6.2.5 ID-TIMS Results

Several subsamples were cut from the aragonite layer in SK-1 for isotope dilution thermal ionization mass spectrometry (ID-TIMS), with an aim to achieve 10 mg of aragonite per aliquot, and a range of U concentrations and U/Pb ratios. Samples were analysed on a Thermo Triton multicollector mass spectrometer. The U/Pb data collected is shown in Table 6.1. These data, when plotted on a Tera-Wasserburg diagram, produce the plot shown in Figure 6.8.

Sample ID	Total Pb (ppb)	U (ppm)	$^{238}\text{U}/^{206}\text{Pb}$	$2\sigma$ (%)	$^{207}\text{Pb}/^{206}\text{Pb}$	$2\sigma$ (%)	$[\text{}^{234}\text{U}/\text{}^{238}\text{U}]$ measured	$2\sigma$ (%)
SK1.1	82	8.610	349.609	0.165	0.81803	0.081		
SK1.2	48	4.265	298.383	0.368	0.82366	0.085		
SK1.5	115	8.865	259.524	0.407	0.82860	0.081		
SK1.6	36	6.957	615.282	0.670	0.77088	0.109		
SK1.7	74	8.949	398.337	0.330	0.80888	0.082		
SK1.8	54	4.716	295.407	0.495	0.82532	0.097		
SK1.9							1.031	i) 0.065 ii) 0.204

**Table 6.1** ID-TIMS U/Pb data for SK-1. The two  $2\sigma$  values for the  $^{234}\text{U}/^{238}\text{U}$  values reflects the 2 uncertainties used when calculating the corrected age, see Table 7.2

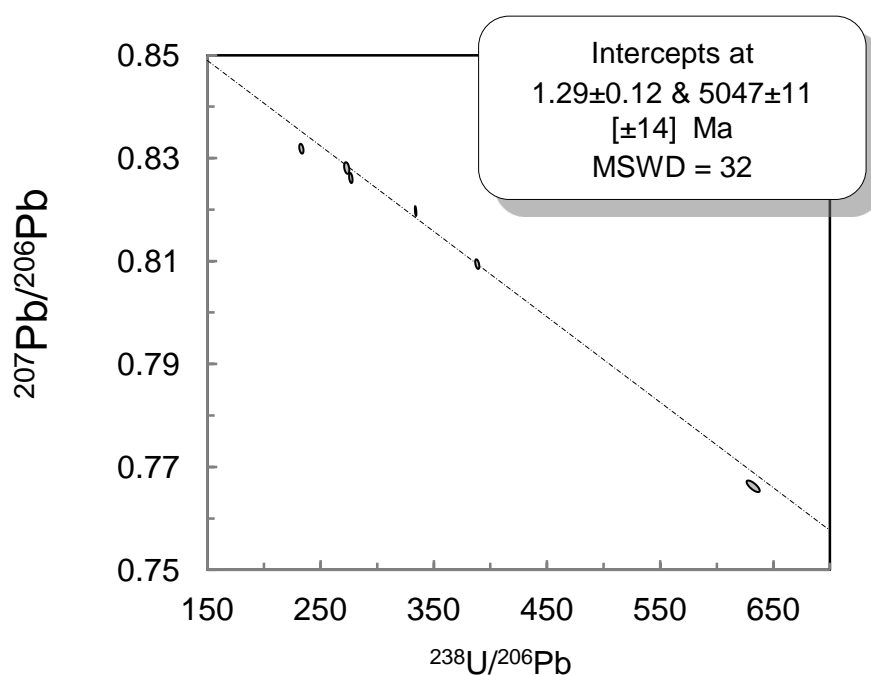


**Figure 6.8** Tera-Wasserburg Diagram for SK-1 ID-TIMS data. Error ellipses are  $2\sigma$ .

The results were then modelled to produce a corrected age. The age of  $1.29 \pm 0.12$  Ma calculated by the Concordia in Figure 7.7 and the measured  $^{234}\text{U}/^{238}\text{U}$  ratio of 1.031 as shown in Table 7.1 were used in this calculation. Two error levels were used on the  $^{234}\text{U}/^{238}\text{U}$  activity ratio; 0.065%  $2\sigma$  and 0.204%  $2\sigma$ . The output of this correction model is shown in Table 7.2. As can be seen, the two different errors used do not produce substantially different results as the uncertainty in the regression dominates the total uncertainty budget.

$[\text{}^{234}\text{U}/\text{}^{238}\text{U}]$ measured	$2\sigma$ (%)	$[\text{}^{234}\text{U}/\text{}^{238}\text{U}]_0$ mean	$2\sigma$ (abs)	$[\text{}^{234}\text{U}/\text{}^{238}\text{U}]_0$ median	Mean corrected age (Ma)	$2\sigma$ (abs)	Median corrected age (Ma)
1.031	0.065	1.756	0.15	1.754	1.129	0.07	1.129
	0.204	1.758	0.15	1.755	1.130	0.07	1.130

**Table 6.2** *Corrected U/Pb data for SK-1 via ID-TIMS analysis*

Both outputs produce an age of approximately  $1.13 \pm 0.07$  Ma. This can be regarded as the most accurate age. The LA-ICP-MS age of  $1.05 \pm 0.09$  Ma agrees within the uncertainty the ID result, both having reasonably small errors. Therefore it seems probable that for some aragonitic or high U samples, LA-ICP-MS analysis may be sufficiently accurate and precise to obtain U/Pb dates, provided an appropriate carbonate standard is used. More comparisons between ages produced by both methods are required verify this.

The fluorescence images from SK-1 indicated that some recrystallisation may have occurred, which may have resulted in open system behaviour. This was further indicated by the fact that 2 samples, which had been spiked with a U/Th solution, returned very different U/Th dating results; one an age of  $700 \pm 100$  kyr BP, typical for a sample that is out of range for U/Th dating, and one an undefined age that did not plot on a  $^{230}\text{Th}/^{238}\text{U}$  vs.  $^{234}\text{U}/^{238}\text{U}$  isochron. This discrepancy may be due to open system behaviour in the second sample. A possible way to avoid this in future samples could be to exclude the outer edges of aragonite layers in suspected recrystallised samples, as these may be more likely to have experienced open system conditions due to proximity to the fluids that caused dissolution-reprecipitation.

# Chapter 7

## Conclusions and Further Work

## 7.1 Introduction

The overall aims of this project were to use speleothems from southwest Turkey and Southern Iran to reconstruct Mid-Late Pleistocene-Holocene palaeoclimate in these little studied areas. The speleothems were analysed geochemically and petrographically, and age models were constructed using U-Series methods. However, two of the three Turkish speleothems and both of the Iranian speleothems exhibited evidence of recrystallisation of aragonite as calcite. This disrupted the U-Series system sufficiently to make the construction of reliable age models difficult. A major component of this project was therefore to investigate whether robust age models could be retrieved from partially recrystallised speleothems, by U/Th dating in the case of DIM-1 from Turkey, and U/Pb dating in the case of SK-1 from Iran.

## 7.2 Dim Cave, SW Turkey

### 7.2.1 Stalagmite DIM-1

DIM-1 was found, by XRD and petrographic analysis, to be composed mainly of calcite, with a change to aragonite just before a hiatus near to the top of the stalagmite. A shift in the growth axis immediately followed the hiatus, above which the stalagmite is again composed of calcite. XRD and SPLS analysis of the 3D structure of DIM-1 revealed extensive recrystallisation of primary aragonite as secondary calcite. It appears that the majority/entirety of DIM-1 was originally composed of aragonite, which has subsequently undergone recrystallisation to calcite, with only the section of aragonite below the hiatus remaining intact.

It is probable that the cause of recrystallisation of primary aragonite in DIM-1 was infiltration by a water film, which occurred soon after the original aragonite growth. The cause of this is inferred to have been periods of high rainfall, which led to flushing events in the epikarst. Drip water flowing over the surface of DIM-1 during these events consequently had a lower Mg/Ca ratio as a result of dilution, allowing calcitisation of the aragonite substrate. This calcitisation due to high rainfall may have occurred annually, with each wet season causing recrystallisation of the previous year's growth, but it is more likely that recrystallisation happened less frequently, perhaps every few years. The extent of the calcitisation implies that the original aragonite was very porous, allowing recrystallising waters to permeate more than one year's growth of carbonate.

For the aragonite below the hiatus to have persisted, an extended arid phase is implied.  $\delta^{18}\text{O}$ ,  $\delta^{13}\text{C}$ , Mg/Ca, Sr/Ca and  $^{87}\text{Sr}/^{86}\text{Sr}$  data also indicate aridity. During the arid phase, waters flowing over the surface of DIM-1 had an elevated Mg/Ca ratio and were not able to calcitize the aragonite surface. The presence of the hiatus supports this conclusion, as it strongly suggests that growth eventually ceased due to aridity. When rainfall began to increase after the dry phase associated with the hiatus, drip waters were only slightly undersaturated with respect to aragonite; this allowed some aragonite to persist on the outer flanks of DIM-1, as waters had reached saturation after flowing over and calcitizing axial sections of DIM-1.

This extensive recrystallisation has important implications for the age model of DIM-1, as uranium may be lost under open system conditions, leading to erroneously old ages. Indeed, the U/Th dating of DIM-1 produced many erroneous ages, although almost all were erroneously young rather than old. Some of these problematic ages were linked to the presence of hiatuses, as in addition to the prominent hiatus, there are probably several “micro-hiatuses”, which are not discernible in hand specimen or thin section, and one of which only became apparent when a stalagmite slab broke along a “micro-hiatus”.

Samples for dating were taken from recrystallised calcite and from primary aragonite. The primary aragonite was sampled from the aragonite region below the main hiatus and from the flanks of the stalagmite where it persisted as the remnants of layers which had been recrystallised in the centre of the stalagmite. 13 out of 23 dates were discarded on geochemical or stratigraphic grounds, the vast majority of these being recrystallised calcite samples, while only 2 out of 7 aragonite samples were discarded for these reasons, both of which were from axial parts of the aragonite region below the hiatus. The five successful aragonite samples were taken from towards the flanks of the stalagmite, however one of these was taken from a layer that projected onto the growth axis above the broken top of the stalagmite and did not directly form part of the age model. The dates from which the age model was constructed all lie within the early part of MIS 5e. There is a high degree of error overlap between dates in the age model, suggesting that any geochemical disruption of the dates from recrystallisation is unlikely to have shifted the calculated errors by more than their  $2\sigma$  error.

The age model for DIM-1 indicates that the speleothem grew between ca 130 kyr BP and 127 kyr BP. This places the growth of DIM-1 during the early Eemian, and the timing of a trend towards more negative  $\delta^{18}\text{O}$  values, indicative of wetter conditions at ca.  $128.6 \pm 0.7$

kyr BP, is similar to the timings of wet periods associated with the Eemian in several other records, such as those from Soreq and Corchia caves (Bar-Matthews et al., 2003, Drysdale et al., 2005). The arid phase recorded in DIM-1 strongly suggests that climate was not stable during early MIS 5e in SW Turkey, and the dating strongly suggests that it can be correlated with arid phases identified in France (Couchoud et al., 2009), Italy (Drysdale et al., 2009), and Israel (Grant et al., 2012) at this time.

### **7.2.2 Stalagmite DIM-3**

DIM-3 grew on the side of DIM-1 after the latter had toppled, and U/Th dating reveals that it was active during the early Holocene (ca 8-7 kyr BP). DIM-3 is composed of primary aragonite. Comparison of DIM-1 and DIM-3 stable isotope data shows that during the brief period of growth of DIM-3, the climate was probably drier than early MIS 5e, and since the period of growth was brief, it appears that the remainder of the Holocene was drier still. The deposition of DIM-3 correlates with a pluvial event which occurred over large parts of the eastern Mediterranean region, known as the Early Holocene Wet Period, and with the formation of Sapropel 1.

The wet period associated with the growth of DIM-3, and likely subsequent aridification that terminated its growth, may have had important implications for local human settlements. For example, the expansion of Neolithic farming methods from the Fertile Crescent into Turkey may have occurred due to the dry conditions at ca 7 kyr BP, as agriculture provided a more stable means of procuring food than the hunter-gatherer methods of the Mesolithic (Frisia et al., 2006).

### **7.2.3 Stalagmite DIM-2**

DIM-2 was identified as a likely recrystallised speleothem by observation in hand specimen, and confirmed by the nature of petrographic fabrics and their boundary morphologies. Aragonite relics observed in calcite regions provided clear evidence of recrystallisation. Therefore, DIM-2 presented an opportunity to investigate in some detail the geochemical properties of primary aragonite and replacement calcite in a speleothem. An attempt was made to date the primary aragonite sections, however this was unsuccessful, as although the bottom section of primary aragonite appeared to produce a reasonable chronology, all dates from the top section were erroneously old. These old ages most likely arose from U loss due to open system behaviour, indicating that although the aragonite looked pristine, recrystallisation had occurred on some scale. Therefore it was not possible to produce an

age model for the stalagmite, although the bottom section of primary aragonite appears to have grown during the period ca 112-110 kyr BP. The trace element and stable isotope data for DIM-2 support the conclusion that the original geochemical signature of the primary aragonite in DIM-2 has been lost, as they appear to record the compositions of the recrystallising waters and bear little resemblance to the geochemical signature of the primary aragonite sections.

## **7.3 Iranian Speleothems**

### **7.3.1 Stalagmite TG-6**

The interpretation of geochemical data from stalagmite TG-6 from Torang Cave in SW Iran was hindered by a poor age model. This was a consequence of large errors on ages, and an erroneous age from a sample taken too close to a depositional hiatus. The onset of growth ( $326 \pm 26$  kyr BP) probably occurred at the start of MIS 9, a very wet interglacial. Two depositional hiatuses probably indicate climatic variability and instability, most likely arid conditions. The lower hiatus is tentatively correlated with a vegetation collapse in Greece ca 280-265 kyr BP (Tzedakis et al., 2003b). It is inferred that growth of TG-6 then continued through MIS 8, at which time cold temperatures reduced evaporation, thereby increasing effective precipitation and allowing speleothem growth. None of the sampled ages are close to the upper hiatus, making pinpointing its duration problematic. However, due to the importance of effective precipitation in controlling the growth of TG-6, it is suggested that growth ceased at the upper hiatus during MIS 7e, and then resumed during MIS 7d.

This interpretation is in large part hypothetical due to the poor age model, and requires further dating before any conclusions can be drawn with certainty.

### **7.3.2 Stalagmite SK-1**

An attempt was made to date SK-1, a speleothem beyond the range of U/Th dating from Sehlak Cave, SW Iran. U/Pb methods were used, with both LA-ICP-MS and ID-TIMS methods combined to determine if LA-ICP-MS could produce dates of sufficient accuracy and precision when using a carbonate standard.

Autoradiography identified only one region of high U, a prerequisite for successful U/Pb dating, in an aragonitic layer. This sample was analysed by both LA-ICP-MS and ID-TIMS, and both approaches were successful, producing ages within error of each other and of comparable precision. ID-TIMS produced an age of  $1.13 \pm 0.07$  Ma, while LA-ICP-MS

produced an age of  $1.05 \pm 0.09$  Ma. Therefore, it appears that LA-ICP-MS may be an appropriate method for dating speleothems beyond the range of U/Th, provided a carbonate standard is used, U content is sufficiently high and common lead content is sufficiently low.

#### **7.4 Future Work**

DIM-1 has demonstrated the presence of a brief arid phase early in MIS 5e, an episode not previously recorded in the region. However, the chronology is partially compromised by recrystallisation and a high priority should be to find another speleothem of similar age to confirm the interpretation and generate a high precision chronology.

Improved dating of TG-6 should be possible, but most of the current dates need to be replicated in order to produce a more coherent chronology. At the current level of precision, it is not possible to draw confident conclusions about the timing of the inferred palaeoclimatic trends.

Use of LA-ICP-MS as a standalone method for dating of older speleothems appears promising; to verify this it is necessary to sample more speleothems beyond the range of U/Th dating, and date them using the U/Pb methodology tested here to date SK-1.

## References

- AL-AASM, I. S. & VEIZER, J. 1986a. DIAGENETIC STABILIZATION OF ARAGONITE AND LOW-MG CALCITE .2. STABLE ISOTOPES IN RUDISTS. *Journal of Sedimentary Petrology*, 56, 763-770.
- AL-AASM, I. S. & VEIZER, J. 1986b. DIAGENETIC STABILIZATION OF ARAGONITE AND LOW-MG CALCITE .1. TRACE-ELEMENTS IN RUDISTS. *Journal of Sedimentary Petrology*, 56, 138-152.
- ALIJANI, B. 1997. *The Weather of Iran*, Payame Nour Publication Series (in Persian).
- ALIJANI, B. & HARMAN, J. R. 1985. SYNOPTIC CLIMATOLOGY OF PRECIPITATION IN IRAN. *Annals of the Association of American Geographers*, 75, 404-416.
- ALMOGI-LABIN, A., BAR-MATTHEWS, M., SHRIKI, D., KOLOSOVSKY, E., PATERNE, M., SCHILMAN, B., AYALON, A., AIZENSHTAT, Z. & MATTHEWS, A. 2009. Climatic variability during the last ~90 ka of the southern and northern Levantine Basin as evident from marine records and speleothems. *Quaternary Science Reviews*, 28, 2882-2896.
- ALONSO-ZARZA, A. M., MARTÍN-PÉREZ, A., MARTÍN-GARCÍA, R., GIL-PEÑA, I., MELÉNDEZ, A., MARTÍNEZ-FLORES, E., HELLSTROM, J. & MUÑOZ-BARCO, P. 2011. Structural and host rock controls on the distribution, morphology and mineralogy of speleothems in the Castañar Cave (Spain). *Geological Magazine*, 148, 211-225.
- ALPERT, P., NEEMAN, B. U. & SHAY-EL, Y. 1990. Intermonthly Variability of Cyclone Tracks in the Mediterranean. *Journal of Climate*, 3, 1474-1478.
- ALPERT, P., OSETINSKY, I., ZIV, B. & SHAFIR, H. 2004. A new seasons definition based on classified daily synoptic systems: An example for the Eastern Mediterranean. *International Journal of Climatology*, 24, 1013-1021.
- AMEMIYA, Y. & MIYAHARA, J. 1988. IMAGING PLATE ILLUMINATES MANY FIELDS. *Nature*, 336, 89-90.
- AN, Z. & PORTER, S. C. 1997. Millennial-scale climatic oscillations during the last interglaciation in central China. *Geology*, 25, 603-606.
- ANDERSEN, M. B., STIRLING, C. H., POTTER, E.-K., HALLIDAY, A. N., BLAKE, S. G., MCCULLOCH, M. T., AYLING, B. F. & O'LEARY, M. 2008. High-precision U-series measurements of more than 500,000 year old fossil corals. *Earth and Planetary Science Letters*, 265, 229-245.
- ANDERSON, T. F. & ARTHUR, M. A. 1983. Stable isotopes of oxygen and carbon and their application to sedimentological and palaeoenvironmental problems. In: ARTHUR, M. A., ANDERSON, T. F., KAPLAN, I. R., VEIZER, J. & LAND, L. S. (eds.) *Stable Isotopes in Sedimentary Geochemistry*. Society of Economic Palaeontologists and Mineralogists Short Course.
- ANTOINE, D., MOREL, A. & ANDRÉ, J.-M. 1995. Algal pigment distribution and primary production in the eastern Mediterranean as derived from coastal zone color scanner observations. *J. Geophys. Res.*, 100, 16193-16209.
- ARIZTEGUI, D., ASIOLI, A., LOWE, J. J., TRINCARDI, F., VIGLIOTTI, L., TAMBURINI, F., CHONDROGIANNI, C., ACCORSI, C. A., MAZZANTI, M. B., MERCURI, A. M., VAN DER KAARS, S., MCKENZIE, J. A. & OLDFIELD, F. 2000. Palaeoclimate and the formation of sapropel S1: inferences from Late Quaternary lacustrine and marine sequences in the central Mediterranean region. *Palaeogeography Palaeoclimatology Palaeoecology*, 158, 215-240.
- ARMITAGE, S. J., DRAKE, N. A., STOKES, S., EL-HAWAT, A., SALEM, M. J., WHITE, K., TURNER, P. & MCLAREN, S. J. 2007. Multiple phases of North African humidity recorded in

- lacustrine sediments from the Fazzan Basin, Libyan Sahara. *Quaternary Geochronology*, 2, 181-186.
- ASRAT, A., BAKER, A., MOHAMMED, M. U., LENG, M. J., VAN CALSTEREN, P. & SMITH, C. 2007. A high-resolution multi-proxy stalagmite record from Mechara, Southeastern Ethiopia: palaeohydrological implications for speleothem palaeoclimate reconstruction. *Journal of Quaternary Science*, 22, 53-63.
- ASTILLEROS, J. M., PINA, C. M., FERNANDEZ-DIAZ, L. & PUTNIS, A. 2003. Metastable phenomena on calcite {101<sup>-4</sup>} surfaces growing from Sr<sup>2+</sup>-Ca<sup>2+</sup>-CO<sub>3</sub><sup>2-</sup> aqueous solutions. *Chemical Geology*, 193, 93-107.
- ATKINSON, T. C. 1977. Carbon dioxide in atmosphere of unsaturated zone - important control of groundwater hardness in limestones. *Journal of Hydrology*, 35, 111-123.
- AULER, A. S. & SMART, P. L. 2004. Rates of condensation corrosion in speleothems of semi-arid northeastern Brazil. *Speleogenesis and Evolution of Karst Aquifers*, 2.
- AYALON, A., BAR-MATTHEWS, M. & SASS, E. 1998. Rainfall-recharge relationships within a karstic terrain in the eastern Mediterranean semi-arid region, Israel: delta O-18 and delta D characteristics. *Journal of Hydrology*, 207, 18-31.
- AYALON, A., BAR-MATTHEWS, M. & KAUFMAN, A. 1999. Petrography, strontium, barium and uranium concentrations, and strontium and uranium isotope ratios in speleothems as palaeoclimatic proxies: Soreq Cave, Israel. *Holocene*, 9, 715-722.
- BAKER, A. & SMART, P. L. 1995. Recent flowstone growth rates: Field measurements in comparison to theoretical predictions. *Chemical Geology*, 122, 121-128.
- BAKER, A. & BOLTON, L. 2000. Speleothem organic acid luminescence intensity ratios: a new palaeoenvironmental proxy. *Cave and Karst Science*, 27, 121-124.
- BAKER, A. & BRUNSDON, C. 2003. Non-linearities in drip water hydrology: an example from Stump Cross Caverns, Yorkshire. *Journal of Hydrology*, 277, 151-163.
- BAKER, A., SMART, P. L., EDWARDS, R. L. & RICHARDS, D. A. 1993a. Annual growth banding in a cave stalagmite. *Nature*, 364, 518-520.
- BAKER, A., SMART, P. L. & FORD, D. C. 1993b. Northwest European palaeoclimate as indicated by growth frequency variations of secondary calcite deposits. *Palaeogeography, Palaeoclimatology, Palaeoecology*, 100, 291-301.
- BAKER, A., SMART, P. L. & EDWARDS, R. L. 1995. PALEOCLIMATE IMPLICATIONS OF MASS-SPECTROMETRIC DATING OF A BRITISH FLOWSTONE. *Geology*, 23, 309-312.
- BAKER, A., ITO, E., SMART, P. L. & MCEWAN, R. F. 1997. Elevated and variable values of <sup>13</sup>C in speleothems in a British cave system. *Chemical Geology*, 136, 263-270.
- BAKER, A., GENTY, D. & SMART, P. L. 1998a. High-resolution records of soil humification and paleoclimate change from variations in speleothem luminescence excitation and emission wavelengths. *Geology*, 26, 903-906.
- BAKER, A., GENTY, D., DREYBRODT, W., BARNES, W. L., MOCKLER, N. J. & GRAPES, J. 1998b. Testing theoretically predicted stalagmite growth rate with Recent annually laminated samples: Implications for past stalagmite deposition. *Geochimica et Cosmochimica Acta*, 62, 393-404.
- BAKER, A., MOCKLER, N. J. & BARNES, W. L. 1999. Fluorescence intensity variations of speleothem-forming groundwaters: Implications for paleoclimate reconstruction. *Water Resources Research*, 35, 407-413.
- BAKER, A., GENTY, D. & FAIRCHILD, I. J. 2000. Hydrological characterisation of stalagmite dripwaters at Grotte de Villars, Dordogne, by the analysis of inorganic species and luminescent organic matter. *Hydrology and Earth System Sciences*, 4, 439-449.
- BAKER, A., ASRAT, A., FAIRCHILD, I. J., LENG, M. J., WYNN, P. M., BRYANT, C., GENTY, D. & UMER, M. 2007. Analysis of the climate signal contained within [delta]18O and growth rate parameters in two Ethiopian stalagmites. *Geochimica et Cosmochimica Acta*, 71, 2975-2988.

- BAKER, P. A., SELTZER, G. O., FRITZ, S. C., DUNBAR, R. B., GROVE, M. J., TAPIA, P. M., CROSS, S. L., ROWE, H. D. & BRODA, J. P. 2001. The history of South American tropical precipitation for the past 25,000 years. *Science*, 291, 640-643.
- BALDINI, J. U. L. 2010. Cave atmosphere controls on stalagmite growth rate and palaeoclimate records. In: PEDLEY, H. M. & ROGERSON, M. (eds.) *Tufas and Speleothems: Unravelling the Microbial and Physical Controls*. London: Geological Society of London Special Publication.
- BALDINI, J. U. L., MCDERMOTT, F. & FAIRCHILD, I. J. 2002. Structure of the 8200-year cold event revealed by a speleothem trace element record (Retracted Article. See vol 317, pg 748, 2007). *Science*, 296, 2203-2206.
- BALDINI, J. U. L., MCDERMOTT, F., BAKER, A., BALDINI, L. M., MATTEY, D. P. & RAILSBACK, L. B. 2005. Biomass effects on stalagmite growth and isotope ratios: A 20th century analogue from Wiltshire, England. *Earth and Planetary Science Letters*, 240, 486-494.
- BALDINI, J. U. L., MCDERMOTT, F. & FAIRCHILD, I. J. 2006a. Spatial variability in cave drip water hydrochemistry: Implications for stalagmite paleoclimate records. *Chemical Geology*, 235, 390-404.
- BALDINI, J. U. L., BALDINI, L. M., MCDERMOTT, F. & CLIPSON, N. 2006b. Carbon dioxide sources, sinks, and spatial variability in shallow temperate zone caves: Evidence from Ballynamindra Cave, Ireland. *Journal of Cave and Karst Studies*, 68, 4-11.
- BALDINI, J. U. L., MCDERMOTT, F., HOFFMANN, D. L., RICHARDS, D. A. & CLIPSON, N. 2008a. Very high-frequency and seasonal cave atmosphere P(CO<sub>2</sub>) variability: Implications for stalagmite growth and oxygen isotope-based paleoclimate records. *Earth and Planetary Science Letters*, 272, 118-129.
- BALDINI, L. M., MCDERMOTT, F., FOLEY, A. M. & BALDINI, J. U. L. 2008b. Spatial variability in the European winter precipitation delta O-18-NAO relationship: Implications for reconstructing NAO-mode climate variability in the Holocene. *Geophysical Research Letters*, 35.
- BANNER, J. L. 1995. APPLICATION OF THE TRACE-ELEMENT AND ISOTOPE GEOCHEMISTRY OF STRONTIUM TO STUDIES OF CARBONATE DIAGENESIS. *Sedimentology*, 42, 805-824.
- BANNER, J. L. & KAUFMAN, J. 1994. THE ISOTOPIC RECORD OF OCEAN CHEMISTRY AND DIAGENESIS PRESERVED IN NONLUMINESCENT BRACHIOPODS FROM MISSISSIPPIAN CARBONATE ROCKS, ILLINOIS AND MISSOURI. *Geological Society of America Bulletin*, 106, 1074-1082.
- BANNER, J. L., MUSGROVE, M. L., ASMEROM, Y., EDWARDS, R. L. & HOFF, J. A. 1996. High-resolution temporal record of Holocene ground-water chemistry: Tracing links between climate and hydrology. *Geology*, 24, 1049-1053.
- BANNER, J. L., GUILFOYLE, A., JAMES, E. W., STERN, L. A. & MUSGROVE, M. 2007. Seasonal variations in modern speleothem calcite growth in Central Texas, USA. *Journal of Sedimentary Research*, 77, 615-622.
- BAR-MATTHEWS, M. & AYALON, A. 2011. Mid-Holocene climate variations revealed by high-resolution speleothem records from Soreq Cave, Israel and their correlation with cultural changes. *Holocene*, 21, 163-171.
- BAR-MATTHEWS, M., MATTHEWS, A. & AYALON, A. 1991. Environmental Controls of Speleothem Mineralogy in a Karstic Dolomitic Terrain (Soreq Cave, Israel). *The Journal of Geology*, 99, 189-207.
- BAR-MATTHEWS, M., AYALON, A., MATTHEWS, A., SASS, E. & HALICZ, L. 1996. Carbon and oxygen isotope study of the active water-carbonate system in a karstic Mediterranean cave: Implications for paleoclimate research in semiarid regions. *Geochimica et Cosmochimica Acta*, 60, 337-347.

- BAR-MATTHEWS, M., AYALON, A. & KAUFMAN, A. 1997. Late quaternary paleoclimate in the eastern Mediterranean region from stable isotope analysis of speleothems at Soreq Cave, Israel. *Quaternary Research*, 47, 155-168.
- BAR-MATTHEWS, M., AYALON, A., KAUFMAN, A. & WASSERBURG, G. J. 1999. The Eastern Mediterranean paleoclimate as a reflection of regional events: Soreq cave, Israel. *Earth and Planetary Science Letters*, 166, 85-95.
- BAR-MATTHEWS, M., AYALON, A. & KAUFMAN, A. 2000. Timing and hydrological conditions of Sapropel events in the Eastern Mediterranean, as evident from speleothems, Soreq cave, Israel. *Chemical Geology*, 169, 145-156.
- BAR-MATTHEWS, M., AYALON, A., GILMOUR, M., MATTHEWS, A. & HAWKESWORTH, C. J. 2003. Sea-land oxygen isotopic relationships from planktonic foraminifera and speleothems in the Eastern Mediterranean region and their implication for paleorainfall during interglacial intervals. *Geochimica Et Cosmochimica Acta*, 67, 3181-3199.
- BAR-YOSEF MAYER, D. E., LENG, M. J., ALDRIDGE, D. C., ARROWSMITH, C., GÜMÜŞ, B. A. & SLOANE, H. J. 2012. Modern and early-middle Holocene shells of the freshwater mollusc *Unio*, from Çatalhöyük in the Konya Basin, Turkey: preliminary palaeoclimatic implications from molluscan isotope data. *Journal of Archaeological Science*, 39, 76-83.
- BARD, E., DELAYGUE, G., ROSTEK, F., ANTONIOLI, F., SILENZI, S. & SCHRAG, D. P. 2002. Hydrological conditions over the western Mediterranean basin during the deposition of the cold Sapropel 6 (ca. 175 kyr BP). *Earth and Planetary Science Letters*, 202, 481-494.
- BARTH, H. J. & STEINKOHL, F. 2004. Origin of winter precipitation in the central coastal lowlands of Saudi Arabia. *Journal of Arid Environments*, 57, 101-115.
- BATHURST 1964. The replacement of aragonite by calcite in the molluscan shell wall. In: IMBRIE, J. & NEWELL, N. D. (eds.) *Approaches to paleo-ecology*. New York: Wiley.
- BAYKARA, O. 2009. *RE: Pers. Comm.*
- BECK, J. W., RICHARDS, D. A., EDWARDS, R. L., SILVERMAN, B. W., SMART, P. L., DONAHUE, D. J., HERERRA-OSTERHELD, S., BURR, G. S., CALSOYAS, L., JULL, A. J. T. & BIDDULPH, D. 2001. Extremely large variations of atmospheric C-14 concentration during the last glacial period. *Science*, 292, 2453-2458.
- BECK, W. C., GROSSMAN, E. L. & MORSE, J. W. 2005. Experimental studies of oxygen isotope fractionation in the carbonic acid system at 15 degrees, 25 degrees, and 40 degrees C. *Geochimica et Cosmochimica Acta*, 69, 3493-3503.
- BERGER, A. & LOUTRE, M. F. 1991. Insolation values for the climate of the last 10 million years. *Quaternary Science Reviews*, 10, 297-317.
- BERGER, J.-F. O. & GUILAINE, J. 2009. The 8200 cal BP abrupt environmental change and the Neolithic transition: A Mediterranean perspective. *Quaternary International*, 200, 31-49.
- BERNER, R. A. 1966. CHEMICAL DIAGENESIS OF SOME MODERN CARBONATE SEDIMENTS. *American Journal of Science*, 264, 1-&.
- BERNER, R. A. 1975. The role of magnesium in the crystal growth of calcite and aragonite from sea water. *Geochimica et Cosmochimica Acta*, 39, 489-494, IN3, 495-504.
- BETHOUX, J. P. 1979. BUDGETS OF THE MEDITERRANEAN SEA - THEIR DEPENDANCE ON THE LOCAL CLIMATE AND ON THE CHARACTERISTICS OF THE ATLANTIC WATERS. *Oceanologica Acta*, 2, 157-163.
- BILLÈS, G., CORTEZ, J. & LOSSAINT, P. 1971. L'activité biologique des sols dans les écosystèmes méditerranéens, I. Minéralisation du carbone. *Rev. Ecol. Biol. Sol.*, 8, 375-395.

- BISCHOFF, J. L. & FYFE, W. S. 1968. CATALYSIS INHIBITION AND CALCITE-ARAGONITE PROBLEM .I. ARAGONITE-CALCITE TRANSFORMATION. *American Journal of Science*, 266, 65-&.
- BITAN, A. & SAARONI, H. 1992. THE HORIZONTAL AND VERTICAL EXTENSION OF THE PERSIAN GULF PRESSURE TROUGH. *International Journal of Climatology*, 12, 733-747.
- BLISNIUK, P. M. & STERN, L. A. 2005. Stable isotope paleoaltimetry: A critical review. *American Journal of Science*, 305, 1033-1074.
- BOCH, R., SPÄTTL, C. & KRAMERS, J. 2009. High-resolution isotope records of early Holocene rapid climate change from two coeval stalagmites of Katerloch Cave, Austria. *Quaternary Science Reviews*, 28, 2527-2538.
- BOCH, R., SPOETL, C. & FRISIA, S. 2011. Origin and palaeoenvironmental significance of lamination in stalagmites from Katerloch Cave, Austria. *Sedimentology*, 58, 508-531.
- BÖGLI, A. 1960. Lakosung unde Karrenbildung. *Zeitschrift fur Geomorphologie, Suppl.*, 2, 4-21 (Translated by M. Fargher in Sweeting, M.M. (Ed.) 1981 *Karst Geomorphology*, Stroudsburg, PA: Hutchinson Ross, pp. 64-89).
- BOHM, F., JOACHIMSKI, M. M., DULLO, W. C., EISENHAEUER, A., LEHNERT, H., REITNER, J. & WORHEIDE, G. 2000. Oxygen isotope fractionation in marine aragonite of coralline sponges. *Geochimica et Cosmochimica Acta*, 64, 1695-1703.
- BORSATO, A., FRISIA, S., FAIRCHILD, I. J., SOMOGYI, A. & SUSINI, J. 2007. Trace element distribution in annual stalagmite laminae mapped by micrometer-resolution X-ray fluorescence: Implications for incorporation of environmentally significant species. *Geochimica et Cosmochimica Acta*, 71, 1494-1512.
- BOSCH, H. J., SINNINGE DAMSTÉ, J. S. & DE LEEUW, J. W. 1998. Molecular paleontology of Eastern Mediterranean sapropels: evidence for photic zone anoxia. In: ROBERTSON, A. H. F., EMEIS, K. C., RICHTER, C. & CAMERLENGHI, A. (eds.) *Proc. ODP Sci Res. 160* College Station, TX: Ocean Drilling Program.
- BOTTRELL, S. H. & ATKINSON, T. C. 1992. TRACER STUDY OF FLOW AND STORAGE IN THE UNSATURATED ZONE OF A KARSTIC LIMESTONE AQUIFER. *Tracer Hydrology*.
- BOURGES, F., MANGIN, A. & D'HULST, D. 2001. Carbon dioxide in karst cavity atmosphere dynamics: the example of the Aven d'Orgnac (Ardeche). *Comptes Rendus De L Academie Des Sciences Serie Ii Fascicule a-Sciences De La Terre Et Des Planetes*, 333, 685-692.
- BOURGES, F., GENTHON, P., MANGIN, A. & D'HULST, D. 2006. Microclimates of l'Aven d'Orgnac and other French limestone caves (Chauvet, Esparros, Marsoulas). *International Journal of Climatology*, 26, 1651-1670.
- BRAND, U. 1989. ARAGONITE-CALCITE TRANSFORMATION BASED ON PENNSYLVANIAN MOLLUSKS. *Geological Society of America Bulletin*, 101, 377-390.
- BRAND, U. & VEIZER, J. 1980. CHEMICAL DIAGENESIS OF A MULTICOMPONENT CARBONATE SYSTEM .1. TRACE-ELEMENTS. *Journal of Sedimentary Petrology*, 50, 1219-1236.
- BROOK, G. A., RAFTER, M. A., RAILSBACK, L. B., SHEEN, S. W. & LUNDBERG, J. 1999. A high-resolution proxy record of rainfall and ENSO since AD 1550 from layering in stalagmites from Anjohibe Cave, Madagascar. *Holocene*, 9, 695-705.
- BROOK, G. A., ELLWOOD, B. B., RAILSBACK, L. B. & COWART, J. B. 2006. A 164 ka record of environmental change in the American Southwest from a Carlsbad Cavern speleothem. *Palaeogeography, Palaeoclimatology, Palaeoecology*, 237, 483-507.
- BUCHARDT, B. & WEINER, S. 1981. DIAGENESIS OF ARAGONITE FROM UPPER CRETACEOUS AMMONITES - A GEOCHEMICAL CASE-STUDY. *Sedimentology*, 28, 423-438.

- BUDD, D. A. 1988. ARAGONITE-TO-CALCITE TRANSFORMATION DURING FRESH-WATER DIAGENESIS OF CARBONATES - INSIGHTS FROM PORE-WATER CHEMISTRY. *Geological Society of America Bulletin*, 100, 1260-1270.
- BURNS, S. J., MATTER, A., FRANK, N. & MANGINI, A. 1998. Speleothem-based paleoclimate record from northern Oman. *Geology*, 26, 499-502.
- BURNS, S. J., FLEITMANN, D., MATTER, A., NEFF, U. & MANGINI, A. 2001. Speleothem evidence from Oman for continental pluvial events during interglacial periods. *Geology*, 29, 623-626.
- BURSTEIN, E. A. & EMELIANENKO, V. I. 1996. Log-normal description of fluorescence spectra of organic fluorophores. *Photochemistry and Photobiology*, 64, 316-320.
- BURTON, E. A. & WALTER, L. M. 1987. RELATIVE PRECIPITATION RATES OF ARAGONITE AND MG CALCITE FROM SEAWATER - TEMPERATURE OR CARBONATE ION CONTROL. *Geology*, 15, 111-114.
- BUTZER, K. W., WASHBOUR, C., RICHARDS, J. L. & ISAAC, G. L. 1972. RADIOCARBON DATING OF EAST AFRICAN LAKE LEVELS. *Science*, 175, 1069-&.
- CABROL, P. 1978. *Contribution à l'étude du concrétionnement carbonaté des grottes du sud de la France, morphologie, génèse, diagénèse.*, Montpellier, France.
- CABROL, P. & COUDRAY, J. 1978. Influence des facteurs hydrologiques sur la localisation la forme, la nature minéralogique et la diagenese des concrétions carbonatées des grottes. *Centre d'Etudes Recherches Geol. Hydrogeol., Univ. Montpellier*, 675-700.
- CABROL, P. & COUDRAY, J. 1982. Climatic Fluctuations Influence the Genesis and Diagenesis of Carbonate Speleothems in Southwestern France. *National Speleological Society Bulletin*, 44, 112-117.
- CALVERT, S. E. & FONTUGNE, M. R. 2001. On the late Pleistocene-Holocene sapropel record of climatic and oceanographic variability in the eastern Mediterranean. *Paleoceanography*, 16, 78-94.
- CAMCI ÇETIN, S., KARACA, A., HAKTANIR, K. & YILDIZ, H. 2007. Global attention to Turkey due to desertification. *Environmental monitoring and assessment*, 128, 489-93.
- CAPO, R. C. & DEPAOLO, D. J. 1990. Seawater Strontium Isotopic Variations from 2.5 Million Years Ago to the Present. *Science*, 249, 51-55.
- CAPO, R. C., STEWART, B. W. & CHADWICK, O. A. 1998. Strontium isotopes as tracers of ecosystem processes: theory and methods. *Geoderma*, 82, 197-225.
- CARL, C., WENDT, I. & WENDT, J. I. 1989. U/PB WHOLE-ROCK AND MINERAL DATING OF THE FALKENBERG GRANITE IN NORTHEAST BAVARIA. *Earth and Planetary Science Letters*, 94, 236-244.
- CERLING, T. E. 1984. The stable isotopic composition of modern soil carbonate and its relationship to climate. *Earth and Planetary Science Letters*, 71, 229-240.
- CHAFETZ, H. S., RUSH, P. F. & UTECH, N. M. 1991. MICROENVIRONMENTAL CONTROLS ON MINERALOGY AND HABIT OF CaCO<sub>3</sub> PRECIPITATES - AN EXAMPLE FROM AN ACTIVE TRAVERTINE SYSTEM. *Sedimentology*, 38, 107-126.
- CHARLES, C. D., RIND, D., JOUZEL, J., KOSTER, R. D. & FAIRBANKS, R. G. 1994. GLACIAL-INTERGLACIAL CHANGES IN MOISTURE SOURCES FOR GREENLAND - INFLUENCES ON THE ICE CORE RECORD OF CLIMATE. *Science*, 263, 508-511.
- CHEDDADI, R. & ROSSIGNOL-STRICK, M. 1995. Eastern Mediterranean Quaternary Paleoclimates from Pollen and Isotope Records of Marine Cores in the Nile Cone Area. *Paleoceanography*, 10, 291-300.
- CHEDDADI, R., LAMB, H. F., GUIOT, J. & VAN DER KAARS, S. 1998. Holocene climatic change in Morocco: a quantitative reconstruction from pollen data. *Climate Dynamics*, 14, 883-890.
- CHENG, H., EDWARDS, R. L., HOFF, J., GALLUP, C. D., RICHARDS, D. A. & ASMEROM, Y. 2000. The half-lives of uranium-234 and thorium-230. *Chemical Geology*, 169, 17-33.

- CHENG, H., EDWARDS, R. L., BROECKER, W. S., DENTON, G. H., KONG, X. G., WANG, Y. J., ZHANG, R. & WANG, X. F. 2009. Ice Age Terminations. *Science*, 326, 248-252.
- CHERNOV, A. A. 1984. *Modern Crystallography III Crystal Growth*, Berlin, Springer-Verlag.
- CHRISTENSEN, J. H., HEWITSON, B., BUSUIOC, A., CHEN, A., GAO, X., HELD, I., JONES, R. & AL., E. 2007. Regional climate projections. In: SOLOMON, S., QIN, D., MANNING, M., CHEN, Z., MARQUIS, M., AVERYT, K. B., TIGNOR, M. & MILLER, H. I. (eds.) *Climate Change 2007: The Physical Science Basis. Contribution of Working Group I to the Fourth Assessment Report of the Intergovernmental Panel on Climate Change. Fourth Assessment Report of the Intergovernmental Panel on Climate Change*. Cambridge University Press.
- CITA, M. B., VERGNAUDGRAZZINI, C., ROBERT, C., CHAMLEY, H., CIARANFI, N. & DONOFRIO, S. 1977. PALEOCLIMATIC RECORD OF A LONG DEEP-SEA CORE FROM EASTERN MEDITERRANEAN. *Quaternary Research*, 8, 205-235.
- CLARK, I. & FRITZ, P. 1997. *Environmental Isotopes in Hydrogeology*, CRC Press.
- CLARK, I. D. & FONTES, J.-C. 1990. Paleoclimatic reconstruction in northern Oman based on carbonates from hyperalkaline groundwaters. *Quaternary Research*, 33, 320-336.
- CLIFF, R. A., SPOETL, C. & MANGINI, A. 2010. U-Pb dating of speleothems from Spannagel Cave, Austrian Alps: A high resolution comparison with U-series ages. *Quaternary Geochronology*, 5, 452-458.
- COBB, K. M., ADKINS, J. F., PARTIN, J. W. & CLARK, B. 2007. Regional-scale climate influences on temporal variations of rainwater and cave dripwater oxygen isotopes in northern Borneo. *Earth and Planetary Science Letters*, 263, 207-220.
- COHMAP MEMBERS 1988. Climatic changes of the last 18,000 years: observations and model simulations. *Science*, 241, 1043-52.
- COLE, J. E., RIND, D., WEBB, R. S., JOUZEL, J. & HEALY, R. 1999. Climatic controls on interannual variability of precipitation delta O-18: Simulated influence of temperature, precipitation amount, and vapor source region. *Journal of Geophysical Research-Atmospheres*, 104, 14223-14235.
- COLE, J. M., NIENSTEDT, J., SPATARO, G., RASBURY, E. T., LANZIROTTI, A., CELESTIAN, A. J., NILSSON, M. & HANSON, G. N. 2003. Phosphor imaging as a tool for in situ mapping of ppm levels of uranium and thorium in rocks and minerals. *Chemical Geology*, 193, 127-136.
- COPLIN, T. B. 1996. New guidelines for reporting stable hydrogen, carbon, and oxygen isotope-ratio data. *Geochimica et Cosmochimica Acta*, 60, 3359-3360.
- COPLIN, T. B. 2007. Calibration of the calcite-water oxygen-isotope geothermometer at Devils Hole, Nevada, a natural laboratory. *Geochimica et Cosmochimica Acta*, 71, 3948-3957.
- COPLIN, T. B., KENDALL, C. & HOPPLE, J. 1983. COMPARISON OF STABLE ISOTOPE REFERENCE SAMPLES. *Nature*, 302, 236-238.
- COSFORD, J., QING, H., EGLINGTON, B., MATTEY, D., YUAN, D., ZHANG, M. & CHENG, H. 2008. East Asian monsoon variability since the Mid-Holocene recorded in a high-resolution, absolute-dated aragonite speleothem from eastern China. *Earth and Planetary Science Letters*, 275, 296-307.
- COSFORD, J., QING, H., MATTEY, D., EGLINGTON, B. & ZHANG, M. 2009. Climatic and local effects on stalagmite delta(13)C values at Lianhua Cave, China. *Palaeogeography Palaeoclimatology Palaeoecology*, 280, 235-244.
- COUCHOUD, I., GENTY, D., HOFFMANN, D., DRYSDALE, R. & BLAMART, D. 2009. Millennial-scale climate variability during the Last Interglacial recorded in a speleothem from south-western France. *Quaternary Science Reviews*, 28, 3263-3274.

- CRAIG, H. 1957. ISOTOPIC STANDARDS FOR CARBON AND OXYGEN AND CORRECTION FACTORS FOR MASS-SPECTROMETRIC ANALYSIS OF CARBON DIOXIDE. *Geochimica et Cosmochimica Acta*, 12, 133-149.
- CRAIG, H. 1961. Isotopic Variations in Meteoric Waters. *Science*, 133, 1702-1703.
- CRAIG, H. 1965. The measurement of oxygen isotope palaeotemperatures. In: TONGIORGI, E. (ed.) *Stable isotopes in oceanographic studies and palaeotemperatures*. Pisa, Italy: Cnpsiglio Nazionale delle Recherche Laboratio di Geologia Nucleare.
- CRAIG, K. D., HORTON, P. D. & REAMS, M. W. 1984. Clastic and Solutinal Boundaries as Nucleation SURfaces for Aragonite in Speleothems. *National Speleological Society Bulletin*, 46, 15-17.
- CRUZ, F. W., KARMANN, I., VIANA, O., BURNS, S. J., FERRARI, J. A., VUILLE, M., SIAL, A. N. & MOREIRA, M. Z. 2005. Stable isotope study of cave percolation waters in subtropical Brazil: Implications for paleoclimate inferences from speleothems. *Chemical Geology*, 220, 245-262.
- CRUZ, F. W., JR., BURNS, S. J., JERCINOVIC, M., KARMANN, I., SHARP, W. D. & VUILLE, M. 2007. Evidence of rainfall variations in Southern Brazil from trace element ratios (Mg/Ca and Sr/Ca) in a Late Pleistocene stalagmite. *Geochimica et Cosmochimica Acta*, 71, 2250-2263.
- CULLEN, H. M. & DEMENOCAL, P. B. 2000. North Atlantic influence on Tigris-Euphrates streamflow. *International Journal of Climatology*, 20, 853-863.
- DANSGAARD, W. 1964. STABLE ISOTOPES IN PRECIPITATION. *Tellus*, 16, 436-468.
- DANSGAARD, W., JOHNSEN, S. J., CLAUSEN, H. B., DAHLJENSEN, D., GUNDESTRUP, N. S., HAMMER, C. U., HVIDBERG, C. S., STEFFENSEN, J. P., SVEINBJORNSDOTTIR, A. E., JOUZEL, J. & BOND, G. 1993. EVIDENCE FOR GENERAL INSTABILITY OF PAST CLIMATE FROM A 250-KYR ICE-CORE RECORD. *Nature*, 364, 218-220.
- DAVIS, K. J., DOVE, P. M. & DE YOREO, J. J. 2000. The Role of Mg<sup>2+</sup> as an Impurity in Calcite Growth. *Science*, 290, 1134-1137.
- DAVIS, K. J., DOVE, P. M., WASYLENKI, L. E. & DE YOREO, J. J. 2004. Morphological consequences of differential Mg<sup>2+</sup> incorporation at structurally distinct steps on calcite. *American Mineralogist*, 89, 714-720.
- DAYEM, K. E., MOLNAR, P., BATTISTI, D. S. & ROE, G. H. 2010. Lessons learned from oxygen isotopes in modern precipitation applied to interpretation of speleothem records of paleoclimate from eastern Asia. *Earth and Planetary Science Letters*, 295, 219-230.
- DE BOER, R. B. 1977. Stability of Mg-Ca carbonates. *Geochimica et Cosmochimica Acta*, 41, 265-270.
- DE CHOUDENS-SÁNCHEZ, V. & GONZÁLEZ, L. A. 2009. Calcite and Aragonite Precipitation Under Controlled Instantaneous Supersaturation: Elucidating the Role of CaCO<sub>3</sub> Saturation State and Mg/Ca Ratio on Calcium Carbonate Polymorphism. *Journal of Sedimentary Research*, 79, 363-376.
- DE LANGE, G. J., THOMSON, J., REITZ, A., SLOMP, C. P., PRINCIPATO, M. S., ERBA, E. & CORSELLI, C. 2008. Synchronous basin-wide formation and redox-controlled preservation of a Mediterranean sapropel. *Nature Geoscience*, 1, 606-610.
- DE RIJK, S., HAYES, A. & ROHLING, E. J. 1999. Eastern Mediterranean sapropel S1 interruption: an expression of the onset of climatic deterioration around 7 ka BP. *Marine Geology*, 153, 337-343.
- DE VILLIERS, J. P. R. 1971. CRYSTAL STRUCTURES OF ARAGONITE, STRONTIANITE, AND WITHERITE. *American Mineralogist*, 56, 758-767.
- DEINES, P. 1980. The Isotopic Composition of Reduced Organic Carbon. In: FRITZ, P. & FONTES, J. C. (eds.) *Handbook of Environmental Isotope Geochemistry - The Terrestrial Environment*, A. Amsterdam: Elsevier.

- DEINES, P., LANGMUIR, D. & HARMON, R. S. 1974. Stable carbon isotope ratios and the existence of a gas phase in the evolution of carbonate ground waters. *Geochimica et Cosmochimica Acta*, 38, 1147-1164.
- DEMENOCAL, P., ORTIZ, J., GUILDERSON, T., ADKINS, J., SARNTHEIN, M., BAKER, L. & YARUSINSKY, M. 2000. Abrupt onset and termination of the African Humid Period: rapid climate responses to gradual insolation forcing. *Quaternary Science Reviews*, 19, 347-361.
- DEMENY, A., KELE, S. & SIKLOSZ, Z. 2010. Empirical equations for the temperature dependence of calcite-water oxygen isotope fractionation from 10 to 70 degrees C. *Rapid Communications in Mass Spectrometry*, 24, 3521-3526.
- DENNISTON, R. F., GONZÁLEZ, L. A., ASMEROM, Y., SHARMA, R. H. & REAGAN, M. K. 2000. Speleothem Evidence for Changes in Indian Summer Monsoon Precipitation over the Last ~2300 Years. *Quaternary Research*, 53, 196-202.
- DENTON, G. H., ALLEY, R. B., COMER, G. C. & BROECKER, W. S. 2005. The role of seasonality in abrupt climate change. *Quaternary Science Reviews*, 24, 1159-1182.
- DESMARCHELIER, J. M., GOEDE, A., AYLIFFE, L. K., MCCULLOCH, M. T. & MORIARTY, K. 2000. Stable isotope record and its palaeoenvironmental interpretation for a late Middle Pleistocene speleothem from Victoria Fossil Cave, Naracoorte, South Australia. *Quaternary Science Reviews*, 19, 763-774.
- DESMARCHELIER, J. M., HELLSTROM, J. C. & MCCULLOCH, M. T. 2006. Rapid trace element analysis of speleothems by ELA-ICP-MS. *Chemical Geology*, 231, 102-117.
- DEVELLE, A.-L., HERREROS, J., VIDAL, L., SURSOCK, A. & GASSE, F. 2010. Controlling factors on a paleo-lake oxygen isotope record (Yammoûneh, Lebanon) since the Last Glacial Maximum. *Quaternary Science Reviews*, 29, 865-886.
- DEVELLE, A. L., GASSE, F., VIDAL, L., WILLIAMSON, D., DEMORY, F., VAN CAMPO, E., GHALEB, B. & THOUVENY, N. 2011. A 250 ka sedimentary record from a small karstic lake in the Northern Levant (Yammoûneh, Lebanon). Paleoclimatic implications. *Palaeogeography, Palaeoclimatology, Palaeoecology*, doi: 10.1016/j.palaeo.2011.02.008.
- DINPASHOH, Y., FAKHERI-FARD, A., MOGHADDAM, M., JAHANBAKHS, S. & MIRNIA, M. 2004. Selection of variables for the purpose of regionalization of Iran's precipitation climate using multivariate methods. *Journal of Hydrology*, 297, 109-123.
- DIRICAN, A., ÜNAL, S., ACAR, Y. & DEMIRCAN, M. 2005. The temporal and seasonal variation of H-2 and O-18 in atmospheric water vapour and precipitation from Ankara, Turkey in relation to air mass trajectories at the Mediterranean Basin. In: (2005), I. (ed.) *Isotopic Composition of Precipitation in the Mediterranean Basin in Relation to Air Circulation Patterns and Climate*.
- DJAMALI, M., AKHANI, H., ANDRIEU-PONEL, V., BRACONNOT, P., BREWER, S., DE BEAULIEU, J. L., FLEITMANN, D., FLEURY, J., GASSE, F., GUIBAL, F., JACKSON, S. T., LÉZINE, A. M., MÉDAIL, F., PONEL, P., ROBERTS, N. & STEVENS, L. 2010. Indian summer Monsoon variations could have affected the early-Holocene woodland expansion in the Near East. *Holocene*, 20, 813-820.
- DODD, J. R. 1966. Processes of conversion of aragonite to calcite with examples from the Cretaceous of Texas. *Journal of Sedimentary Research*, 36, 733-741.
- DOMENICO, P. A. & SCHWARTZ, F. W. 1990. *Physical and Chemical Hydrogeology*, New York, John Wiley & Sons.
- DOMÍNGUEZ-VILLAR, D., WANG, X., CHENG, H., MARTÍN-CHIVELET, J. & EDWARDS, R. L. 2008. A high-resolution late Holocene speleothem record from Kaite Cave, northern Spain:  $\delta^{18}\text{O}$  variability and possible causes. *Quaternary International*, 187, 40-51.

- DORALE, J. A., GONZALEZ, L. A., REAGAN, M. K., PICKETT, D. A., MURRELL, M. T. & BAKER, R. G. 1992. A HIGH-RESOLUTION RECORD OF HOLOCENE CLIMATE CHANGE IN SPELEOTHEM CALCITE FROM COLD WATER CAVE, NORTHEAST IOWA. *Science*, 258, 1626-1630.
- DORALE, J. A., EDWARDS, R. L., ITO, E. & GONZALEZ, L. A. 1998. Climate and vegetation history of the midcontinent from 75 to 25 ka: A speleothem record from Crevice Cave, Missouri, USA. *Science*, 282, 1871-1874.
- DRAKE, B. L. 2012. The influence of climatic change on the Late Bronze Age Collapse and the Greek Dark Ages. *Journal of Archaeological Science*.
- DRAKE, J. J. 1983. The effects of geomorphology and seasonality on the chemistry of carbonate groundwater. *Journal of Hydrology*, 61, 223-236.
- DREYBRODT, W. 1980. DEPOSITION OF CALCITE FROM THIN-FILMS OF NATURAL CALCAREOUS SOLUTIONS AND THE GROWTH OF SPELEOTHEMS. *Chemical Geology*, 29, 89-105.
- DREYBRODT, W. 1988. *Processes in Karst Systems: Physics, Chemistry and Geology*, New York, Springer-Verlag.
- DREYBRODT, W. 1999. Chemical kinetics, speleothem growth and climate. *Boreas*, 28, 347-356.
- DREYBRODT, W. & SCHOLZ, D. 2010. Climatic dependence of stable carbon and oxygen isotope signals recorded in speleothems: From soil water to speleothem calcite. *Geochimica et Cosmochimica Acta*, doi: 10.1016/j.gca.2010.11.002.
- DREYBRODT, W. 2011a. Comments on processes contributing to the isotope composition of <sup>13</sup>C and <sup>18</sup>O in calcite deposited to speleothems. *Acta Carsologica*, 40, 233-238.
- DREYBRODT, W. 2008. Evolution of the isotopic composition of carbon in a calcite precipitating H<sub>2</sub>O-CO<sub>2</sub>-CaCO<sub>3</sub> solution and the related isotopic composition of calcite in stalagmites. *Geochimica et Cosmochimica Acta*, 72, 4712-4724.
- DREYBRODT, W. 2011b. COMMENTS ON PROCESSES CONTRIBUTING TO THE ISOTOPE COMPOSITION OF C-13 AND O-18 IN CALCITE DEPOSITED TO SPELEOTHEMS. *Acta Carsologica*, 40, 233-238.
- DREYBRODT, W. & SCHOLZ, D. 2011. Climatic dependence of stable carbon and oxygen isotope signals recorded in speleothems: From soil water to speleothem calcite. *Geochimica et Cosmochimica Acta*, doi: 10.1016/j.gca.2010.11.002.
- DRYSDALE, R., ZANCHETTA, G., HELLSTROM, J., MAAS, R., FALLICK, A., PICKETT, M., CARTWRIGHT, I. & PICCINI, L. 2006. Late Holocene drought responsible for the collapse of Old World civilizations is recorded in an Italian cave flowstone. *Geology*, 34, 101-104.
- DRYSDALE, R. N., ZANCHETTA, G., HELLSTROM, J. C., FALLICK, A. E., ZHAO, J.-X., ISOLA, I. & BRUSCHI, G. 2004. Palaeoclimatic implications of the growth history and stable isotope ( $\delta^{18}\text{O}$  and  $\delta^{13}\text{C}$ ) geochemistry of a Middle to Late Pleistocene stalagmite from central-western Italy. *Earth and Planetary Science Letters*, 227, 215-229.
- DRYSDALE, R. N., ZANCHETTA, G., HELLSTROM, J. C., FALLICK, A. E. & ZHAO, J. X. 2005. Stalagmite evidence for the onset of the Last Interglacial in southern Europe at 129 +/- 1 ka. *Geophysical Research Letters*, 32, 4.
- DRYSDALE, R. N., ZANCHETTA, G., HELLSTROM, J. C., FALLICK, A. E., MCDONALD, J. & CARTWRIGHT, I. 2007. Stalagmite evidence for the precise timing of North Atlantic cold events during the early last glacial. *Geology*, 35, 77-80.
- DRYSDALE, R. N., HELLSTROM, J. C., ZANCHETTA, G., FALLICK, A. E., GONI, M. F. S., COUCHOUD, I., MCDONALD, J., MAAS, R., LOHMANN, G. & ISOLA, I. 2009. Evidence for Obliquity Forcing of Glacial Termination II. *Science*, 325, 1527-1531.

- DULINSKI, M. & ROZANSKI, K. 1990. FORMATION OF C-13 C-12 ISOTOPE RATIOS IN SPELEOTHEMS - A SEMIDYNAMIC MODEL. *Radiocarbon*, 32, 7-16.
- DYKOSKI, C. A., EDWARDS, R. L., CHENG, H., YUAN, D., CAI, Y., ZHANG, M., LIN, Y., QING, J., AN, Z. & REVENAUGH, J. 2005. A high-resolution, absolute-dated Holocene and deglacial Asian monsoon record from Dongge Cave, China. *Earth and Planetary Science Letters*, 233, 71-86.
- EASTWOOD, W. J., LENG, M. J., ROBERTS, N. & DAVIS, B. 2007. Holocene climate change in the eastern Mediterranean region: a comparison of stable isotope and pollen data from Lake Golhisar, southwest Turkey. *Journal of Quaternary Science*, 22, 327-341.
- EDWARDS, L. R., CHEN, J. H. & WASSERBURG, G. J. 1987.  $^{238}\text{U}$  -  $^{234}\text{U}$  -  $^{230}\text{Th}$  -  $^{232}\text{Th}$  systematics and the precise measurement of time over the past 500,000 years. *Earth and Planetary Science Letters*, 81, 175-192.
- EDWARDS, R. L., CHEN, J. H. & WASSERBURG, G. J. 1988.  $^{238}\text{U}$ - $^{234}\text{U}$ - $^{230}\text{Th}$ - $^{232}\text{Th}$  systematics and the precise measurement of time over the past 500,000 years. *Earth and Planetary Science Letters*, 81, 175-192.
- EMEIS, K. C., SAKAMOTO, T., WEHAUSEN, R. & BRUMSACK, H. J. 2000. The sapropel record of the eastern Mediterranean Sea - results of Ocean Drilling Program Leg 160. *Palaeogeography Palaeoclimatology Palaeoecology*, 158, 371-395.
- EMEIS, K. C., SCHULZ, H., STRUCK, U., ROSSIGNOL-STRICK, M., ERLLENKEUSER, H., HOWELL, M. W., KROON, D., MACKENSEN, A., ISHIZUKA, S., OBA, T., SAKAMOTO, T. & KOIZUMI, I. 2003. Eastern Mediterranean surface water temperatures and delta O-18 composition during deposition of sapropels in the late Quaternary. *Paleoceanography*, 18, -.
- ESHEL, G. & FARRELL, B. F. 2000. Mechanisms of Eastern Mediterranean Rainfall Variability. *Journal of the Atmospheric Sciences*, 57, 3219-3232.
- FAIRCHILD, I. J. & MCMILLAN, E. A. 2007. Speleothems as indicators of wet and dry periods. *International Journal of Speleology*, 36, 69-74.
- FAIRCHILD, I. J. & TREBLE, P. C. 2009. Trace elements in speleothems as recorders of environmental change. *Quaternary Science Reviews*, 28, 449-468.
- FAIRCHILD, I. J. & BAKER, A. 2012. *Speleothem Science - From Process to Past Environments*, Wiley-Blackwell.
- FAIRCHILD, I. J., BRADBY, L., SHARP, M. & TISON, J. L. 1994. HYDROCHEMISTRY OF CARBONATE TERRAINS IN ALPINE GLACIAL SETTINGS. *Earth Surface Processes and Landforms*, 19, 33-54.
- FAIRCHILD, I. J., KILLAWEE, J. A., SHARP, M. J., SPIRO, B., HUBBARD, B., LORRAIN, R. D. & TISON, J. L. 1999. Solute generation and transfer from a chemically reactive alpine glacial-proglacial system. *Earth Surface Processes and Landforms*, 24, 1189-1211.
- FAIRCHILD, I. J., BORSATO, A., TOOTH, A. F., FRISIA, S., HAWKESWORTH, C. J., HUANG, Y., MCDERMOTT, F. & SPIRO, B. 2000. Controls on trace element (Sr-Mg) compositions of carbonate cave waters: implications for speleothem climatic records. *Chemical Geology*, 166, 255-269.
- FAIRCHILD, I. J., BAKER, A., BORSATO, A., FRISIA, S., HINTON, R. W., MCDERMOTT, F. & TOOTH, A. F. 2001. Annual to sub-annual resolution of multiple trace-element trends in speleothems. *Journal of the Geological Society*, 158, 831-841.
- FAIRCHILD, I. J., SMITH, C. L., BAKER, A., FULLER, L., SPÖTL, C., MATTEY, D., MCDERMOTT, F. & E.I.M.F. 2006. Modification and preservation of environmental signals in speleothems. *Earth-Science Reviews*, 75, 105-153.
- FAIRCHILD, I. J., FRISIA, S., BORSATO, A. & TOOTH, A. F. 2007. Speleothems. In: NASH, D. J. & MCLAREN, S. J. (eds.) *Geochemical Sediments and Landscapes*. Oxford: Blackwell Publishing.

- FAURE, G. & MENSING, T. M. 2005. *Isotopes: Principles and Applications*, John Wiley and Sons.
- FERNÁNDEZ-DÍAZ, L., PUTNIS, A., PRIETO, M. & PUTNIS, C. V. 1996. The role of magnesium in the crystallization of calcite and aragonite in a porous medium. *Journal of Sedimentary Research*, 66, 482-491.
- FIELD, M. H., HUNTLEY, B. & MULLER, H. 1994. EEMIAN CLIMATE FLUCTUATIONS OBSERVED IN A EUROPEAN POLLEN RECORD. *Nature*, 371, 779-783.
- FILIPOV, A. F. 1990. Formation conditions of aragonite in some caves from Pester karst region, W. Rhodopes: Ann. Sofia Univ. *Geol. Geogr.*, 79, 162-173.
- FINCH, A. A. & ALLISON, N. 2007. Coordination of Sr and Mg in calcite and aragonite. *Mineralogical Magazine*, 71, 539-552.
- FINCH, A. A., SHAW, P. A., WEEDON, G. P. & HOLMGREN, K. 2001. Trace element variation in speleothem aragonite: potential for palaeoenvironmental reconstruction. *Earth and Planetary Science Letters*, 186, 255-267.
- FINCH, A. A., SHAW, P. A., HOLMGREN, K. & LEE-THORP, J. 2003. Corroborated rainfall records from aragonitic stalagmites. *Earth and Planetary Science Letters*, 215, 265-273.
- FISCHBECK, R. & MÜLLER, G. 1971. Monohydrocalcite, hydromagnesite, nesquehonite, dolomite, aragonite, and calcite in speleothems of the Fränkische Schweiz, Western Germany. *Contributions to Mineralogy and Petrology*, 33, 87-92.
- FISHER, W. B. 1968. *The Land of Iran*, Cambridge, Cambridge University Press.
- FLANNERY, K. V. 1973. Origins of agriculture. *Annual Review of Anthropology*, 2, 271-310.
- FLEITMANN, D., BURNS, S. J., MUDELSEE, M., NEFF, U., KRAMERS, J., MANGINI, A. & MATTER, A. 2003a. Holocene forcing of the Indian monsoon recorded in a stalagmite from Southern Oman. *Science*, 300, 1737-1739.
- FLEITMANN, D., BURNS, S. J., NEFF, U., MANGINI, A. & MATTER, A. 2003b. Changing moisture sources over the last 330,000 years in Northern Oman from fluid-inclusion evidence in speleothems. *Quaternary Research*, 60, 223-232.
- FLEITMANN, D., BURNS, S. J., NEFF, U., MUDELSEE, M., MANGINI, A. & MATTER, A. 2004. Palaeoclimatic interpretation of high-resolution oxygen isotope profiles derived from annually laminated speleothems from Southern Oman. *Quaternary Science Reviews*, 23, 935-945.
- FLEITMANN, D., BURNS, S. J., MANGINI, A., MUDELSEE, M., KRAMERS, J., VILLA, I., NEFF, U., AL-SUBBARY, A. A., BUETTNER, A., HIPPLER, D. & MATTER, A. 2007. Holocene ITCZ and Indian monsoon dynamics recorded in stalagmites from Oman and Yemen (Socotra). *Quaternary Science Reviews*, 26, 170-188.
- FLEITMANN, D., CHENG, H., BADERTSCHER, S., EDWARDS, R. L., MUDELSEE, M., GOKTURK, O. M., FANKHAUSER, A., PICKERING, R., RAIBLE, C. C., MATTER, A., KRAMERS, J. & TUYSUZ, O. 2009. Timing and climatic impact of Greenland interstadials recorded in stalagmites from northern Turkey. *Geophysical Research Letters*, 36.
- FOLK, R. L. 1965. Some aspects of recrystallization in ancient dolomites. In: PRAY, L. C. & MURRAY, R. C. (eds.) *Dolomitization and Limestone Diagenesis - A Symposium*. Tulsa, Oklahoma, U.S.A.: Society of Economic Paleontologists and Mineralogists.
- FOLK, R. L. 1974. NATURAL-HISTORY OF CRYSTALLINE CALCIUM-CARBONATE - EFFECT OF MAGNESIUM CONTENT AND SALINITY. *Journal of Sedimentary Petrology*, 44, 40-53.
- FOLK, R. L. 1994. INTERACTION BETWEEN BACTERIA, NANNOBACTERIA, AND MINERAL PRECIPITATION IN HOT-SPRINGS OF CENTRAL ITALY. *Geographie Physique Et Quaternaire*, 48, 233-246.
- FOLK, R. L. & ASSERETO, R. 1976. COMPARATIVE FABRICS OF LENGTH-SLOW AND LENGTH-FAST CALCITE AND CALCITIZED ARAGONITE IN A HOLOCENE SPELEOTHEM, CARLSBAD CAVERNS, NEW-MEXICO. *Journal of Sedimentary Petrology*, 46, 486-496.

- FONTES, J.-C., GASSE, F. & ANDREWS, J. N. Climatic conditions of Holocene groundwater recharge in the Sahel zone of Africa. *Isotope Techniques in the Study of Past and Current Environmental Changes in the Hydrosphere and the Atmosphere*, 1993 Vienna, Austria. IAEA.
- FORD, D. 1988. Characteristics of Dissolutional Cave Systems in Carbonate Rocks. *In: JAMES, N. P. & CHOQUETTE, P. W. (eds.) Paleokarst*. New York: Springer-Verlag.
- FORD, D. C. & WILLIAMS, P. W. 1989. *Karst Geomorphology and Hydrology*, London, Unwin Hyman.
- FORD, D. C. & WILLIAMS, P. W. 2007. *Karst Hydrogeology and Geomorphology*, Chichester, England, Wiley.
- FRICKE, H. C. & O'NEIL, J. R. 1999. The correlation between O-18/O-16 ratios of meteoric water and surface temperature: its use in investigating terrestrial climate change over geologic time. *Earth and Planetary Science Letters*, 170, 181-196.
- FRIEDMAN, I. & O'NEIL, J. R. 1977. Compilation of stable isotope fractionation factors of geochemical interest. *In: FLEISCHER, M. (ed.) Data of Geochemistry*. U.S.G.S. Professional Paper.
- FRIEDMAN, I., HARRIS, J. M., SMITH, G. I. & JOHNSON, C. A. 2002. Stable isotope composition of waters in the Great Basin, United States - 1. Air-mass trajectories. *Journal of Geophysical Research-Atmospheres*, 107.
- FRISIA, S., BORSATO, A., MANGINI, A., SPÖTL, C., MADONIA, G. & SAURO, U. 2006. Holocene climate variability in Sicily from a discontinuous stalagmite record and the Mesolithic to Neolithic transition. *Quaternary Research*, 66, 388-400.
- FRISIA, S. 1996. Petrographic evidences of diagenesis in some speleothems: some examples. *Speleochronos*, 7, 21-30.
- FRISIA, S. & WENK, H. R. 1993. TEM AND AEM STUDY OF PERVASIVE, MULTISTEP DOLOMITIZATION OF THE UPPER TRIASSIC DOLOMIA PRINCIPALE (NORTHERN ITALY). *Journal of Sedimentary Petrology*, 63, 1049-1058.
- FRISIA, S. & BORSATO, A. 2010. Karst. *In: ALONSO-ZARZA, A. M. & TANNER, L. H. (eds.) Carbonates in Continental Settings: Facies, environments and processes*. Amsterdam: Elsevier.
- FRISIA, S., BORSATO, A., FAIRCHILD, I. J. & MCDERMOTT, F. 2000. Calcite fabrics, growth mechanisms, and environments of formation in speleothems from the Italian Alps and southwestern Ireland. *Journal of Sedimentary Research*, 70, 1183-1196.
- FRISIA, S., BORSATO, A., FAIRCHILD, I. J., MCDERMOTT, F. & SELMO, E. M. 2002. Aragonite-calcite relationships in speleothems (Grotte de Clamouse, France): Environment, fabrics, and carbonate geochemistry. *Journal of Sedimentary Research*, 72, 687-699.
- FRISIA, S., BORSATO, A., PRETO, N. & MCDERMOTT, F. 2003. Late Holocene annual growth in three Alpine stalagmites records the influence of solar activity and the North Atlantic Oscillation on winter climate. *Earth and Planetary Science Letters*, 216, 411-424.
- FRISIA, S., BORSATO, A., SPÖTL, C., VILLA, I. M. & CUCCHI, F. 2005. Climate variability in the SE Alps of Italy over the past 17 000 years reconstructed from a stalagmite record. *Boreas*, 34, 445-455.
- FRISIA, S., FAIRCHILD, I. J., FOHLMEISTER, J., MIORANDI, R., SPÖTL, C. & BORSATO, A. 2011. Carbon mass-balance modelling and carbon isotope exchange processes in dynamic caves. *Geochimica et Cosmochimica Acta*, 75, 380-400.
- FRONVAL, T. & JANSEN, E. 1996. Rapid changes in ocean circulation and heat flux in the Nordic seas during the last interglacial period. *Nature*, 383, 806-810.

- FRUMKIN, A. & STEIN, M. 2004. The Sahara-East Mediterranean dust and climate connection revealed by strontium and uranium isotopes in a Jerusalem speleothem. *Earth and Planetary Science Letters*, 217, 451-464.
- FRUMKIN, A.,MAGARITZ, M.,CARMİ, I. & ZAK, I. 1991. The Holocene climatic record of the salt caves of Mount Sedom Israel. *The Holocene*, 1, 191-200.
- FRUMKIN, A.,FORD, D. C. & SCHWARCZ, H. P. 1999. Continental oxygen isotopic record of the last 170,000 years in Jerusalem. *Quaternary Research*, 51, 317-327.
- FRUMKIN, A.,FORD, D. C. & SCHWARCZ, H. P. 2000. Paleoclimate and vegetation of the last glacial cycles in Jerusalem from a speleothem record. *Global Biogeochemical Cycles*, 14, 863-870.
- FYFE, W. S. & BISCHOFF, J. L. 1965. The Calcite-Aragonite Problem. In: PRAY, L. C. & MURRAY, J. W. (eds.) *Dolomitization and Limestone Diagenesis - A Symposium*. Tulsa, Oklahoma, USA: Society of Economical Paleontologists and Mineralogists.
- GAMS, I. 1981. Contribution to morphometrics of stalagmites. *Proceedings of the 8th International Congress of Speleology*, 276-278.
- GANOR, E. & MAMANE, Y. 1982. Transport of Saharan dust across the eastern Mediterranean. *Atmospheric Environment (1967)*, 16, 581-587.
- GARRELS, R. M.,THOMPSON, M. E. & SIEVER, R. 1960. Stability of some carbonates at 25 degrees C and one atmosphere total pressure. *Am J Sci*, 258, 402-418.
- GARRELS, R. M.,THOMPSON, M. E. & SIEVER, R. 1961. Control of carbonate solubility by carbonate complexes. *Am J Sci*, 259, 24-45.
- GASCOYNE, M. 1992. Paleoclimate determination from cave calcite deposits. *Quaternary Science Reviews*, 11, 609-632.
- GASCOYNE, M.,SCHWARCZ, H. P. & FORD, D. C. 1980. A PALAEOTEMPERATURE RECORD FOR THE MID-WISCONSIN IN VANCOUVER ISLAND. *Nature*, 285, 474-476.
- GASSE, F. 2000. Hydrological changes in the African tropics since the Last Glacial Maximum. *Quaternary Science Reviews*, 19, 189-211.
- GAT, J. R. 1980. The isotopes of hydrogen and oxygen in precipitation. In: FRITZ, P. & FONTES, J. C. (eds.) *Handbook of Environmental Isotope Geochemistry*.
- GAT, J. R. 1996. Oxygen and hydrogen isotopes in the hydrologic cycle. *Annual Review of Earth and Planetary Sciences*, 24, 225-262.
- GAT, J. R. & CARMİ, I. 1970. Evolution of the isotopic composition of atmospheric waters in the Mediterranean Sea area. *Journal of Geophysical Research*, 75, 3039-3048.
- GAT, J. R. & DANSGAARD, W. 1972. Stable isotope survey of the fresh water occurrences in Israel and the Northern Jordan Rift Valley. *Journal of Hydrology*, 16, 177-211.
- GAT, J. R. & MAGARITZ, M. 1980. Climatic variations in the Eastern Mediterranean Sea area. *Naturwissenschaften*, 67, 80-87.
- GAT, J. R. & CARMİ, I. Effect of climate changes on the precipitation patterns and isotopic composition of water in a climate transition zone: Case of the Eastern Mediterranean Sea area. In: SOLOMON, S. I., BERAN, M. & HOGG, W., eds. *The Influence of Climate Change and Climatic Variability on the Hydrologic Regime and Water Resources*, 1987 Vancouver. IAHS.
- GAT, J. R.,SHEMESH, A.,TZIPERMAN, E.,HECHT, A.,GEORGOPOULOS, D. & BASTURK, O. 1996. The stable isotope composition of waters of the eastern Mediterranean Sea. *Journal of Geophysical Research C: Oceans*, 101, 6441-6451.
- GENTY, D. 2008. Palaeoclimate Research in Villars Cave (Dordogne, SW-France). *International Journal of Speleology*, 37, 173-191.
- GENTY, D. & QUINIF, Y. 1996. Annually laminated sequences in the internal structure of some Belgian stalagmites - Importance for paleoclimatology. *Journal of Sedimentary Research*, 66, 275-288.

- GENTY, D. & MASSAULT, M. 1997. Bomb C-14 recorded in laminated speleothems: Calculation of dead carbon proportion. *Radiocarbon*, 39, 33-48.
- GENTY, D. & MASSAULT, M. 1999. Carbon transfer dynamics from bomb-<sup>14</sup>C and  $\delta^{13}\text{C}$  time series of a laminated stalagmite from SW France - modelling and comparison with other stalagmite records. *Geochimica et Cosmochimica Acta*, 63, 1537-1548.
- GENTY, D., VOKAL, B., OBELIC, B. & MASSAULT, M. 1998. Bomb <sup>14</sup>C time history recorded in two modern stalagmites -- importance for soil organic matter dynamics and bomb <sup>14</sup>C distribution over continents. *Earth and Planetary Science Letters*, 160, 795-809.
- GENTY, D., MASSAULT, M., GILMOUR, M., BAKER, A., VERHEYDEN, S. & KEPENS, E. 1999. Calculation of past dead carbon proportion and variability by the comparison of AMS(<sup>14</sup>C) and TIMS U/Th ages on two holocene stalagmites. *Radiocarbon*, 41, 251-270.
- GENTY, D., BAKER, A., MASSAULT, M., PROCTOR, C., GILMOUR, M., PONS-BRANCHU, E. & HAMELIN, B. 2001a. Dead carbon in stalagmites: carbonate bedrock paleodissolution vs. ageing of soil organic matter. Implications for <sup>13</sup>C variations in speleothems. *Geochimica et Cosmochimica Acta*, 65, 3443-3457.
- GENTY, D., BAKER, A. & VOKAL, B. 2001b. Intra- and inter-annual growth rate of modern stalagmites. *Chemical Geology*, 176, 191-212.
- GENTY, D., BLAMART, D., OUAHDI, R., GILMOUR, M., BAKER, A., JOUZEL, J. & VAN-EXTER, S. 2003. Precise dating of Dansgaard-Oeschger climate oscillations in western Europe from stalagmite data. *Nature*, 421, 833-837.
- GIUNTA, S., NEGRI, A., MORIGI, C., CAPOTONDI, L., COMBOURIEU-NEBOUT, N., EMEIS, K. C., SANGIORGI, F. & VIGLIOTTI, L. 2003. Coccolithophorid ecostratigraphy and multi-proxy paleoceanographic reconstruction in the Southern Adriatic Sea during the last deglacial time (Core AD91-17). *Palaeogeography Palaeoclimatology Palaeoecology*, 190, 39-59.
- GIVEN, R. K. & WILKINSON, B. H. 1985. KINETIC CONTROL OF MORPHOLOGY, COMPOSITION, AND MINERALOGY OF ABIOTIC SEDIMENTARY CARBONATES. *Journal of Sedimentary Petrology*, 55, 109-119.
- GLUECK, N. 1960. *Rivers in the Desert*, New York, Grove Press.
- GOEDE, A., GREEN, D. C. & HARMON, R. S. 1986. LATE PLEISTOCENE PALEOTEMPERATURE RECORD FROM A TASMANIAN SPELEOTHEM. *Australian Journal of Earth Sciences*, 33, 333-342.
- GOEDE, A., MCCULLOCH, M., MCDERMOTT, F. & HAWKESWORTH, C. 1998. Aeolian contribution to strontium and strontium isotope variations in a Tasmanian speleothem. *Chemical Geology*, 149, 37-50.
- GOKTURK, E. H., HILLEGONDS, D. J., LIPSCHUTZ, M. E. & HODDER, I. 2002. Accelerator mass spectrometry dating at Catalhoyuk. *Radiochimica Acta*, 90, 407-410.
- GOMBERG, D. N. & BONATTI, E. 1970. HIGH-MAGNESIAN CLACITE - LEACHING OF MAGNESIUM IN DEEP SEA. *Science*, 168, 1451-&.
- GONFIANTINI, R. 1978. STANDARDS FOR STABLE ISOTOPE MEASUREMENTS IN NATURAL COMPOUNDS. *Nature*, 271, 534-536.
- GONFIANTINI, R., ROCHE, M. A., OLIVRY, J. C., FONTES, J. C. & ZUPPI, G. M. 2001. The altitude effect on the isotopic composition of tropical rains. *Chemical Geology*, 181, 147-167.
- GONZÁLEZ, L. A. & LOHMANN, K. C. 1988. Controls on mineralogy and composition of spelean carbonates: Carlsbad Caverns, New Mexico. In: JAMES, N. P. & CHOQUETTE, P. W. (eds.) *Paleokarst*. New York: Springer-Verlag.
- GONZÁLEZ, L. A., CARPENTER, S. J. & LOHMANN, K. C. 1992. INORGANIC CALCITE MORPHOLOGY - ROLES OF FLUID CHEMISTRY AND FLUID-FLOW. *Journal of Sedimentary Petrology*, 62, 382-399.

- GOODFRIEND, G. A. 1988. MID-HOLOCENE RAINFALL IN THE NEGEV DESERT FROM C-13 OF LAND SNAIL SHELL ORGANIC-MATTER. *Nature*, 333, 757-760.
- GOODFRIEND, G. A. 1991. Holocene trends in  $^{18}\text{O}$  in land snail shells from the Negev Desert and their implications for changes in rainfall source areas. *Quaternary Research*, 35, 417-426.
- GOODFRIEND, G. A. 1999. Terrestrial stable isotope records of Late Quaternary paleoclimates in the eastern Mediterranean region. *Quaternary Science Reviews*, 18, 501-513.
- GRANT, K. M., ROHLING, E. J., BAR-MATTHEWS, M., AYALON, A., MEDINA-ELIZALDE, M., RAMSEY, C. B., SATOW, C. & ROBERTS, A. P. 2012. Rapid coupling between ice volume and polar temperature over the past 150,000 years. *Nature*, 491, 744-747.
- GRATZ, A. J., HILLNER, P. E. & HANSMA, P. K. 1993. Step dynamics and spiral growth on calcite. *Geochimica et Cosmochimica Acta*, 57, 491-495.
- GROOTES, P. M. 1993. Interpreting continental oxygen isotope records. In: SWART, P. K., LOHMANN, K. C., MCKENZIE, J. & SAVIN, S. (eds.) *Climate change in continental isotopic records*. Washington, D.C.: American Geophysical Union.
- GROOTES, P. M., STUIVER, M., WHITE, J. W. C., JOHNSEN, S. & JOUZEL, J. 1993. COMPARISON OF OXYGEN-ISOTOPE RECORDS FROM THE GISP2 AND GRIP GREENLAND ICE CORES. *Nature*, 366, 552-554.
- GROSSMAN, E. L. & KU, T.-L. 1981. Aragonite-water isotopic paleotemperature scale based on benthic foraminifer *Hoeglundia elegans*. *Geol. Soc. Am. Annu. Meet.*
- GROSSMAN, E. L. & KU, T.-L. 1986. Oxygen and carbon isotope fractionation in biogenic aragonite: Temperature effects. *Chemical Geology: Isotope Geoscience section*, 59, 59-74.
- GUIOT, J., DEBEAULIEU, J. L., CHEDDADI, R., DAVID, F., PONEL, P. & REILLE, M. 1993. THE CLIMATE IN WESTERN-EUROPE DURING THE LAST GLACIAL INTERGLACIAL CYCLE DERIVED FROM POLLEN AND INSECT REMAINS. *Palaeogeography Palaeoclimatology Palaeoecology*, 103, 73-93.
- GUNN, J. 1983. POINT-RECHARGE OF LIMESTONE AQUIFERS - A MODEL FROM NEW-ZEALAND KARST. *Journal of Hydrology*, 61, 19-29.
- GUNN, J. 2004. *Encyclopedia of Caves and Karst Science*, New York, Fitzroy Dearborn.
- GUTJAHR, A., DABRINGHAUS, H. & LACMANN, R. 1996. Studies of the growth and dissolution kinetics of the  $\text{CaCO}_3$  polymorphs calcite and aragonite I. Growth and dissolution rates in water. *Journal of Crystal Growth*, 158, 296-309.
- GVIRTZMAN, G. & WIEDER, M. 2001. Climate of the last 53,000 Years in the eastern Mediterranean, based on soil-sequence Stratigraphy in the coastal plain of Israel. *Quaternary Science Reviews*, 20, 1827-1849.
- HAKL, J., HUNYADI, I., CSIGE, I., GECZY, G., LENART, L. & VARHEGYI, A. 1997. Radon transport phenomena studied in karst caves - International experiences on radon levels and exposures. *Radiation Measurements*, 28, 675-684.
- HARMON, R. S. 1979. ISOTOPIC STUDY OF GROUNDWATER SEEPAGE IN THE CENTRAL KENTUCKY KARST. *Water Resources Research*, 15, 476-480.
- HARMON, R. S., WHITE, W. B., DRAKE, J. J. & HESS, J. W. 1975. REGIONAL HYDROCHEMISTRY OF NORTH-AMERICAN CARBONATE TERRAINS. *Water Resources Research*, 11, 963-967.
- HARMON, R. S., ATKINSON, T. C. & ATKINSON, J. L. 1983. THE MINERALOGY OF CASTLEGUARD CAVE, COLUMBIA ICEFIELDS, ALBERTA, CANADA. *Arctic and Alpine Research*, 15, 503-516.
- HATZAKI, M., FLOCAS, H. A., ASIMAKOPOULOS, D. N. & MAHERAS, P. 2007. The eastern Mediterranean teleconnection pattern: identification and definition. *International Journal of Climatology*, 27, 727-737.

- HAUG, G. H., HUGHEN, K. A., SIGMAN, D. M., PETERSON, L. C. & ROHL, U. 2001. Southward migration of the intertropical convergence zone through the Holocene. *Science*, 293, 1304-1308.
- HEAL, O. W. & FRENCH, D. D. 1974. Decomposition of organic matter in tundra. In: HOLDING, A. J. (ed.) *Soil organisms and decomposition in tundra*. Stockholm: Tundra Biome Steering Committee.
- HELGESON, H. C., DELANY, J. M., NESBITT, H. W. & BIRD, D. K. 1978. SUMMARY AND CRITIQUE OF THE THERMODYNAMIC PROPERTIES OF ROCK-FORMING MINERALS. *American Journal of Science*, 278, 1-229.
- HELLSTROM, J. C. & MCCULLOCH, M. T. 2000. Multi-proxy constraints on the climatic significance of trace element records from a New Zealand speleothem. *Earth and Planetary Science Letters*, 179, 287-297.
- HENDERSON, G. M., SLOWEY, N. C. & HADDAD, G. A. 1999. Fluid flow through carbonate platforms: constraints from  $^{234}\text{U}/^{238}\text{U}$  and  $\text{Cl}^-$  in Bahamas pore-waters. *Earth and Planetary Science Letters*, 169, 99-111.
- HENDY, C. H. 1971. Isotopic geochemistry of speleothems. 1. Calculation of effects of different modes of formation on isotopic composition of speleothems and their applicability as palaeoclimatic indicators. *Geochimica et Cosmochimica Acta*, 35, 801-&.
- HENDY, C. H. & WILSON, A. T. 1968. PALAEOCLIMATIC DATA FROM SPELEOTHEMS. *Nature*, 219, 48-&.
- HIESS, J., CONDON, D. J., MCLEAN, N. & NOBLE, S. R. 2012. U-238/U-235 Systematics in Terrestrial Uranium-Bearing Minerals. *Science*, 335, 1610-1614.
- HILGEN, F. J. 1991. Astronomical Calibration of Gauss to Matuyama Sappropels in the Mediterranean and Implication for the Geomagnetic Polarity Time Scale. *Earth and Planetary Science Letters*, 104, 226-244.
- HILL, C. & FORTI, P. 1997. *Cave Minerals of the World*, Huntsville, Alabama, National Speleological Society.
- HOFFMANN, D. L., SPOETL, C. & MANGINI, A. 2009. Micromill and in situ laser ablation sampling techniques for high spatial resolution MC-ICPMS U-Th dating of carbonates. *Chemical Geology*, 259, 253-261.
- HOLLAND, H. D., KIRSIPU, T. V., HUEBNER, J. S. & OXBURGH, U. M. 1964. ON SOME ASPECTS OF THE CHEMICAL EVOLUTION OF CAVE WATERS. *Journal of Geology*, 72, 36-67.
- HOLMGREN, K., KARLÉN, W. & SHAW, P. A. 1995. Paleoclimatic Significance of the Stable Isotopic Composition and Petrology of a Late Pleistocene Stalagmite from Botswana. *Quaternary Research*, 43, 320-328.
- HOLZKÄMPER, S., SPÖTL, C. & MANGINI, A. 2005. High-precision constraints on timing of Alpine warm periods during the middle to late Pleistocene using speleothem growth periods. *Earth and Planetary Science Letters*, 236, 751-764.
- HOPLEY, P. J., MARSHALL, J. D. & LATHAM, A. G. 2009. Speleothem preservation and diagenesis in South African hominin sites: implications for paleoenvironments and geochronology. *Geoarchaeology*, 24, 519-547.
- HOU, W. T. & FENG, Q. L. 2005. A simple method to control the polymorphs of calcium carbonate in  $\text{CO}_2$ -diffusion precipitation. *Journal of Crystal Growth*, 282, 214-219.
- HOWSON, M. R., PETHYBRIDGE, A. D. & HOUSE, W. A. 1987. SYNTHESIS AND DISTRIBUTION COEFFICIENT OF LOW-MAGNESIUM CALCITES. *Chemical Geology*, 64, 79-87.
- HOYOS, M., SOLER, V., CANAVERAS, J. C., SANCHEZ-MORAL, S. & SANZ-RUBIO, E. 1998. Microclimatic characterization of a karstic cave: human impact on microenvironmental parameters of a prehistoric rock art cave (Candamo Cave, northern Spain). *Environmental Geology*, 33, 231-242.

- HSIEH, J. C. C., CHADWICK, O. A., KELLY, E. F. & SAVIN, S. M. 1998. Oxygen isotopic composition of soil water: Quantifying evaporation and transpiration. *Geoderma*, 82, 269-293.
- [HTTP://WWW.DIMCAVE.COM.TR](http://www.dimcave.com.tr). 2009].
- HUANG, Y. & FAIRCHILD, I. J. 2001. Partitioning of Sr<sup>2+</sup> and Mg<sup>2+</sup> into calcite under karst-analogue experimental conditions. *Geochimica et Cosmochimica Acta*, 65, 47-62.
- HUANG, Y., FAIRCHILD, I. J., BORSATO, A., FRISIA, S., CASSIDY, N. J., MCDERMOTT, F. & HAWKESWORTH, C. J. 2001. Seasonal variations in Sr, Mg and P in modern speleothems (Grotta di Ernesto, Italy). *Chemical Geology*, 175, 429-448.
- HURRELL, J. W. 1995. DECADAL TRENDS IN THE NORTH-ATLANTIC OSCILLATION - REGIONAL TEMPERATURES AND PRECIPITATION. *Science*, 269, 676-679.
- IAEA & WMO 2006. Global Network of Isotopes in Precipitation. The GNIP Database.
- JALUT, G., DEDOUBAT, J. J., FONTUGNE, M. & OTTO, T. 2009. Holocene circum-Mediterranean vegetation changes: Climate forcing and human impact. *Quaternary International*, 200, 4-18.
- JEX, C. N., BAKER, A., FAIRCHILD, I. J., EASTWOOD, W. J., LENG, M. J., SLOANE, H. J., THOMAS, L. & BEKAROGLU, E. 2010. Calibration of speleothem [ $\delta$ ]<sup>18</sup>O with instrumental climate records from Turkey. *Global and Planetary Change*, 71, 207-217.
- JIMÉNEZ-LÓPEZ, C., CABALLERO, E., HUERTAS, F. J. & ROMANEK, C. S. 2001. Chemical, mineralogical and isotope behavior, and phase transformation during the precipitation of calcium carbonate minerals from intermediate ionic solution at 25°C. *Geochimica et Cosmochimica Acta*, 65, 3219-3231.
- JOHNSON, K. R., HU, C., BELSHAW, N. S. & HENDERSON, G. M. 2006a. Seasonal trace-element and stable-isotope variations in a Chinese speleothem: The potential for high-resolution paleomonsoon reconstruction. *Earth and Planetary Science Letters*, 244, 394-407.
- JOHNSON, K. R., INGRAM, B. L., SHARP, W. D. & ZHANG, P. Z. 2006b. East Asian summer monsoon variability during Marine Isotope Stage 5 based on speleothem  $\delta$ O-18 records from Wanxiang Cave, central China. *Palaeogeography Palaeoclimatology Palaeoecology*, 236, 5-19.
- JONES, B. & KAHLE, C. F. 1993. MORPHOLOGY, RELATIONSHIP, AND ORIGIN OF FIBER AND DENDRITE CALCITE CRYSTALS. *Journal of Sedimentary Petrology*, 63, 1018-1031.
- JONES, B. & KAHLE, C. F. 1995. ORIGIN OF ENDOGENETIC MICRITE IN KARST TERRAINS - A CASE-STUDY FROM THE CAYMAN ISLANDS. *Journal of Sedimentary Research Section a-Sedimentary Petrology and Processes*, 65, 283-293.
- KALLEL, N., PATERNE, M., LABEYRIE, L., DUPLESSY, J.-C. & ARNOLD, M. 1997a. Temperature and salinity records of the Tyrrhenian Sea during the last 18,000 years. *Palaeogeography, Palaeoclimatology, Palaeoecology*, 135, 97-108.
- KALLEL, N., PATERNE, M., DUPLESSY, J. C., VERGNAUDGRAZZINI, C., PUJOL, C., LABEYRIE, L., ARNOLD, M., FONTUGNE, M. & PIERRE, C. 1997b. Enhanced rainfall in the Mediterranean region during the last sapropel event. *Oceanologica Acta*, 20, 697-712.
- KARABORK, M. C., KAHYA, E. & KARACA, M. 2005. The influences of the Southern and North Atlantic Oscillations on climatic surface variables in Turkey. *Hydrological Processes*, 19, 1185-1211.
- KARACA, M., DENIZ, A. & TAYANC, M. 2000. Cyclone track variability over Turkey in association with regional climate. *International Journal of Climatology*, 20, 1225-1236.
- KARMANN, I., CRUZ, F. W., JR., VIANA, O., JR. & BURNS, S. J. 2007. Climate influence on geochemistry parameters of waters from Santana-Perolas cave system, Brazil. *Chemical Geology*, 244, 232-247.

- KAUFMAN, A. 1969. TH232 CONCENTRATION OF SURFACE OCEAN WATER. *Geochimica et Cosmochimica Acta*, 33, 717-&.
- KAUFMAN, A., WASSERBURG, G. J., PORCELLI, D., BAR-MATTHEWS, M., AYALON, A. & HALICZ, L. 1998. U-Th isotope systematics from the Soreq cave, Israel and climatic correlations. *Earth and Planetary Science Letters*, 156, 141-155.
- KAUFMANN, G. 2003. Stalagmite growth and palaeo-climate: the numerical perspective. *Earth and Planetary Science Letters*, 214, 251-266.
- KEHL, M. 2009. Quaternary Climate Change in Iran - the State of Knowledge. *Erdkunde*, 63, 1-17.
- KENDALL, A. C. & BROUGHTON, P. L. 1978. ORIGIN OF FABRICS IN SPELEOTHEMS COMPOSED OF COLUMNAR CALCITE CRYSTALS. *Journal of Sedimentary Petrology*, 48, 519-538.
- KENDREW, W. G. 1961. *Climates of the Continents*, London, Oxford University Press.
- KIM, S.-T., HILLAIRE-MARCEL, C. & MUCCI, A. 2006. Mechanisms of equilibrium and kinetic oxygen isotope effects in synthetic aragonite at 25 degrees C. *Geochimica et Cosmochimica Acta*, 70, 5790-5801.
- KIM, S. T. & O'NEIL, J. R. 1997. Equilibrium and nonequilibrium oxygen isotope effects in synthetic carbonates. *Geochimica et Cosmochimica Acta*, 61, 3461-3475.
- KIM, S. T., O'NEIL, J. R., HILLAIRE-MARCEL, C. & MUCCI, A. 2007. Oxygen isotope fractionation between synthetic aragonite and water: Influence of temperature and Mg<sup>2+</sup> concentration. *Geochimica et Cosmochimica Acta*, 71, 4704-4715.
- KINSMAN, D. J. J. 1969. Interpretation of Sr<sup>+2</sup> concentrations in carbonate minerals and rocks. *Journal of Sedimentary Petrology*, 39, 486-508.
- KINSMAN, D. J. J. & HOLLAND, H. D. 1969. The co-precipitation of cations with CaCO<sub>3</sub>: IV. The co-precipitation of Sr<sup>2+</sup> with aragonite between 16° and 96°C. *Geochimica et Cosmochimica Acta*, 33, 1-17.
- KITANO, Y. 1962. A STUDY OF THE POLYMORPHIC FORMATION OF CALCIUM CARBONATE IN THERMAL SPRINGS WITH AN EMPHASIS ON THE EFFECT OF TEMPERATURE. *Bulletin of the Chemical Society of Japan*, 35, 1980-1985.
- KITANO, Y. & HOOD, D. W. 1965. The influence of organic material on the polymorphic crystallization of calcium carbonate. *Geochimica et Cosmochimica Acta*, 29, 29-41.
- KITANO, Y., HOOD, D. W. & PARK, K. 1962. Pure aragonite synthesis. *Journal of Geophysical Research*, 67, 4873-&.
- KLIMCHOUK, A. 2009. Morphogenesis of hypogenic caves. *Geomorphology*, 106, 100-117.
- KNUDSEN, K. L., SEIDENKRANTZ, M. S. & KRISTENSEN, P. 2002. Last interglacial and early glacial circulation in the northern North Atlantic Ocean. *Quaternary Research*, 58, 22-26.
- KOSTER, R. D., DEVALPINE, D. P. & JOUZEL, J. 1993. CONTINENTAL WATER RECYCLING AND (H<sub>2</sub>O)-O-18 CONCENTRATIONS. *Geophysical Research Letters*, 20, 2215-2218.
- KOTRONI, V., LAGOUVARDOS, K. & LALAS, D. 2001. The effect of the island of Crete on the Etesian winds over the Aegean Sea. *Quarterly Journal of the Royal Meteorological Society*, 127, 1917-1937.
- KOTTHOFF, U., PROSS, J., MUELLER, U. C., PEYRON, O., SCHMIEDL, G., SCHULZ, H. & BORDON, A. 2008. Climate dynamics in the borderlands of the Aegean Sea during formation of sapropel S1 deduced from a marine pollen record. *Quaternary Science Reviews*, 27, 832-845.
- KOWALCZK, A. J. & FROELICH, P. N. 2010. Cave air ventilation and CO(2) outgassing by radon-222 modeling: How fast do caves breathe? *Earth and Planetary Science Letters*, 289, 209-219.

- KRICHAK, S. O. & ALPERT, P. 2005. Signatures of the NAO in the atmospheric circulation during wet winter months over the Mediterranean region. *Theoretical and Applied Climatology*, 82, 27-39.
- KU, T. L. & LI, H. C. 1998. Speleothems as high-resolution paleoenvironment archives: Records from northeastern China. *Proceedings of the Indian Academy of Sciences-Earth and Planetary Sciences*, 107, 321-330.
- KUCZUMOW, A., GENTY, D., CHEVALLIER, P., NOWAK, J. & RO, C. U. 2003. Annual resolution analysis of a SW-France stalagmite by X-ray synchrotron microprobe analysis. *Spectrochimica Acta Part B-Atomic Spectroscopy*, 58, 851-865.
- KUTIEL, H. & MAHERAS, P. 1998. Variations in the temperature regime across the Mediterranean during the last century and their relationship with circulation indices. *Theoretical and Applied Climatology*, 61, 39-53.
- KUTIEL, H. & BENAROCH, Y. 2002. North Sea-Caspian Pattern (NCP) - an upper level atmospheric teleconnection affecting the Eastern Mediterranean: Identification and definition. *Theoretical and Applied Climatology*, 71, 17-28.
- KUTIEL, H., MAHERAS, P. & GUIKA, S. 1998. Singularity of atmospheric pressure in the eastern Mediterranean and its relevance to interannual variations of dry and wet. *International Journal of Climatology*, 18, 317-327.
- KUTIEL, H., MAHERAS, P., TURKES, M. & PAZ, S. 2002. North Sea Caspian Pattern (NCP) - an upper level atmospheric teleconnection affecting the eastern Mediterranean - implications on the regional climate. *Theoretical and Applied Climatology*, 72, 173-192.
- LACHNIET, M. S. 2009. Climatic and environmental controls on speleothem oxygen-isotope values. *Quaternary Science Reviews*, 28, 412-432.
- LACHNIET, M. S. & PATTERSON, W. P. 2006. Use of correlation and stepwise regression to evaluate physical controls on the stable isotope values of Panamanian rain and surface waters. *Journal of Hydrology*, 324, 115-140.
- LACHNIET, M. S., BERNAL, J. P., ASMEROM, Y. & POLYAK, V. 2012. Uranium loss and aragonite-calcite age discordance in a calcitized aragonite stalagmite. *Quaternary Geochronology*.
- LAKOWICZ, J. R., MALIWAL, B. P., CHEREK, H. & BALTER, A. 1983. ROTATIONAL FREEDOM OF TRYPTOPHAN RESIDUES IN PROTEINS AND PEPTIDES. *Biochemistry*, 22, 1741-1752.
- LAMBERT, W. J. & AHARON, P. 2010. Oxygen and hydrogen isotopes of rainfall and dripwater at DeSoto Caverns (Alabama, USA): Key to understanding past variability of moisture transport from the Gulf of Mexico. *Geochimica et Cosmochimica Acta*, 74, 846-861.
- LAMBERT, W. J. & AHARON, P. 2011. Controls on dissolved inorganic carbon and  $\delta^{13}\text{C}$  in cave waters from DeSoto Caverns: Implications for speleothem  $\delta^{13}\text{C}$  assessments. *Geochimica et Cosmochimica Acta*, In Press, Corrected Proof.
- LAND, L. S. 1967. DIAGENESIS OF SKELETAL CARBONATES. *Journal of Sedimentary Petrology*, 37, 914-&.
- LANGMUIR, D. 1978. URANIUM SOLUTION-MINERAL EQUILIBRIA AT LOW-TEMPERATURES WITH APPLICATIONS TO SEDIMENTARY ORE-DEPOSITS. *Geochimica et Cosmochimica Acta*, 42, 547-569.
- LANGMUIR, D. & HERMAN, J. S. 1980. The mobility of thorium in natural waters at low temperatures. *Geochimica et Cosmochimica Acta*, 44, 1753-1766.
- LASAGA, A. C. 1981. Implications of a concentration-dependent growth rate on the boundary layer crystal-melt model. *Earth and Planetary Science Letters*, 56, 429-434.
- LATHAM, A., SCHWARCZ, H. P., FORD, D. C. & PEARCE, G. W. 1982. THE PALEOMAGNETISM AND U-TH DATING OF 3 CANADIAN SPELEOTHEMS - EVIDENCE FOR THE

- WESTWARD DRIFT, 5.4-2.1-KA-BP. *Canadian Journal of Earth Sciences*, 19, 1985-1995.
- LAURITZEN, S. E. 1995. HIGH-RESOLUTION PALEOTEMPERATURE PROXY RECORD FOR THE LAST INTERGLACIATION BASED ON NORWEGIAN SPELEOTHEMS. *Quaternary Research*, 43, 133-146.
- LAURITZEN, S. E. & LUNDBERG, J. 1999. Speleothems and climate: a special issue of The Holocene. *Holocene*, 9, 643-647.
- LEA, D. W., MARTIN, P. A., PAK, D. K. & SPERO, H. J. 2002. Reconstructing a 350 ky history of sea level using planktonic Mg/Ca and oxygen isotope records from a Cocos Ridge core. *Quaternary Science Reviews*, 21, 283-293.
- LEE, J.-E., FUNG, I., DEPAOLO, D. J. & OTTO-BLIESNER, B. 2008. Water isotopes during the Last Glacial Maximum: New general circulation model calculations. *J. Geophys. Res.*, 113, D19109.
- LEGRANDE, A. N. & SCHMIDT, G. A. 2006. Global gridded data set of the oxygen isotopic composition in seawater. *Geophysical Research Letters*, 33.
- LEMCKE, G. & STURM, M. 1997.  $\delta$  O-18 and trace element measurements as proxy for the reconstruction of climate changes at Lake Van (Turkey): Preliminary results. *Third Millennium Bc Climate Change and Old World Collapse*.
- LEMMEN, C., GRONENBORN, D. & WIRTZ, K. W. 2011. A simulation of the Neolithic transition in Western Eurasia. *Journal of Archaeological Science*.
- LENG, M. J. & MARSHALL, J. D. 2004. Palaeoclimate interpretation of stable isotope data from lake sediment archives. *Quaternary Science Reviews*, 23, 811-831.
- LENG, M. J., ROBERTS, N., REED, J. M. & SLOANE, H. J. 1999. Late Quaternary palaeohydrology of the Konya Basin, Turkey, based on isotope studies of modern hydrology and lacustrine carbonates. *Journal of Paleolimnology*, 22, 187-204.
- LENG, M. J., BANESCHI, I., ZANCHETTA, G., JEX, C. N., WAGNER, B. & VOGEL, H. 2010. Late Quaternary palaeoenvironmental reconstruction from Lakes Ohrid and Prespa (Macedonia/Albania border) using stable isotopes. *Biogeosciences*, 7, 3109-3122.
- LI, H.-C., KU, T.-L., YOU, C.-F., CHENG, H., EDWARDS, R. L., MA, Z.-B., TSAI, W.-S. & LI, M.-D. 2005.  $^{87}\text{Sr}/^{86}\text{Sr}$  and  $\text{Sr}/\text{Ca}$  in speleothems for paleoclimate reconstruction in Central China between 70 and 280 kyr ago. *Geochimica et Cosmochimica Acta*, 69, 3933-3947.
- LI, H.-C., LEE, Z.-H., WAN, N.-J., SHEN, C.-C., LI, T.-Y., YUAN, D.-X. & CHEN, Y.-H. 2010. The  $[\delta]^{18}\text{O}$  and  $[\delta]^{13}\text{C}$  records in an aragonite stalagmite from Furong Cave, Chongqing, China: A 2000-year record of monsoonal climate. *Journal of Asian Earth Sciences*, In Press, Corrected Proof.
- LI, T.-Y., SHEN, C.-C., LI, H.-C., LI, J.-Y., CHIANG, H.-W., SONG, S.-R., YUAN, D.-X., LIN, C. D. J., GAO, P., ZHOU, L., WANG, J.-L., YE, M.-Y., TANG, L.-L. & XIE, S.-Y. 2011. Oxygen and carbon isotopic systematics of aragonite speleothems and water in Furong Cave, Chongqing, China. *Geochimica et Cosmochimica Acta*, 75, 4140-4156.
- LIPPMANN, F. 1973. *Sedimentary Carbonate Minerals*, Berlin, Springer-Verlag.
- LISIECKI, L. E. & RAYMO, M. E. 2005. A Pliocene-Pleistocene stack of 57 globally distributed benthic  $\delta$  O-18 records. *Paleoceanography*, 20.
- LISKER, S., VAKS, A., BAR-MATTHEWS, M., PORAT, R. & FRUMKIN, A. 2010. Late Pleistocene palaeoclimatic and palaeoenvironmental reconstruction of the Dead Sea area (Israel), based on speleothems and cave stromatolites. *Quaternary Science Reviews*, 29, 1201-1211.
- LIU, Z. Y., KUTZBACH, J. & WU, L. X. 2000. Modeling climate shift of El Nino variability in the Holocene. *Geophysical Research Letters*, 27, 2265-2268.
- LORENS, R. B. 1981. Sr, Cd, Mn and Co distribution coefficients in calcite as a function of calcite precipitation rate. *Geochimica et Cosmochimica Acta*, 45, 553-561.

- LOURENS, L. J., ANTONARAKOU, A., HILGEN, F. J., VANHOOF, A. A. M., VERGNAUDGRAZZINI, C. & ZACHARIASSE, W. J. 1996. Evaluation of the Plio-Pleistocene astronomical timescale. *Paleoceanography*, 11, 391-413.
- LUDWIG, K. R. 1998. On the treatment of concordant uranium-lead ages. *Geochimica et Cosmochimica Acta*, 62, 665-676.
- LUDWIG, K. R. 2003a. Mathematical-Statistical Treatment of Data and Errors for  $^{230}\text{Th}/\text{U}$  Geochronology. *Reviews in Mineralogy and Geochemistry*, 52, 631-656.
- LUDWIG, K. R. 2003b. ISOPLOT 3.00: a geochronology toolkit for Microsoft Excel. *Berkeley Geochronological Center Special Publication, Berkeley*.
- LUTERBACHER, J. & XOPLAKI, E. 2003. 500-year winter temperature and precipitation variability over the Mediterranean area and its connection to the large-scale atmospheric circulation. *Mediterranean Climate: Variability and Trends*.
- MAGNY, M., MIRAMONT, C. & SIVAN, O. 2002. Assessment of the impact of climate and anthropogenic factors on Holocene Mediterranean vegetation in Europe on the basis of palaeohydrological records. *Palaeogeography Palaeoclimatology Palaeoecology*, 186, 47-59.
- MAGNY, M., DE BEAULIEU, J.-L., DRESCHER-SCHNEIDER, R., VANNIERE, B., WALTER-SIMONNET, A.-V., MIRAS, Y., MILLETA, L., BOSSUETA, G., PEYRON, O., BRUGLAPAGLIA, E. & LEROUX, A. 2007. Holocene climate changes in the central Mediterranean as recorded by lake-level fluctuations at Lake Accesa (Tuscany, Italy). *Quaternary Science Reviews*, 26, 1736-1758.
- MALANOTTE-RIZZOLI, P., MANCA, B. B., D'ALCALA, M. R., THEOCHARIS, A., BRENNER, S., BUDILLON, G. & OZSOY, E. 1999. The Eastern Mediterranean in the 80s and in the 90s: the big transition in the intermediate and deep circulations. *Dynamics of Atmospheres and Oceans*, 29, 365-395.
- MALIVA, R. G. & DICKSON, J. A. D. 1992. The mechanism of skeletal aragonite neomorphism: evidence from neomorphosed mollusks from the upper Purbeck Formation (Late Jurassic-Early Cretaceous), southern England. *Sedimentary Geology*, 76, 221-232.
- MALIVA, R. G., MISSIMER, T. M. & DICKSON, J. A. D. 2000. Skeletal aragonite neomorphism in Plio-Pleistocene sandy limestones and sandstones, Hollywood, Florida, USA. *Sedimentary Geology*, 136, 147-154.
- MANGINI, A., SPÖTL, C. & VERDES, P. 2005. Reconstruction of temperature in the Central Alps during the past 2000 yr from a  $\delta(18)\text{O}$  stalagmite record. *Earth and Planetary Science Letters*, 235, 741-751.
- MARTÍN-GARCÍA, R., ALONSO-ZARZA, A. M. & MARTÍN-PÉREZ, A. 2009. Loss of primary texture and geochemical signatures in speleothems due to diagenesis: Evidences from Castañar Cave, Spain. *Sedimentary Geology*, 221, 141-149.
- MARTIN, G. D., WILKINSON, B. H. & LOHMANN, K. C. 1986. THE ROLE OF SKELETAL POROSITY IN ARAGONITE NEOMORPHISM - STROMBUS AND MONTASTREA FROM THE PLEISTOCENE KEY LARGO LIMESTONE, FLORIDA. *Journal of Sedimentary Petrology*, 56, 194-203.
- MATTEY, D., LOWRY, D., DUFFET, J., FISHER, R., HODGE, E. & FRISIA, S. 2008. A 53 year seasonally resolved oxygen and carbon isotope record from a modern Gibraltar speleothem: Reconstructed drip water and relationship to local precipitation. *Earth and Planetary Science Letters*, 269, 80-95.
- MAYLE, F. E., BURBRIDGE, R. & KILLEEN, T. J. 2000. Millennial-scale dynamics of southern Amazonian rain forests. *Science*, 290, 2291-+.
- MAZZULLO, S. J. 1980. CALCITE PSEUDOSPAR REPLACIVE OF MARINE ACICULAR ARAGONITE, AND IMPLICATIONS FOR ARAGONITE CEMENT DIAGENESIS. *Journal of Sedimentary Petrology*, 50, 409-422.

- MCARTHUR, J. M., HOWARTH, R. J. & BAILEY, T. R. 2001. Strontium isotope stratigraphy: LOWESS version 3: Best fit to the marine Sr-isotope curve for 0-509 Ma and accompanying look-up table for deriving numerical age. *Journal of Geology*, 109, 155-170.
- MCCLURE, H. A. 1976. RADIOCARBON CHRONOLOGY OF LATE QUATERNARY LAKES IN ARABIAN DESERT. *Nature*, 263, 755-756.
- MCCREA, J. M. 1950. ON THE ISOTOPIC CHEMISTRY OF CARBONATES AND A PALEOTEMPERATURE SCALE. *Journal of Chemical Physics*, 18, 849-857.
- MCDERMOTT, F. 2004. Palaeo-climate reconstruction from stable isotope variations in speleothems: a review. *Quaternary Science Reviews*, 23, 901-918.
- MCDERMOTT, F., FRISIA, S., HUANG, Y. M., LONGINELLI, A., SPIRO, B., HEATON, T. H. E., HAWKESWORTH, C. J., BORSATO, A., KEPPENS, E., FAIRCHILD, I. J., VAN DER BORG, K., VERHEYDEN, S. & SELMO, E. 1999. Holocene climate variability in Europe: Evidence from delta O-18, textural and extension-rate variations in three speleothems. *Quaternary Science Reviews*, 18, 1021-1038.
- MCDERMOTT, F., SCHWARCZ, H. P. & ROWE, P. J. 2006. Isotopes in Speleothems. In: LENG, M. J. (ed.) *Isotopes in Palaeoenvironmental Research*. Heidelberg: Springer.
- MCDERMOTT, F., ATKINSON, T. C., FAIRCHILD, I. J., BALDINI, L. M. & MATTEY, D. P. 2011. A first evaluation of the spatial gradients in [delta]18O recorded by European Holocene speleothems. *Global and Planetary Change*, In Press, Corrected Proof.
- MCGARRY, S. F. & BAKER, A. 2000. Organic acid fluorescence: applications to speleothem palaeoenvironmental reconstruction. *Quaternary Science Reviews*, 19, 1087-1101.
- MCGILLEN, M. R. & FAIRCHILD, I. J. 2005. An experimental study of incongruent dissolution of CaCO<sub>3</sub> under analogue glacial conditions. *Journal of Glaciology*, 51, 383-390.
- MCKINNEY, C. R., MCCREA, J. M., EPSTEIN, S., ALLEN, H. A. & UREY, H. C. 1950. IMPROVEMENTS IN MASS SPECTROMETERS FOR THE MEASUREMENT OF SMALL DIFFERENCES IN ISOTOPE ABUNDANCE RATIOS. *Review of Scientific Instruments*, 21, 724-730.
- MCLAREN, S. J., GILBERTSON, D. D., GRATTAN, J. P., HUNT, C. O., DULLER, G. A. T. & BARKER, G. A. 2004. Quaternary palaeogeomorphologic evolution of the Wadi Faynan area, southern Jordan. *Palaeogeography, Palaeoclimatology, Palaeoecology*, 205, 131-154.
- MCMANUS, J. F., BOND, G. C., BROECKER, W. S., JOHNSEN, S., LABEYRIE, L. & HIGGINS, S. 1994. HIGH-RESOLUTION CLIMATE RECORDS FROM THE NORTH-ATLANTIC DURING THE LAST INTERGLACIAL. *Nature*, 371, 326-329.
- MCMANUS, J. F., OPPO, D. W. & CULLEN, J. L. 1999. A 0.5-million-year record of millennial-scale climate variability in the North Atlantic. *Science*, 283, 971-975.
- MCMILLAN, E. A., FAIRCHILD, I. J., FRISIA, S., BORSATO, A. & MCDERMOTT, F. 2005. Annual trace element cycles in calcite-aragonite speleothems: evidence of drought in the western Mediterranean 1200-1100 yr BP. *Journal of Quaternary Science*, 20, 423-433.
- MEENTMEYER, V. 1978. Macroclimate and lignin control of decomposition rates. *Ecology*, 59, 465-472.
- MELKI, T., KALLEL, N. & FONTUGNE, M. 2010. The nature of transitions from dry to wet condition during sapropel events in the Eastern Mediterranean Sea. *Palaeogeography Palaeoclimatology Palaeoecology*, 291, 267-285.
- MEYER, M. C., CLIFF, R. A., SPÖTL, C., KNIPPING, M. & MANGINI, A. 2009. Speleothems from the earliest Quaternary: Snapshots of paleoclimate and landscape evolution at the northern rim of the Alps. *Quaternary Science Reviews*, 28, 1374-1391.

- MICKLER, P. J., BANNER, J. L., STERN, L., ASMEROM, Y., EDWARDS, R. L. & ITO, E. 2004. Stable isotope variations in modern tropical speleothems: Evaluating equilibrium vs. kinetic isotope effects. *Geochimica Et Cosmochimica Acta*, 68, 4381-4393.
- MICKLER, P. J., STERN, L. A. & BANNER, J. L. 2006. Large kinetic isotope effects in modern speleothems. *Geological Society of America Bulletin*, 118, 65-81.
- MIGOWSKI, C., STEIN, M., PRASAD, S., NEGENDANK, J. R. F. W. & AGNON, A. 2006. Holocene climate variability and cultural evolution in the Near East from the Dead Sea sedimentary record. *Quaternary Research*, 66, 421-431.
- MODARRES, R. & SARHADI, A. 2011. Statistically-based regionalization of rainfall climates of Iran. *Global and Planetary Change*, 75, 67-75.
- MOORE, G. W. 1956. Aragonite speleothems as indicators of paleotemperature. *American Journal of Science*, 254, 746-753.
- MOORE, G. W. 1962. The Growth of Stalactites. *Bulletin of the National Speleological Society*, 24, 95-106.
- MORSE, J. W. & MACKENZIE, F. T. 1990. *Geochemistry of Sedimentary Carbonates*, Amsterdam, Elsevier.
- MORSE, J. W. & BENDER, M. L. 1990. PARTITION-COEFFICIENTS IN CALCITE - EXAMINATION OF FACTORS INFLUENCING THE VALIDITY OF EXPERIMENTAL RESULTS AND THEIR APPLICATION TO NATURAL SYSTEMS. *Chemical Geology*, 82, 265-277.
- MORSE, J. W., WANG, Q. W. & TSIU, M. Y. 1997. Influences of temperature and Mg:Ca ratio on CaCO<sub>3</sub> precipitates from seawater. *Geology*, 25, 85-87.
- MOULIN, C., LAMBERT, C. E., DULAC, F. & DAYAN, U. 1997. Control of atmospheric export of dust from North Africa by the North Atlantic oscillation. *Nature*, 387, 691-694.
- MUCCI, A. & MORSE, J. W. 1983. The incorporation of Mg<sup>2+</sup> and Sr<sup>2+</sup> into calcite overgrowths: influences of growth rate and solution composition. *Geochimica et Cosmochimica Acta*, 47, 217-233.
- MUCCI, A. & MORSE, J. W. 1985. Auger-spectroscopy determination of the surface-most adsorbed layer composition on aragonite, calcite, dolomite, and magnesite in synthetic seawater. *American Journal of Science*, 285, 306-317.
- MÜHLINGHAUS, C., SCHOLZ, D. & MANGINI, A. 2009. Modelling fractionation of stable isotopes in stalagmites. *Geochimica et Cosmochimica Acta*, 73, 7275-7289.
- MÜNNICH, K. O. 1957. Messungen des <sup>14</sup>C-Gehaltes von hartem Grundwasser. *Naturwissenschaften*, 44, 32-33.
- MULLER, U. C., KLOTZ, S., GEYH, M. A., PROSS, J. & BOND, G. C. 2005. Cyclic climate fluctuations during the last interglacial in central Europe. *Geology*, 33, 449-452.
- MURRAY, J. W. 1954. The deposition of calcite and aragonite in caves. *Journal of Geology*, 62, 481-&.
- MUSGROVE, M. & BANNER, J. L. 2004. Controls on the spatial and temporal variability of vadose dripwater geochemistry: Edwards aquifer, central Texas. *Geochimica et Cosmochimica Acta*, 68, 1007-1020.
- MYERS, P. G. & ROHLING, E. J. 2000. Modeling a 200-yr interruption of the Holocene Sapropel S-1. *Quaternary Research*, 53, 98-104.
- NASAB, H. V., CLARK, G. A. & TORKAMANDI, S. 2012. Late Pleistocene dispersal corridors across the Iranian Plateau: A case study from Mirak, a Middle Paleolithic site on the northern edge of the Iranian Central desert (Dasht-e Kavir). *Quaternary International*.
- NAZEMOSADAT, M. J. & CORDERY, I. 2000. On the relationships between ENSO and autumn rainfall in Iran. *International Journal of Climatology*, 20, 47-61.
- NEEV, D. & HALL, J. K. 1979. GEOPHYSICAL INVESTIGATIONS IN THE DEAD SEA. *Sedimentary Geology*, 23, 209-238.

- NIER, A. O. 1950. A REDETERMINATION OF THE RELATIVE ABUNDANCES OF THE ISOTOPES OF CARBON, NITROGEN, OXYGEN, ARGON, AND POTASSIUM. *Physical Review*, 77, 789-793.
- O'NEIL, J. R., CLAYTON, R. N. & MAYEDA, T. K. 1969. OXYGEN ISOTOPE FRACTIONATION IN DIVALENT METAL CARBONATES. *Journal of Chemical Physics*, 51, 5547-&.
- ONAC, B. P. 2005. Minerals. In: CARVER, D. C. & WHITE, W. B. (eds.) *Encyclopedia of Caves*. London: Elsevier Academic Press.
- OOMORI, T., KANESHIMA, H., MAEZATO, Y. & KITANO, Y. 1987. Distribution coefficient of  $Mg^{2+}$  ions between calcite and solution at 10-50°C. *Marine Chemistry*, 20, 327-336.
- ORTEGA, R., MAIRE, R., DEVÈS, G. & QUINIF, Y. 2005. High-resolution mapping of uranium and other trace elements in recrystallized aragonite-calcite speleothems from caves in the Pyrenees (France): Implication for U-series dating. *Earth and Planetary Science Letters*, 237, 911-923.
- OSMOND, J. K. 1980. Uranium series disequilibrium in hydrologic studies. In: FRITZ, P. & FONTES, J. C. (eds.) *Handbook of Environmental Isotope Geochemistry*. Amsterdam: Elsevier.
- OSMOND, J. K. & IVANOVICH, M. 1992. Uranium-series mobilization and surface hydrology. In: IVANOVICH, M. & HARMON, R. S. (eds.) *Uranium-Series Disequilibrium*. Oxford: Oxford Science Publishers.
- OSTER, J. L., MONTAÑEZ, I. P., SHARP, W. D. & COOPER, K. M. 2009. Late Pleistocene California droughts during deglaciation and Arctic warming. *Earth and Planetary Science Letters*, 288, 434-443.
- OSTER, J. L., MONTAÑEZ, I. P., GUILDERSON, T. P., SHARP, W. D. & BANNER, J. L. 2010. Modeling speleothem  $\delta^{13}C$  variability in a central Sierra Nevada cave using  $^{14}C$  and  $^{87}Sr/^{86}Sr$ . *Geochimica et Cosmochimica Acta*, 74, 5228-5242.
- PANNO, S. V., LUNDSTROM, C. C., HACKLEY, K. C., CURRY, B. B., FOUKE, B. W. & ZHANG, Z. F. 2009. Major Earthquakes Recorded by Speleothems in Midwestern US Caves. *Bulletin of the Seismological Society of America*, 99, 2147-2154.
- PAPE, J. R., BANNER, J. L., MACK, L. E., MUSGROVE, M. & GUILFOYLE, A. 2010. Controls on oxygen isotope variability in precipitation and cave drip waters, central Texas, USA. *Journal of Hydrology*, 385, 203-215.
- PAQUETTE, J. & REEDER, R. J. 1995. Relationship between surface structure, growth mechanism, and trace element incorporation in calcite. *Geochimica et Cosmochimica Acta*, 59, 735-749.
- PARTIN, J. W., COBB, K. M., ADKINS, J. F., CLARK, B. & FERNANDEZ, D. P. 2007. Millennial-scale trends in west Pacific warm pool hydrology since the Last Glacial Maximum. *Nature*, 449, 452-U3.
- PASSIER, H. F., BOSCH, H. J., NIJENHUIS, I. A., LOURENS, L. J., BOTTCHER, M. E., LEENDERS, A., DAMSTE, J. S. S., DE LANGE, G. J. & DE LEEUW, J. W. 1999. Sulphidic Mediterranean surface waters during Pliocene sapropel formation. *Nature*, 397, 146-149.
- PAULING, A., LUTERBACHER, J., CASTY, C. & WANNER, H. 2006. Five hundred years of gridded high-resolution precipitation reconstructions over Europe and the connection to large-scale circulation. *Climate Dynamics*, 26, 387-405.
- PAULSEN, D. E., LI, H.-C. & KU, T.-L. 2003. Climate variability in central China over the last 1270 years revealed by high-resolution stalagmite records. *Quaternary Science Reviews*, 22, 691-701.
- PEDONE, V. A., CERCONE, K. R. & BURRUSS, R. C. 1990. ACTIVATORS OF PHOTOLUMINESCENCE IN CALCITE - EVIDENCE FROM HIGH-RESOLUTION, LASER-EXCITED LUMINESCENCE SPECTROSCOPY. *Chemical Geology*, 88, 183-190.

- PERDIKOURI, C., KASIOPTAS, A., PUTNIS, C. V. & PUTNIS, A. 2008. The effect of fluid composition on the mechanism of the aragonite to calcite transition. *Mineralogical Magazine*, 72, 111-114.
- PERDIKOURI, C., KASIOPTAS, A., GEISLER, T., SCHMIDT, B. C. & PUTNIS, A. 2011. Experimental study of the aragonite to calcite transition in aqueous solution. *Geochimica et Cosmochimica Acta*, In Press, Accepted Manuscript.
- PERKINS, A. M. 1996. Observations under electron microscopy of magnetic minerals extracted from speleothems. *Earth and Planetary Science Letters*, 139, 281-289.
- PERRETTE, Y., DELANNOY, J. J., DESMET, M., LIGNIER, V. & DESTOMBES, J. L. 2005. Speleothem organic matter content imaging. The use of a Fluorescence Index to characterise the maximum emission wavelength. *Chemical Geology*, 214, 193-208.
- PERRIER, F., RICHON, P. & SABROUX, J. C. 2005. Modelling the effect of air exchange on Rn-222 and its progeny concentration in a tunnel atmosphere. *Science of the Total Environment*, 350, 136-150.
- PERRIN, K., JEANNIN, P. Y. & ZWAHLEN, F. 2003. Epikarst storage in a karst aquifer: a conceptual model based on isotopic data, Milandre test site, Switzerland. *Journal of Hydrology*, 279, 106-124.
- PETIT, J. R., JOUZEL, J., RAYNAUD, D., BARKOV, N. I., BARNOLA, J. M., BASILE, I., BENDER, M., CHAPPELLAZ, J., DAVIS, M., DELAYGUE, G., DELMOTTE, M., KOTLYAKOV, V. M., LEGRAND, M., LIPENKOV, V. Y., LORIUS, C., PEPIN, L., RITZ, C., SALTZMAN, E. & STIEVENARD, M. 1999. Climate and atmospheric history of the past 420,000 years from the Vostok ice core, Antarctica. *Nature*, 399, 429-436.
- PEYRON, O., GORING, S., DORMOY, I., KOTTHOFF, U., PROSS, J., DE BEAULIEU, J. L., DRESCHER-SCHNEIDER, R., VANNIÉRE, B. & MAGNY, M. 2011. Holocene seasonality changes in the central mediterranean region reconstructed from the pollen sequences of Lake Accesa (Italy) and Tenaghi Philippon (Greece). *Holocene*, 21, 131-146.
- PFLITSCH, A. & PIASECKI, J. 2003. Detection of an airflow system in Niedzwiedzia (Bear) Cave, Kletno, Poland. *Journal of Cave and Karst Studies*, 65, 160-173.
- PICKERING, R., KRAMERS, J. D., PARTRIDGE, T., KODOLANYI, J. & PETTKE, T. 2010. U-Pb dating of calcite-aragonite layers in speleothems from hominin sites in South Africa by MC-ICP-MS. *Quaternary Geochronology*, 5, 544-558.
- PIERRE, C. 1999. The oxygen and carbon isotope distribution in the Mediterranean water masses. *Marine Geology*, 153, 41-55.
- PINARDI, N. & MASETTI, E. 2000. Variability of the large scale general circulation of the Mediterranean Sea from observations and modelling: a review. *Palaeogeography Palaeoclimatology Palaeoecology*, 158, 153-174.
- PINGITORE, N. E. 1976. VADOSE AND PHREATIC DIAGENESIS - PROCESSES, PRODUCTS AND THEIR RECOGNITION IN CORALS. *Journal of Sedimentary Petrology*, 46, 985-1006.
- PINGITORE, N. E. 1982. THE ROLE OF DIFFUSION DURING CARBONATE DIAGENESIS. *Journal of Sedimentary Petrology*, 52, 27-40.
- PINHASI, R. & PLUCIENNIK, M. 2004. A Regional Biological Approach to the Spread of Farming in Europe: Anatolia, the Levant, South-Eastern Europe, and the Mediterranean. *Current Anthropology*, 45, S59-S82.
- PLAGNES, V., CAUSSE, C., GENTY, D., PATERNE, M. & BLAMART, D. 2002. A discontinuous climatic record from 187 to 74 ka from a speleothem of the Clamouse Cave (south of France). *Earth and Planetary Science Letters*, 201, 87-103.
- POAGE, M. A. & CHAMBERLAIN, C. P. 2001. Empirical relationships between elevation and the stable isotope composition of precipitation and surface waters: Considerations for studies of paleoelevation change. *American Journal of Science*, 301, 1-15.
- POLYAK, V. J. & ASMEROM, Y. 2001. Late Holocene climate and cultural changes in the southwestern United States. *Science*, 294, 148-151.

- PRUYERS, P. A., DELANGE, G. J. & MIDDELBURG, J. J. 1991. GEOCHEMISTRY OF EASTERN MEDITERRANEAN SEDIMENTS - PRIMARY SEDIMENT COMPOSITION AND DIAGENETIC ALTERATIONS. *Marine Geology*, 100, 137-154.
- RAICH, J. W. & SCHLESINGER, W. H. 1992. THE GLOBAL CARBON-DIOXIDE FLUX IN SOIL RESPIRATION AND ITS RELATIONSHIP TO VEGETATION AND CLIMATE. *Tellus Series B-Chemical and Physical Meteorology*, 44, 81-99.
- RAICICH, F., PINARDI, N. & NAVARRA, A. 2003. Teleconnections between Indian monsoon and Sahel rainfall and the Mediterranean. *International Journal of Climatology*, 23, 173-186.
- RAIKES, R. 1967. *Water, Weather and Prehistory*, Aberdeen, The University Press.
- RAILSBACK, L. B., BROOK, G. A., CHEN, J., KALIN, R. & FLEISHER, C. J. 1994. Environmental controls on the petrology of a late Holocene speleothem from Botswana with annual layers of aragonite and calcite. *Journal of Sedimentary Research Section A-Sedimentary Petrology and Processes*, 64, 147-155.
- RAILSBACK, L. B., DABOUS, A. A., OSMOND, J. K. & FLEISHER, C. J. 2002. Petrographic and Geochemical Screening of Speleothems for U-series Dating: An Example from Recrystallized Speleothems from Wadi Sannur Cavern, Egypt. *Journal of Cave and Karst Studies*, 64.
- RAILSBACK, L. B., LIANG, F., VIDAL ROMANI, J. R., GRANDAL-D'ANGLADE, A., VAQUEIRO RODRIGUEZ, M., SANTOS FIDALGO, L., FERNANDEZ MOSQUERA, D., CHENG, H. & EDWARDS, R. L. 2011. Petrographic and isotopic evidence for Holocene long-term climate change and shorter-term environmental shifts from a stalagmite from the Serra do Courel of northwestern Spain, and implications for climatic history across Europe and the Mediterranean. *Palaeogeography Palaeoclimatology Palaeoecology*, 305, 172-184.
- RAZIEI, T., BORDI, I. & PEREIRA, L. S. 2008. A precipitation-based regionalization for Western Iran and regional drought variability. *Hydrology and Earth System Sciences*, 12, 1309-1321.
- REDDY, M. M. & WANG, K. K. 1980. Crystallization of calcium carbonate in the presence of metal ions : I. Inhibition by magnesium ion at pH 8.8 and 25°C. *Journal of Crystal Growth*, 50, 470-480.
- REEDER, R. J. & GRAMS, J. C. 1987. Sector zoning in calcite cement crystals: Implications for trace element distributions in carbonates. *Geochimica et Cosmochimica Acta*, 51, 187-194.
- REEVE, A. S. & PERRY, E. C. 1994. CARBONATE GEOCHEMISTRY AND THE CONCENTRATIONS OF AQUEOUS  $Mg^{2+}$ ,  $SR^{2+}$  AND  $CA^{2+}$  - WESTERN NORTH COAST OF THE YUCATAN, MEXICO. *Chemical Geology*, 112, 105-117.
- REVEL, M., DUCASSOU, E., GROUSSET, F. E., BERNASCONI, S. M., MIGEON, S., REVILLON, S., MASCLE, J., MURAT, A., ZARAGOSI, S. & BOSCH, D. 2010. 100,000 Years of African monsoon variability recorded in sediments of the Nile margin. *Quaternary Science Reviews*, 29, 1342-1362.
- RICHARDS, D. A. & DORALE, J. A. 2003. Uranium-series Chronology and Environmental Applications of Speleothems *In*: BOURDON, B., HENDERSON, G. M., LUNDSTROM, C. C. & TURNER, S. P. (eds.) *Uranium-series Geochemistry*. Reviews in Mineralogy.
- RICHARDS, D. A., BOTTRELL, S. H., CLIFF, R. A., STROHLE, K. & ROWE, P. J. 1998. U-Pb dating of a speleothem of Quaternary age. *Geochimica et Cosmochimica Acta*, 62, 3683-3688.
- RICHON, P., PERRIER, F., SABROUX, J. C., TRIQUE, M., FERRY, C., VOISIN, V. & PILI, E. 2005. Spatial and time variations of radon-222 concentration in the atmospheres of a dead-end horizontal tunnel. *Journal of Environmental Radioactivity*, 78, 179-198.

- RIGHTMIRE, C. T. 1978. Seasonal variation in  $p\text{CO}_2$  and  $^{13}\text{C}$  content of soil atmosphere. *Water Resources Research*, 14, 691-692.
- ROBERTS, M. S., SMART, P. L. & BAKER, A. 1998. Annual trace element variations in a Holocene speleothem. *Earth and Planetary Science Letters*, 154, 237-246.
- ROBERTS, M. S., SMART, P. L., HAWKESWORTH, C. J., PERKINS, W. T. & PEARCE, N. J. G. 1999a. Trace element variations in coeval holocene speleothems from GB cave, southwest England. *Holocene*, 9, 707-713.
- ROBERTS, N., KUZUCUOĞLU, C. & KARABIYIKOĞLU, M. 1999b. The Late Quaternary in the Eastern Mediterranean region: an introduction. *Quaternary Science Reviews*, 18, 497-499.
- ROBERTS, N., REED, J. M., LENG, M. J., KUZUCUOĞLU, C., FONTUGNE, M., BERTAUX, J., WOLDRING, H., BOTTEMA, S., BLACK, S., HUNT, E. & KARABIYIKOĞLU, M. 2001. The tempo of Holocene climatic change in the eastern Mediterranean region: New high-resolution crater-lake sediment data from central Turkey. *Holocene*, 11, 721-736.
- ROBINSON, L. F., HENDERSON, G. M. & SLOWEY, N. C. 2002. U-Th dating of marine isotope stage 7 in Bahamas slope sediments. *Earth and Planetary Science Letters*, 196, 175-187.
- ROBINSON, S. A., BLACK, S., SELLWOOD, B. W. & VALDES, P. J. 2006. A review of palaeoclimates and palaeoenvironments in the Levant and Eastern Mediterranean from 25,000 to 5000 years BP: setting the environmental background for the evolution of human civilisation. *Quaternary Science Reviews*, 25, 1517-1541.
- RODWELL, M. J. & HOSKINS, B. J. 1996. Monsoons and the dynamics of deserts. *Quarterly Journal of the Royal Meteorological Society*, 122, 1385-1404.
- ROHLING, E. J. 1994. REVIEW AND NEW ASPECTS CONCERNING THE FORMATION OF EASTERN MEDITERRANEAN SAPROPELS. *Marine Geology*, 122, 1-28.
- ROHLING, E. J. & HILGEN, F. J. 1991. THE EASTERN MEDITERRANEAN CLIMATE AT TIMES OF SAPROPEL FORMATION - A REVIEW. *Geologie En Mijnbouw*, 70, 253-264.
- ROHLING, E. J. & PALIKE, H. 2005. Centennial-scale climate cooling with a sudden cold event around 8,200 years ago. *Nature*, 434, 975-979.
- ROHLING, E. J., JORISSEN, F. J. & DESTIGTER, H. C. 1997. 200 year interruption of Holocene sapropel formation in the Adriatic Sea. *Journal of Micropalaeontology*, 16, 97-108.
- ROMANEK, C. S., GROSSMAN, E. L. & MORSE, J. W. 1992. Carbon isotopic fractionation in synthetic aragonite and calcite - Effects of temperature and precipitation rate. *Geochimica et Cosmochimica Acta*, 56, 419-430.
- ROSHOLT, J. N. 1982. Mobilization and weathering. In: IVANOVICH, R. S. & HARMON, R. S. (eds.) *Uranium Series Disequilibrium: Applications to Environmental Problems*. Oxford: Clarendon Press.
- ROSSIGNOL-STRICK, M. 1983. AFRICAN MONSOONS, AN IMMEDIATE CLIMATE RESPONSE TO ORBITAL INSOLATION. *Nature*, 304, 46-49.
- ROSSIGNOL-STRICK, M. 1985. MEDITERRANEAN QUATERNARY SAPROPELS, AN IMMEDIATE RESPONSE OF THE AFRICAN MONSOON TO VARIATION OF INSOLATION. *Palaeogeography Palaeoclimatology Palaeoecology*, 49, 237-263.
- ROSSIGNOL-STRICK, M. 1995. Sea-land correlation of pollen records in the Eastern Mediterranean for the glacial-interglacial transition: Biostratigraphy versus radiometric time-scale. *Quaternary Science Reviews*, 14, 893-915.
- ROSSIGNOL-STRICK, M. & PATERNE, M. 1999. A synthetic pollen record of the eastern Mediterranean sapropels of the last 1 Ma: implications for the time-scale and formation of sapropels. *Marine Geology*, 153, 221-237.

- ROSSIGNOL-STRICK, M.,NESTEROFF, W.,OLIVE, P. & VERGNAUD-GRAZZINI, C. 1982. AFTER THE DELUGE - MEDITERRANEAN STAGNATION AND SAPROPEL FORMATION. *Nature*, 295, 105-110.
- ROZANSKI, K.,SONNTAG, C. & MUNNICH, K. O. 1982. FACTORS CONTROLLING STABLE ISOTOPE COMPOSITION OF EUROPEAN PRECIPITATION. *Tellus*, 34, 142-150.
- ROZANSKI, K.,ARAGUAS-ARAGUAS, L. & GONFIANTINI, R. 1993. Isotopic patterns in modern precipitation. In: SWART, P. K., LOHMANN, K. C., MCKENZIE, J. & SAVIN, S. (eds.) *Climate Change in Continental Isotopic Records*. Washington, D.C.: American Geophysical Union.
- RYAN, J. L. & RAI, D. 1987. THORIUM(IV) HYDROUS OXIDE SOLUBILITY. *Inorganic Chemistry*, 26, 4140-4142.
- SADORI, L. & NARCISI, B. 2001. The Postglacial record of environmental history from Lago di Pergusa, Sicily. *Holocene*, 11, 655-671.
- SALAH, M. 2005. Wonder of Kerman and Torang Cave. *Kouh*. Tehran, Iran: <http://tehranavenue.com/print.php?ln=en&id=449>.
- SALOMONS, W. & MOOK, W. G. 1986. Isotope Geochemistry of Carbonates in the Weathering Zone. In: FRITZ, P. & FONTES, J. C. (eds.) *Handbook of Environmental Isotope Geochemistry - The Terrestrial Environment*, B. Amsterdam: Elsevier.
- SANDBERG, P. A. & HUDSON, J. D. 1983. ARAGONITE RELIC PRESERVATION IN JURASSIC CALCITE-REPLACED BIVALVES. *Sedimentology*, 30, 879-892.
- SARIS, F.,HANNAH, D. M. & EASTWOOD, W. J. 2010. Spatial variability of precipitation regimes over Turkey. *Hydrological Sciences Journal-Journal Des Sciences Hydrologiques*, 55, 234-249.
- SCHOLZ, D. & HOFFMANN, D. L. 2011. StalAge - An algorithm designed for construction of speleothem age models. *Quaternary Geochronology*, 6, 369-382.
- SCHOLZ, D.,MUEHLINGHAUS, C. & MANGINI, A. 2009. Modelling delta C-13 and delta O-18 in the solution layer on stalagmite surfaces. *Geochimica et Cosmochimica Acta*, 73, 2592-2602.
- SCHRAG, D. P.,HAMPT, G. & MURRAY, D. W. 1996. Pore fluid constraints on the temperature and oxygen isotopic composition of the glacial ocean. *Science*, 272, 1930-1932.
- SCHRAG, D. P.,ADKINS, J. F.,MCINTYRE, K.,ALEXANDER, J. L.,HODELL, D. A.,CHARLES, C. D. & MCMANUS, J. F. 2002. The oxygen isotopic composition of seawater during the Last Glacial Maximum. *Quaternary Science Reviews*, 21, 331-342.
- SCHROEDE, J. H. 1969. EXPERIMENTAL DISSOLUTION OF CALCIUM, MAGNESIUM, AND STRONTIUM FROM RECENT BIOGENIC CARBONATES - A MODEL OF DIAGENESIS. *Journal of Sedimentary Petrology*, 39, 1057-&.
- SCHWARCZ, H. P. 1986. Geochronology and isotopic geochemistry of speleothems. In: FRITZ, P. & FONTES, G. (eds.) *Handbook of Environmental Isotope Geochemistry*. Amsterdam: Elsevier.
- SCHWARCZ, H. P.,HARMON, R. S.,THOMPSON, P. & FORD, D. C. 1976. STABLE ISOTOPE STUDIES OF FLUID INCLUSIONS IN SPELEOTHEMS AND THEIR PALEOCLIMATIC SIGNIFICANCE. *Geochimica et Cosmochimica Acta*, 40, 657-665.
- SCOFFIN, T. P. 1987. *An Introduction to Carbonate Sediments and Rocks*, New York, Chapman and Hall.
- SCRIVNER, A. E.,VANCE, D. & ROHLING, E. J. 2004. New neodymium isotope data quantify Nile involvement in Mediterranean anoxic episodes. *Geology*, 32, 565-568.
- SEIDENKRANTZ, M. S.,KRISTENSEN, P. & KNUDSEN, K. L. 1995. MARINE EVIDENCE FOR CLIMATIC INSTABILITY DURING THE LAST INTERGLACIAL IN SHELF RECORDS FROM NORTHWEST EUROPE. *Journal of Quaternary Science*, 10, 77-82.

- SENESI, N.,MIANO, T. M.,PROVENZANO, M. R. & BRUNETTI, G. 1991. CHARACTERIZATION, DIFFERENTIATION, AND CLASSIFICATION OF HUMIC SUBSTANCES BY FLUORESCENCE SPECTROSCOPY. *Soil Science*, 152, 259-271.
- SHARP, Z. 2007. *Principles of Stable Isotope Geochemistry*, Upper Saddle River, NJ., Pearson Education, Inc.
- SHAY-EL, Y. & ALPERT, P. 1991. A diagnostic study of winter diabatic heating in the Mediterranean in relation to cyclones. *Quarterly Journal of the Royal Meteorological Society*, 117, 715-747.
- SHERWIN, C. M. & BALDINI, J. U. L. 2011. Cave air and hydrological controls on prior calcite precipitation and stalagmite growth rates: Implications for palaeoclimate reconstructions using speleothems. *Geochimica et Cosmochimica Acta*, 75, 3915-3929.
- SHINDELL, D. T.,MILLER, R. L.,SCHMIDT, G. A. & PANDOLFO, L. 1999. Simulation of recent northern winter climate trends by greenhouse-gas forcing. *Nature*, 399, 452-455.
- SHOPOV, Y. Y.,FORD, D. C. & SCHWARCZ, H. P. 1994. LUMINESCENT MICROBANDING IN SPELEOTHEMS - HIGH-RESOLUTION CHRONOLOGY AND PALEOCLIMATE. *Geology*, 22, 407-410.
- SHURBAJI, A. R. M. & PHILLIPS, F. M. 1995. A NUMERICAL-MODEL FOR THE MOVEMENT OF H<sub>2</sub>O, H-2 O-18, AND (HHO)-H-2 IN THE UNSATURATED ZONE. *Journal of Hydrology*, 171, 125-142.
- SINCLAIR, D. J. 2011. Two mathematical models of Mg and Sr partitioning into solution during Incongruent Calcite Dissolution. Implications for dripwater and speleothem studies. *Chemical Geology*, 283, 119-133.
- SINHA, A.,CANNARIATO, K. G.,STOTT, L. D.,CHENG, H.,EDWARDS, R. L.,YADAVA, M. G.,RAMESH, R. & SINGH, I. B. 2007. A 900-year (600 to 1500 A. D.) record of the Indian summer monsoon precipitation from the core monsoon zone of India. *Geophysical Research Letters*, 34.
- SIROCKO, F.,SARNTHEIN, M.,ERLENKEUSER, H.,LANGE, H.,ARNOLD, M. & DUPLESSY, J. C. 1993. CENTURY-SCALE EVENTS IN MONSOONAL CLIMATE OVER THE PAST 24,000 YEARS. *Nature*, 364, 322-324.
- SMART, P. L. & FRIEDERICH, H. Water movement and storage in the unsaturated zone of a maturely karstified aquifer, Mendip Hills, England. Conference on environmental problems in karst terrains and their solution, 1987 Bowling Green, Kentucky. National Water Well Association, 57-87.
- SÖNMEZ, F. K.,KOMUSCU, A. U.,ERKAN, A. & TURGU, E. 2005. An analysis of spatial and temporal dimension of drought vulnerability in Turkey using the standardized precipitation index. *Natural Hazards*, 35, 243-264.
- SPEER, J. A. 1983. Crystal chemistry and phase relations of orthorhombic carbonates. In: REEDER, R. J. (ed.) *Carbonates: Mineralogy and Chemistry*. Chelsea, Michigan: Mineralogical Society of America.
- SPÖTL, C. & MANGINI, A. 2002. Stalagmite from the Austrian Alps reveals Dansgaard-Oeschger events during isotope stage 3: Implications for the absolute chronology of Greenland ice cores. *Earth and Planetary Science Letters*, 203, 507-518.
- SPÖTL, C.,MANGINI, A.,FRANK, N.,EICHSTADTER, R. & BURNS, S. J. 2002a. Start of the last interglacial period at 135 ka: Evidence from a high Alpine speleothem. *Geology*, 30, 815-818.
- SPÖTL, C.,UNTERWURZACHER, M.,MANGINI, A. & LONGSTAFFE, F. J. 2002b. Carbonate speleothems in the dry, inneralpine Vinschgau Valley, northernmost Italy: Witnesses of changes in climate and hydrology since the last glacial maximum. *Journal of Sedimentary Research*, 72, 793-808.

- SPÖTL, C., FAIRCHILD, I. J. & TOOTH, A. F. 2005. Cave air control on dripwater geochemistry, Obir Caves (Austria): Implications for speleothem deposition in dynamically ventilated caves. *Geochimica et Cosmochimica Acta*, 69, 2451-2468.
- STEPANOV, V. I. 1997. Notes on mineral growth from the archive of V.I. Stepanov (1924-1988). *Proceedings of the University of Bristol Speleological Society*, 21, 25-42.
- STEVENS, L. R., WRIGHT, H. E. & ITO, E. 2001. Proposed changes in seasonality of climate during the Lateglacial and Holocene at Lake Zeribar, Iran. *Holocene*, 11, 747-755.
- STEWART, B. W., CAPO, R. C. & CHADWICK, O. A. 1998. Quantitative strontium isotope models for weathering, pedogenesis and biogeochemical cycling. *Geoderma*, 82, 173-195.
- STOTT, L., CANNARIATO, K., THUNELL, R., HAUG, G. H., KOUTAVAS, A. & LUND, S. 2004. Decline of surface temperature and salinity in the western tropical Pacific Ocean in the Holocene epoch. *Nature*, 431, 56-59.
- STREET-PERROTT, F. A. & PERROTT, R. A. 1990. ABRUPT CLIMATE FLUCTUATIONS IN THE TROPICS - THE INFLUENCE OF ATLANTIC-OCEAN CIRCULATION. *Nature*, 343, 607-612.
- STREET, F. A. & GROVE, A. T. 1979. GLOBAL MAPS OF LAKE-LEVEL FLUCTUATIONS SINCE 30,000 YR BP. *Quaternary Research*, 12, 83-118.
- STUIVER, M., GROOTES, P. M. & BRAZIUNAS, T. F. 1995. The GISP2 delta O-18 climate record of the past 16,500 years and the role of the sun, ocean, and volcanoes. *Quaternary Research*, 44, 341-354.
- SWIFT, M. J., HEAL, O. W. & ANDERSON, J. M. 1979. *Decomposition in Terrestrial Ecosystems*, Oxford, London, Edinburgh, Melbourne, Blackwell Scientific Publications.
- TAHA, M. F., HARB, S. A., NAGIB, M. K. & TANTAWY, A. H. 1981. The Climate of the Near East. In: TAKAHASHI, K. & ARAKAWA, H. (eds.) *Climates of Southern and Western Asia*. Amsterdam: Elsevier.
- TALMA, A. S. & VOGEL, J. C. 1992. LATE QUATERNARY PALEOTEMPERATURES DERIVED FROM A SPELEOTHEM FROM CANGO CAVES, CAPE PROVINCE, SOUTH-AFRICA. *Quaternary Research*, 37, 203-213.
- TAN, M., BAKER, A., GENTY, D., SMITH, C., ESPER, J. & CAI, B. 2006. Applications of stalagmite laminae to paleoclimate reconstructions: Comparison with dendrochronology/climatology. *Quaternary Science Reviews*, 25, 2103-2117.
- TARUTANI, T., CLAYTON, R. N. & MAYEDA, T. K. 1969. The effect of polymorphism and magnesium substitution on oxygen isotope fractionation between calcium carbonate and water. *Geochimica et Cosmochimica Acta*, 33, 987-996.
- TATLI, H., NÜZHET DALFES, H. & SIBEL MENTEŞ, Ş. 2004. A statistical downscaling method for monthly total precipitation over Turkey. *International Journal of Climatology*, 24, 161-180.
- TERA, F. & WASSERBURG, G. J. 1972. U-TH-PB SYSTEMATICS IN 3 APOLLO 14 BASALTS AND PROBLEM OF INITIAL PB IN LUNAR ROCKS. *Earth and Planetary Science Letters*, 14, 281-&.
- THORNTHWAITE, C. 1948. An approach toward a rational classification of climate. *Geographical Review*, 38, 55-94.
- THORROLD, S. R., CAMPANA, S. E., JONES, C. M. & SWART, P. K. 1997. Factors determining delta C-13 and delta O-18 fractionation in aragonitic otoliths of marine fish. *Geochimica et Cosmochimica Acta*, 61, 2909-2919.
- TREBLE, P., SHELLEY, J. M. G. & CHAPPELL, J. 2003. Comparison of high resolution sub-annual records of trace elements in a modern (1911-1992) speleothem with instrumental climate data from southwest Australia. *Earth and Planetary Science Letters*, 216, 141-153.

- TREBLE, P. C., CHAPPELL, J. & SHELLEY, J. M. G. 2005a. Complex speleothem growth processes revealed by trace element mapping and scanning electron microscopy of annual layers. *Geochimica et Cosmochimica Acta*, 69, 4855-4863.
- TREBLE, P. C., CHAPPELL, J., GAGAN, M. K., MCKEEGAN, K. D. & HARRISON, T. M. 2005b. In situ measurement of seasonal  $\delta^{18}\text{O}$  variations and analysis of isotopic trends in a modern speleothem from southwest Australia. *Earth and Planetary Science Letters*, 233, 17-32.
- TREMAINE, D. M., FROELICH, P. N. & WANG, Y. 2011. Speleothem calcite farmed in situ: Modern calibration of  $\delta^{18}\text{O}$  and  $\delta^{13}\text{C}$  paleoclimate proxies in a continuously-monitored natural cave system. *Geochimica et Cosmochimica Acta*, 75, 4929-4950.
- TREWARTHA, G. T. 1980. *An Introduction to Climate*, New York, McGraw-Hill.
- TRITAKIS, B. P. 1982. ETESIANS DISTRIBUTION WITHIN THE BARTEL ROTATIONS NO-1938-2027 (1975-1981). *Geophysical Research Letters*, 9, 1225-1226.
- TROESTER, J. W. & WHITE, W. B. 1984. SEASONAL FLUCTUATIONS IN THE CARBON-DIOXIDE PARTIAL-PRESSURE IN A CAVE ATMOSPHERE. *Water Resources Research*, 20, 153-156.
- TRUDGILL, S. T., PICKLES, A. M., SMETTEM, K. R. J. & CRABTREE, R. W. 1983. SOIL-WATER RESIDENCE TIME AND SOLUTE UPTAKE .1. DYE TRACING AND RAINFALL EVENTS. *Journal of Hydrology*, 60, 257-279.
- TÜRKEŞ, M. 1996. Spatial and temporal analysis of annual rainfall variations in Turkey. *International Journal of Climatology*, 16, 1057-1076.
- TÜRKEŞ, M., KOÇ, T. & SARIŞ, F. 2009. Spatiotemporal variability of precipitation total series over Turkey. *International Journal of Climatology*, 29, 1056-1074.
- TURKES, M., SUMER, U. M. & DEMIR, I. 2002. Re-evaluation of trends and changes in mean, maximum and minimum temperatures of Turkey for the period 1929-1999. *International Journal of Climatology*, 22, 947-977.
- TURNER, J. V. 1982. Kinetic fractionation of carbon-13 during calcium carbonate precipitation. *Geochimica et Cosmochimica Acta*, 46, 1183-1191.
- TZEDAKIS, P. C., FROGLEY, M. R. & HEATON, T. H. E. 2003a. Last Interglacial conditions in southern Europe: evidence from Ioannina, northwest Greece. *Global and Planetary Change*, 36, 157-170.
- TZEDAKIS, P. C., MCMANUS, J. F., HOOGHIEMSTRA, H., OPPO, D. W. & WIJMSTRA, T. A. 2003b. Comparison of changes in vegetation in northeast Greece with records of climate variability on orbital and suborbital frequencies over the last 450 000 years. *Earth and Planetary Science Letters*, 212, 197-212.
- UNAL, Y., KINDAP, T. & KARACA, M. 2003. Redefining the climate zones of Turkey using cluster analysis. *International Journal of Climatology*, 23, 1045-1055.
- VAKS, A., BAR-MATTHEWS, M., AYALON, A., SCHILMAN, B., GILMOUR, M., HAWKESWORTH, C. J., FRUMKIN, A., KAUFMAN, A. & MATTHEWS, A. 2003. Paleoclimate reconstruction based on the timing of speleothem growth and oxygen and carbon isotope composition in a cave located in the rain shadow in Israel. *Quaternary Research*, 59, 182-193.
- VAKS, A., BAR-MATTHEWS, M., MATTHEWS, A., AYALON, A. & FRUMKIN, A. 2010. Middle-Late Quaternary paleoclimate of northern margins of the Saharan-Arabian Desert: reconstruction from speleothems of Negev Desert, Israel. *Quaternary Science Reviews*, 29, 2647-2662.
- VAKS, A., GUTAREVA, O. S., BREITENBACH, S. F. M., AVIRMED, E., MASON, A. J., THOMAS, A. L., OSINZEV, A. V., KONONOV, A. M. & HENDERSON, G. M. 2013. Speleothems Reveal 500,000-Year History of Siberian Permafrost. *Science*, 340, 183-186.
- VAN BEYNEN, P., BOURBONNIERE, R., FORD, D. & SCHWARCZ, H. 2001. Causes of colour and fluorescence in speleothems. *Chemical Geology*, 175, 319-341.

- VAN BEYNEN, P. E., SOTO, L. & PACE-GRACZYK, K. 2008. Paleoclimate reconstruction derived from speleothem strontium and delta C-13 in Central Florida. *Quaternary International*, 187, 76-83.
- VAN ZEIST, W. & BOTTEMA, S. 1977. Palynological investigation in Western Iran. *Palaeohistorica*, 19, 18-85.
- VAN ZEIST, W. & WOLDRING, H. 1978. A postglacial pollen diagram from Lake Van in east Anatolia. *Review of Palaeobotany and Palynology*, 26, 249-276.
- VAN ZEIST, W., WOLDRING, H. & STAPERT, D. 1975. Late Quaternary vegetation and climate of south-western Turkey. *Paleohistoria*, 17, 53-143.
- VAN DEN BORRE, J., GRAMBOW, B. & ABDELOUAS, A. 2010. Discrepancies in Thorium Oxide Solubility Values: Study of Attachment/Detachment Processes at the Solid/Solution Interface. *Inorganic Chemistry*, 49, 8736-8748.
- VERGNAUD-GRAZZINI, C., RYAN, W. B. F. & CITA, M. B. 1977. STABLE ISOTOPIC FRACTIONATION, CLIMATE CHANGE AND EPISODIC STAGNATION IN EASTERN MEDITERRANEAN DURING LATE QUATERNARY. *Marine Micropaleontology*, 2, 353-370.
- VERHEYDEN, S., KEPPENS, E., FAIRCHILD, I. J., MCDERMOTT, F. & WEIS, D. 2000. Mg, Sr and Sr isotope geochemistry of a Belgian Holocene speleothem: implications for paleoclimate reconstructions. *Chemical Geology*, 169, 131-144.
- VERHEYDEN, S., NADER, F. H., CHENG, H. J., EDWARDS, L. R. & SWENNEN, R. 2008. Paleoclimate reconstruction in the Levant region from the geochemistry of a Holocene stalagmite from the Jeita cave, Lebanon. *Quaternary Research*, 70, 368-381.
- VERMOERE, M., DEGRYSE, P., VANHECKE, L., MUCHEZ, P., PAULISSEN, E., SMETS, E. & WAELKENS, M. 1999. Pollen analysis of two travertine sections in Basköy (southwestern Turkey): implications for environmental conditions during the early Holocene. *Review of Palaeobotany and Palynology*, 105, 93-110.
- VISBECK, M. H., HURRELL, J. W., POLVANI, L. & CULLEN, H. M. 2001. The North Atlantic Oscillation: Past, present, and future. *Proceedings of the National Academy of Sciences of the United States of America*, 98, 12876-12877.
- WALKER, G. T. & BLISS, E. W. 1932. World weather V. *Memoirs of the Royal Meteorological Society*, 44, 53-83.
- WALLACE, J. M. & GUTZLER, D. S. 1981. TELECONNECTIONS IN THE GEOPOTENTIAL HEIGHT FIELD DURING THE NORTHERN HEMISPHERE WINTER. *Monthly Weather Review*, 109, 784-812.
- WANG, G., DOLMAN, A. J. & ALESSANDRI, A. 2011. A summer climate regime over Europe modulated by the North Atlantic Oscillation. *Hydrology and Earth System Sciences*, 15, 57-64.
- WANG, X., AULER, A. S., EDWARDS, R. L., CHENG, H., ITO, E. & SOLHEID, M. 2006. Interhemispheric anti-phasing of rainfall during the last glacial period. *Quaternary Science Reviews*, 25, 3391-3403.
- WANG, X. F., AULER, A. S., EDWARDS, R. L., CHENG, H., CRISTALLI, P. S., SMART, P. L., RICHARDS, D. A. & SHEN, C. C. 2004. Wet periods in northeastern Brazil over the past 210 kyr linked to distant climate anomalies. *Nature*, 432, 740-743.
- WANG, Y. J., CHENG, H., EDWARDS, R. L., AN, Z. S., WU, J. Y., SHEN, C. C. & DORALE, J. A. 2001. A high-resolution absolute-dated Late Pleistocene monsoon record from Hulu Cave, China. *Science*, 294, 2345-2348.
- WANG, Y. J., CHENG, H., EDWARDS, R. L., KONG, X. G., SHAO, X. H., CHEN, S. T., WU, J. Y., JIANG, X. Y., WANG, X. F. & AN, Z. S. 2008. Millennial- and orbital-scale changes in the East Asian monsoon over the past 224,000 years. *Nature*, 451, 1090-1093.

- WARDLAW, N., OLDERSHAW, A. & STOUT, M. 1978. TRANSFORMATION OF ARAGONITE TO CALCITE IN A MARINE GASTEROPOD. *Canadian Journal of Earth Sciences*, 15, 1861-1866.
- WASYLENKI, L. E., DOVE, P. M., WILSON, D. S. & DE YOREO, J. J. 2005. Nanoscale effects of strontium on calcite growth: An in situ AFM study in the absence of vital effects. *Geochimica et Cosmochimica Acta*, 69, 3017-3027.
- WEBSTER, J. W., BROOK, G. A., RAILSBACK, L. B., CHENG, H., EDWARDS, R. L., ALEXANDER, C. & REEDER, P. P. 2007. Stalagmite evidence from Belize indicating significant droughts at the time of Preclassic Abandonment, the Maya Hiatus, and the Classic Maya collapse. *Palaeogeography, Palaeoclimatology, Palaeoecology*, 250, 1-17.
- WEISS, H. & BRADLEY, R. S. 2001. Archaeology - What drives societal collapse? *Science*, 291, 609-610.
- WENDT, I. 1984. A three-dimensional U<sup>-</sup>, Pb discordia plane to evaluate samples with common lead of unknown isotopic composition. *Chemical Geology*, 46, 1-12.
- WENINGER, B., ALRAM-STERN, E., BAUER, E., CLARE, L., DANZEGLOCKE, U., JÖRIS, O., KUBATZKI, C., ROLLEFSON, G., TODOROVA, H. & VAN ANDEL, T. 2006. Climate forcing due to the 8200 cal yr BP event observed at Early Neolithic sites in the eastern Mediterranean. *Quaternary Research*, 66, 401-420.
- WENINGER, B., CLARE, L., ROHLING, E. J., BAR-YOSEF, O., BOEHNER, U., BUDJA, M., BUNDSCHUH, M., FEURDEAN, A., GEBEL, H.-G., JOERIS, O., LINSTAEDTER, J., MAYEWSKI, P., MUEHLENBRUCH, T., REINGRUBER, A., ROLLEFSON, G., SCHYLE, D., THISSEN, L., TODOROVA, H. & ZIELHOFER, C. 2009. The Impact of Rapid Climate Change on prehistoric societies during the Holocene in the Eastern Mediterranean. *Documenta Praehistorica, Vol Xxxvi*.
- WENK, H. R., BARBER, D. J. & REEDER, R. J. 1983. Microstructures in carbonates. In: REEDER, R. J. (ed.) *Carbonates: Mineralogy and Chemistry*. Washington D.C.: Mineralogical Society of America.
- WHITE, S. 1976. The Effects of Strain on the Microstructures, Fabrics, and Deformation Mechanisms in Quartzites. *Philosophical Transactions of the Royal Society of London. Series A, Mathematical and Physical Sciences*, 283, 69-86.
- WHITE, W. B. 1981. Reflectance Spectra and Color in Speleothems. *National Speleological Society Bulletin*, 43, 20-26.
- WICK, L., LEMCKE, G. & STURM, M. 2003. Evidence of Lateglacial and Holocene climatic change and human impact in eastern Anatolia: High-resolution pollen, charcoal, isotopic and geochemical records from the laminated sediments of Lake Van, Turkey. *Holocene*, 13, 665-675.
- WIEDNER, E., SCHOLZ, D., MANGINI, A., POLAG, D., MUEHLINGHAUS, C. & SEGL, M. 2008. Investigation of the stable isotope fractionation in speleothems with laboratory experiments. *Quaternary International*, 187, 15-24.
- WIGLEY, T. M. L. & FARMER, G. 1982. Climate of the Eastern Mediterranean and Near East. In: BINTLIFF, J. L. & VAN ZEIST, W. (eds.) *Palaeoclimates, Palaeoenvironments and Human Communities in the Eastern Mediterranean Region in Later Prehistory*. Oxford: British Archaeological Reports International Series 133.
- WILLIAMS, M., DUNKERLEY, D., DE DECKKER, P., KERSHAW, P. & CHAPPELL, J. 1998. *Quaternary Environments*, London, Arnold.
- WILLIAMS, P. W. 1983. THE ROLE OF THE SUBCUTANEOUS ZONE IN KARST HYDROLOGY. *Journal of Hydrology*, 61, 45-67.
- WILLIAMS, P. W. 2008. The role of the epikarst in karst and cave hydrogeology: a review. *International Journal of Speleology*, 37, 1-10.

- WILLIAMS, P. W., KING, D. N. T., ZHAO, J. X. & COLLERSON, K. D. 2004. Speleothem master chronologies: combined Holocene O-18 and C-13 records from the North Island of New Zealand and their palaeoenvironmental interpretation. *Holocene*, 14, 194-208.
- WILSON, T. R. S., THOMSON, J., COLLEY, S., HYDES, D. J., HIGGS, N. C. & SORENSEN, J. 1985. EARLY ORGANIC DIAGENESIS - THE SIGNIFICANCE OF PROGRESSIVE SUBSURFACE OXIDATION FRONTS IN PELAGIC SEDIMENTS. *Geochimica et Cosmochimica Acta*, 49, 811-822.
- WINLAND, H. D. 1969. STABILITY OF CALCIUM CARBONATE POLYMORPHS IN WARM, SHALLOW SEAWATER. *Journal of Sedimentary Petrology*, 39, 1579-&.
- WINOGRAD, I. J. 2002. Evidence from Uranium-Series-Dated Speleothems for the Timing of the Penultimate Deglaciation of Northwestern Europe. *Quaternary Research*, 58, 60-61.
- WINOGRAD, I. J., SZABO, B. J., COPLEN, T. B. & RIGGS, A. C. 1988. A 250,000-YEAR CLIMATIC RECORD FROM GREAT-BASIN VEIN CALCITE - IMPLICATIONS FOR MILANKOVITCH THEORY. *Science*, 242, 1275-1280.
- WINOGRAD, I. J., COPLEN, T. B., LANDWEHR, J. M., RIGGS, A. C., LUDWIG, K. R., SZABO, B. J., KOLESAR, P. T. & REVESZ, K. M. 1992. CONTINUOUS 500,000-YEAR CLIMATE RECORD FROM VEIN CALCITE IN DEVILS-HOLE, NEVADA. *Science*, 258, 255-260.
- WINOGRAD, I. J., LANDWEHR, J. M., LUDWIG, K. R., COPLEN, T. B. & RIGGS, A. C. 1997. Duration and Structure of the Past Four Interglaciations. *Quaternary Research*, 48, 141-154.
- WOO, K. S. & CHOI, D. W. 2006. Calcitization of aragonite speleothems in limestone caves in Korea: Diagenetic process in a semiclosed system. *Geological Society of America Special Papers*, 404, 297-306.
- WOODHEAD, J. & PICKERING, R. 2012. Beyond 500 ka: Progress and prospects in the U-Pb chronology of speleothems, and their application to studies in palaeoclimate, human evolution, biodiversity and tectonics. *Chemical Geology*, 322, 290-299.
- WOODHEAD, J., HELLSTROM, J., MAAS, R., DRYSDALE, R., ZANCHETTA, G., DEVINE, P. & TAYLOR, E. 2006. U-Pb geochronology of speleothems by MC-ICPMS. *Quaternary Geochronology*, 1, 208-221.
- WOODHEAD, J., HELLSTROM, J., PICKERING, R., DRYSDALE, R., PAUL, B. & BAJO, P. 2012. U and Pb variability in older speleothems and strategies for their chronology. *Quaternary Geochronology*, 14, 105-113.
- WRIGHT, H. E., MCANDREW, J. H. & VANZEIST, W. 1967. MODERN POLLEN RAIN IN WESTERN IRAN AND ITS RELATION TO PLANT GEOGRAPHY AND QUATERNARY VEGETATIONAL HISTORY. *Journal of Ecology*, 55, 415-&.
- WURTH, G., NIGGEMANN, S., RICHTER, D. K. & MANGINI, A. 2004. The younger dryas and holocene climate record of a stalagmite from Holloch cave (Bavarian Alps, Germany). *Journal of Quaternary Science*, 19, 291-298.
- YONGE, C. J., FORD, D. C., GRAY, J. & SCHWARCZ, H. P. 1985. Stable isotope studies of cave seepage water. *Chemical Geology: Isotope Geoscience section*, 58, 97-105.
- YUAN, D. X., CHENG, H., EDWARDS, R. L., DYKOSKI, C. A., KELLY, M. J., ZHANG, M. L., QING, J. M., LIN, Y. S., WANG, Y. J., WU, J. Y., DORALE, J. A., AN, Z. S. & CAI, Y. J. 2004. Timing, duration, and transitions of the Last Interglacial Asian Monsoon. *Science*, 304, 575-578.
- ZANCHETTA, G., DRYSDALE, R. N., HELLSTROM, J. C., FALLICK, A. E., ISOLA, I., GAGAN, M. K. & PARESCHI, M. T. 2007. Enhanced rainfall in the Western Mediterranean during deposition of sapropel S1: stalagmite evidence from Corchia cave (Central Italy). *Quaternary Science Reviews*, 26, 279-286.

- ZANGVIL, A., KARAS, S. & SASSON, A. 2003. Connection between eastern mediterranean seasonal mean 500 hPa height and sea-level pressure patterns and the spatial rainfall distribution over Israel. *International Journal of Climatology*, 23, 1567-1576.
- ZHAO, J. X., XIA, Q. K. & COLLERSON, K. D. 2001. Timing and duration of the Last Interglacial inferred from high resolution U-series chronology of stalagmite growth in Southern Hemisphere. *Earth and Planetary Science Letters*, 184, 635-644.
- ZHENG, Y. F. 1999. Oxygen isotope fractionation in carbonate and sulfate minerals. *Geochemical Journal*, 33, 109-126.
- ZHONG, S. & MUCCI, A. 1989. Calcite and aragonite precipitation from seawater solutions of various salinities: Precipitation rates and overgrowth compositions. *Chemical Geology*, 78, 283-299.
- ZHORNYAK, L. V., ZANCHETTA, G., DRYSDALE, R. N., HELLSTROM, J. C., ISOLA, I., REGATTIERI, E., PICCINI, L., BANESCHI, I. & COUCHOUD, I. 2011. Stratigraphic evidence for a "pluvial phase" between ca 8200-7100 ka from Renella cave (Central Italy). *Quaternary Science Reviews*, 30, 409-417.
- ZHOU, G. T. & ZHENG, Y. F. 2003. An experimental study of oxygen isotope fractionation between inorganically precipitated aragonite and water at low temperatures. *Geochimica et Cosmochimica Acta*, 67, 387-399.
- ZHOU, H., ZHAO, J., ZHANG, P., SHEN, C.-C., CHI, B., FENG, Y., LIN, Y., GUAN, H. & YOU, C.-F. 2008a. Decoupling of stalagmite-derived Asian summer monsoon records from North Atlantic temperature change during marine oxygen isotope stage 5d. *Quaternary Research*, 70, 315-321.
- ZHOU, H., CHI, B., LAWRENCE, M., ZHAO, J., YAN, J., GREIG, A. & FENG, Y. 2008b. High-resolution and precisely dated record of weathering and hydrological dynamics recorded by manganese and rare-earth elements in a stalagmite from Central China. *Quaternary Research*, 69, 438-446.
- ZHOU, H., WANG, Q., ZHAO, J., ZHENG, L., GUAN, H., FENG, Y. & GREIG, A. 2008c. Rare earth elements and yttrium in a stalagmite from Central China and potential paleoclimatic implications. *Palaeogeography, Palaeoclimatology, Palaeoecology*, 270, 128-138.
- ZHOU, H., FENG, Y.-X., ZHAO, J.-X., SHEN, C.-C., YOU, C.-F. & LIN, Y. 2009. Deglacial variations of Sr and  $87\text{Sr}/86\text{Sr}$  ratio recorded by a stalagmite from Central China and their association with past climate and environment. *Chemical Geology*, 268, 233-247.
- ZHOU, J. Z., LUNDSTROM, C. C., FOUKE, B., PANNO, S., HACKLEY, K. & CURRY, B. 2005. Geochemistry of speleothem records from southern Illinois: Development of (U-234)/(U-238) as a proxy for paleoprecipitation. *Chemical Geology*, 221, 1-20.
- ZIV, B., SAARONI, H. & ALPERT, P. 2004. The factors governing the summer regime of the eastern Mediterranean. *International Journal of Climatology*, 24, 1859-1871.

# Methods Appendix

## Sawing of Stalagmites

Iranian stalagmites were previously sawed by Dr Sa'ad Al-Omari. Turkish stalagmites were sawed by myself on a diamond tipped, water cooled rock saw.

## Carbonate Stable Isotope Measurements

Powders were drilled from speleothem slabs using a hand held dentist's drill at 1 mm intervals along the growth axis, then weighed into stainless steel capsules. Sample analyses were carried out by myself under the supervision of Dr Alina Marca-Bell in the Stable Isotope Laboratory, UEA, with the exception of those measurements performed by Dr Sa'ad Al-Omari, as noted in the text. Approximately 100 µg samples were analysed for carbon and oxygen isotopic compositions on a Europa SIRA II dual inlet isotope ratio mass spectrometer following reaction with 100% phosphoric acid at 90°C using an on-line common acid bath system built in house. The precision of the measurements was better than 0.1 ‰ for both  $^{13}\text{C}$  and  $^{18}\text{O}$ , representing the standards deviation of repeat analyses of the UEACMST carbonate material lab standard (n=7, analysed in each batch of samples). In some batches, precision of the standard  $^{13}\text{C}$  was not as precise as 0.1 ‰, however this was identified as being due to particularly negative samples causing a memory effect in the acid. When less negative samples were measured and this memory effect wasn't a factor, precision was much higher.

## Water Stable Isotope Measurements

Oxygen and hydrogen isotopic measurements were performed using a Picarro cavity ring-down spectroscopy (CDRS) laser instrument. Due to memory effects in this type of instrumentation, each sample was injected 6 times (0.1 ml volume). Data are reported as delta values (per mil) vs. VSMOW. The measurement precision was 0.3 ‰ for  $\delta^{18}\text{O}$  and 0.5 ‰ for  $\delta\text{D}$ , based on the repeat analysis of the laboratory internal standard (NTW) (n= 9).

## Trace Element Measurements

All sample preparations were carried out by myself; all analyses were carried out by myself and Mr Graham Chilvers at the UEA. Laser analysis was carried out on a Thermo-Electron

X-Series ICP-MS using a NIST glass standard. Lines were pre-ablated to remove surface contamination, before sample spots were performed. To calibrate these data, solution analyses were also carried out:

Carbonate samples of 2.5mg were dissolved in 5ml of 10% acetic acid, and then diluted to 50 ml with MilliQ water. Water samples of 0.8 ml were acidified with 0.2 ml double distilled concentrated nitric acid, then diluted to 10 ml with MilliQ water. Carbonate and water samples were then analysed on a Varian ICPOES. Trace element concentrations were determined relative to mixed standard solutions of precisely known concentration.

## Uranium Series Dating

Method courtesy of Steve Noble, NIGL, BGS.

All analytical work was done at the NERC Isotope Geosciences Laboratory. Chemical preparation was done in a HEPA-filtered class 100 workstation. Reagents were prepared by sub-boiling in either quartz or Teflon, both in house and purchased from Romil UK (UpA grade). All vessels used for sample processing were Savillex PFA.

Samples (~200-250 mg powder) were dissolved in water and 15 M HNO<sub>3</sub>, the latter dispensed dropwise into the water in which the sample was immersed, to avoid overly vigorous reaction. Dissolved samples were then spiked with a mixed <sup>229</sup>Th-<sup>236</sup>U tracer calibrated against gravimetric solutions prepared from CRM 112a U metal and Ames Laboratory high purity Th metal. Sample-spike equilibration was achieved by refluxing samples overnight in sealed Savillex PFA vials, drying down, and taking up and refluxing in 7 M HNO<sub>3</sub>.

Samples were then dried down and reacted in 15 M HNO<sub>3</sub> and 30% H<sub>2</sub>O<sub>2</sub> (10:1 ratio to maximize oxidation) to consume organic materials that could potentially negatively impact column chemistry. Two oxidation steps preceded chemistry. Pre-concentration by Fe co-precipitation using an FeCl solution prepared from Puratronic Fe nitrate and the initial chemical separation of U and Th on homemade 0.6 ml columns (polypropylene with hydrophilic polyethylene frits) using AG-1 x 8 anion resin followed procedures established by Edwards et al. (1988).

Prior to co-precipitation the samples were taken up in 2 M HCl. 4-8 mg of Fe was added as FeCl and U and Pb precipitated with the Fe by adding 22 M ammonia solution. The samples

were centrifuged at 2500 rpm for 5 minutes in tightly sealed precleaned PP tubes and the supernatant liquid pipetted off and discarded. The precipitates were washed and centrifuged 3x with Milli Q water to remove unwanted sample matrix prior to dissolution in acid ready for column chemistry.

Samples were loaded and washed on cleaned and equilibrated columns in 7 M HNO<sub>3</sub>. Th was eluted in 8 M HCl followed by U elution in 0.2 M HCl. After an initial separation on AG-1 x 8, the separated Th aliquots were further purified using a second pass through AG-1 x 8 columns, while separated U was purified on UTEVA columns following Andersen et al. (2008). The U and Th separates were once again subjected to repeated 15 M HNO<sub>3</sub> and 30% H<sub>2</sub>O<sub>2</sub> oxidation steps to minimize potential organic contamination from the resins, particularly UTEVA. U and Th separates were taken up in 1 ml 0.2 M HCl - 0.05 M HF and centrifuged to remove any resin beads prior to mass spectrometry to avoid of nebulizer tip clogging and introduction of unwanted organic material into the instruments.

Early in this study U isotope data were obtained on an Axiom multicollector inductively coupled mass spectrometer (MC-ICP-MS). The Axiom was operated in static mode using an Aridus 1 desolvating nebulizer, measuring <sup>234</sup>U on an SEM. U sensitivity was ca. 100 V/ppm at an introduction rate of ~50 microlitres/minute. Mass bias and SEM gain was monitored via replicate CRM 112a analyses. Corresponding Th data were obtained on a Nu instruments Nu HR MC-ICP-MS using a DSN desolvating nebulizer (sensitivity was ca. 200 V/ppm U).

The bulk of the U and Th data for this study, however, were obtained on a recently acquired Thermo Neptune Plus MC-ICP-MS (sensitivity ca. 350-500 V/ppm U) using an Aridus II desolvating nebulizer. U mass bias and SEM/Faraday gain correction of unknowns was based on standard-sample bracketing. Exponential correction for U mass bias was based on measurements of CRM 112a spiked with a <sup>233</sup>U/<sup>236</sup>U tracer (IRMM 3636), while SEM gain was monitored using measured <sup>234</sup>U/<sup>235</sup>U of mass bias-corrected unspiked CRM 112a analyses, with the mass-bias and spike-corrected <sup>234</sup>U/<sup>238</sup>U values of the spiked CRM 112a runs used as a check on the SEM gain. Hydride and tailing corrections on the Neptune measurements followed Hiess et al. (2012). Both hydride and down-mass tailing were on the order of 2 ppm of the adjacent peaks and was very consistent on a timescale of several days on the Neptune.

Mass bias and SEM gain for Th measurements on both the Nu HR and Neptune instruments were corrected using an in-house  $^{229}\text{Th}$ - $^{230}\text{Th}$ - $^{232}\text{Th}$  reference solution calibrated by ICP-MS against CRM 112a. On the Neptune Th isotopes were measured in static multicollection mode with  $^{229}\text{Th}$  and  $^{232}\text{Th}$  measured on Faraday detectors while  $^{230}\text{Th}$  was measured on an SEM. The Nu HR collector block at NIGL is optimized for U-Pb geochronology and therefore a dynamic peak-jumping routine was necessary to obtain all relevant Th ratios, with  $^{229}\text{Th}/^{230}\text{Th}$  and  $^{229}\text{Th}/^{232}\text{Th}$  being measured statically in successive peak jumps. Total  $^{238}\text{U}$  and  $^{232}\text{Th}$  blanks were generally <10 pg and <4 pg during the course of this study and were negligible relative to the sample U and Th. On the Neptune, standard accuracy (within 0.1%) and reproducibility (within 0.2%) of  $^{234}\text{U}/^{238}\text{U}$  was monitored by replicate analyses of Harwell uraninite HU-1. Equivalent data from the Axiom was on the order of  $\pm 0.2$  and 0.3%, accuracy and reproducibility respectively. Replicate measurements of the in-house  $^{229}\text{Th}$ - $^{230}\text{Th}$ - $^{232}\text{Th}$  reference solution indicate that accuracy and reproducibility for  $^{229}\text{Th}/^{230}\text{Th}$  as measured on the Neptune is on the order of  $\pm 0.2$ -0.3% for  $^{230}\text{Th}$  ion beams > 5000 cps and ca. 0.4% for the Nu HR. Data were reduced using an in-house Excel spreadsheet and ages calculated using the Isoplot version 3 add-in (Ludwig, 2003b) following Ludwig, (2003a) and the decay constants of Cheng et al. (2000).

## U/Pb Dating

Method courtesy of Dan Condon, NIGL, BGS.

Samples were screened via LA-ICP-MS using a Nu Plasma HR Inductively Coupled Plasma Multi-collector Mass Spectrometer with a Nu Instruments DSN-100 dry aerosol nebuliser. The laser ablation system was a New Wave Research UP-193 with solid state Nd/YAG laser. The data was collected simultaneously in two Faraday Cups ( $^{238}\text{U}$  and  $^{235}\text{U}$ ) and six ion counters ( $^{207}\text{Pb}$ ,  $^{206}\text{Pb}$ ,  $^{205}\text{Tl}$ ,  $^{204}\text{Pb}+^{204}\text{Hg}$ ,  $^{203}\text{Tl}$ , and  $^{202}\text{Hg}$ ).

Samples for ID-TIMS were cut from the speleothem using a dentist's drill, ensuring not to incorporate any detritus. Samples were spiked with a mixed  $^{205}\text{Pb}$ - $^{233}\text{U}$ - $^{235}\text{U}$  tracer and dissolved using established protocols for the dissolution of carbonate. Following chemical purification, U was measured by multi-collector ICP-MS using a Nu Plasma HR at NIGL using a static faraday cup array. IRMM-184 was used as a reference material to correct for mass bias, and any residual mass bias was resolved using the corrected  $^{233}\text{U}/^{235}\text{U}$  double spike ratio. Pb was measured by thermal ionisation mass spectrometry (TIMS) using a ThermoScientific Triton and a static faraday cup array. Mass bias was determined by

measurement of NBS 981 and NBS 982. Up to 1 pg of common Pb was assumed to be procedural blank.

For  $^{234}\text{U}/^{238}\text{U}$  measurements, samples were dissolved as for U/Pb analysis, but no spike was used. Only U was measured, using the Neptune plus MC-ICP-MS at NIGL.

## **Autoradiography**

Digital autoradiography was carried out using an Amersham Biosciences Storm 860 Laser Stimulated Photoluminescence Scanner. Samples were placed on BaClF digital storage phosphor imaging plates, which were doped with Europium. Laser light of wavelength 635 nm (red) and 450 nm (blue) was used to release the energy stored by the crystals in the plate.

## **Sr Isotopes**

Method courtesy of Ian Millar, NIGL, BGS

All sample preparation was performed by Dr Ian Millar and myself at NIGL, BGS. Samples were pre-leached in 1% acetic acid in order to remove labile Sr, and subsequently leached in dilute (10%) acetic acid in order to preferentially dissolve carbonate material. For the Dim Cave soil sample, the residue after acetic acid leaching was also analysed. Samples were dried and reweighed, and spiked with an enriched  $^{84}\text{Sr}$  tracer in order to allow calculation of Sr concentration by isotope dilution. The samples were then converted to nitrate form by addition of concentrated (16M) nitric acid, and again evaporated. Sr was separated using c. 150 microlitres of Eichrom Sr-SPEC ion exchange resin in disposable 1ml columns.

Sr was loaded onto single rhenium filaments using a TaO activator, and analysed in a Thermo Triton mass spectrometer at NIGL in multi-dynamic mode. Nine analyses of the NBS987 standard run with the samples gave a value of  $0.710251 \pm 0.000003$  (4.9 ppm,  $1\sigma$  uncertainty).